Crystallization, Micro- and Nano-structure, and Melting Behavior of Polymer Blends

3

G. Groeninckx, C. Harrats, M. Vanneste, and V. Everaert

Contents

G. Groeninckx (✉) • V. Everaert
Department of Chemistry, Division of Molecular and Nanomaterials, Laboratory of Macromolecular Structure Chemistry, Catholic University of Leuven, Heverlee, Belgium
e-mail: gabriel.groeninckx@chem.kuleuven.ac.be; valja.everaert@gmail.com

C. Harrats
Laboratoire de Chimie Appliquée (LAC) DGRSDT, Institut des Sciences et Technologies, Ctr Univ Ain Temouchent, Ain Temouchent, Algeria
e-mail: charrats@gmail.com

M. Vanneste
Textile Functionalisation & Surface Modification, R&D/CENTEXBEL, Zwijnaarde, Algeria
e-mail: myriam.vanneste@centexbel.be

L.A. Utracki, C.A. Wilkie (eds.), *Polymer Blends Handbook*,
DOI 10.1007/978-94-007-6064-6_5,

Abstract

When the melt of a crystalline polymer is cooled to a temperature between the glass transition and the equilibrium melting point, the thermodynamic requirement for crystallization is fulfilled.

In a crystallizable miscible blend, however, the presence of an amorphous component, either thermoplastic or thermosetting, can either increase or decrease the tendency to crystallize depending on the effect of the composition of the blend on its glass transition and on the equilibrium melting point of the crystallizable component and also on the curing extent and conditions in case of thermosetting amorphous component. The type of segregation of the amorphous component, influenced by parameters such as crystallization conditions, chain microstructure, molecular weight, blend composition, and curing extent, determines to a large extent the crystalline morphology of a crystallizable binary blend. Separate crystallization, concurrent crystallization, or cocrystallization can occur in a blend of two crystallizable components. The spherulite growth of the crystallizable component in miscible blends is influenced by the type and molecular weight of the amorphous component, the former affecting the intermolecular interactions between both components and the latter the diffusion of the amorphous component. The blend composition, the crystallization conditions, the degree of miscibility and the mobility of both blend components, and the nucleation activity of the amorphous component are important factors with respect to the crystallization kinetics. The melting behavior of crystallizable miscible blends often reveals multiple DSC endotherms, which can be ascribed to recrystallization, secondary crystallization, or liquid-liquid phase separation. Complex crystallization behavior develops in miscible blends containing a crystallizable thermoplastic and a curable thermosetting component. That depends on the temperature and time of curing the thermosetting and also on whether crystallization is initiated before, during, or after the curing process.

For the discussion of the crystallization and melting behavior in immiscible polymer blends, a division into three main classes is proposed.

In blends with a crystallizable matrix and an amorphous dispersed phase, both the nucleation behavior and the spherulite growth rate of the matrix can be affected. Nucleation of the matrix always remains heterogeneous; however, the amount of nuclei can be altered due to migration of heterogeneous nuclei during melt-mixing. Blending can also influence the spherulite growth rate of the matrix. During their growth, the spherulites can have to reject, occlude, or deform the dispersed droplets. In general, the major influence of blending is a change in the spherulite size and semicrystalline morphology of the matrix.

A completely different behavior is reported for blends in which the *crystallizable phase is dispersed*. Fractionated crystallization of the dispersed droplets, associated with different degrees of undercooling and types of nuclei, is the rule. The most important reason is a lack of primary heterogeneous nuclei within each crystallizable droplet. An important consequence of fractionated crystallization may be a drastic reduction in the degree of crystallinity.

When two crystallizable components are blended, a more complex behavior due to the influence of both phases on each other is expected. In general, the discussion for matrix crystallization and droplet crystallization can be combined. However, crystallization of one of the phases can sometimes directly induce crystallization in the second phase. As a consequence, the discussion of blends of this type has been subdivided with respect to the physical state of the second phase during crystallization. The special case of "coincident crystallization," in which the two phases crystallize at the same time, is discussed. Finally, the effect of compatibilization of crystalline/crystalline polymer blends is briefly reviewed.

A new section has been added, introduced to deal with crystallization phenomena in immiscible polymer blends containing nanoparticles. Recent reports, although few, discuss the effect of nanoparticles on crystallization and melting in immiscible polymer blends.

3.1 General Introduction

The study of the processing-morphology-property relations of polymer blends has become a topic of major scientific importance during the past three decades mainly because of intensified technological interest in this area.

The science and technology of polymer blends has now acquired an important position in the area of development of new polymeric materials. Moreover, the application of polymer blends has increased significantly and is expected to continue to grow. Of the total consumption of engineering polymers, more than 20 % is currently thought to be composed of blends with important and various applications in the automotive, electrical, and electronic industry, in computer and business equipment housings, in medical components, etc. Annually about 4,900 patents related to polymer blends are published worldwide.

These are various reasons for today's focus on polymer blends. Design of new polymers with special properties by chemical synthesis is always more expensive than the costs of the constituent existing polymers and the blending operation. A proper selection and combination of polymeric components in a certain ratio might result in a blend material with optimal properties for a specific application. The resulting blend will be the more successful; the more of the desired properties of the components are expressed in its property profile. A remarkable broad spectrum of properties can often be achieved by blending. These properties include mostly mechanical strength and stiffness, toughness, processability, heat distortion

temperature, chemical and weathering resistance, flame retardancy, thermal and dimensional stability, aging resistance, elongation, permeability, transparency, and gloss.

A fundamental question, which has to be addressed first about any blend system of interest, is of course whether the components are miscible or not. Polymer mixtures of chemically dissimilar polymers can be divided on the basis of the miscibility of their components being miscible, partially miscible, or fully immiscible.

While miscibility of polymers was considered as rather rare three decades ago, it is now recognized as an achievable phenomenon with probably well over 500 noted miscible combinations. The conceptual key toward forming miscible polymer blends is to choose polymer pairs with chemical structures capable of specific interactions leading to exothermic heats of mixing. Miscibility studies on homopolymer/copolymer blends indicate that strong repulsive interactions between the segments of the copolymer larger than those between its segments and the homopolymer might also lead to miscibility.

Miscible polymer blends behave similar to what is expected of a single-phase system. Their properties are a combination of the properties of the pure components, and in many cases, they are intermediate between those of the components. The characteristics of the components affecting the properties of miscible blends are their chemical structure and molecular weight, their concentration, and their intermolecular interactions, including crystallizability.

While miscible blend systems are of considerable scientific and practical interest, it should not be concluded that miscibility is always the preferred situation with respect to the properties. In fact, immiscibility leading to two or multiple phases during blending is desired in various cases since the property combinations that one seeks require essentially a system in which each phase can contribute its own characteristics to the blend material.

For thermodynamic reasons, i.e., small entropy gain on mixing, most arbitrary selected polymer pairs are immiscible and, as a consequence, display a two-phase behavior. Melt-mixing of immiscible polymers can result in a variety of phase morphologies depending on the blend composition, the rheological characteristics of the components such as viscosity and elasticity, the interfacial tension between the phases, and the intensity and type of flow that is applied. In the case of immiscible polymer blends, important characteristics with respect to their properties are the chemical nature of the components, the blend composition, the phase morphology (size and shape), the degree of crystallinity and semicrystalline structure of the phases in the case of crystallizable components, and the interfacial interactions between the phases.

A number of miscible polymer blends are only completely miscible and form one-phase systems over a limited concentration, temperature, and pressure range. Under certain conditions of temperature, pressure, and composition, miscible binary blends may phase separate into two liquid phases with different compositions, called partially miscible blends. Important characteristics of this type of blends are the overall blend composition, the morphology, and the composition of the different phases as well as the nature of the interface between the phases.

A large number of polymer blends contain one or two crystallizable components. The crystallization behavior of a polymer component in a blend is expected to be altered by the presence of the second blend component, whether both are completely miscible, partially miscible, or totally immiscible. Therefore, a profound scientific understanding of the crystallization behavior and the resulting semicrystalline structure in polymer blends is necessary for effective manipulation and control of their properties.

There are a number of important factors governing the change of the crystallization rate and semicrystalline structure of a polymer in blend systems. Those include the degree of miscibility of the constituent polymers, their concentration, their glass-transition and melting temperature, the phase morphology and the interface structure in the case of immiscible blends, etc.

This chapter, related to the crystallization, morphological structure, and melting of polymer blends, has been divided into two main parts. The first part (Sect. 3.2) deals with the crystallization kinetics, semicrystalline morphology, and melting behavior of miscible polymer blends. The crystallization, morphological structure, and melting properties of immiscible polymer blends are described in the second part of this chapter (Sect. 3.3).

3.2 Crystallization, Morphological Structure, and Melting Behavior of Miscible Polymer Blends

The crystallization of miscible and immiscible polymer blends can differ remarkably from that of the neat crystallizable component(s). In the case of crystallizable miscible blends (discussed in this section), important polymer characteristics with respect to crystallization are the chemical nature and molecular mass of the components, their concentration in the blend, and the intermolecular interactions between the components.

The thermodynamic requirement for crystallization in a miscible blend is that the blend exhibits a free energy on crystallization that is more negative than the free energy of the liquid-liquid mixture. A liquid-solid phase separation can occur when the miscible melt is cooled to a temperature between the glass transition of the blend and the equilibrium melting point of the crystallizable component(s) (Sect. 3.2.1). The presence of an amorphous component in a crystallizable binary blend can either increase or decrease the tendency to crystallize, depending on the effect of composition on the glass transition of the blend and on the equilibrium melting point of the crystallizable component.

The morphology of a semicrystalline polymer blend is largely determined by the type of segregation of the amorphous component (Sect. 3.2.2.1). In the case of interspherulitic segregation of the amorphous component, where the spherulites of the crystalline component are imbedded in an amorphous matrix, the semicrystalline morphology will be influenced to a lesser extent than when the amorphous component is located within the spherulites (interlamellar and interfibrillar segregation). The parameters determining the type of segregation are not fully understood.

Recent studies (Defieuw 1989) indicate that the crystallization conditions, blend composition, chain rigidity and microstructure, and molecular weight of the components are important. Blends consisting of two crystallizable components (Sect. 3.2.2.2) can exhibit separate crystallization or concurrent crystallization (cocrystallization).

Spherulite growth of the crystallizable component in miscible blend (Sect. 3.2.3) will be influenced by the type and molecular weight of the amorphous component (the former affecting the intermolecular interactions between both components and the latter the diffusion of the amorphous component).

The blend composition, the crystallization condition, the degree of miscibility and the mobility of both blend components, and the nucleation activity of the amorphous component are important factors with respect to the crystallization kinetics (Sect. 3.2.4).

The melting behavior of miscible crystallizable blends (Sect. 3.2.5) is often complex, revealing multiple DSC endotherms, which can be ascribed to several causes such as recrystallization, secondary crystallization, liquid-liquid phase separation (Sect. 3.2.6), etc.

3.2.1 Crystallization Temperature Range of Crystallizable Miscible Blends

The crystallization of a polymer can only proceed in a temperature range limited on the low temperature side by the glass-transition temperature (T_g) and on the high temperature side by the equilibrium melting point (T_m°). Below T_g the mobility of the polymer chains is hindered, while in the proximity of T_m°, crystal nucleation is inhibited.

When dealing with crystallizable miscible blends, the glass transition is located in between those of the neat components (Fig. 3.1). The presence of an amorphous component in a crystallizable miscible polymer blend can increase or decrease the tendency to crystallize depending on the T_g of the amorphous component with respect to that of the crystallizable one. If the T_g of the amorphous component is lower than that of the crystallizable one, the crystallization envelope ($T_m^\circ - T_g$) is widened, and the crystallization is facilitated. In the opposite case, where the T_g of the amorphous component is higher than that of the crystallizable one, the blend T_g is increased and the temperature range over which crystallization can occur becomes smaller. A limiting case of this is the inhibition of crystallization due to the fact that the blend T_g is higher than the T_m° of the crystallizing component, a phenomenon that is often seen in blends with a high concentration of amorphous component. An even more complex situation is observed when two miscible components are crystallizable.

Some examples are given in Table 3.1. In PCL/CPE blends, the PCL crystallization is enhanced when CPE is added (Defieuw et al. 1989a). The crystallization range becomes narrower in blends such as PCL/PECH (Runt and Martynowicz 1986), PEG/PEMA (Cimmino et al. 1989), PCL/SAN (Defieuw et al. 1989d), and

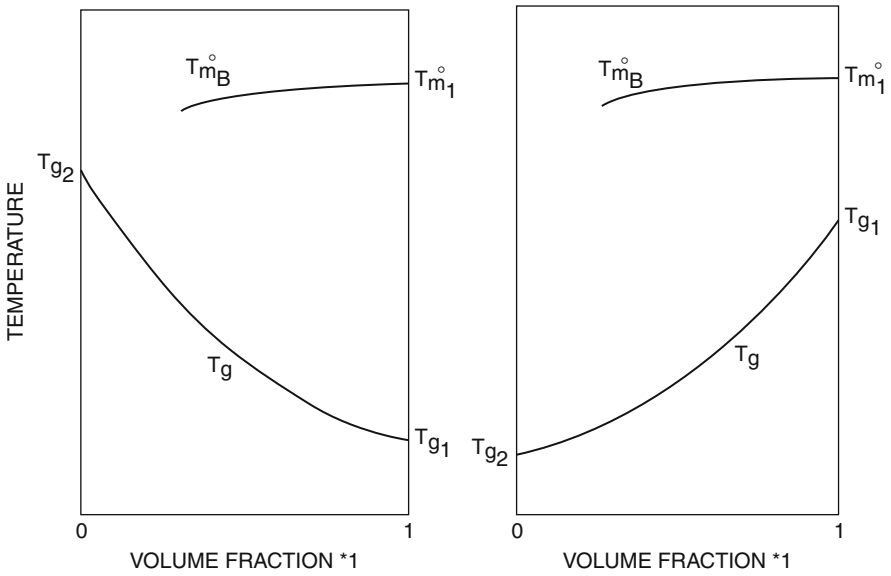

Fig. 3.1 Possible crystallization temperature ranges for a crystallizable miscible polymer blend (*1* crystallizable component, *2* amorphous component) (Runt and Martynowicz 1986)

PBT/PAr (Iruin et al. 1989), PEO/Aramide 34I (Dreezen et al. 1999a), and PEO/PES (Dreezen et al. 1999b). It should be noted that the PBT/PAr 10/90 blend does not show any tendency to crystallize although the blend's T_g is located beneath the melting point of PBT. A possible explanation for this observation is that crystallization is too slow to be noticed within the observation time limit.

3.2.2 Crystallization Phenomena in Miscible Polymer Blends

When crystallized from the melt, most polymers show a spherulitic texture (Fig. 3.2). The spherulites then consist of lamellar stacks of alternating crystalline and amorphous layers, radiating from the center (the primary nucleus).

3.2.2.1 Modes of Segregation of the Amorphous Component During Crystallization in Crystalline/Amorphous blends

In blends of a crystallizable polymer with an amorphous one, the morphology is largely determined by the type of segregation of the amorphous component. Crystallization in a miscible blend involves two types of polymer transport: diffusion of the crystallizable component toward the crystallization front and simultaneous rejection of the amorphous component. This latter phenomenon is called segregation; it can take place at three different levels: interspherulitic, interfibrillar, and interlamellar (Fig. 3.3).

Table 3.1 Influence of T_g of the amorphous component on the crystallization ability of the crystallizable component in miscible binary polymer blends

Polymer blend[a]	Blend composition (wt/wt)	T_g and T_m° (°C) of crystallizable component		T_g (°C) of amorphous component	Blend T_g (°C)	Crystallization[b]	References
PCL/CPE42	50/50[c]	−63	60	1.5	34	y	Defieuw et al. (1989a)
PCL/CPE49	50/50[c]	−63	60	18.5	44	y	
PCL/PECH	10/90	−60	60	−15	Ns[d]	y	Runt and Martynowicz (1986)
PCL/PSMA14	90/10 step −10 %/+10 %	−63, 4	56.7	127.1	Na	y	Balsamo et al. (2006)
PCL/SAN24	50/50[c]	−63	60	110	30	y	Defieuw et al. (1989c)
PBT/PAr	70/30	31	219	179	43	y	Iruin et al. (1989)
	50/50				51	y	
	30/70				87	y	
	10/90				147	n	
PEG/PEMA	90/10	−55	75	71	−47[e]	y	Cimmino et al. (1989)
	80/20				−39[e]	y	
	70/30				−30[e]	y	
PEO/PA (Aramide 34I)	95/05 to 50/50 step −5 %/+5 %	−60	73	224			Dreezen et al. (1999a)
PEO/PES	85/15	−60	73	225	−50	y	Dreezen et al. (1999b)
	80/20				−40	y	
	75/25				−30	y	

[a]The crystallizable component is listed first
[b]Ability to crystallize: yes (y) or no (n)
[c]More compositions are reported in the article
[d]*ns* not stated
[e]Calculated from the Fox equation

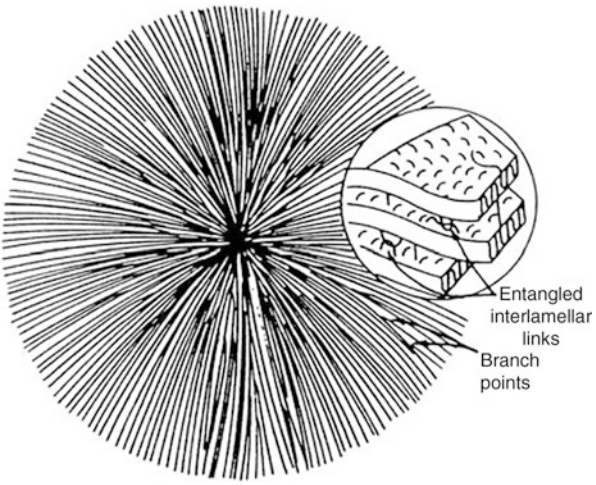

Fig. 3.2 Schematic representation of the spherulitic texture of a semicrystalline polymer (Hoffman et al. 1976)

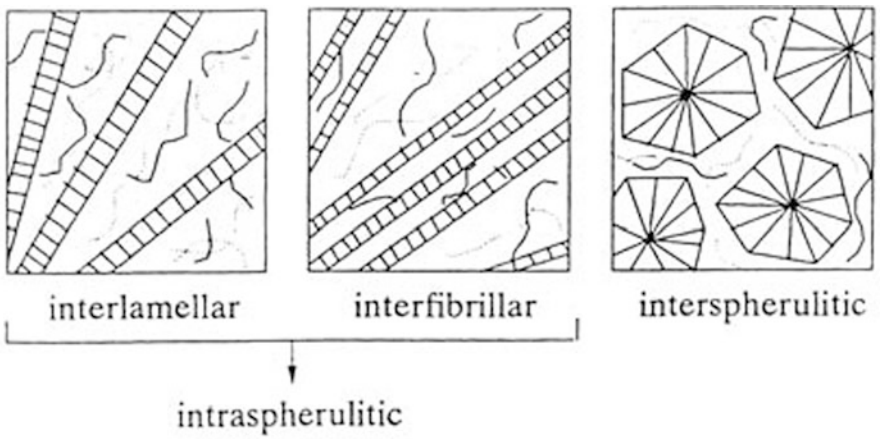

Fig. 3.3 Schematic representation of the different types of segregation of the amorphous component in crystallizable miscible polymer blends (*full lines*: crystallizable component, *dotted lines*: amorphous component)

Interspherulitic segregation, in which the spherulites are imbedded in an amorphous matrix, can be distinguished from the other two types using optical microscopy. In the case of intraspherulitic segregation, a volume-filling texture is observed; the amorphous components can be located either between the lamellae (interlamellar) or between stacks of lamellae (interfibrillar). To find out whether or not interlamellar segregation occurs, small-angle X-ray scattering (SAXS) can be used. The increase of the long spacing, which is the sum of the average thickness of the crystalline and amorphous layers, as well as the increase of the thickness of the

amorphous layers between the crystalline lamellae, with increasing concentration of the amorphous component, are parameters that are often used as indications for interlamellar segregation. In Table 3.2 some examples are presented together with the parameter and/or technique used to make conclusions about the type of segregation.

Most studies concerning the segregation behavior of amorphous components in a miscible crystallizable blend deal with PCL as the crystallizable component. In their blends with PCL, PVC has shown to segregate interlamellar (Stein et al. 1978, 1981; Khambatta et al. 1976a, b; Ong and Price 1978a; Russell and Stein 1980, 1983), PC interfibrillar or interspherulitic (Vandermarliere 1986; Cruz et al. 1979; Fernandez et al. 1986), CPE either interfibrillar or interspherulitic (depending on the amount of amorphous component) (Defieuw et al. 1989a), SMA interlamellar (Defieuw et al. 1989a; Defieuw et al. 1989b, c; Vanneste et al. 1995), SAN interlamellar (Defieuw et al. 1989c; Vanneste et al. 1995), and Phenoxy interlamellar/interfibrillar (Defieuw et al. 1989d; Vanneste 1993).

An intensively studied blend is the PEEK/PEI blend for which interlamellar (Chen and Porter 1994), interfibrillar (Crevecoeur and Groeninckx 1991: Hsiao and Sauer 1993), and interspherulitic segregations (Crevecoeur and Groeninckx 1991) were reported. In PEKK/PEI blends, PEI is segregated interspherulitically (Hsiao and Sauer 1993).

Warner et al. (1977) have shown that in iPS/PS blends the noncrystallizable atactic PS was mainly segregated between the fibrils inside the spherulites. Similar observations have been reported recently by Chi Wang et al. (2006) by using TEM and SEM tools on 50 wt% atactic PS/50 wt% syndiotactic PS miscible blends. On the other hand, Wenig et al. (1975) determined the segregation of PPE to be interlamellar region in the iPS/PPE blends. The influence of the tacticity of PMMA on segregation in PEG/PMMA blends was investigated by Silvestre et al. (1987a). Atactic and syndiotactic PMMA were found located in between the lamellae of PEG, whereas isotactic PMMA was reported to segregate interfibrillar or interspherulitic. It should, however, be noted that a low molecular weight iPMMA was used in this study. In other PEG blends, the amorphous component resided in the interlamellar (EVAc; Cimmino et al. 1994), interspherulitic (PEMA; Cimmino et al. 1989), and interlamellar and interfibrillar regions (PVAc; Silvestre et al. 1987b; Kalfoglou et al. 1988). Atactic PMMA (Canetti et al. 1994) and atactic polyhydroxybutyrate (PBH; Abe et al. 1994) were located between the lamellae in blends with iPHB. Interlamellar segregation was also reported in blends of 1-octene LLDPE fractions with different short-chain branching contents (Defoor et al. 1993).

Blends of PVDF with PMMA have been studied by several authors. All three types of segregation were detected, which was attributed to variation of the crystallization temperature by Stein et al. (1981) and Morra and Stein (1982). Hahn et al. (1987) reported the existence of a compositional interphase (a region of varying polymer composition) between the lamellae and the amorphous interlayer. The order-disorder interphase seemed to contain pure PMMA, while in the remaining interlamellar region, a homogeneous mixture of PMMA and amorphous PVDF was located.

Table 3.2 Type of segregation of the amorphous component in some crystallizable miscible polymer blends

Polymer blend	Amorphous comp. (wt%)[a]	Type of segregation	Parameter	Technique[b]	References
PCL/PVC	0–50% PVC	Interlamellar	Long spacing	SAXS, OM	Stein et al. (1978, 1981), Khambatta et al. (1976a, b), Ong and Price (1978a), Russell and Stein (1980, 1983)
PCL/PC		Interfibrillar or interspherulitic	Long spacing	SAXS	Vandermarliere (1986), Cruz et al. (1979), Fernandez et al. (1986)
PCL/CPE	0–30% CPE[c]	Interfibrillar	Long spacing	SAXS, OM	Defieuw et al. (1989a), Defieuw (1989)
	>30% CPE[c]	Interspherulitic	Long spacing	SAXS, OM	Defieuw et al. (1989a)
PCL/SMAx[d]	0–40% SMA	Interlamellar	Long spacing	SAXS, OM	Defieuw (1989), Defieuw et al. (1989b, c)
PCL/PSMA14	0–10% SMA14	Interlamellar	Amorphous layer thickness	SAXS	Vanneste (1993)
	0–100% PCL	Interlamellar		TEM	Balsam et al. (2006)
PCL/SANy[e]	0–50% SAN24	Interlamellar	Long spacing	SAXS, OM	Defieuw et al. (1989c)
	0–20% SAN15	Interlamellar	Amorphous layer thickness	SAXS	Vanneste and Groeninckx (1995)
PCL/Phenoxy	0–50% Phenoxy	Interlamellar/interfibrillar	Long spacing	SAXS, OM	Defieuw (1989), Defieuw et al. (1989d)
	0–10% Phenoxy	Interlamellar	Amorphous layer thickness	SAXS	Vanneste (1993)
PEG/aPMMA	0–40% PMMA	Interlamellar	Long spacing	SAXS	Silvestre et al. (1987a)
PEG/sPMMA	0–40% PMMA	Interlamellar	Long spacing	SAXS	Silvestre et al. (1987a)
PEG/iPMMA	0–40% PMMA	Interfibrillar or interspherulitic	Long spacing	SAXS	Silvestre et al. (1987a)
PEG/PVAc	0–40% PVAc	Interlamellar and interfibrillar	Amorphous thickness	SAXS, OM	Silvestre et al. (1987b)
		Interfibrillar			Kalfoglou et al. (1988)

(*continued*)

Table 3.2 (continued)

Polymer blend	Amorphous comp. (wt%)[a]	Type of segregation	Parameter	Technique[b]	References
PEG/PEMA		Intraspherulitic			Cimmino et al. (1989)
PEG/EVA[f]	0–20% EVA	Interlamellar		OM	Cimmino et al. (1993b)
PEO/Aramid 34I	0–50% Armd	Intraspherulitic		OM,SAXS	Dreezen et al. (1999)
PEO/PES		Intraspherulitic		OM, SAXS	Dreezen et al. (1999)
aPHB/iPHB		Interlamellar and interfibrillar[g]			Abe et al. (1994)
aPMMA/iPHB		Interlamellar			Canetti et al. (1994)
PVDF/PMMA	ns	Interlamellar, interfibrillar, or interspherulitic[h]	Amorphous layer thickness	SAXS, OM	Morra et al. (1982, 1984), Stein et al. (1981)
PVDF/PMMA	0% and 40% PMMA	Partially interlamellar/partially interfibrillar		SAXS, OM	Saito and Stuhn (1994)
PVDF/PMMA	0–75% PMMA	Interlamellar	Amorphous layer thickness	SAXS	Ullmann and Wendorff (1985)
PVDF/iPEMA[i]	0–50% iPEMA	Interlamellar	Long spacing	SAXS	Eshuis et al. (1982)
iPS/PPE	0–30% PPE	Interlamellar	Lamellar thickness	SAXS	Wenig et al. (1975)
iPS/PS	0–30% PS	Interfibrillar	Amorphous layer thickness	SAXS	Warner et al. (1977), Stein et al. (1981), Russell and Stein (1980)
aPS/sPs	0–80% aPS	Interfibrillar	Long spacing	SAXS, TEM	Wang et al. (2004)
LLDPE/LLDPE[j]		Interlamellar	Long spacing	SAXS	Defoor et al. (1993)
PEEK/PEI	0–50% PEI	Interfibrillar or interspherulitic	Long spacing	SAXS	Crevecoeur and Groeninckx (1991)

PEEK/PEI	0–50% PEI	Interlamellar	Melting behavior	DSC	Chen and Porter (1994)
PEEK/PEI[k]	<50% PEI	Interfibrillar	Long spacing	SAXS	Hsiao and Sauer (1993)
PEKK/PEI[l]	0–50% PEI	Interspherulitic	Long spacing	SAXS	Hsiao and Sauer (1993)

[a]*ns* not specified
[b]*SAXS* small-angle X-ray scattering, *OM* optical microscopy
[c]CPE containing 42.1 and 49.1 wt% chlorine
[d]x = wt% MA in SMA, i.e., 14 and 25 wt% MA
[e]y = wt% AN in SAN, i.e., 15 and 24 wt% AN
[f]PEG/EVA is only miscible for a vinyl acetate content of 56% and higher (Cimmino et al. 1993)
[g]Two different molecular weights were used
[h]Depending on the crystallization temperature (Stein et al. 1981)
[i]PVDF/iPEMA shows an LCST phase behavior (LCST = 183 °C), the experiments were performed on blends prepared and studied below this temperature
[j]A blend of 1-octene LLDPE fractions with different short-chain branching contents was investigated, i.e., 3 and 33 methyl groups per 1000 carbon atoms
[k]Rapid crystallization conditions, interfibrillar segregation occurred in blends with a PEI concentration below 50 %; at higher contents of the amorphous component, interspherulitic segregation was observed
[l]Slow crystallization conditions

Miscibility, isothermal crystallization kinetics, crystal structure, and microstructure of biodegradable PBSA/PVPh blends were investigated with DSC, Polarized OM, WAXD, and SAXS (Yang et al. 2009).

The investigation revealed the following features with respect to the crystallization of PBSA in the presence of PVPh:

1. PBSA and PVPh are miscible crystalline/amorphous polymer blends. Miscibility of PBSA/PVPh blends was evidenced by the single composition-dependent glass-transition temperature over the entire blend compositions. The negative polymer-polymer interaction parameter, obtained from the melting depression of PBSA, indicates that PBSA/PVPh blends are thermodynamically miscible.
2. Isothermal crystallization kinetics study of neat and blended PBSA indicates that the crystallization mechanism of PBSA does not change, but the crystallization rate decreases with increasing the PVPh content in the blends.
3. The crystal structure of PBSA is not modified in the PBSA/PVPh blends. However, the values of LP, Lc, and La become larger with increasing the PVPh content, indicating that PVPh mainly resides in the interlamellar region of PBSA spherulites.

Typical Examples of Supramolecular and Semicrystalline Morphology

PEO (semicrystalline)/Aramide 34I (amorphous) blend was observed by polarized microscope to identify the supramolecular structure and characterized by SAXS to identify the type of semicrystalline morphology (Dreezen et al. 1999). The supramolecular structure of pure PEO consists of different types depending on the molecular weight and the crystallization temperature. Allen and Mandelkern (1982) compiled a morphological map for PEO in which three different supramolecular structures are present: a spherulitic, a hedritic, and an intermediate spherulitic-hedritic structure. Figure 3.4 reveals that pure PEO displays a non-structured-birefringence structure. Blending PEO with Aramide 34I results in the formation of well-defined Maltese-cross spherulites above 15 % Aramide 34I. Figure 3.4a represents an intermediate pattern of spherulitic-hedritic structure. All the blends containing up to 25 % amorphous Aramide 34I exhibit volume-filling spherulites indicating intraspherulitic segregation of the amorphous component. This change was attributed to lower diffusion rate and increased secondary nucleation when crystallizing PEO in blends with Aramide 34I, the T_g of which is very high. Calculation from SAXS reveals that both the long period and the amorphous thickness increase with the amount of the amorphous component, whereas the crystalline lamellae thickness slightly decreases; this effect is synonymous of interlamellar segregation. A model in which thin lamellae are located between the primary formed thick lamellae in the same stack was proposed to describe the secondary crystallization of PEO in PEO/Aramide 34I blends (Fig. 3.4). Similar crystallization, melting, and supramolecular structure and mode of segregation behavior were also reported when PEO is blended with polyethersulfone (Dreezen et al. 1999b; Fig. 3.5).

The concept of a crystal-amorphous (also order-disorder) interface was first proposed by Flory (1962) for binary semicrystalline/amorphous blends.

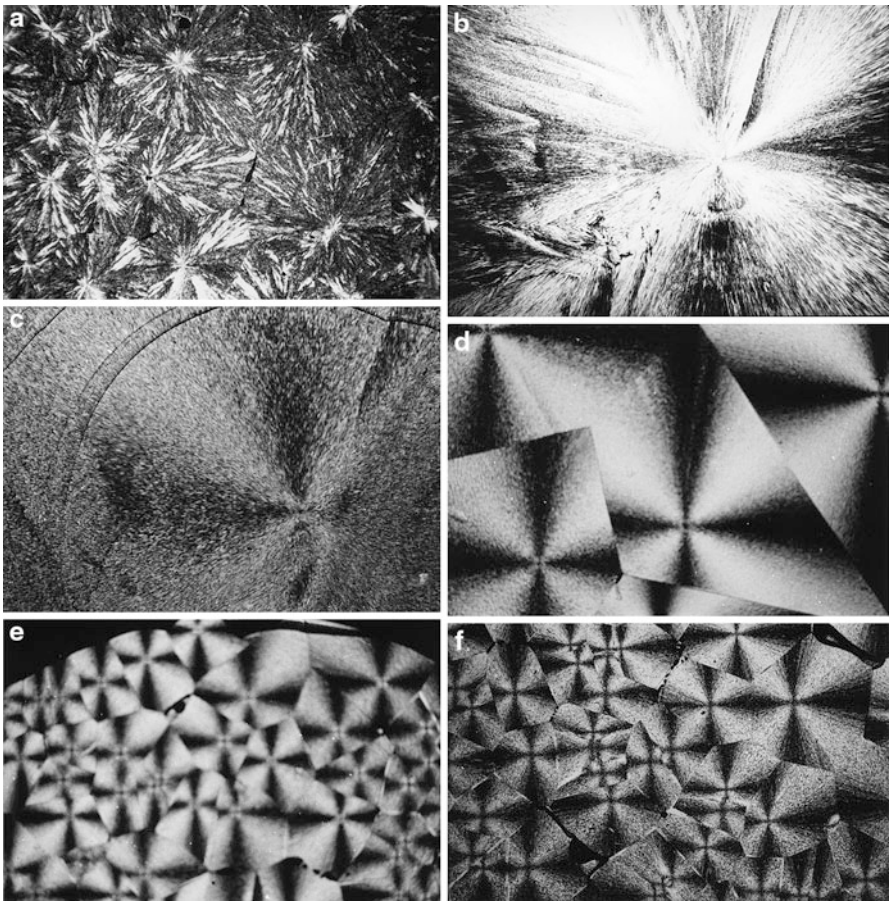

Fig. 3.4 Optical micrographs of PEO/Aramide 34I blends: (**a**) 100/0 $T_c = 47$ °C, magn. 5×; (**b**) 95/5 $T_c = 42$ °C, magn. 5×; (**c**) 90/10 $T_c = 44$ °C, magn. 10×; (**d**) 85/15 $T_c = 32$ °C, magn. 10×; (**e**) 80/20 $T_c = 28$ °C, magn. 10×; (**f**) 75/25 $T_c = 28$ °C, magn. 10× (Dreezen et al. 1999)

The *order-disorder interphase* was defined as the region of loss of crystalline order. Kumar and Yoon (1991) examined this interface and found that in blends the thickness of this transition zone was essentially independent of the interaction parameter between the two polymers (when χ_{12} varied from -1 to -0.005). Following the theoretical predictions, the thickness of this region increases only slightly when stiffer chains are considered. Due to the higher degree of order of segments of the crystallizable component in this zone, the penetration of the amorphous component is limited. The *compositional interphase*, however, is influenced by the stiffness of both chains and by the interaction parameter (the interfacial thickness varies with the reciprocal of $|\chi_{12}|^{1/2}$). This prediction seems to be confirmed by experiments. Blends of iPS and PS as well as HDPE/LDPE blends (at a temperature above the melting point for the latter blend) have a χ_{12} that is

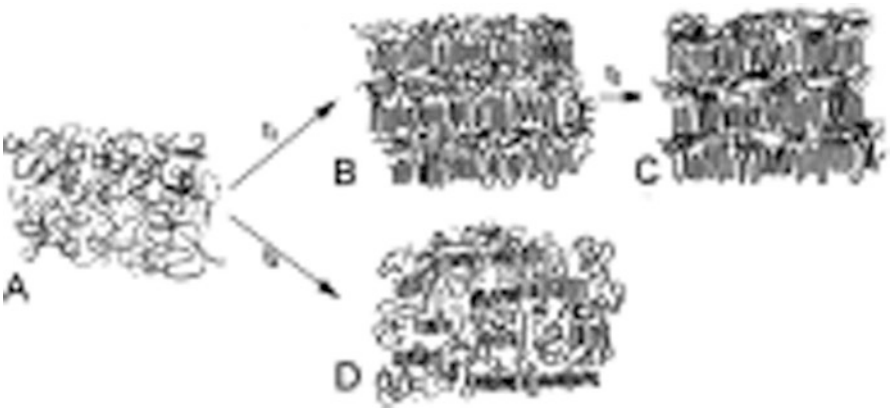

Fig. 3.5 Model describing the crystallization behavior of (**a**) 80/20 PEO/Aramide 34I blend; (**b**) after fast primary crystallization; (**c**) secondary crystallization; and (**d**) a 65/35 PEO/Aramide blend after crystallization (Dreezen et al. 1999)

nearly zero; as a consequence, they will not form a mixed phase in the interlamellar region – the amorphous polymer will be excluded from the interlamellar zone. This seems to be in agreement with the experimental observations for iPS/PS (Warner et al. 1977) and HDPE/LDPE (Song et al. 1988). The presence of a pure order-disorder interphase has been observed in PVDF/PMMA blends (Wenig et al. 1975) using small-angle X-ray scattering and dielectric relaxation experiments. Jonas et al. (1995) estimated the spatial extension of the order-disorder interphase of PEEK in its blends with PEI.

A check of the theoretical predictions of Kumar and Yoon can be made comparing several miscible crystallizable blends with components having a similar stiffness but exhibiting variable interactions (i.e., different values of χ_{12}). Such experimental work was done by Runt et al. (1991) who examined blends of crystallizable PEG with three different amorphous components (PMMA, PVAc and polyhydroxystyrene, PHS). The first two amorphous polymers (PMMA and PVAc) exhibited a small interaction with PEG, while PHS (being able to form hydrogen bonds with PEG) displayed large interactions. A pure PEG interphase was found for the PEG blends with PMMA and PVAc, whereas a relaxation suggestive for the presence of a mixed interphase for the PEG/PHS blend was observed. Barron et al. (1992) studied strongly interacting PCL blends with PC, PVC, Phenoxy, etc., by means of dielectric relaxation measurements. The blends exhibit a dielectric relaxation in between the relaxation of the pure components, indicating the presence of a mixed amorphous interphase. The possibility to observe this transitional behavior depended on the frequency used; a frequency of 10Hz was used in this case. Therefore, it was impossible to study these transitions by means of dynamic mechanical experiments (DMA, usually 1Hz is used) or differential scanning calorimetry (DSC). For the PCL/PVC blends (PVC segregates interlamellar (Russell and Stein 1983), three transitions were noticed: (1) a pure amorphous PCL region (γ-relaxation); (2) a mixed amorphous phase,

located at a higher temperature than the former and which shifts to higher temperatures with increasing PVC content; and (3) an interphase transition that shifts to higher temperatures the stronger the interaction between both polymers. A frequency lower than 10Hz results in an overlap of the transitions associated with the mixed and phase and with the interphase, while at higher frequencies, the γ-relaxation merges with the interphase transition.

Excellent work was reported by Balsamo et al. (2006) on the semicrystalline morphology of PCL/PSMA14 miscible blends as well as on their crystallization kinetics. The authors used a combination of dielectric, calorimetric, and microscopy characterization tools to investigate crystallization features of PCL in miscible PCL/PSMA14 blends over the whole composition range. The results achieved allowed to draw the following conclusions with respect to the miscibility effect on the blend relaxation dynamics and crystallization kinetics of PCL:

(a) Crystallization of PCL in the blend occurs when the PCL content reaches 30 wt% or more. A depression of the PCL melting point and a significant cold crystallization process are detected for the 40/60 blend, showing the intimate mixing of the components with the existence of interactions on a molecular level. This is supported by the interlamellar insertion of the PSMA14, the formation of ring-banded spherulites, and the significant increase in the half-crystallization times.
(b) The existence of a miscible interlamellar region leads to a spherulitic extinction ring spacing that becomes larger upon increasing crystallization temperature. Interestingly, it also increases with PSMA14 content. The latter differentiates the PSMA14/PCL system from other PCL blends.
(c) With respect to the chain dynamics, the thermally stimulated depolarization current (TSDC) results indicate that even the short-range reorientations of the PCL dipoles are affected by blending. The addition of the rigid PSMA14 to PCL causes the hindering of the pre-cooperative motions usually assigned to the β relaxation in the presence of PCL crystalline regions.

For example, Fig. 3.6 shows the spherulites formed after isothermal crystallization at the indicated temperatures. Indeed, in addition to the typical Maltese-cross, extinction rings appear, leading to ring-banded spherulites. This kind of superstructures has been observed, for example, in blends of PCL with SAN (Wang and Jiang 1997; Li et al. 1992; Wang et al. 1998) and PVC (Eastmond 2000) as well as in block copolymers (Balsamo et al. 1996; Albuerne et al. 2003; Nojima et al. 1991). Note that the spherulites fill all the space, indicating the absence of interspherulitic segregation. In all cases, a linear increase of the radii of the spherulites with time was found until their impingement, evidencing that the growth rate is not controlled by diffusion. These results are in agreement with the interlamellar location of the PSMA14 evidenced here with TEM and are the consequence of the low flexibility of the PSMA chains and its affinity toward the PCL.

It is well known that banding is the result of the cooperative twisting of the lamellae during growth. Although such twisting has been associated with internal stresses produced on the lamellae surfaces, the reason for its occurrence is still controversial (Lotz and Cheng 2005). It has also been reported in case of polymer

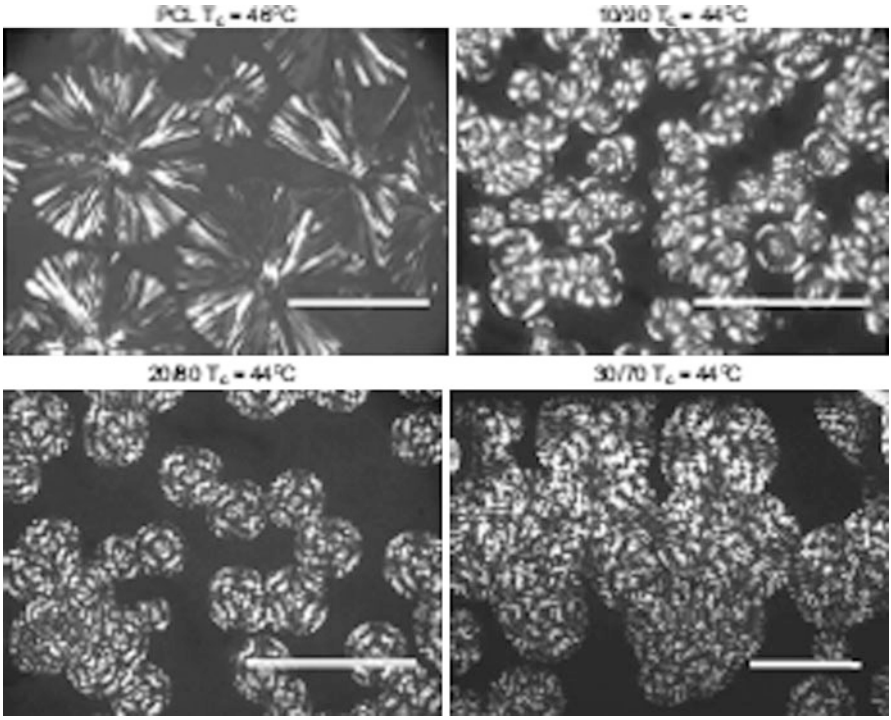

Fig. 3.6 POM images obtained during isothermal crystallization of PSMA14/PCL blends at the indicated crystallization temperatures. The *bars* represent 100 μm. Top left: PCL Tc = 46 °C, Top right: 10/90 Tc = 44 °C, Bottom left: 20/80 Tc = 44 °C, Bottom right: 30/70 Tc = 44 °C. (Balsamo et al. 2006 with Permission)

blends that the periodicity of the rings depends on composition (Morin et al. 2001). To characterize the superstructure, the periodicity of the rings was measured in PSMA14/PCL 20/80 and 30/70. The results presented in Fig. 3.7 reveal that the periodicity increases with the content of the amorphous component, a fact that is contrary to the results obtained by other authors in blends containing PCL (Nojima et al. 1991; Wang et al. 1996; Schulze et al. 1993). Nevertheless, Briber and Khoury (1987, 1993) reported a similar trend in poly(vinylene fluoride)/poly(ethyl acrylate) blends. This could be related to the dependence of the interaction parameter on composition. Additionally, the periodicity markedly increases with the crystallization temperature, due to the higher segmental mobility within the blend.

3.2.2.2 Modes of Crystallization in Crystalline/Crystalline Blends

When dealing with miscible blends containing two crystalline components, several modes of crystallization are possible: separate crystallization, concurrent crystallization, cocrystallization, etc. Only those blends in which both components are miscible in the melt are considered here (Table 3.3). PET/PBT blends were reported to be an example of separate crystallization (Escala and Stein 1979;

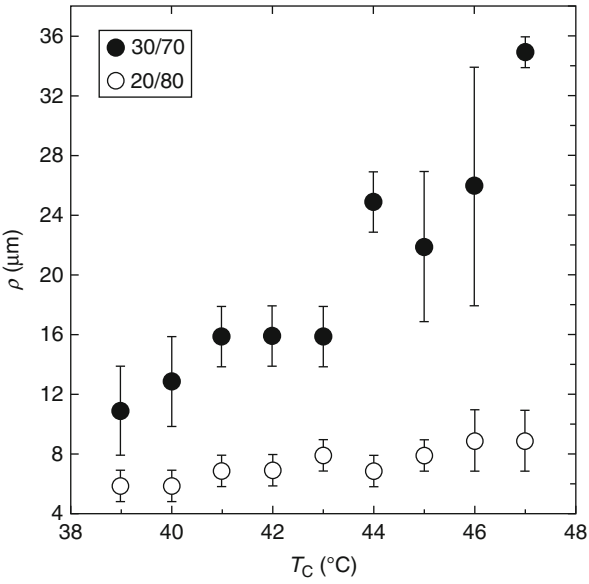

Fig. 3.7 Dependence of the ring periodicity measured from POM micrographs as a function of crystallization temperature for PSMA14/PCL 30/70 and 20/80 (Balsamo et al. 2006)

Stein et al. 1981). A spherulitic crystallization was observed for the neat components as well as for blends with small amounts of one component, and the crystals of the minor component were included within the spherulites of the major component, which results in a coarsening of the spherulitic texture. Transesterification is, however, the reason for the homogenous amorphous phase.

Run et al. (2009) have recently shown that in the miscible blends of PET and PTT, PET component will crystallize first, and the formed crystallites serve as the nucleating agent for PTT crystallization at higher temperatures. The content of each component in the blend affects the crystallization growth rate of the other blend partner. PTT constitutes a diluting agent for the PET crystallization process. The spherulite's size, however, is much smaller than that of those formed in pure PTT. A completely different situation was reported by Chen et al. (2009) when the crystallization of miscible PET/PLA blend was considered. Due to the phenomenon of rigid amorphous fraction (RAF) formed by one component, the crystallization of the other partner is perturbed or even altered. PET can crystallize in all blends, regardless of whether PLA is amorphous or crystalline, and the degree of crystallinity of PET decreased as the fraction of PLA was increased in the blend. Whereas, the PLA crystallization is strongly affected by the mobility of the PET fraction. In the presence of an amorphous PET, PLA can crystallize, albeit weakly, even in a 70PLA/30PET blend. But when the PET is crystalline, PLA cannot crystallize below a 0.9 fraction in the blend. This phenomenon has been attributed of the ability of PET and PLA to form rigid amorphous fractions (RAF) which, like crystals, may inhibit the growth of crystals of the other blend partner.

A simultaneous (or concurrent) crystallization can only occur when the crystallization temperature ranges overlap and if the crystallizability of both blend's

Table 3.3 Crystallization types of miscible polymer blends consisting of two crystallizable components

Polymer blend	Crystallization type[a]	References
LDPE/LLDPE	Concurrent crystallization	Hu et al. (1977)
	Separate crystallization	Kyu et al. (1987)
LDPE/VLDPE	Cocrystallization	Chen et al. (2001)
UHMWPE/HDPE	Concurrent crystallization	Kyu and Vadhar (1986)
UHMWPE/LLDPE	Concurrent crystallization	Kyu and Vadhar (1986)
	Cocrystallization/ separate[b]	Vadhar and Kyu (1987)
UHMWPE/LDPE	Separate crystallization	Kyu and Vadhar (1986, 1987)
LLDPE/LLDPE[c]	Cocrystallization	Rego Lopez and Gedde (1988)
LDPE/EPDM[d]	Cocrystallization	Starkweather, Jr. (1980)
HDPE/LLDPE[e]	Cocrystallization[f]	Hu et al. (1987), Edward (1986), Gupta et al. (1994)
LLDPE/VLDPE	Cocrystallization	Huang et al. (1990)
LDPE/VLDPE	Partial cocrystallization	Huang et al. (1990)
HDPE/VLDPE	Cocrystallization	Huang et al. (1990)
DHDPE[g]/LLDPE[h]	Cocrystallization[i]	Tashiro et al. (1992a, b; 1994a, b, c, d)
DHDPE/LLDPE[j]	Partial cocrystallization	Tashiro et al. (1994a, b, c, d)
DHDPE/HDPE	Partial cocrystallization[k]	Tashiro et al. (1994a, b, c, d)
PEEK/PEK	Cocryst./separate cryst.[l]	Sham et al. (1988)
PEEK/PEK	Cocrystallization	Harris and Robeson (1987)
PEEK/PEEEK	Cocrystallization	Harris and Robeson (1987)
PEEK/PEEKK	Cocrystallization	Harris and Robeson (1987)
PEEK/$P(E)_{0.43}(K)_{0.57}$[m]	Cocrystallization	Harris and Robeson (1987)
PEEK/PEK/PEI	Cocryst. of PEEK and PEK	Harris and Robeson (1988)
PVF/PVDF	Cocrystallization	Natta et al. (1965)
VDF-TFE/VDF-HFA	Cocrystallization[n]	Cho et al. (1993)
iPS/iP(p-Me-S)[o]	Cocrystallization	Natta et al. (1961)
P(iPr-vinylether)/P(sec-But-vinyl ether)	Cocrystallization	Wunderlich (1973)
P(4-Me-pentene)/P (4-Me-hexene)	Cocrystallization	Wunderlich (1973)
PBT/PEE[p]	Cocrystallization	Gallagher et al. (1993)
PET/PBT	Separate crystallization	Stein et al. (1978)

(*continued*)

Table 3.3 (continued)

Polymer blend	Crystallization type[a]	References
PET/PTT	Separate crystallization	Run et al. (2009)
iPMMA/sPMMA	Cocrystallization	Liquori et al. (1965)
PCL/PC	Separate crystallization	Vandermarliere (1986)
PCL/PBT	Separate crystallization	Righetti et al. (2007)
PPE/iPS	Separate crystallization	Hammel et al. (1975)
PED/EVAc[q]	Cocrystallization	Clough et al. (1994)
PET/PLA	Separate crystallization	Chen et al. (2009)

[a]It should be noted that not all authors use the same terminology concerning the type of crystallization. Especially the terms "cocrystallization" and "concurrent crystallization" are often confused. Since some authors did not examine whether the lattice parameters change or not, it is not possible to decide if they mean cocrystallization or concurrent crystallization
[b]Depending on the blend preparation: cocrystallization when sequentially mixed and separate crystallization when simultaneously mixed
[c]Different molecular weight fractions
[d]Ethylene/propylene/1,4-hexadiene with an ethylene/propylene ratio of 4.5 mol%
[e]LLDPE: ethylene butene-1 copolymer, 18 branches/1,000 C
[f]Valid as well for slowly as rapidly (quenched) cooled blends
[g]DHDPE: deuterated HDPE
[h]LLDPE with a branching content of ca. 17 ethyl groups/1,000 carbons
[i]The lattice parameters vary continuously with composition of the blend, and the cocrystallization process is ascribed to the closeness of the crystallization rate of both species
[j]LLDPE with a branching content of ca. 41 ethyl groups/1,000 carbons
[k]The tendency to cocrystallize increases with increasing HDPE concentration
[l]Cocrystallization occurs when the blends are quenched rapidly from the melt (±100 °C/min); separate crystallites are formed when isothermally crystallized, annealed at high temperatures, precipitated from solution, or slowly cooled from the melt (1 °C/min)
[m]$P(E)_{0.43}(K)_{0.57}$ is a random copolymer composed of phenyl ether and phenyl ketone units
[n]The type of crystallization depends on the thermal treatment of the samples: cocrystallization takes place in samples that are quenched or annealed at 110 °C for 6 h; separate crystallization is observed when annealed at 100 °C for 6 h. This is due to the existence of an UCST phase behavior between 100°C and 110 °C
[o]Copolymer of styrene and *p*-methyl styrene containing 30 mol% of the latter comonomer
[p]Miscibility of PBT/PEE depends on the copolymer composition of PEE, and cocrystallization occurs under all crystallization conditions and is possible because the unit cell parameters of PBT and PEE are the same. To avoid interchain chemical reactions, the blends were prepared by solvent casting
[q]EVAc has a molar ratio of ethylene to vinyl acetate of 7:1 and is amorphous, an increase of the lattice parameters was noticed when adding EVAc

components is similar. Cocrystallization is only possible when the components are isomorphic or miscible in the amorphous as well as in the crystalline phase. In both cases, mixed crystals can result, but in the case of concurrent crystallization, no changes in crystal structure may be induced. Cocrystallization requires chemical

compatibility, close matching of the chain conformations, lattice symmetry, and comparable lattice dimensions (Olabisi et al. 1979). Some examples of miscible polymer blends with two crystalline components are given in Table 3.3 together with the type of crystallization.

3.2.3 Spherulite Growth of the Crystallizable Component

3.2.3.1 Spherulite Growth Rate in Homopolymers

In the case of homopolymers, the growth rate of a lamellar crystal is controlled by two processes: on the one hand by the ability of forming a surface nucleus (determined by the degree of undercooling, $\Delta T = T_m^\circ - T_g$) and on the other hand by the ability of diffusion of the chain molecules toward the crystal growth front (determined by the difference between the crystallization temperature, T_c, and the glass-transition temperature, T_g). Both processes are inversely dependent on temperature; a maximum rate of crystal growth is usually observed at temperatures close to $T_{\max} \approx (T_g + T_m)/2$.

The growth rate kinetics of bulk semicrystalline homopolymers have been described in the past by Mandelkern et al. (1954) and Hoffman and Lauritzen (1976, 1973), using a modified version of the theory of nucleation of Turnbull and Fisher (1949):

$$G = G^\circ \exp[-\Delta E/R(T_c - T_o)]\exp[-\Delta F^*/k_B T] \tag{3.1}$$

G° is a constant dependent on the regime of crystallization, independent of temperature, and inversely proportional to the polymer molecular weight (Van Antwerpen and Van Krevelen 1972); T_o is the temperature at which motions necessary for the transport of molecules through the liquid-solid boundary cease; T_c is the temperature of crystallization; and k_B is the Boltzmann constant.

The rate of growth of a crystal, G, is governed by two processes: the activation energy required to transport crystalline molecules across the solid-liquid interface (ΔE) and the work necessary to form a critical nucleus (ΔF^*). At low supercooling, the growth rate is nucleation controlled, while at high supercooling, it is diffusion controlled; as a consequence, Eq. 3.1 produces a bell-shaped curve. Such a behavior for iPS (curve a) is shown in Fig. 3.8.

3.2.3.2 Spherulite Growth Rate in Miscible Polymer Blends

When dealing with crystallizable miscible polymer blends containing a noncrystallizable component, some refinements had to be made. Some modifications were proposed by Alfonso and Russell (1986) and by Cimmino et al. (1989) for blends in which the amorphous component is segregated into the interlamellar region (see also Sect. 3.2.2.1). First, the chemical potential of the liquid phase might be altered by the specific interactions that are often responsible for the miscibility of polymers (Olabisi et al. 1979). Such interactions may change the free energy required to form a critical nucleus as well as the mobility of both the crystalline and amorphous components. Second, the noncrystallizable component has to

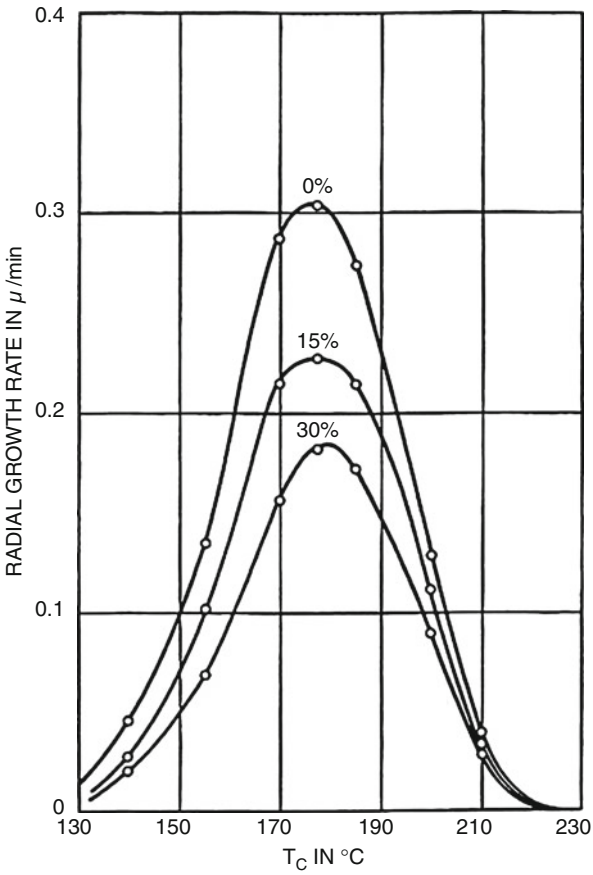

Fig. 3.8 Spherulitic growth rate in iPS and iPS/PS blends (the values represent the percentage of atactic PS present in the blend) (Keith and Padden 1964)

diffuse away from the crystal growth front into the interlamellar region. Thus, the rate at which the growth front progresses depends on the competition between the inherent capability of the crystal to grow and on the rate of rejection (segregation) of the amorphous component. The kinetics of crystal growth will ultimately be determined by the slower of these two phenomena. A direct consequence of this consideration is the dependence of the crystal growth rate on the molecular weight of both components. Third, the concentration of the crystallizable component at the growth front will decrease during crystallization. And finally, the glass-transition temperature and the melting temperature can be influenced by addition of an amorphous polymer. As already mentioned in Sect. 3.2.1, the T_g of miscible blend lies in between the glass-transition temperatures of the neat components, its value being a function of the blend's composition. Depending on the T_g value of the noncrystallizable component (higher or lower than the T_g of the crystallizable component), the crystallization temperature range will be, respectively, narrowed or widened.

Incorporating the concepts discussed above, the equation describing the crystal growth rate in a miscible polymer blend can be expressed as

$$G_m = (\phi_2 k_1 k_2)/(k_1 + k_2)\exp(-\Delta F_m{}^*/k_B T_c) \tag{3.2}$$

ϕ_2 is the volume fraction of the crystallizable component; T_c is the crystallization temperature; k_1 is the rate of transport of the crystallizable molecules across the liquid-solid boundary:

$$k_1 = G^\circ \exp[-\Delta E/R(T_c - T_o')] \tag{3.3}$$

T_o' is the value of T_o in the blend and can be written in terms of the glass transition and a constant C (associated with the WLF constant C_2) (Rostami 1990); and k_2 is the rate at which the amorphous component segregates

$$k_2 = D/d = 2\overline{D}/L \tag{3.4}$$

d is the maximum distance over which the amorphous component has to diffuse away during crystallization ($d = L/2$, with L the crystal lamellae thickness), and D is the diffusion coefficient. Since a simultaneous diffusion of the amorphous and the crystalline component takes place, the diffusion coefficient of interest is the mutual diffusion coefficient, $\overline{D}$; $\Delta F_m{}^*$ is the free energy of nucleus formation (secondary nucleation) in the presence of a noncrystallizable component.

The rate of crystal growth in a semicrystalline blend, G_m, will depend on the magnitude of k_1, k_2, and $\Delta F_m{}^*$. At low undercooling, $\Delta T = T_m{}^\circ - T_c$, $\Delta F_m{}^*$ is high and hence G_m is small. However, if the blend T_g approaches or exceeds the melting point ($T_m{}^\circ$), k_2 can prohibit crystallization regardless of the value of $\Delta F_m{}^*$.

Table 3.4 refers to a number of crystallizable miscible polymer blends for which the spherulite growth rate as a function of the crystallization temperature has been investigated. For most blends, only a part of the bell-shaped curve could be measured. In Fig. 3.8, the complete bell-shaped spherulitic growth rate curve of iPS in iPS/PS blends containing 0, 15, and 30 wt% PS is shown. Due to the addition of impurity (e.g., the amorphous PS), a suppression of the growth rate is observed, which is greater than the concentration of the impurity added. Important parameters of the impurity added to the crystallizable component are the type, concentration, and molecular weight (Keith and Padden 1964).

By means of several optical techniques, viz., small-angle laser light scattering (SALLS), optical microscopy, etc., the spherulite structure can be studied. From the photographic scattering pattern, the spherulitic radius, R, can be calculated as a function of the crystallization time and/or blend composition (Stein 1964):

$$R = 4.1\lambda/4\pi\{1/\sin(0.5\ \theta_m)\} \tag{3.5}$$

θ_m represents the azimuthal angle of the intensity maximum; R the spherulite radius; and λ the light wavelength in the medium.

A general observation is a decrease of the spherulitic radius with increasing content of the amorphous polymer when a same crystallization time is used (see Fig. 3.9 and Table 3.5: PCL/PVC).

Table 3.4 Spherulitic growth rate measurements in miscible polymer blends (G vs. T_c)

Polymer blend	Amorphous comp. (wt%)	Temperature range studied (T_c, °C)	Bell-shaped curve	References
iPS/PS	0–30% PS	130–230	Complete	Keith and Padden (1964)
PEG/PMMA	0–30% PMMA	40–55	Part	Cimmino et al. (1989)
PEG/PMMA[a]	0–30% PMMA	10–60	Part	Alfonso and Russell (1986)
PEG/PMMA[b]	0–40% PMMA	35–55	Part	Martuscelli (1984)
PEG/PMMA	0–40% PMMA	44–58	Part	Calahorra et al. (1982)
PEG/PVAc	0–40% PVAc	45–55	Part	Martuscelli (1984)
PEO/PES	0–50 % PES	17–55	Part	Dreezen et al. (1999)
PEO/Aramid	0–50 % Aramid	25–45	Part	Dreezen et al. (1999)
PVDF/PMMA	0–50% PMMA	110–160	Part	Wang and Nishi (1977)
	30% PMMA	148–162	Complete[c]	Okabe et al. (2010)
PCL/PVC	25–50% PVC	20–35	Part	Ong and Price (1978)
	0–10% PVC	30–41	Part	Nojima et al. (1986)

[a]Several PMMA polymers with different molecular weights were used
[b]Several PEG polymers with different molecular weights were used
[c]A temperature of 162 °C has been used and allowed a spherulite growth rate of bell-shaped curve

3.2.3.3 Determination of the Lateral and Fold Surface Free Energies from the Growth Rate

Alfonso and Russell (1986) related the different terms in Eq. 3.2 to the measurable or characteristic properties of the blend, which resulted in the following relation for blends in which the amorphous component segregated into the interlamellar regions:

$$G_m = \left\{\phi_2 G^{\circ} \exp[-\Delta E/R(T_c - T_o')]2\overline{D}/L\right\}/\left\{G^{\circ} \exp[-\Delta E/R(T_c - T_o')] + 2\overline{D}/L\right\} \exp\left\{(-2b\sigma\sigma_e)/\left(k_B T \Delta h_u f\left[1 - T_c/T_m^{\circ} - RTV_{2u}\chi(1-\phi_2)^2/\Delta h_u f\, V_{1u}\right]\right)\right\} \tag{3.6}$$

where b is the thickness of a monomolecular layer; $\sigma\sigma_e$ is the product of the lateral and fold surface free energies; V_{iu} is the molar volume of component i; χ is the Huggins-Flory interaction parameter; and Δh_u is the heat of fusion per mole of monomer of the crystallizable component, the temperature dependence of which is taken into account by the parameter f:

$$f = \left[2T_c/\left(T_c + T_m^{\circ}\right)\right] \tag{3.7}$$

Both $\sigma\sigma_e$ and χ are assumed to be independent of temperature and composition.

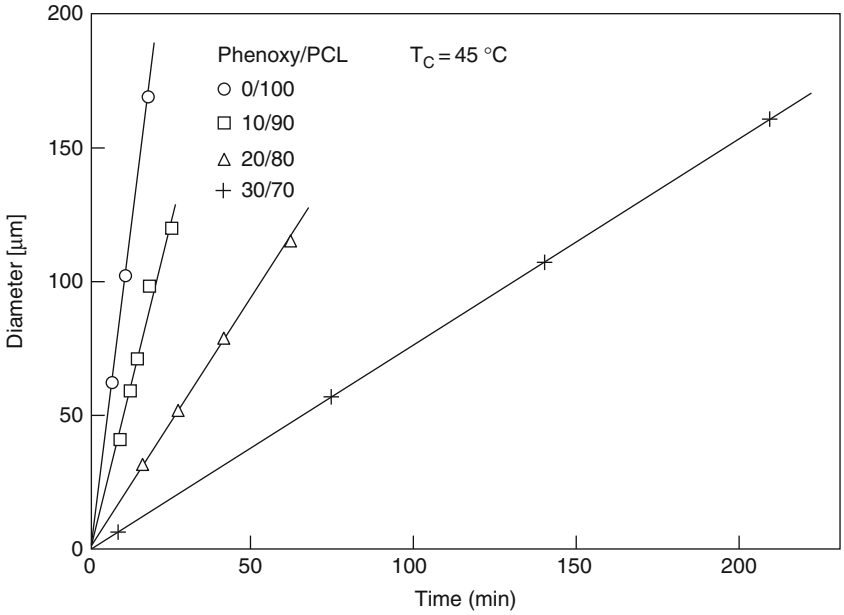

Fig. 3.9 Spherulite growth of PCL/Phenoxy blends at $T_c = 45$ °C (Defieuw et al. 1989d)

In Eq. 3.6 the ratio $\overline{D}/G$, a modified version of the δ-parameter (Keith and Padden, 1963, 1964), appears. This length, relative to the thickness of the crystalline lamellae (L), is critical for the consideration of the crystal growth in crystallizable miscible polymer blends.

Equation 3.6 can be written as

$$\alpha = -\sigma\sigma_{ei}\beta \tag{3.8}$$

where

$$\begin{aligned}\alpha = \ln G_m - \ln\phi_2 - \ln G^{\circ} + \Delta E/R(T_c - T_o') \\ + \ln\left\{1 + \left[G^{\circ} L \exp[-\Delta E/R(T_c - T_o')]/2\overline{D}\right]\right\}\end{aligned} \tag{3.9}$$

and

$$\alpha = \ln G^{\circ} - \left(K_g/T_c\Delta T f\right) \tag{3.10}$$

with

$$K_g = \left(n\, b\sigma\sigma_e T_m^{\circ}\right)/(\Delta h_u k_B) \tag{3.11}$$

Table 3.5 Maximum spherulite radius, R, as a function of crystallization time (t_c) and blend composition

Polymer blend	Composition (wt%)	T_c (°C)	R_{max} measured (μm)[a]	t_c (min) required to obtain R_{max}[a]	References
PCL/PVC	100/0	30	21[b]	[c]	Khambatta et al. (1976a, b)
	90/10	30	36[b]	[c]	
	80/20	30	31[b]	[c]	
	70/30	30	26[b]	[c]	
	60/40	30	19[b]	[c]	
	50/50	30	10[b]	[c]	
	75/25	20	33	7	Ong and Price (1978b)
		25	32	9	
		30	60	20	
		35	63	33	
	90/10	33.2	136	8	Nojima et al. (1986)
		35.1	157	12	
		37.8	150	19	
		39.2	122	31	
PCL/CPE 42.1[d]	100/0	45	70	3	Defieuw et al. (1989a)
	90/10	45	150	25	
	80/20	45	119	43	
PCL/Phenoxy	100/0	45	168	19	Defieuw et al. (1989b)
	90/10	45	119	25	
	80/20	45	114	61	
	70/30	45	160	209	
PCL/SMA 14[e]	100/0	45	165	16	Defieuw et al. (1989b)
	90/10	45	169	77	
	80/20	45	111	187	
PEG/iPS	100/0	Ns	Ns		Wenig et al. (1975)
	90/10				
	70/30				

[a]Extrapolated values from figures
[b]A mean value is given, obtained by various optical techniques
[c]The crystallization was allowed to proceed for more than five halftimes of crystallization for each composition
[d]CPE with 42.1 wt% chlorine; PCL/CPE 42.1 shows an LCST behavior (LCST = 147 °C); the experiments were performed on specimens prepared below the LCST
[e]SMA with 14 wt% MA

where n is 2 or 4 depending on the regime of crystallization (Hoffman 1982; Ong and Price 1978b; Runt and Martynowicz 1986). The value of $n = 2$ refers to intermediate growth behavior (regime II), while the value of $n = 4$ corresponds with regime I and III in which low and high undercooling, respectively, is taking place. Furthermore, based on the WLF relation (Williams et al. 1955), the growth rate can be written as (Ong and Price 1978b)

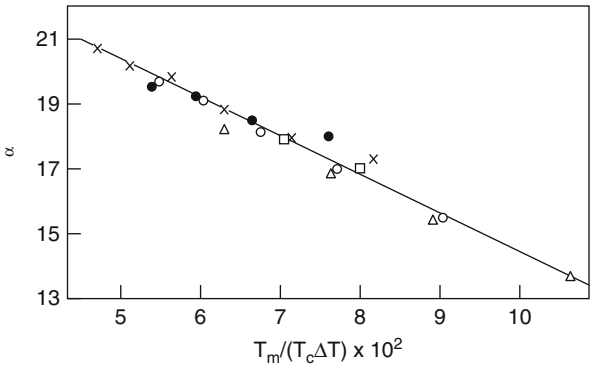

Fig. 3.10 Plot of α versus $T_m/(T_c\Delta T)$ for various compositions of a PEG/PMMA blend (*triangles*, 100/0; *circles*, 90/10; *squares*, 80/20; *crosses*, 70/30; *filled circles*, 60/40) (Calahorra et al. 1982)

$$\alpha = \ln G^{\circ} - C_3\left\{T_m{}^{\circ}/T_c\left(T_m{}^{\circ} - T_c\right)\right\} \tag{3.12}$$

where

$$C_3 = (4b\sigma\sigma_e)/(k_B\,\Delta h_u) \tag{3.13}$$

Note that $K = C_3\,T_m$ when $n = 4$ (regime I or III) and

$$\beta = (2b/k_B T_c)\left\{\left(\Delta h_u f \Delta T/Tm^{\circ}\right) - \left[RTV_{2u}\chi(1-\phi_2)^2\right]/V_{1u}\right\}^{-1} \tag{3.14}$$

α contains parameters associated with the kinetic processes, while thermodynamic variables are met in β. If the product $\sigma\sigma_e$ is independent of the blend composition and temperature, then, according to Eq. 3.8, a curve of α versus β should produce a straight line, regardless of the concentration and molecular weight of the amorphous component. The slope of such a plot is a measure of the product $\sigma\sigma_e$.

Another way to rewrite Eq. 3.6 is (Cimmino et al. 1989)

$$\alpha = \ln G_m - \ln\phi_2 + C_1/[R(C_2 + T_c - T_o] - \left[\left(0.2T_m{}^{\circ}\ln\phi_2\right)/\left(T_m{}^{\circ} - T_c\right)\right] \tag{3.15}$$

Although equilibrium melting points, $T_m{}^{\circ} = T_c$, should be used in Eq. 3.13, generally the experimental T_m values are used.

Considering the Eqs. 3.11 and 3.13, a plot of α versus $1/(T_c\Delta Tf)$ and $T_m{}^{\circ}/(T_c\Delta T)$, respectively, should result in a straight line from which $\sigma\sigma_e$ can be obtained – see Fig. 3.10 where a plot of α as a function of $T_m{}^{\circ}/(T_c\Delta T)$ is shown.

The straight line in Fig. 3.10 represents a fit of Eq. 3.13 to the experimental values using the WLF constants, $C_1 = 17{,}250$ cal/mol and $C_2 = 72$ K (see Eq. 3.15), the latter value being higher than the true WLF value of 51.6. Other authors,

however, also had to use higher C_2 values to fit their growth rate data (Hoffman and Weeks 1962a; Magill 1964; Boon et al. 1968). The good fit in Fig. 3.10 indicates that the temperature dependence of the spherulite growth rate of a crystallizable component in miscible blends is quite similar to that of homopolymers. It is also obvious from this figure that σ_e is independent of the concentration of the amorphous component (PMMA). Caution should be taken to generalize these data since (1) the high concentration diluent was not investigated and (2) the temperature range was near the melting point. The same observations were, however, made by Ong and Price (1978b) and by Wang and Nishi (1977).

3.2.3.4 Influence of the Molecular Weight of the Amorphous Component

Alfonso and Russell (1986) found a significant curvature in the α versus β plots of PEG/PMMA blends (see Eq. 3.8) while they were linear for neat PEG. The curvature could be due to an increase of $\sigma\sigma_e$ with a decreasing temperature. These authors also studied the influence of the molecular weight of the amorphous component (PMMA) on the spherulite growth rate of PEG. Noteworthy is the discrepancy seen at low undercooling for one of the blends containing PMMA with a molecular weight corresponding to the critical molecular weight for entanglement. Superposing all data for different molecular weights (above the critical value) results in a true master curve (see Fig. 3.11), which shows that Eq. 3.8 accounts quite well for the effect of molecular weight.

3.2.3.5 Influence of the Molecular Weight of the Crystallizable Component

Martuscelli (1984) studied the influence of the molecular weight of the crystallizable component (PEG) on the spherulite growth rate of PEG/PMMA blend. In contrary to Calahorra et al. (1982), they found that the fold surface free energy, σ_e, decreases with increasing PMMA content in the blend. It should be mentioned, however, that the molecular weight of PEG used by Calahorra is much higher ($M_w = 400$ kg/mol) compared to the PEG used by Martuscelli (2 and 10 kg/mol). The value of σ_e was seen to depend on the molecular weight of PEG (Martuscelli 1984), being smaller in the case of blends containing PEG with lower molecular weight (see Fig. 3.12).

Several authors (Ong and Price 1978b; Alfonso and Russell 1986; Runt and Martynowicz 1986; Cimmino et al. 1989) used one of the equations mentioned above to calculate G°, σ, σ_o, and/or $\sigma\sigma_o$ (see Table 3.6). The following empirical relationship (Thomas and Staveley 1952; Geil 1963; Vidotto et al. 1969) was developed:

$$\sigma = 0.1\, b\, \Delta h_u \tag{3.16}$$

3.2.3.6 Influence of Copolymer Composition

The influence of the SAN copolymer composition on the spherulitic growth rate of PCL has been studied at a fixed crystallization temperature by

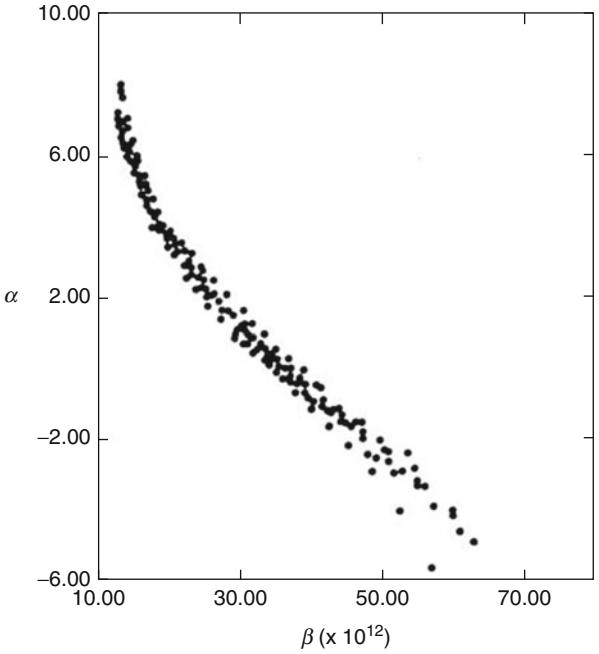

Fig. 3.11 Master curve of α versus β for blends of PEG (145) with PMMA (125) and PMMA (525) (values between brackets refer to the molecular weight of the components in kg/mol) (Alfonso and Russell 1986)

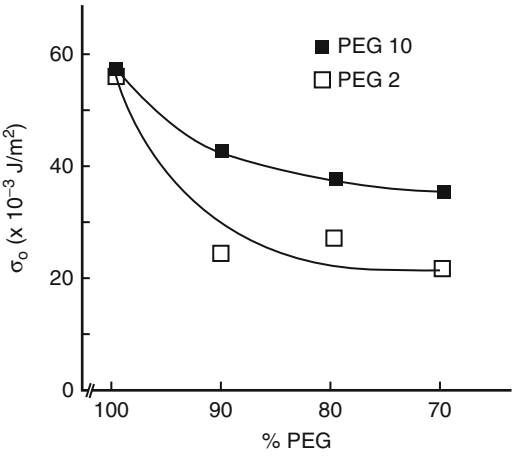

Fig. 3.12 Surface free energy of folding, σ_o, as a function of the PMMA content for PEG/PMMA blends using two PEG polymers differing in molecular weight (2 and 10 kg/mol) (Martuscelli 1984)

Kressler et al. (1992, 1993). A minimum has been observed at about 20 wt% AN in SAN for several compositions (see Fig. 3.13), due to a minimum in the value of the interaction parameter, χ, at the same copolymer composition that is responsible for a reduced chain mobility.

Table 3.6 Pre-exponential factor (G°), lateral (σ), and fold surface (σ_e) free energy and/or their product ($\sigma\sigma_e$) as calculated from Eqs. 3.8, 3.11, or 3.13

Polymer blend	Composition	G° ($\times 10^{-3}$ m/s)	$\sigma\sigma_e$ ($\times 10^6$ J^2/m^4)	σ_e ($\times 10^3$ J/m^2)	σ ($\times 10^3$ J/m^2)	References
PEG/PMMA	100/0[a]					Alfonso and Russell (1986)
	13,000	3.6	363			
	145,000	2.2	496			
	594,000	8.0	627			
	990,000	48.3	724			
PEG/PMMA	0–40% PMMA	4.1	186	18.8	9.9[b]	Calahorra et al. (1982)
PEG/PMMA	100/0			58/60/57[c]		Martuscelli et al. (1984)
	90/10			43/48/26[c]		
	80/20			38/39/27[c]		
	70/30			36/39/22[c]		
	60/40			36/37/—[c]		
PEG/PEMA	100/0			58	[d]	Cimmino et al. (1989)
	90/10			28	[d]	
	80/20			24	[d]	
	70/30			14	[d]	
PCL/PVC	25–50 wt% PVC[e]	0.72	175	27	6.5[f]	Ong and Price (1978b)
PCL/SAN19.5[g]	90/10		567			Kressler et al. (1993)
	80/20		507			
	70/30		518			
	60/40		491			

(*continued*)

Table 3.6 (continued)

Polymer blend	Composition	G° ($\times 10^{-3}$ m/s)	$\sigma\sigma_e$ ($\times 10^6$ J^2/m^4)	σ_e ($\times 10^3$ J/m^2)	σ ($\times 10^3$ J/m^2)	References
PVDF/PMMA[h]	100/0	0.182	464	47	9.76[h]	Wang and Nishi (1977)
	75/25	0.131	495	51	9.76[h]	
	50/50	0.012	396	40	9.76[h]	

[a]Several molecular weight PEG polymers were used
[b]Other compositions have been studied too
[c]This parameter has been calculated using a modified version of Eq 3.16: $\sigma = 0.1\ (\Delta h_u)\ (a_o b_o)^{0.5}$, where $a_o = 5.43$ A, $b_o = 4.45$ A, and $\Delta h_u = 1.986 \times 10^6$ J/m^3
[d]σ was calculated by Eq. 3.16, using $b = 4.65$ A (Vidotto et al. 1969)
[f]σ was calculated by Eq. 3.16, using $b = 4.38$ A and $\Delta h_u = 1.48 \times 10^{+8}$ J/m^3
[g]Since all compositions could be superposed on one straight line in the α versus $T_m/T\Delta T$ plot, all blend compositions have the same value for G°, σ, σ_e, and $\sigma\sigma_e$
[h]SAN with 19.5% AN; other copolymers have been used by the author leading to the same tendencies
[i]The first value is calculated from the spherulitic growth rate data of PEG(10)/PMMA, the second one from the overall crystallization data of PEG(10)/PMMA, and the third one from the spherulitic growth rate data of PEG(2)/PMMA (Martuscelli and Demma 1980) (the value between brackets refers to the molecular weight of PEG in kg/mol)
[j]This parameter has been calculated using Eq. 3.16 where $b_o = 4.65$A and $\Delta h_u = 2.13 \times 10^6$ J/m^3 (Van Krevelen 1976)

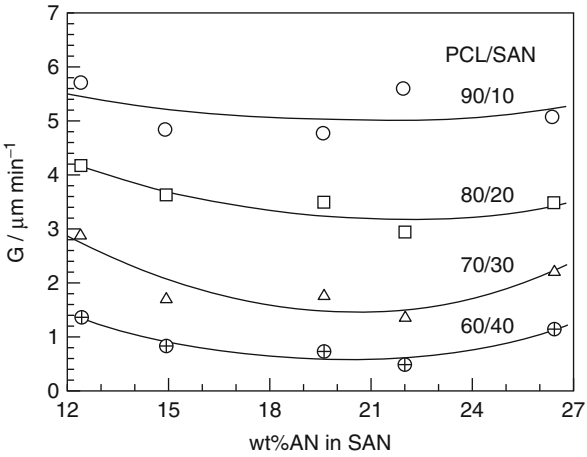

Fig. 3.13 Dependence of the spherulite growth rate G on the copolymer composition of SAN in PCL/SAN blends at 45 °C (Kressler et al. 1992, 1993)

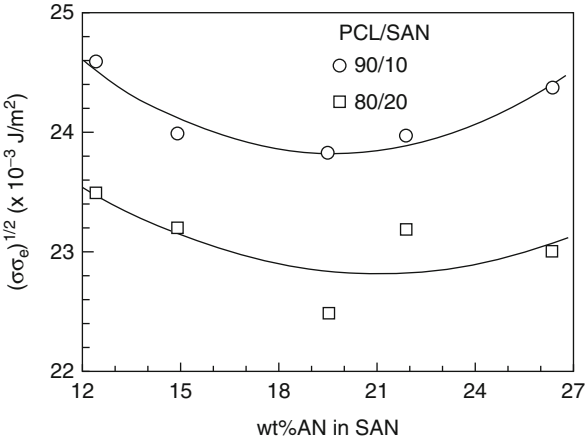

Fig. 3.14 Values of $(\sigma\sigma_e)^{1/2}$ versus the copolymer composition of SAN in PCL/SAN blends (Kressler et al. 1992, 1993)

The same authors also investigated the influence of the copolymer composition of SAN in PCL/SAN blends on G° and $(\sigma\sigma_e)^{1/2}$. The plot of $(\sigma\sigma_e)^{1/2}$ versus the acrylonitrile content in SAN shows a minimum (Fig. 3.14), suggesting that the addition of SAN results in a stabilization of the growing PCL crystallites. This effect was more pronounced when the interactions between SAN and PCL, indicated by χ, are more favorable. Since G° is proportional to $|\chi - \chi_s|$ (Saito et al. 1991), with χ_s the interaction parameter at the spinodal, a minimum was also noticed in the G° versus the copolymer composition of SAN (see Figs. 3.14 and 3.15).

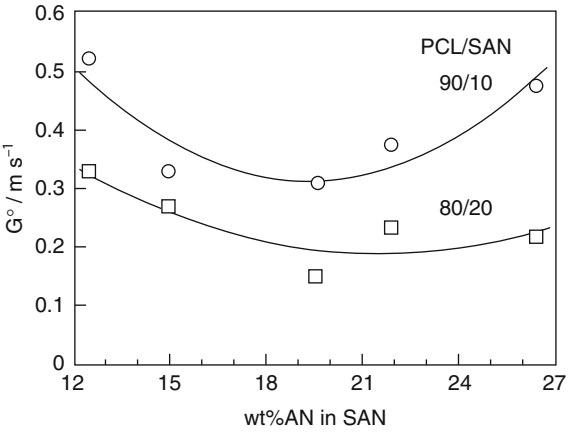

Fig. 3.15 The pre-exponential factor G° SAN in PCL/SAN blends (Kressler et al. 1992, 1993)

3.2.3.7 Other Aspects Related to Crystallization in Miscible Blends

(a) Chen et al. (2001) are among the few authors who considered the study of the effect of chain branching on the crystallization behavior of polyethylenes blends. Simple DSC techniques were used to differentiate, in terms of crystallization and melting, between blends of LDPE and VLDPE containing short branches. A stepwise isothermal crystallization was applied to thermally fractionate species based on their branching densities. The fractionated curves were used to determine the short-chain branching distribution, crystallization, and miscibility of the blends. When the two blend partners have similar unbranched segments, they may cocrystallize provided miscibility exists in the melt. Cocrystallization was found in all series of blends investigated but to varying extent depending on the branches densities of each blend couple.

(b) Svoboda et al. (2008) by choosing PCL/SAN containing 27.5 wt% AN could elucidate an interesting phenomenon of the competition between the phase dissolution and the crystallization of PCL in the blend. The authors qualified the crystallization as the liquid-solid phase transition and the phase dissolution as the liquid-liquid phase transition. A blend of 80/20 PCL/SAN phase separates via spinodal decomposition (SD) above the LCST, yielding a regularly phase-separated SD structure. By quenching a sample at temperatures below the Tm of the crystallizable PCL component, it was possible to have both crystallization and phase separation. TEM observations revealed that during isothermal annealing (after quenching to temperature as 51 °C close to T_m of PCL), the SD structure disappeared, and then the crystallization started from a single-phase mixture to yield normal crystalline structure similar to a neat PCL phase. At lower temperatures (e.g., 40 °C), crystallization set in quickly, and the SD was preserved implying the crystallization prevailed over the dissolution process, resulting in a bi-continuous structure consisting of amorphous (SAN-rich) and crystalline (PCL-rich) regions. At intermediate temperatures (e.g., 45 °C), the phase dissolution competed with the crystallization,

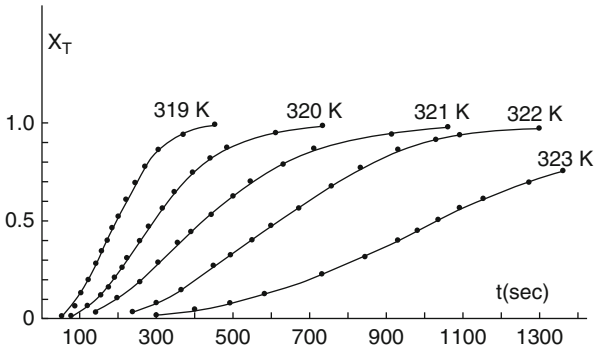

Fig. 5.16 Crystallization isotherms for the PEG/PEMA 80/20 blend crystallized at different T_c (Cimmino et al. 1989)

resulting in a bi-continuous structure with longer periodic distance and a broad boundary having a gradient in composition of amorphous region between PCL lamellae crystals.

3.2.4 Overall Crystallization Kinetics

3.2.4.1 General Aspects of the Avrami Theory Under Isothermal Conditions

The overall crystallization kinetics of blends can often be described by the Avrami equation (Avrami 1939):

$$\alpha = 1 - \exp\{-kt^n\} \tag{3.17}$$

α is the weight fraction of crystallinity at time t, n is the Avrami index depending on the type of nucleation and the crystal growth geometry, and k is the Avrami constant related to the crystallization rate:

$$k = \ln\left(2/t^n{}_{1/2}\right) \tag{3.18}$$

where $t^n{}_{1/2}$ is the halftime of crystallization (the time for half the crystallinity to develop), which is often used as a measure for the overall rate of crystallization. The theory was applied to polymer systems, e.g., by Morgan (1954) and Mandelkern et al. (1954).

In Fig. 3.16 typical crystallization isotherms were obtained by plotting α versus the crystallization time for the PEG/PEMA 80/20 blend at different crystallization temperatures. From such curves, the halftime of crystallization, $t^n{}_{1/2}$, can be deduced.

Equation 3.17 can be rewritten as

$$\log\{-\ln(1-\alpha)\} = \log k + n\log t \tag{3.19}$$

Plotting the left part of this equation against log t should result in a straight line, from which both Avrami parameters, n (slope) and k (intercept), can be obtained.

In Table 3.7 some literature data on the Avrami constants and the halftime of crystallization are presented. The Avrami n index (smaller than three for all the crystallization temperatures studied) of PCL/PBT system as investigated recently by Righetti et al. (2007) suggests a not fully three-dimensional crystalline growth. For the calculation of the crystallization growth rate, the authors plotted the reciprocal of the crystallization time needed to reach 20 % (and not half) of the crystallinity as a function of undercooling. As illustrated in Fig. 3.17, the dependence of the crystallization rate on the PCL molecular weight for both miscible and phase-separated PBT/PCL 80/20 blends, at the undercoolings accessible to DSC, parallels perfectly the trends exhibited by the linear growth rate curves that refer to lower undercoolings. Indeed and in contrast to many miscible systems, the low molecular weight PCL induces an increase in the crystallization rate of the PBT because of the higher molecular mobility the PCL oligomer causes as a plasticizer.

Cimmino et al. (1989) calculated the halftime of crystallization ($t_{1/2}$) for some PEG blends, PEG/PEMA, PEG/PVAc, and PEG/PMMA, using the same blend composition and the crystallization temperature. Blends of PEG with PVAc had the smallest $t_{1/2}$, while the PEG/PEMA blends showed the highest values for the halftime of crystallization. The type of amorphous component added to PEG seems to be important. The differences observed in $t_{1/2}$ (and also in the values of G) depend on:

- The degree of miscibility and mobility of the crystallizable and amorphous components
- The influence of the amorphous component on the nucleation of PEG
- Influence of the noncrystallizable component on the secondary nucleation or the crystallization regime (neat PEG and PEG/PEMA crystallize in regime I, whereas PEG/PVAc and PEG/PMMA crystallize in regime II)

Adding PMMA to PEG results in a decrease of $k = \ln 2/t^n{}_{1/2}$ (see Eq. 3.18), an effect that is clearly seen in Fig. 3.18 where $1/t_{1/2}$ is plotted against crystallization temperature (Martuscelli et al. 1984).

3.2.4.2 Modified Avrami Expression

It was often found that, contrary to the theoretical prediction, the value of n is noninteger (Avrami 1939). The Avrami model is based on several assumptions, such as constancy in shape of the growing crystal, constant rate of radial growth, lack of induction time, uniqueness of the nucleation mode, complete crystallinity of the sample, random distribution of nuclei, constant value of radial density, primary nucleation process (no secondary nucleation), and absence of overlap between the growing crystallization fronts. These assumptions are often not met in polymer (blend) crystallization. Also, erroneous determination of the "zero" time and an overestimation of the enthalpy of fusion of the polymer at a given time can lead to noninteger values for n (Grenier and Prud'homme 1980).

Pérez-Cardenas et al. (1991) developed a modified Avrami expression, taking into account the secondary crystallization effects. The weight fraction of crystallinity, α, can be written as the sum of two terms:

Table 3.7 Overall kinetic rate constant, k; Avrami index, n; and halftime of crystallization, $t^n_{1/2}$; as function of the crystallization temperature and blend composition for some crystallizable miscible blends

Polymer blend	Composition	T_c (°C)	k (s^{-n})	n	$t^n_{1/2}$ (min)	Reference
PCL/PVC	70/30	5	4.36×10^{-2}	2.86	3.6	Ong and Price (1978b)
		15	1.41×10^{-2}	2.60	6.2	
		25	1.95×10^{-3}	2.55	20	
	65/35	5	1.99×10^{-3}	2.82	10	
		15	7.60×10^{-4}	2.70	15	
		25	9.57×10^{-5}	2.93	37	
	60/40	5	4.57×10^{-6}	3.23	46	
		15	8.50×10^{-6}	3.14	35	
		25	2.62×10^{-6}	3.26	58	
	50/50	5	2.45×10^{-9}	3.16	630	
		15	3.98×10^{-9}	3.22	480	
		25	3.16×10^{-9}	3.08	595	
PCL/PVC[a]	100/0	29.6	19.95×10^{-3}	3.5	45[b]	Nojima et al. (1986)
		38.0	3.88×10^{-3}	2.2	217[b]	
		42.1	1.01×10^{-3}	2.4	848[b]	
	90/10	28.4	13.80×10^{-3}	2.1	61[b]	
		38.4	2.16×10^{-3}	1.7	374[b]	
		40.4	0.87×10^{-3}	1.9	949[b]	

(*continued*)

Table 3.7 (continued)

Polymer blend	Composition	T_c (°C)	k (s^{-n})	n	$t^n_{1/2}$ (min)	Reference
PEG/PMMA[a]	100/0	47	1.09[c]	2.53	0.8	Martuscelli et al. (1984)
		51	5.18×10^{-3}[c]	2.78	5.8	
		54	3.52×10^{-5}[c]	2.63	42.9	
	90/10	46	2.84×10^{-1}[c]	2.52	1.4	
		50	7.53×10^{-3}[c]	2.67	5.4	
		53	8.46×10^{-5}[c]	2.57	33.3	
	80/20	42	3.57×10^{-2}[c]	2.45	3.4	
		47	4.94×10^{-4}[c]	2.46	19.0	
		50	5.40×10^{-5}[c]	2.50	39.1	
	70/30	39	9.26×10^{-3}[c]	2.56	5.7	
		44	2.90×10^{-4}[c]	2.82	16.8	
		49	6.05×10^{-6}[c]	2.72	72.4	
PEG/PEMA[a]	100/0	47	4.171×10^{-4}	2.1	0.5	Cimmino et al. (1989)
		50	6.144×10^{-5}	2.0	1.2	
		53	2.840×10^{-6}	2.4	4.7	
	90/10	47	2.068×10^{-6}	2.5	4.2	
		49	4.614×10^{-7}	2.1	8.1	
		51	3.306×10^{-8}	2.3	30.5	
	80/20	47	5.082×10^{-7}	2.4	4.7	
		49	7.686×10^{-8}	2.8	10.1	
		51	4.823×10^{-9}	2.3	30.5	
	70/30	43	2.497×10^{-7}	2.8		
		45	5.829×10^{-8}	2.1		
		47	1.315×10^{-8}	2.4		

PBT/PCL MW = 1250; Miscible blend	80/20	$T_m^\circ - T_c = 47.4$	n.a	2.4	n.a.	Righetti et al. (2007)
		45.4	–	2.5	–	
		43.4	–	2.4	–	
		41.4	–	2.2	–	
		39.4	–	2.3	–	
		37.4	–	2.5	–	
		35.4	–	2.8	–	
		33.4	–	2.8	–	
		31.4	–	2.7	–	

[a]The authors investigated a wide range of crystallization temperatures, from which only a few are presented here
[b]The halftime of crystallization is expressed in seconds (!)
[c]The overall kinetic rate constant is expressed in min^{-n} (!)

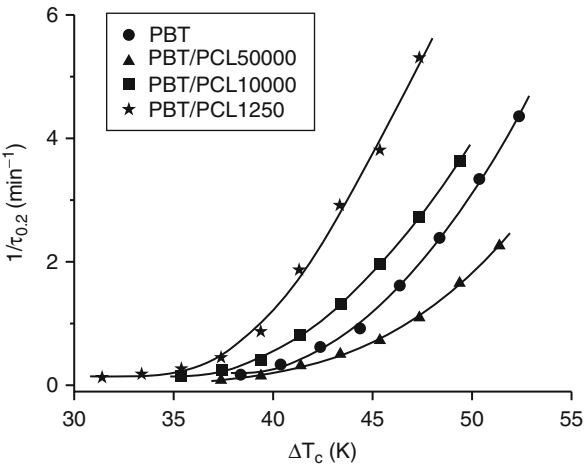

Fig. 3.17 Reciprocal of the time needed to reach 20 % of the final crystallinity (1/τ0.2) for PBT and PBT/PCL blends, plotted as a function of the undercooling. The *lines* are a guide for eyes (Righetti et al. 2007)

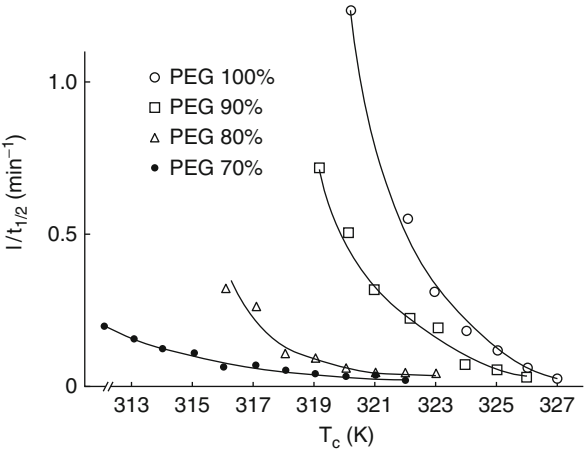

Fig. 3.18 Reciprocal of the halftime of crystallization, $t_{1/2}$, versus T_c for neat PEG (10) and PEG (10) blends with PMMA (the value between brackets refers to the molecular weight of PEG in kg/mol) (Martuscelli 1984)

$$\alpha = \alpha_p + \alpha_s \tag{3.20}$$

where the subscripts "p" and "s" refer to primary and secondary crystallization, respectively.

The crystallization process is divided in three regions (Fig. 3.19): (I) the initial primary crystallization region, (II) a region in which both primary and secondary crystallization takes place, and finally (III) a region in which only secondary crystallization occurs.

A parameter, ζ, was introduced, which is the weight fraction of the polymer crystallized by primary and secondary crystallization at the moment that the primary crystallization has ended (end of region II). The whole crystallization process is then described by two equations:

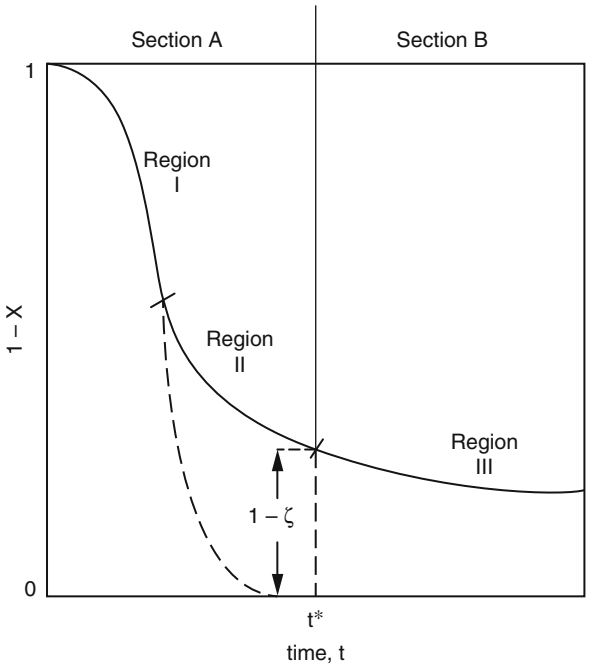

Fig. 3.19 Comparison between a typical experimental crystallization isotherm (*solid line*) and the Avrami equation (Eq. 3.17, *broken line*). The three regions I, II, and III correspond to primary, primary and secondary, and secondary crystallization, respectively (Pérez-Cardenas et al. 1991)

$$1-\alpha=\exp\left(-kt^{n}-k't^{n'}\right)\left[kn(1-\zeta)\int_{o}^{t}\exp\left(k\tau^{n}+k'\tau^{n'}\right)\tau^{n-1}\mathrm{d}\tau+1\right] \tag{3.21}$$

$$1-\alpha=(1-\zeta)\exp(k't^{*}n')\exp\left(-k't^{n'}\right) \tag{3.22}$$

Equation 3.21 is valid for $\alpha \leq \zeta$ and Eq. 3.22 for $\alpha > \zeta$. Instead of two Avrami parameters, five parameters are required to describe the process. They have the following physical meaning: k and n (the primary crystallization parameters) depend on crystallization temperature, nature of primary nucleation, and the fast growth; the secondary crystallization parameters, k' and n', depend on the conditions under which the slow crystallization of the remaining amorphous regions takes place; and a fifth parameter, ζ, indicates the weight fraction of material crystallized up to the moment the primary crystallization ends. t^* is the moment at which the third region starts (e.g., pure secondary crystallization).

Some literature data concerning isothermal crystallization experiments of linear PE at 128 °C (Doremus et al. 1958) have been fitted using different values for the parameters in Eqs. 3.21 and 3.22 (Fig. 3.20). The most accurate fit was obtained using the following parameters: $n = 4$, $k = 3.7 \times 10^{-10}$, $n' = 2$, $k' = 4 \times 10^{-6}$, and $\zeta = 0.68$.

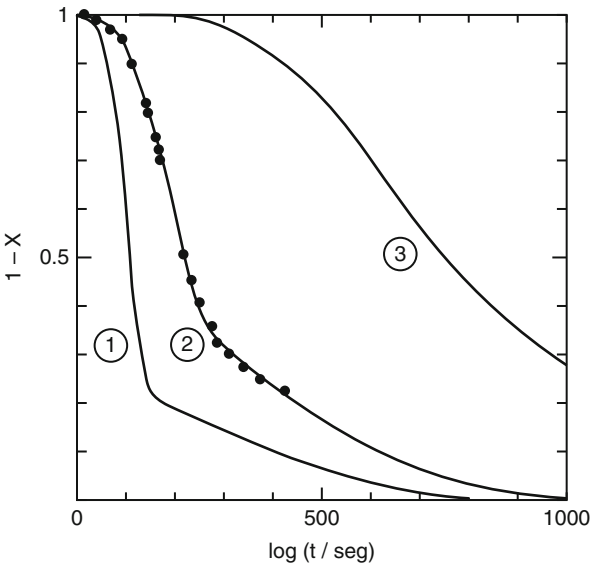

Fig. 3.20 Theoretical isotherms (*solid lines*) using Eqs. 3.21 and 3.22 for three different sets of values of the five parameters (Pérez-Gardenas et al. 1991) fitted to the experimental values (*points*) of Doremus et al. (1958)

In the case of miscible polymer blends, the temperature dependence of the overall kinetic rate constant, k, can be calculated from (Boon and Azcue 1968; Wunderlich 1973; Hoffman 1982)

$$1/n\ln k - \ln\phi_2 + \Delta E/\{R(T_c - T_o)\} - \left\{\left(0.2T_m^{\circ}\ln\phi_2\right)/\Delta T\right\} = \alpha_2 = \ln A_n - \left\{K_g/T_c\Delta Tf\right\} \tag{3.23}$$

with K_g the same as in Eq. 3.12

3.2.4.3 Determination of the Surface Free Energy of Folding from Overall Kinetic Data

A plot of α_2 versus $1/(T_c\Delta Tf)$ results in a straight line and from the slope, values of σ_e can be obtained. In Table 3.8 and Fig. 3.21, the free energy of folding, σ_e, for some PEG/PEMA and PEG/PMMA blends, respectively, derived from the overall kinetics of crystallization (Eq. 3.23), is compared with the values obtained from the radial growth rate data (Eq. 3.11). The compositional dependence of σ_e derived from both methods is similar, although higher values were obtained using Eq. 3.23 (overall kinetics of crystallization).

The σ_e values obtained from both analyses almost coincide. The dependence of σ_e on the composition of the PEG/PMMA blends may be partly accounted for by the effect of concentration, since the concentration-dependent part of σ_e is only a few joule per square meter (Martuscelli 1984). It is possible that PMMA molecules located in the interlamellar regions easily form entanglements with PEG molecules, favoring the formation of large loops on the surface of the PEG crystals.

Table 3.8 Free energy of folding (σ_e) for some PEG/PEMA blends calculated using Eqs. 3.11 and 3.23

Polymer blend	Composition (wt%)	σ_e ($\times 10^3$J/m^2) (Eq. 3.11)	σ_e ($\times 10^3$J/m^2) (Eq. 3.23)	References
PEG/PEMA	100/0	58	75	Cimmino et al. (1989)
	90/10	28	42	
	80/20	24	34	
	70/30	14	29	
PEG/PMMA	100/0	58	60	Martuscelli et al. (1984)
	90/10	43	48	
	80/20	38	39	
	70/30	36	39	
	60/40	36	37	

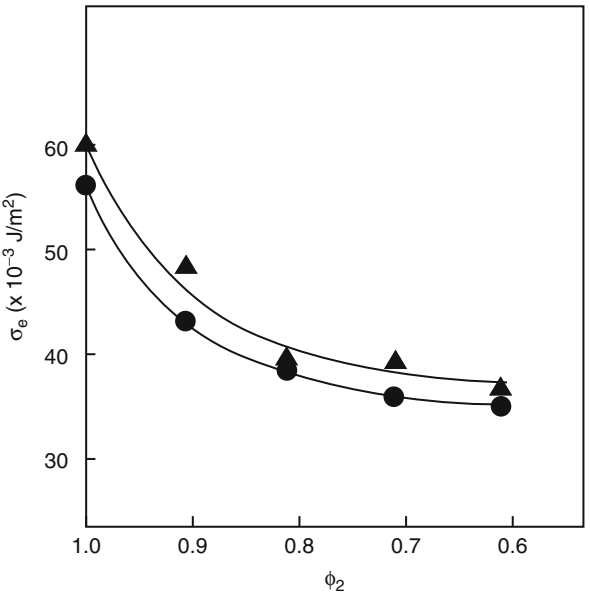

Fig. 3.21 Surface free energy of folding, σ_e, versus the volume fraction of the crystallizable component, ϕ_2, for blends of PEG (10) with PMMA from spherulite growth rate data (*circles*) and from overall rates of crystallization data (*triangles*) (the value between brackets refers to the molecular weight of PEG in kg/mol) (Martuscelli et al. 1984)

This can lead to an increase of both the surface enthalpy and the entropy of folding which contribute to σ_e ($\sigma_e = H_e - TS_e$). The decrease of σ_e when adding PMMA suggests that the entropic term overwhelms the enthalpic one.

3.2.4.4 Nonisothermal Kinetics

The theory of Avrami is limited to isothermal processes. Since polymer processing is mostly performed under nonisothermal conditions, the theory has been extended (Ziabicki 1967; Ozawa 1971; Ziabicki 1976).

According to Ozawa (1971), the crystallinity at any temperature is given by

$$-\ln(1-\alpha) = C(t)/q^{n''} \tag{3.24}$$

where q is the heating or cooling rate; $C(t)$ is a cooling function of the process; and n'' is the Ozawa exponent.

Ziabicki (1967, 1976) based his analysis on the assumption that any nonisothermal process can be treated as a combination of several isothermal crystallization steps:

$$E(t) = kt^n = \ln 2 \left\{ \int_0^t ds/t_{1/2}[\alpha(s)] \right\}^n \tag{3.25}$$

This equation is an analogue of Eq. 3.18.

Under nonisothermal conditions, the ultimate Avrami parameters will be averages of the parameters of the subsequent steps.

Gupta et al. (1994) used the following equation, based on the theory described by Ziabicki (1967, 1976) and by Kamal and Chu (1983), to describe the nonisothermal behavior of cocrystallizing HDPE/LLDPE blends.

$$\left[\alpha_p{}' \left(T_p - T_{ons}\right)\right] / \left[\beta\left(1-\alpha_p\right)\right] = (n-1) - \left[E\left(T_p - T_{ons}\right)\right] / \left[RT_p^2\right] \tag{3.26}$$

where $\alpha' = \mathrm{d}\alpha/\mathrm{d}t = nkt^{(n-1)}(1-\alpha)$ and β is the heating rate. In the case of a cooling experiment, β will be negative and β should be replaced by $-\beta$ in the equation.

T_{ons} is the onset temperature and T_p is the temperature after time t ($T_p - T_{ons} = \beta t$), where the subscript "p" denotes the peak temperature and E is the activation energy of the crystallization process.

A plot of the left part of Eq. 3.26 against $(T_p - T_{ons})/T_p{}^2$ should be linear with slope and intercept equal to E/R and $(n-1)$, respectively (see Fig. 3.22). The quantity α was evaluated from the ratio of the area under the crystallization peak per unit mass of the sample. α_p is the extent of crystallization at the peak maximum and is determined by the fractional area under the exotherm from the onset temperature T_{ons} to the peak temperature T_p relative to the total area under the exotherm.

The Avrami exponent and the activation energy decrease with increasing LLDPE content (see Table 3.9).

The authors suggested that the Avrami constant could be seen as the sum of two processes: a contribution due to nucleation and a contribution due to growth:

$$n = n_{\text{ucleation}} + n_{\text{growth}} \tag{3.27}$$

Since both components cocrystallize (Edward 1986; Hu et al. 1987; Gupta et al. 1994), the crystalline growth can be considered to be identical. As a consequence, the differences seen in the Avrami exponent, n, in the blends

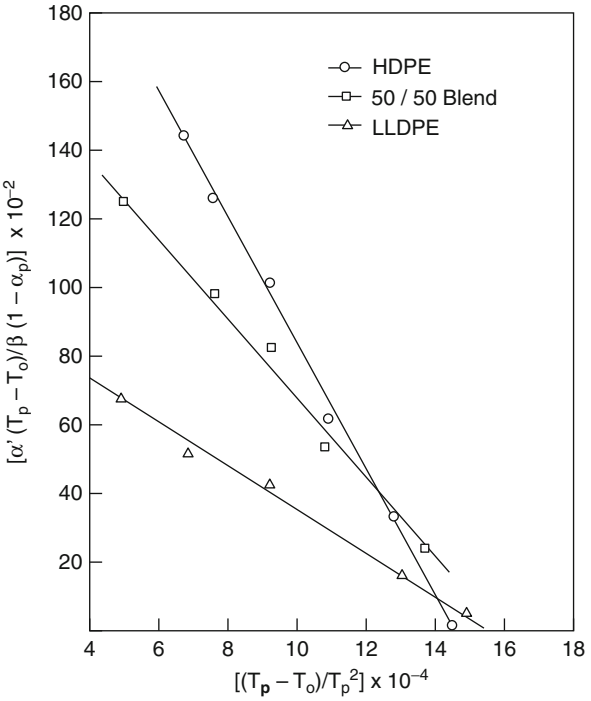

Fig. 3.22 Plot of $[\alpha_p' (T_p - T_o)]/[\beta (1 - \alpha_p)]$ versus $(T_p - T_o)/T_p^2$ for HDPE, LLDPE, and the 50/50 blend (Gupta et al. 1994)

Table 3.9 Avrami exponent, n, for HDPE, LLDPE, and their blends

Blend composition (wt%)[a] HDPE/LLDPE	Avrami exponent, n	Activation energy, E (kJ/mol)
100/0	2.94	121.67
75/25	2.65	99.44
50/50	2.30	85.83
20/80	1.93	59.04
0/100	1.72	49.16

[a]More compositions were mentioned in the article (Gupta et al. 1994)

must be due to a difference in the nucleation behavior that depends on the blend composition. A value varying from 0 (instantaneous nucleation) to 1 (sporadic nucleation) was attributed to the contribution of the nucleation of LLDPE and HDPE, respectively, to the Avrami constant, n. The remaining part of n (e.g., 1.94 for HDPE and 1.74 for LLDPE) represents the value for the growth process.

The lower activation energy for LLDPE compared to HDPE seems to be due to a storage of thermal energy by the crystallites caused by the presence of bulky pendant groups at the crystalline boundary that exert repulsive forces. Cocrystallization enhances these forces due to the greater abundance of the bulky groups that results in a decrease of the activation energy.

3.2.5 Melting Behavior of Crystallizable Miscible Blends

3.2.5.1 The Equilibrium Melting Temperature in Miscible Blends: Hoffman-Weeks Plot

In a semicrystalline homopolymer, the change in free energy of melting per mole of monomer unit is given by

$$\Delta G_u(T) = \Delta H_u - T\Delta S_u \tag{3.28}$$

where ΔH_u and ΔS_u are the enthalpy and the entropy changes on melting, respectively. For blends, the difference in free energy of the crystalline unit can be written as (Sanchez and Di Marzio 1971)

$$\Delta G_{ub}(T) = \Delta G_u(T) + \Delta g_M = \Delta H_u - T\Delta S_u + \Delta h_M - T\Delta s_M \tag{3.29}$$

where $\Delta G_u(T)$ has the same meaning as in Eq. 3.28, i.e., the heat of fusion of the crystalline component in the blend is assumed to be equal to that of the homopolymer. For athermal blends ($\Delta h_M = 0$) Eq. 3.29 becomes

$$\Delta G_{ub}(T) = \Delta H_u - T\Delta S_u - T\Delta s_M = \Delta H_u - T\Delta S_{ub} \tag{3.30}$$

For an infinitely thick crystal with an equilibrium melting temperature in the blend of T_{mb}°, $\Delta G_{ub}(T_{mb}^{\circ})$ is equal to 0 and

$$T_{mb}^{\circ} = \Delta H_u / \Delta S_{ub} \tag{3.31}$$

substituting Eq. 3.31 into Eq. 3.30 results in

$$\Delta G_{ub}(T_{mb}) = \Delta H_u(1 - T_{mb}/T_{mb}^{\circ}) - T_{mb}\Delta s_M \tag{3.32}$$

At T_m:

$$\Delta G_{ub}(T_{mb}) = 2(\sigma_{eb}/n_b) \tag{3.33}$$

Combining and rearranging Eqs. 3.32 and 3.33 gives a relation between the experimental and equilibrium melting point in athermal polymer blends:

$$1/T_{mb} = \{1/T_{mb}^{\circ} + \Delta s_M/\Delta H_u\}\{1/[1 - (2\sigma_{eb}/\Delta H_u n_b)]\} \tag{3.34}$$

with $\sigma_{eb} = \phi_1{}^{\alpha}\,\sigma_e$ and $n_b = (1 - \phi_1)^{\beta} n$ with α and β constants which need to be evaluated for each system (Cimmino et al. 1988). For $\Delta s_M \to 0$, the dependence can be simplified to

$$T_{mb} = T_{mb}^{\circ}[1 - (2\sigma_{eb}/\Delta H_u n_b)] \tag{3.35}$$

If the heat of mixing is not ignored ($\Delta h_M \neq 0$), then the same treatment of Eq. 3.29 as used to obtain Eq. 3.35 results in

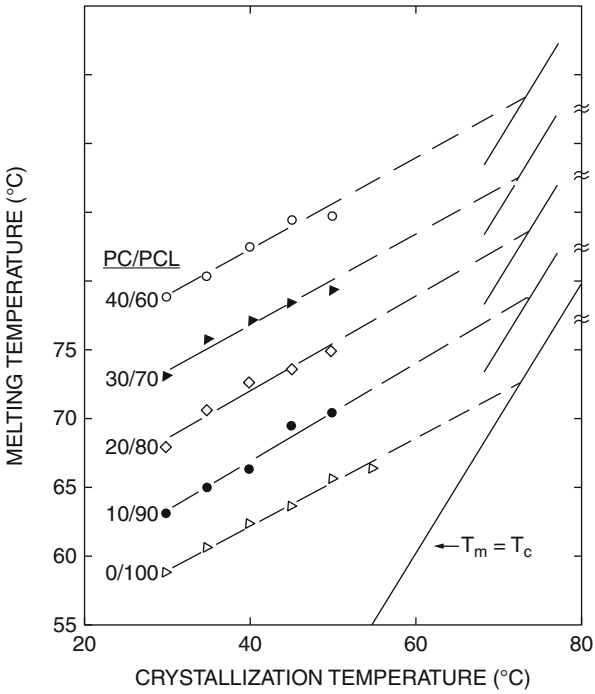

Fig. 3.23 Hoffman-Weeks plot for PCL-rich PCL/PC blends (the data are displaced by 5 °C to discern the different blend compositions) (Jonza and Porter 1986)

$$T_{mb} = T_{mb}^{\circ}\{1 - [(2\sigma_{eb}/\Delta H_u n_b) + (\Delta g_M/\Delta H_u)]\} \tag{3.36}$$

This equation is a general form of the relation between the experimental and equilibrium melting temperature of the blend.

The equilibrium temperature of a polymer (blend) can experimentally be determined by a Hoffman-Weeks plot, which is a plot of the experimental melting point versus the crystallization temperature (T_m vs. T_c) as presented in Fig. 3.23. Extrapolation from experimental data to the $T_m = T_c$ line results in the value of T_{mb}°.

The influence of T_c on T_m is due to morphological contributions such as degree of perfection and the finite size of crystals (Hoffman and Weeks 1962b; Mandelkern 1964). If the crystals are perfect, of finite size and no recrystallization takes place during the melting, the T_m versus T_c data can be described by Nishi and Wang (1975)

$$T_m^{\circ} - T_m = \phi\left(T_m^{\circ} - T_c\right) \tag{3.37}$$

or

$$T_m = T_m^{\circ}(1 - \phi) + \phi T_c \tag{3.38}$$

T_m° and T_m are the equilibrium and observed melting point, respectively; ϕ is the stability parameter that depends on the crystal thickness and assumes

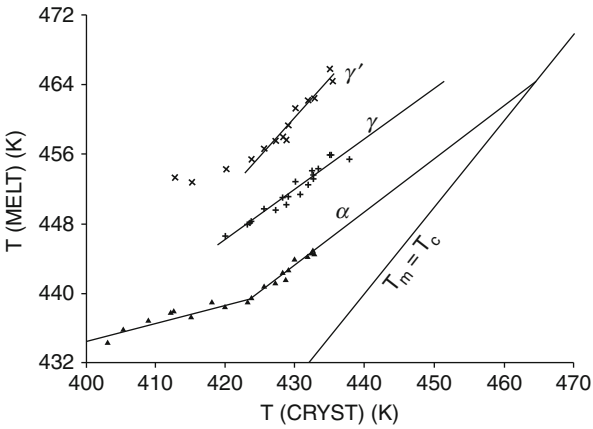

Fig. 3.24 Hoffman-Weeks plot for PVDF/PMMA blends with 50.1 vol% of PVDF (Stein et al. 1981)

values between 0 and 1 (sometimes ϕ is replaced by $1/\gamma$, where γ is the thickening factor of the crystal).

The value of $\phi = 0$ implies $T_m = T_m^\circ$ for all T_c, whereas $\phi = 1$ implies $T_m = T_c$. Therefore, the crystals are most stable at $\phi = 0$ and inherently unstable at $\phi = 1$. Nishi and Wang (1975) examined the polymer system PVDF/PMMA and found a value for $\phi = 0.2$ for all compositions studied, which suggests that the crystals are fairly stable. A comparable value has been found for other polymer crystals (Hoffman and Weeks 1962b).

The same polymer blend was studied by Stein et al. (1981), Morra and Stein (1984). Since PVDF crystallizes into several types of morphologies, different lines are shown in the Hoffman-Weeks plot (Fig. 3.24). The curve representing the melting point of PVDF as a function of the crystallization temperature for the α modification shows a break that was associated with defect exclusion from the crystal (Stein et al. 1981) and by entrapment of head-to-head defects of the PVDF chains into the crystals during rapid crystallization at large undercooling (Morra and Stein 1984).

Hoffman-Weeks plots have also been drawn for several other amorphous/crystalline miscible blends, such as PVDF/PEMA (Eshuis et al. 1982), PEG/PMMA (Martuscelli 1984), PCL/SARAN (Zhang and Prud'homme 1987), as well as for some miscible blends containing two semicrystalline components, PCL/PC (Jonza and Porter 1986) and PCL/Penton (Guo 1990). Table 3.10 represents equilibrium melting points derived from T_m versus T_c plots for some of these systems.

In Fig. 3.25 Hoffman-Weeks plot for PCL/PBT blends is compared to pure PBT sample. A nonlinear extrapolation procedure was applied for the determination of the equilibrium melting temperature of the crystallizing phase. The linear extrapolation as proposed initially by Hoffman-Weeks neglects the contribution of the increment of the lamellar thickness. Note that the PCL is miscible with PBT only when the PCL molecular weight is equal or lower than MW = 1,250. The blend samples having a PCL molecular weight of 10,000 or 50,000 form immiscible mixture for which the crystallization behavior of pure PBT is recovered. The T_m° of

Table 3.10 Equilibrium melting points derived from Hoffman-Weeks plots for several crystallizable miscible blends

Polymer blend	Composition[a]	T_m° (°C)	References
PVDF/PMMA	100/0	173.8	Nishi and Wang (1975)
	50/50	165.2	
PCL/PC[b]	100/0	71	Jonza and Porter (1986)
	10–40 % PC	71 ± 2	
PCL/P(VCl_2-VC)[c]	100/0	58.1	Zhang and Prud'homme (1987)
	50/50	55.4	
PCL/P(VCl_2-VA)[c]	50/50	55.3	
PCL/P(VCl_2-AN)	50/50	53.6	
PCL/Penton	0/100	185	Guo (1990)
	50/50	172.5	
PEEK/PEI	0–60 % PEI	384	Chen and Porter (1993)
		389	Lee and Porter (1987)
iPS/PPE	0–35 % PPE	240	Plans et al. (1984)

[a]Most authors studied more compositions than the ones presented here
[b]Both polymers crystallize in this blend, but no $T_m - T_c$ plots could be made for PC since the blends are reactive at the higher crystallization temperatures required for this component
[c]Both polymers crystallize in this blend

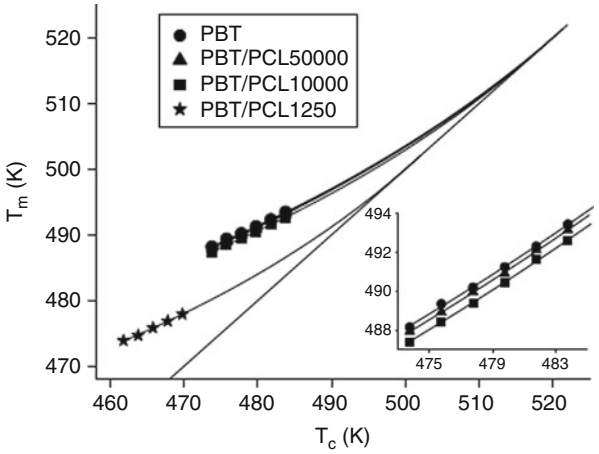

Fig. 3.25 Melting temperature of non-thickened crystals ($\beta = 1$) as a function of T_c for PBT and PBT/PCL blends. The *curved* lines are the nonlinear fit to the experimental data. The *straight* line $T_m = T_c$ is also depicted. The *inset* shows an enlargement of the plot (Righetti et al. 2007)

the PBT/PCL1250 is equal to 501 °K, much lower than that of pure PBT (522 °K) or its blends with higher MW PCL samples (PCL10000: $T_m^\circ = 519$°K; PCL50000: $T_m^\circ = 521$ °K).

It should, however, be noted that several blends do not show a linear T_m versus T_c relation (Rim and Runt 1984; Jonza and Porter 1986). The absence of linearity originates from several effects, such as recrystallization, crystal defects, etc.

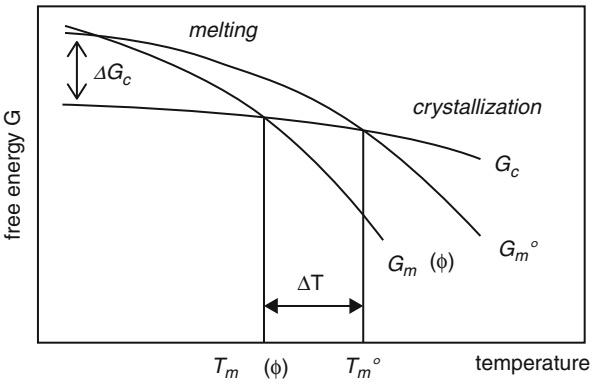

Fig. 3.26 Schematic diagram of the free energy of a crystalline phase (G_c) and the free energy of a melt phase of a homopolymer (G_m°) and a miscible blend (G_{mb}°) as function of the temperature

3.2.5.2 Melting-Point Depression

The melting behavior of a semicrystalline component in a miscible blend strongly depends on the blend composition. In several blends, a depression of the melting point has been observed after addition of an amorphous polymer. This behavior results from the kinetic, morphological, and thermodynamic factors (Cimmino et al. 1989). *Kinetic* effects originate from the crystal formation at temperatures below the equilibrium melting point. They can be avoided by using equilibrium values derived from Hoffman-Weeks plots. Melting-point depression, caused by *morphological* effects (see Eq. 3.38), is associated with changes in crystal thickness, perfection and geometry, as well as different thermal histories of the samples. When a miscible diluent is added to a semicrystalline polymer, the equilibrium melting point of the crystallizable component can be depressed due to interaction between both components. The free energy of the crystallizable component will decrease from G_m° to G_{mb}°, when the crystallites are surrounded by a mixed melt phase. The free energy of the crystalline phase, G_c, is not affected by mixing. The melting temperature, defined as the cross section of G_c and G_m (e.g., when $\Delta G = 0$), may be depressed (Fig. 3.26).

The melting-point depression resulting from *thermodynamic* effects can be described by the following equation (Flory 1953; Nishi and Wang 1975):

$$\begin{aligned}&\left(1/T_{mb}^{\circ}\right) - \left(1/T_{m}^{\circ}\right) = -[(RV_{2u})/(\Delta h_u V_{1u})] \\ &\left[(\ln\phi_2/m_2) + (1/m_2 - 1/m_1)(1-\phi_2) + \chi_{12}(1-\phi_2)^2\right]\end{aligned} \tag{3.39}$$

T_{mb}° and T_m° are the equilibrium melting point of the blend and the neat crystallizable component, respectively; V_u is the molar volume of the repeating unit of the components (1 = amorphous component and 2 = crystallizable component); Δh_u is the heat of fusion per mole of repeating unit; m is the number of units in the molecule, i.e., the degree of polymerization; ϕ is the volume fraction; and χ_{12} is the polymer-polymer interaction parameter.

Since, for polymers $m \to \infty$, Eq. 3.39 can be reduced to

$$\left(1/T_{mb}^{\circ}\right) - \left(1/T_{m}^{\circ}\right) = -[(RV_{2u})/(\Delta h_u V_{1u})]\chi_{12}(1-\phi_2)^2 \tag{3.40}$$

Instead of χ_{12}, the interaction energy density, B_{12}, can be used; both parameters are related by

$$\chi_{12} = B_{12}V_{1u}/RT \tag{3.41}$$

Melting-point depression data are often used to determine the Huggins-Flory interaction parameter, χ_{12} (see Table 3.11), that is a measure for the miscibility of the blend, i.e., χ_{12} is negative for a miscible blend. A lack of melting-point depression means that χ_{12} is zero. Equation 3.39 is only valid for systems in which the crystalline morphology is not affected by the composition.

Many authors (Hay 1976; Kwei and Frisch 1978; Rim and Runt 1984; Plans et al. 1984; Alfonso and Russell 1986), however, encountered difficulties when fitting Eq. 3.40 to their experimental data, due to (Rostami 1990):

- The use of observable melting temperatures instead of the thermodynamic equilibrium temperatures.
- The plot of the left-hand side of Eq. 3.40 versus the right-hand side has no zero-intercept. The intercept contains information about the crystalline morphology (Kwei and Frisch 1978; Walsh et al. 1985) that has been ignored. Following Eq. 3.39 the intercept should equal $1/m_1$. When high molecular weight polymers are used, $1/m_1$ equals zero. This was observed for PVDF/PMMA and PVDF/PEMA blends (Kwei and Frisch 1978).
- The concentration dependence of the interaction parameter adds a restriction on plotting the left-hand side of Eq. 3.40 versus ϕ_1 to obtain a single value for χ_{12} (Kwei and Frisch 1978; Plans et al. 1984; Walsh et al. 1985).

A modified version of this equation has been used by some other authors (Kwei and Frisch 1978; Walsh et al. 1985), who added a constant that is related to the morphology of the crystalline region:

$$\Delta h_u\left(T_m^{\circ} - T_{mb}^{\circ}\right)/\phi_1 RT_m^{\circ} - T_{mb}^{\circ}/m_1 - \phi_1 T_{mb}^{\circ}/2m_2 = C/R - b\phi_1 \tag{3.42}$$

where C is a constant taking into account the morphological contributions (which were assumed to be proportional to ϕ_1) and b is a constant derived from the equation relating the interaction parameter with temperature: $\chi_{12} = a + b/T$ with $a \ll b/T$ near the melting point. This approach was, however, not satisfactory (Walsh et al. 1985).

It should be noted that in Eq. 3.42 the assumption of infinite molecular weights has not been included as was done in Eq. 3.40.

Balsamo et al. (2006) presented a nice comparison in Fig. 3.27 of the effect of equilibrium melting-point depression in miscible blends of PCL with various partners including PVC, PSMA14 (14 wt% MA), Phenoxy, and SAN19,5 (19,5 wt% AN). It is clear that PSMA14 caused the greatest depression of the T_m° of PCL compared to the other partners. The authors ascribed this effect to the

highest interaction PCL develops with PSMA14 and that hinders the formation of perfect and complete lamellae. The peak temperature was used for the calculations instead of the onset due to the presence of a low melting endotherm that introduces some error in the determination of the onset of the melting point corresponding to the primary crystallization. Using at least eight experimental points, a linear dependence was observed in the T_c range used in this work. Thus, the extrapolation to $T_c = T_m$ by a linear least squares fit could be performed to calculate T_m°. For neat PCL, a T_m° of 69.9 °C, was observed in agreement with values reported in the

Table 3.11 Interaction parameters, χ_{12} and B_{12}, derived from the melting-point depression data

Polymer blend	Interaction parameter, χ_{12}	Interaction parameter, B_{12} ($\times 10^6$J/m^3)	References
PVDF/PMMA	−0.295 (160 °C)	−12.48	Nishi and Wang (1975)
PVDF/PEMA	−0.34 (160 °C)	−11.94	Kwei et al. (1976)
		−13.11	Imken et al. (1976)
PEG(20,000)/PMMA[a]	−1.93 (76 °C)	−65.32	Martuscelli and Demma (1980)
PEG(100,000)/PMMA	−0.35 (74 °C)	−11.93	Martuscelli et al. (1984)
PEG/PVC[b]	−0.094 (65 °C)	−6.56 (65 °C)	Marco et al. (1993)
PCL/SAN 19.2[c]	−0.18		Kressler and Kammer (1988)
PBA/Phenoxy		−16.20 (61 °C)	Harris et al. (1982)
PEA/Phenoxy		−9.67 (49 °C)	Harris et al. (1982)
PCL/Phenoxy		−10.09 (56 °C)	Harris et al. (1982)
PCL/Penton[d]		−15	Guo (1990)
PCL/P(VCl_2-VC) 80/20[e,d]	−0.46		Zhang and Prud'homme (1987)
PCL rich	−0.02		Aubin et al. (1983)
P(VCl_2-VC) rich	−0.21		Aubin et al. (1983)
PCL/P(VCl_2-VA) 80/20[e,d]	−0.53		Zhang and Prud'homme (1987)
PCL rich	−0.01		Aubin et al. (1983)
P(VCl_2-VA) rich	−0.28		Aubin et al. (1983)
PCL/P(VCl_2-AN) 80/20[e,d]	−0.37		Zhang and Prud'homme (1987)
P(VCl_2/VCl)/PDPS[d]		−0.84	Woo et al. (1983)
P(VCl_2/VCl)/PDPA[d]		−4.60	Woo et al. (1983)
P(VCl_2/VCl)/PCL[d]		−8.37	Woo et al. (1983)
P(VCl_2/VCl)/PCDS[d]		−12.98	Woo et al. (1983)
PCL/PVDF[d,f]	−1.5		Jo et al. (1992)
FVA/EVAc[g]	−0.06	−15.07	Clough et al. (1994)
PI/EVAc[g]	−0.02	−7.12	Clough et al. (1994)

(*continued*)

Table 3.11 (continued)

Polymer blend	Interaction parameter, χ_{12}	Interaction parameter, B_{12} ($\times 10^6$J/m^3)	References
PED/EVAc[g]	−0.38	−115.56	Clough et al. (1994)
PEEK/PEI	−0.40 (400 °C)	−5.02	Chen and Porter (1993)
iPS/PS (2,200)	−0.002		Runt (1981)
iPS/PS (50,000)	−0.003		Runt (1981)
iPS/PPE	0.17		Plans et al. (1984)
	−0.022		Runt (1981)

[a]The absolute value of χ_{12} is too large in comparison with the other literature data on miscible blends. The authors (Martuscelli et al. 1984) suggested that for this blend non-negligible entropic effects occur during mixing of the two polymers, noncompliance with the assumption inherent in the extrapolation of T_m (observed melting point) by using the Hoffman-Weeks plot and the inadequacies of the Huggins-Flory theory to describe the melting behavior of such polymer-polymer system
[b]EVAc (molar ratio ethylene to vinyl acetate: 7:1) is amorphous
[c]SAN containing 19.2 wt% AN
[d]Both polymers are semicrystalline
[e]More compositions have been investigated by the authors
[f]Units: J/mL
[g]This system shows an LCST behavior for PCL-rich blends, while blends with a high concentration on PVDF are phase separated; the blends considered here are only the miscible ones below their LCST (blends with a content of PVDF less than 30 wt%)
[h]The polymer blend PEG/PVC is only miscible when the concentration on PVC is ≥40 %

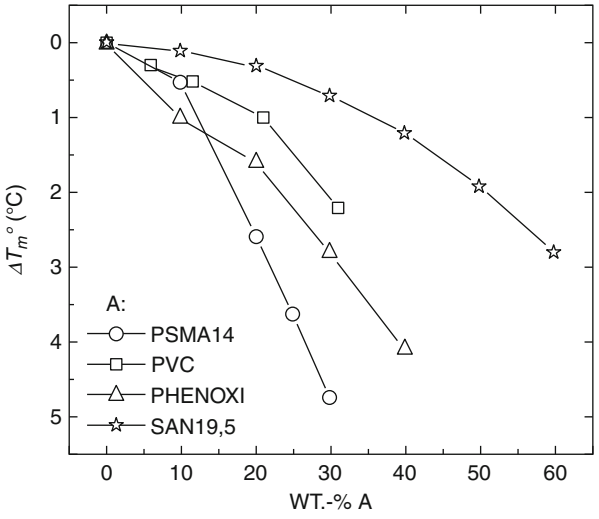

Fig. 3.27 Equilibrium melting-point depression of the PCL fraction in blends A/PCL as a function of the amorphous polymer A content. (○) Author's work, (Δ) (10), (□) (5), (☆) (15) (Balsamo et al. 2006)

literature (Balsamo et al. 2001; Wang and Jian 1997; Jonza and Porter 1986; Neo and Goh 1991). The melting-point depression exhibited by the PCL fraction with increasing PSMA14 (68.3 ± 2.2 °C and 64.2±1.4 °C for PSMA14/PCL 10/90 and 30/70, respectively) indicates miscibility between PCL and PSMA14 as was previously discussed from the standard DSC scans.

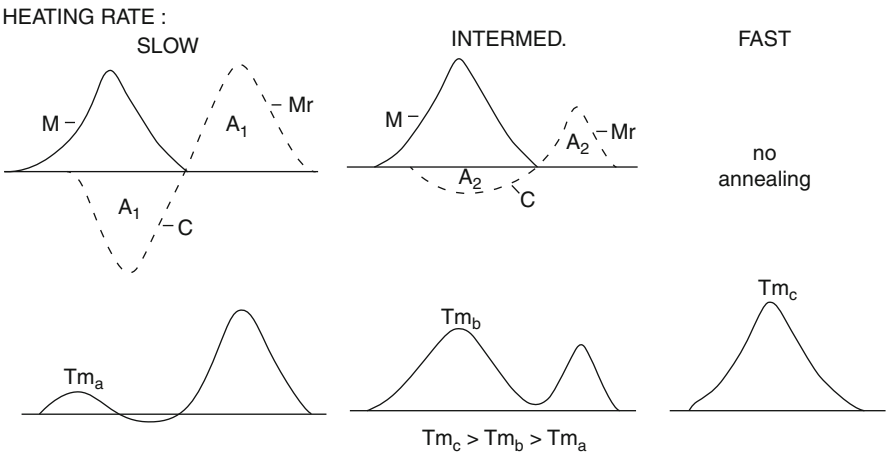

Fig. 3.28 Schematic representation of the melting mechanism proposed to account for the heating rate dependence of recrystallizing material. The *top* of the figure shows the melting of the original crystals (M), recrystallization (C), and remelting (M_r). The *bottom* portion of the figure shows the resultant thermograms that are experimentally observed (Rim and Runt 1983)

For some miscible blends, a melting-point elevation has been reported with respect to that of the neat crystallizable component, both crystallized at the same temperature (Eshuis et al. 1982; Rim and Runt 1983, 1984). These observations may originate from recrystallization, enhanced crystal perfection, and increased crystal size.

3.2.5.3 Multiple Melting Endotherms

The melting behavior of binary crystallizable blends often reveals multiple melting endotherms that can be ascribed to recrystallization, secondary crystallization effects, phase separation, etc.

Recrystallization is a process in which the initial, rather imperfect, lamellae melt and recrystallize to produce thicker and more perfect lamellae that as a consequence melt at a higher temperature. As a result of this process, a double melting behavior may be observed. Recrystallization has been observed for neat polymers and blends.

A method that is often used to determine if the dual melting behavior is caused by recrystallization is the variation of the heating rate in DSC experiments. It is suggested that during the DSC run, an annealing of the crystalline lamellae occurs (see Fig. 3.28; Rim and Runt 1983). At slow heating rates, the original crystals are given sufficient time to reorganize, and the melting behavior is then mainly caused by lamellae originating from recrystallization (C) and melting of the recrystallized material (M_r). The resulting behavior is a composite of the peaks due to the melting of the original crystals (M), the recrystallization exotherm, and the melting of the recrystallized material. As the heating rate is increased, the crystals have less time to reorganize, thus C and M decrease in magnitude.

A plot of the observed melting point of both melting endotherms as function of the crystallization temperature (Hoffman-Weeks plot) is another method to detect whether recrystallization occurs. The melting point of recrystallized material is independent of T_c; thus a horizontal line is observed in the T_m versus T_c plot.

During crystallization of a miscible polymer blend, the composition of the amorphous phase changes, i.e., becomes poorer on the crystallizable component. In some cases, a liquid-liquid phase separation can take place as a result of the crystallization. This phenomenon will be discussed more in detail in the next section.

A complex melting behavior is also observed when a semicrystalline polymer exhibits two different types of crystal structure. A second crystal structure can be introduced by a variation in temperature, pressure, elongation, etc. This phenomenon is known for neat PE. Adding an amorphous polymer to a crystallizable component can result in a change of the unit cell dimensions of the crystal structure. This has been observed for LDPE blended with EPDM (Starkweather 1980), where the unit cell expanded in the a-direction (a raises from 7.515–8.350 A) when increasing the amount of EPDM, while the b- and c-directions remained almost unchanged. The composition of EPDM plays also an important role. EPDM with an ethylene/propylene mole ratio of 4:5 (EPDM-1) exhibits the behavior as mentioned above. Decreasing the ethylene content in the EPDM copolymer results in an amorphous polymer (designated EPDM-2 and EPDM-3; Starkweather 1980) that do not alter the unit cell dimensions as much as EPDM-1 does. The latter copolymer is thought to cocrystallize (at least partially) with LDPE.

Several blends prepared by coprecipitation followed by crystallization from the melt exhibit a double melting behavior, due to the occurrence of the secondary crystallization process. The amorphous component causes a retarded crystallization of some of the crystallizable chains, which form lamellae smaller than and located between the primary ones constituting the spherulites (see Fig. 3.29).

This is a phenomenon often observed in PCL blends. In DSC scans as a function of crystallization time (t_c), a single melting behavior is observed after short t_c, while a second melting endotherm is noticed at long t_c (see Fig. 3.30). This second melting endotherm becomes more important as the more amorphous component is added (Vanneste and Groeninckx 1995; Fig. 3.31).

In Table 3.12 some blends are presented exhibiting a complex melting behavior due to one or more of the abovementioned reasons.

It should be mentioned that several homopolymers (of which polyethylene is probably the best known sample) also exhibit a complex melting behavior. Branched polyethylenes (LDPE, LLDPE, and VLDPE) show multiple melting endotherms, due to the presence of fractions with different branching contents (Schouterden et al. 1985; Defoor et al. 1993). This was clearly illustrated by Defoor et al. who fractionated LLDPE with respect to the short-chain branching content and blended the fractions with the highest and the lowest branching content. It was shown that they both crystallized and melted separately. Both fractions determined the spherulitic morphology in a cooperative way.

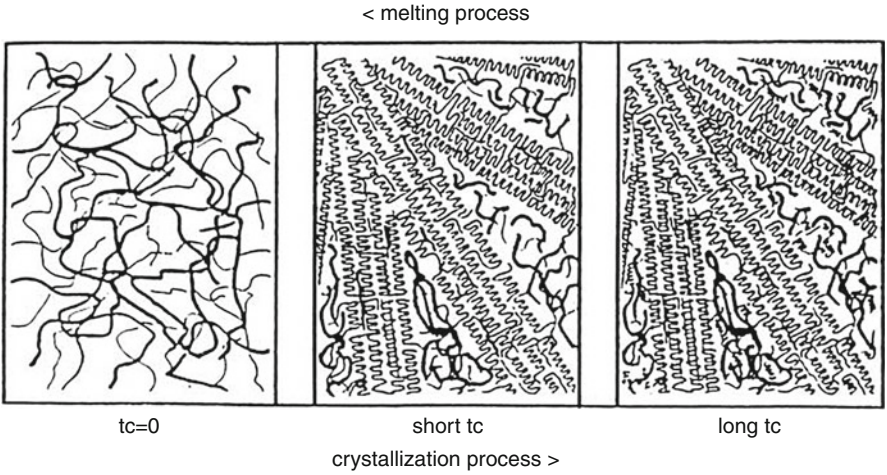

Fig. 3.29 Schematic presentation illustrating the secondary crystallization process (*thin lines*: crystallizable component, *thick lines*: amorphous component)

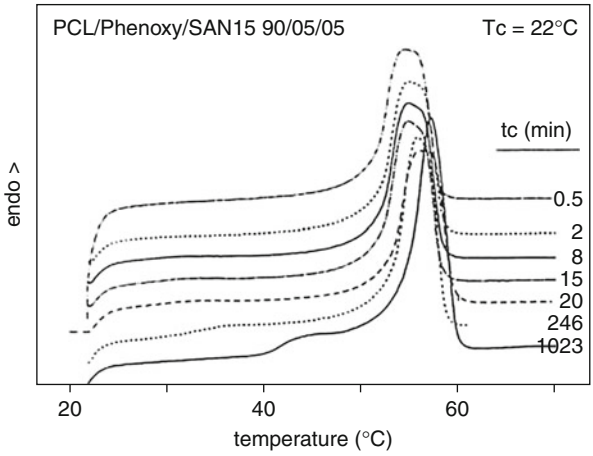

Fig. 3.30 Influence of the crystallization time on the melting behavior of the ternary PCL/Phenoxy/SAN 15 = 90/05/05 blend (Vanneste and Groeninckx 1994)

Other examples are PPS (which shows a double melting behavior due to the obstructive effect of branching or cross-linking of the molecules on crystallization at high temperature; Mai et al. 1994) and PEEK. Much controversy exists about the cause of the double melting behavior of PEEK – recrystallization or secondary crystallization. According to one group of authors (Prasad et al. 1991; Hudson et al. 1991; Bassett et al. 1992; Lattimer et al. 1992), PEEK that was crystallized

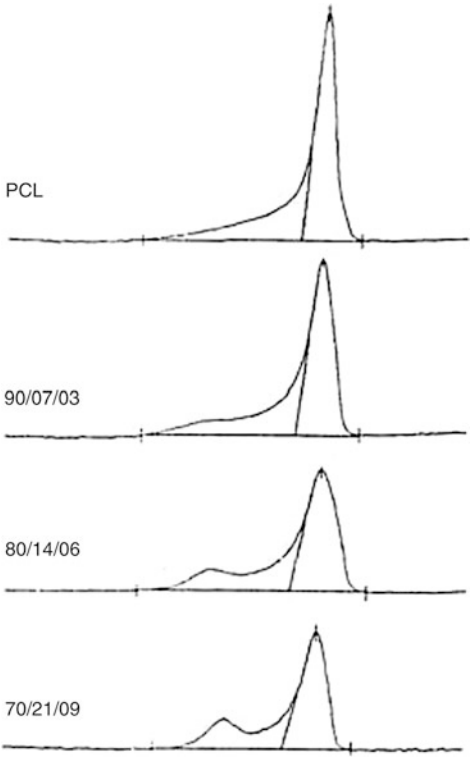

Fig. 3.31 Influence of the concentration of the amorphous component on the amount of secondary crystallization in PCL/SAN 15/SMA 14 polymer blends (Vanneste and Groeninckx 1995)

from the melt contains crystals with two types of lamellar thickness. The thicker ones grow first, while the smaller ones grow later within the thicker lamellae. Thermal analysis, however, indicates that a process of melting, recrystallization, and remelting occurs (Cheng et al. 1986; Lee and Porter 1987; Lee et al. 1989; Crevecoeur and Groeninckx 1991).

PEO/amorphous polyamide (Aramide 34I) blends investigated by Dreezen et al. (1999) displayed a double melting behavior. By varying the crystallization time of a 85 wt% PEO/15 wt% Aramide 34I from 33 to 451 h, the authors could demonstrate that the primary melting endotherm visible at 65 °C does not change, whereas the second melting endotherm increased in intensity and shifted to higher temperatures (from 41 °C to 50 °C) with increasing crystallization time (Fig. 3.32). They attributed the presence of a second melting endotherm, situated at lower temperatures than the main peak, to secondary crystallization of PEO after the primary crystallization process. The crystallization of some PEO-chains was retarded and crystallized slowly after the formation of the spherulitic structure. With time the thin lamellae thicken and melt at higher temperatures. During heating at low heating rates,

Table 3.12 Examples of crystallizable miscible polymer blends exhibiting a complex melting behavior

Polymer system	Type of melting behavior	Required conditions	References
PCL/SAN	Recrystallization	Melt crystallized	Rim and Runt (1983, 1984)
PCL/SAN	Dual melting behavior[a]	Melt crystallized	Kressler and Kammer (1988)
PCL/SAN	Recrystallization	Melt crystallized	Vandermarliere (1986)
PCL/Phenoxy/SAN 15[b]	Recrystallization	Short crystallization times	Vanneste (1993), Vanneste and Groeninckx (1994)
PEEK/PEI[c]	Recrystallization	Melt crystallized	Crevecoeur and Groeninckx (1991)
LDPE/EPDM	Different crystal types	Ethylene/propylene ratio: 4:5	Starkweather(1980)
PCL/P(VCl_2-VC)	Secondary crystallization	High P(VCl_2-VC) content[d]	Zhang and Prud'homme (1987)
PCL/CPE[e]	Secondary crystallization	Coprecipitation technique + melt crystallization	Defieuw et al. (1989b)
PCL/SMA x[f]	Secondary crystallization	Coprecipitation technique + melt crystallization	Defieuw et al. (1989b)
PCL/Phenoxy	Secondary crystallization	Coprecipitation technique + melt crystallization	Defieuw et al. (1989d)
PCL/SAN x/SAN y[g]	Secondary crystallization	Coprecipitation technique + melt crystallization	Defieuw et al. (1989c), Vanneste (1993)
PCL/Phenoxy/SAN 15[b]	Secondary crystallization	Coprecipitation technique + melt crystallization[h]	Vanneste and Groeninckx (1994)
PEEK/PEI	Secondary crystallization	Melt blended and crystallized	Bassett et al. (1992), Hsiao and Sauer (1994)
LLDPE/LLDPE[c]	Secondary crystallization	Coprecipitation technique + melt crystallization	Defoor et al. (1993)
PCL/PSMA14	Dual crystallization	Melt crystallized	Balsamo et al. (2006)

[a]Reason for this dual melting behavior "is not completely clear," but recrystallization is possibly occurring
[b]SAN containing 15 wt% AN
[c]A blend of 1-octene LLDPE fractions with different short-chain branching content was investigated, i.e., 3 and 33 methyl groups per 1,000 carbon atoms
[d]Solution cast blends followed by melt crystallization
[e]PCL/CPE is only totally miscible for CPE containing 49.1 wt% chlorine
[f]$x = 14$ and 25 wt%
[g]x and y are 25 and 24 wt% and 15 and 14 w%, respectively, in both references
[h]Only the blends with 90 wt% are dealt with since only those combinations were found to be miscible

the lamellae melt and recrystallize, resulting in lower melting endotherm that shifted to lower temperatures the recrystallized lamellae melt at slightly higher temperatures than the thick primary lamellae with a shift to higher temperature and an increase in intensity of the higher melting endotherm (Fig. 3.33).

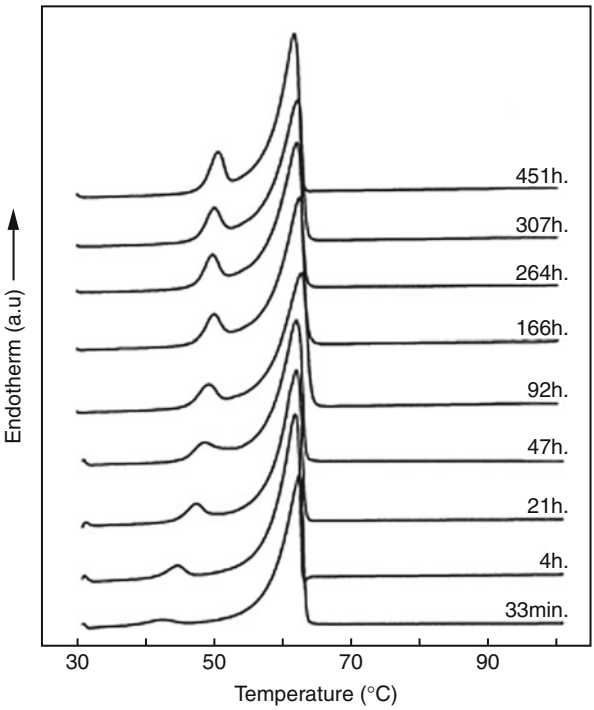

Fig. 3.32 DSC-heating curves of 85/15 PEO/Aramide blends crystallized at 28 °C for different times (Dreezen et al. 1999)

3.2.6 Crystallization Phenomenon in Miscible Thermoplastic/Thermosetting Blends

Because of the additional parameter of curing a phase, crystallization of blends of a curable amorphous thermosetting with a crystallizable thermoplastic has been poorly reported in literature. Nevertheless, the few blend systems covered are very interesting and show attractive phenomena in terms of crystallization, melting, and phase separation when the thermosetting is cured. Crystallization in thermosetting polymer blends containing a crystallizable thermoplastic component will be affected by the miscibility of the components, the phase behavior of the cross-linked blends, and the topological effect of the formed network. Except for the particular three-dimensional network formed upon chemical curing, the effect of thermosetting curing is almost similar to that of a solidifying phase (cooling below T_g for an amorphous phase or crystallization of a crystallizable phase) in thermoplastic/thermoplastic blend system. Therefore, we can consider that the utmost effect of the cured phase on the crystallizable phase is the chain mobility restriction. How does the segregation of the cured thermosetting component take place during the crystallization of the semicrystalline component? Prior to any deep investigation of the crystallization phenomenon, a deep understanding of the miscibility of the thermosetting/thermoplastic blends is crucial. The determination of the glass

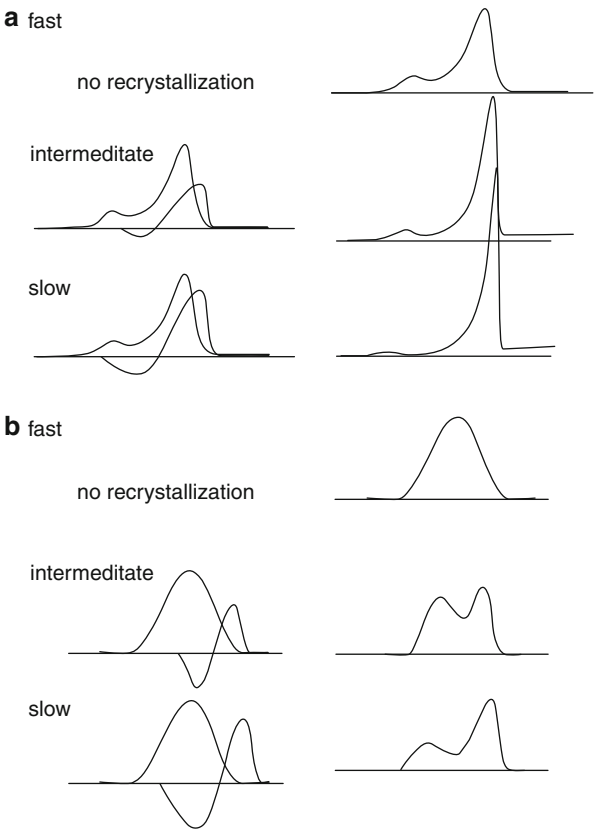

Fig. 3.33 Schematic representation of the melting mechanism proposed to account for the heating rate dependence of recrystallizing blends. The *left* side of the figure shows the melting of the original crystals (*full line*) and the recrystallization, remelting phenomenon (*dashed line*), while the *right* side shows the resulting experimentally observed thermogram: (**a**) for an 80/20 PEO/Aramide blend; (**b**) for a 65/35 PEO/Aramide blend at fast, intermediate, and slow heating rates (Dreezen et al. 1999)

transition as a function of the extent of curing of the thermosetting resin helps for the interpretation of the crystallization results. Other questions remain poorly elucidated including, e.g., to which extent the chains of the thermoplastic component remain intimately in contact to the thermosetting network when curing is achieved. One can expect that a part of the crystallizable phase is entrapped in the formed network of the thermosetting and does not participate to the overall crystallization.

Blends of bisphenol A type epoxy resin (ER) with PEO (Guo et al. 2001a), PCL (Guo et al. 2001b), and POM (Goossens et al. 2006a, b, 2007) are typical examples of thermosetting/thermoplastic blend system studied. The curing of the epoxy resin is usually ensured by using MCDEA curing agent. In Fig. 3.34 the T_g of the blend and the T_c and T_m of the PEO component as a function of the ER/PEO blend composition are plotted. It is clear that the presence of PEO phase reduces the cross-linking density of the ER resin, and hence it is T_g via a dilution and eventually a plasticizing mechanism. Blends with 60 wt% or more ER do not exhibit any crystallization and behave as an amorphous phase. Blends with 50–60 wt% PEO crystallize at higher T_c, indicating chain mobility constraints imposed by the formation of a cross-linked ER network.

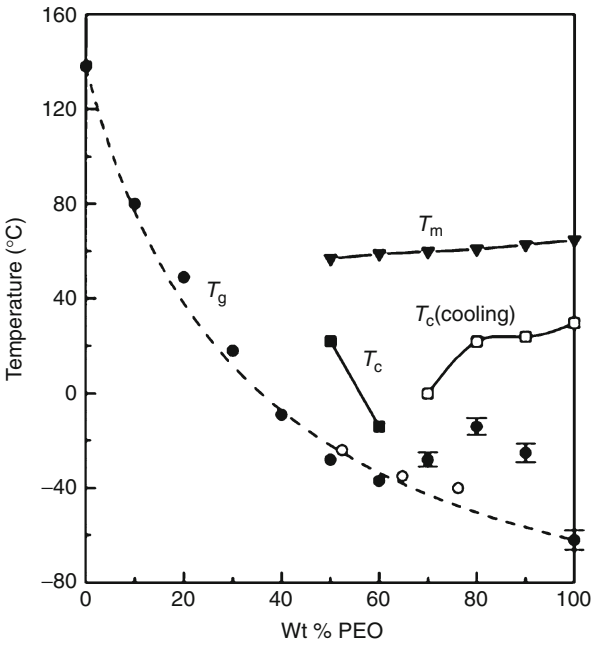

Fig. 3.34 Thermal properties of the second scan of the MCDEA-cured ER/PEO blends. (●) Experimental plot of T_g versus overall blend composition, (□) plot of T_g versus calculated amorphous composition, and (————) theoretical curve of T_g versus composition as predicted by the Gordon-Taylor equation using a k value of 0.25. The T_c (cooling) (□) as a function of composition is also given (Guo et al. 2001)

Blends of uncured thermosetting component DGEBA with PCL were compared to blends of cured resin ER with PCL (Guo et al. 2001). In Fig. 3.35 are plotted the measured experimental T_g of the uncured DGEBA/PCL blends as a function of composition. The curve exhibits a mixing rule trend indicating a strong miscibility of the two components. Note that in blends containing 70 wt% or more PCL, the T_g exhibits a positive deviation with respect to the fox mixing rule (broken line), indicating a high crystallinity of the PCL phase. Figure 3.36 shows the T_g of the cured ER/PCL blends, the T_c and T_m as a function of the blend composition. Comparison of the two figures reveals that the uncured DGEBA resin is less constraining the crystallinity of the PCL phase than the cured ER resin. Indeed, the crystallization temperature, T_c, increases with increasing ER content synonymous of the difficult crystallization of PCL in the presence of the cured resin.

The melting depression is less pronounced in the uncured blend than in the cured one. A smaller difference of the Tm's of the two endothermic peaks is depicted between the cured and the uncured DGEBA/PCL blend system. Big differences with respect to the melting behavior compared to classical thermoplastic/thermoplastic miscible blends are revealed. The crystallization of the crystallizable phase was found to be very sensitive to the thermal history as manifested by crystallization peaks observed during the first heating scan, the second heating scan, or the phenomenon of the double melting behavior. Figure 3.37 illustrates these effects for the degree of crystallinity as a function of the PCL content in the cured ER/blend. Substantial differences exist between samples as-prepared, cooled from the melt or quenched. No significant effect is depicted for the cooled or the quenched samples when the content

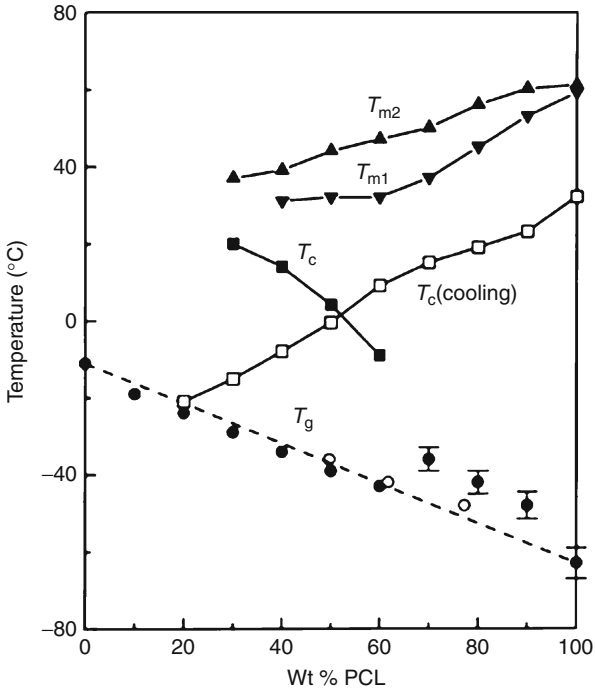

Fig. 3.35 Thermal transitions of the quenched samples of uncured DGEBA/PCL blends. (●) Experimental T_g versus overall blend composition, (□) T_g versus calculated amorphous composition, (——) theoretical curve of T_g according to the fox equation, and (□) T_c cooling (Guo et al. 2001)

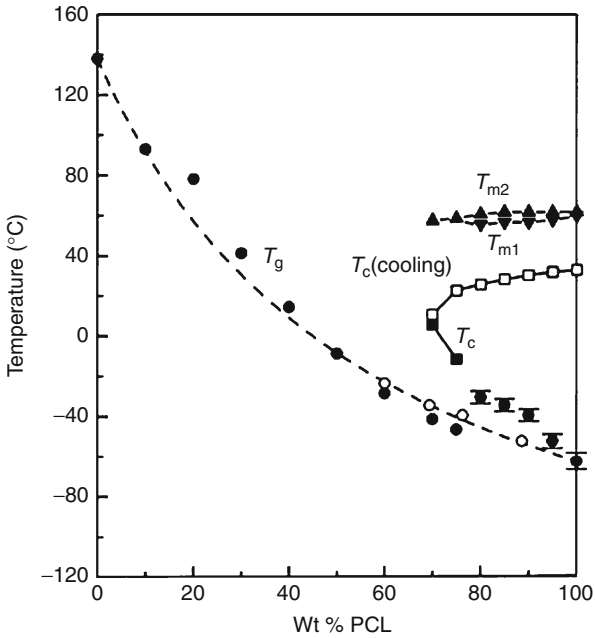

Fig. 3.36 Thermal transitions of the quenched samples of uncured MCDEA-cured ER/PCL blends. (●) Experimental T_g versus overall blend composition, (□) T_g versus calculated amorphous composition, (——) theoretical curve of T_g versus blend composition as predicted by the Gordon-Taylor equation using a value of $k = 0.37$, and (□) T_c cooling (Guo et al. 2001)

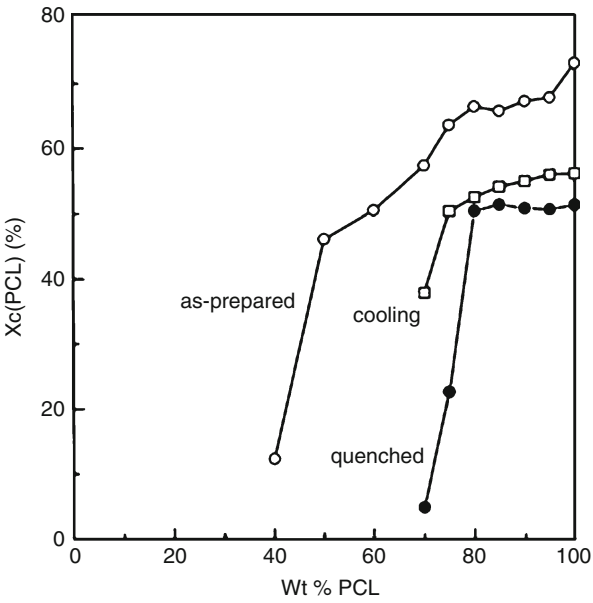

Fig. 3.37 X_c PCL versus PCL weight fraction of the MCDEA-cured ER/PCL blends. (□) as-prepared samples, (●) quenched samples, and (□) X_c PCL developed during the cooling scan (Guo et al. 2001)

of PCL is equal or above 80 wt%. A drastic decrease of crystallinity is however registered below this critical concentration. The as-prepared samples exhibit a decreasing degree of crystallinity when the concentration of PCL is between 100 and 40 wt%.

3.2.6.1 Crystallization Kinetics

The overall crystallization rate of the crystallizable phase in thermosetting/thermoplastic miscible blends is greatly affected by the presence of the thermosetting resin either cured or not (ER cured with MCDEA or uncured DGEBA resin). The crystallinity of PCL in the cured ER/PCL blend decreases much more rapidly with increasing amorphous cured ER content than that of the uncured amorphous DGEBA/PCL blends. The authors ascribed this behavior to the higher T_g of the cured ER restraining the chain mobility for the PCL and thus limiting the extent and rate of crystallization ($T_g = 138$ °C for the cured ER and $T_g = -11$ °C for the uncured DGEBA system).

Halftime of crystallization $t_{1/2}$ as a function of crystallization T_c for cured ER/EO blend reveals that addition of cured ER resin to PEO crystallizable thermoplastic depresses the overall crystallization rate of PEO, and at a fixed T_c, the overall crystallization rate decreases significantly with increasing the concentration of the cured resin ER (Fig. 3.38). Application of the Avrami extrapolation resulted in n values comprised between 3.5 and 5, not changing as the content of ER in the blend is increased. That means the incorporation of cured ER does not affect significantly the nucleation, and growth process is under the conditions the authors selected for the crystallization of PEO.

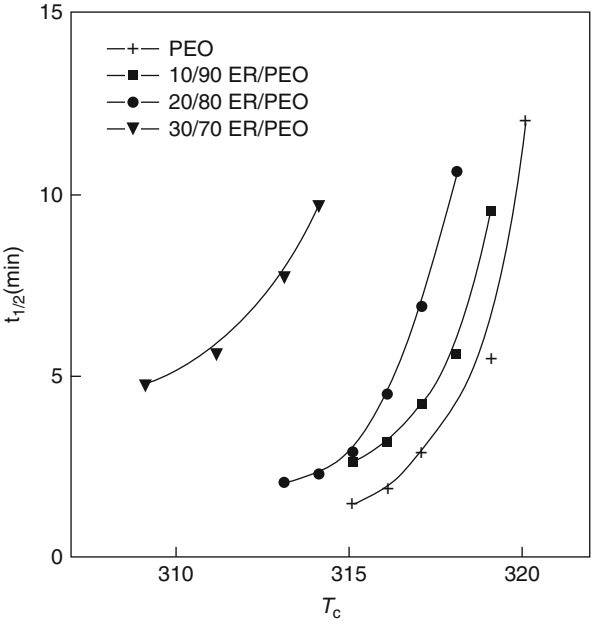

Fig. 3.38 Halftime of crystallization $t_{1/2}$ as a function of crystallization temperature T_c (Guo et al. 2001)

Goossens et al. (2006b, 2007) studied the most challenging aspect which consists of curing the DGEBA and monitoring the crystallization of the POM phase in the DGEBA thermosetting/POM thermoplastic blends system.

The influence of the curing reaction and the resulting reaction-induced phase separation on the crystallization and melting of POM in POM/DGEBA has been studied at two different cure temperatures (180 °C situated above the melting point of POM and 145 °C below it). Various phase morphologies have been generated which allows to investigate the POM crystallization in either a particle-in-matrix or in a phase-inverted phase morphology of POM/DGEBA blends. By using DSC and OM characterization techniques, the authors could demonstrate that at the curing temperature of 180 °C, large differences exist between particle-in-matrix (for 10 wt% POM blends) and phase-inverted structures (20 wt% POM blends) with respect to crystallization behavior. The melting temperatures were almost similar, indicating reorganization in the small POM-rich droplets in the 10 wt% POM blend upon heating. When lowering the curing temperature to 145 °C, isothermal crystallization was induced followed by interspherulitic reaction-induced phase separation (RIPS). Substantial differences were noticed between dynamically and isothermally crystallized POM.

3.2.6.2 Semicrystalline Morphology Development

As in classical amorphous thermoplastic/crystallizable thermoplastic miscible blends, the chains of the thermosetting are rejected from the crystallizing front when the crystallizable thermoplastic is crystallizing in thermosetting/thermoplastic blends. The curing process allows the formation of a network that is not involved

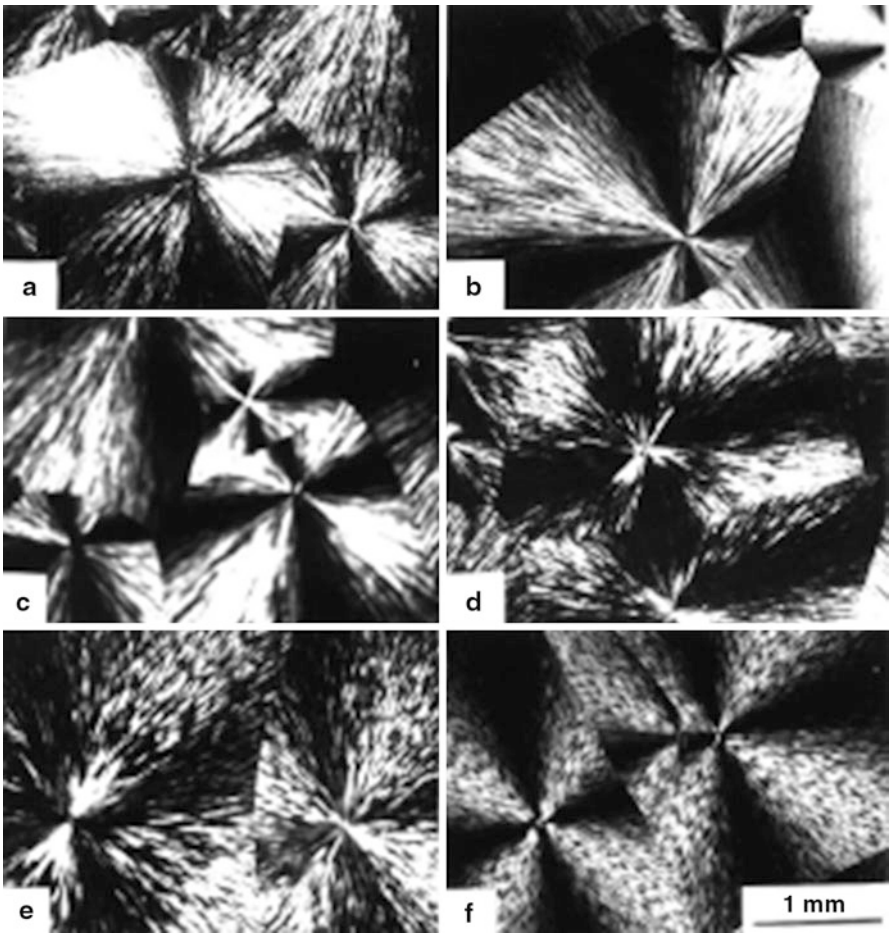

Fig. 3.39 Optical micrographs of ER/PEO blends crystallized at 23 °C. ER/PEO: (**a**) 0/100; (**b**) 10/90; (**c**) 20/80; (**d**) 30/70; (**e**) 40/60; and (**f**) 50/50 (Guo et al. 2001)

in crystallization and is segregated in own domain upon crystallization. The liquid-solid phase separation occurring during the crystallization process of PEO in miscible MCDEA-cured ER/PEO blends requires the segregation and diffusion of amorphous ER away from the crystalline nucleus. The cured ER molecules have a rather limited mobility compared to the linear polymer diluents. Well-defined spherulites were observed in cured ER/PEO blends with ER content up to 50 wt% isothermally crystallized at 23 °C (Fig. 3.39). The spherulitic morphology does not become irregular or coarser with increasing ER content as revealed by OM characterization tools. That indicates that the MCDEA-cured ER is not segregated in the interspherulitic space but must be interlamellarly or interfibrillarly segregated during the process of PEO crystallization. This semicrystalline morphology has been confirmed by using SAXS characterization. The long period increased

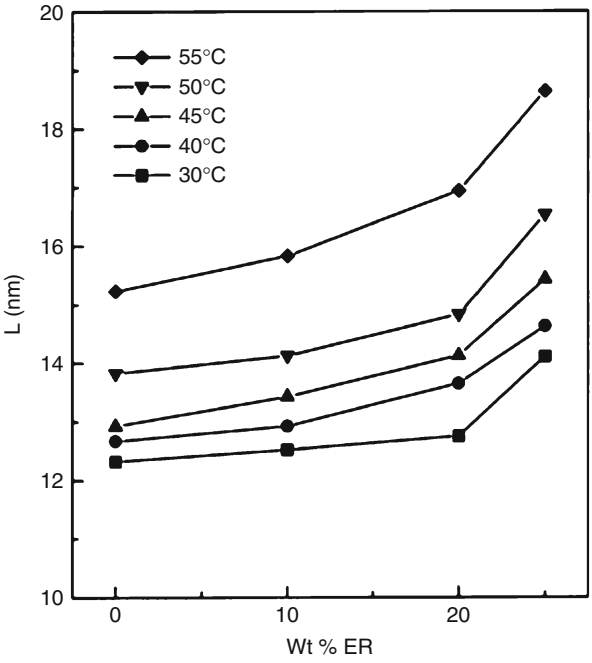

Fig. 3.40 Long period, *L*, as a function of composition for MCDEA-cured ER/PCL blends (Guo et al. 2001)

drastically with increasing ER content at all crystallization temperatures. The interlamellar segregation resulting in an increase of the long period has been reported in a number of cases of miscible polymer blends as, e.g., PVC/PCL (Khambatta et al. 1976a, b) or PSMA/PCL (Defieuw et al. 1989a). In contrast to linear (not cross-linked) polymers, cured resins exhibit high viscosity and slow chain mobility which makes its diffusion at the crystallizing front difficult. Similar trends of the long period increase have been reported for PCL/MCDEA-cured ER blends using SAXS techniques (Guo et al. 2001). When the content of the cured ER was increased from 0 to 25 wt%, the long period was increased by almost 1.5 nm at all crystallization temperatures (Fig. 3.40). That is synonymous of interlamellar segregation of the ER resin upon crystallization of PCL.

3.2.7 Coupling of Demixing and Crystallization Phenomena

3.2.7.1 Thermoplastic/Thermoplastic Blends

Tanaka and Nishi (1985) were the first to report about the existence of coupling between crystallization and demixing in crystallizable blends. A competition between demixing and crystallization is seen in binary blends of a semicrystalline and an amorphous polymer when the crystallization curve and the miscibility gap intersect. The morphology of blends exhibiting such behavior is determined by the ratio of the rate of crystallization and of demixing. Four important situations can be distinguished (Fig. 3.41):

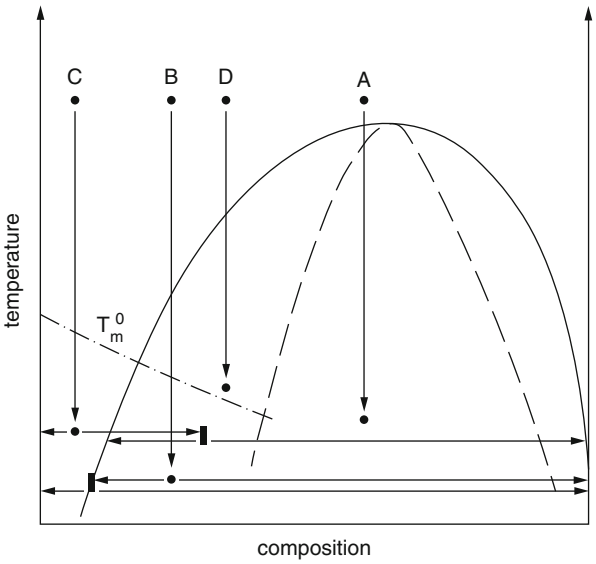

Fig. 3.41 Phase diagram of a binary polymer blend with miscibility gap (UCST) and intersecting crystal/melt coexistence curve. The T_m° curve is extrapolated into the miscibility gap. Quenching routes *A* to *D* are explained in the text. For routes *B* and *C*, the quenching-induced phase separation and crystallization are indicated. —— binodal, ——— spinodal, and —. crystal/melt coexistence curve (Li et al. 1991)

A. Simultaneous spinodal decomposition and crystallization
   The blend is quenched into the unstable region of the miscibility gap and to a temperature below the crystallization/melt coexistence curve.
B. Simultaneous binodal decomposition and crystallization
   This type is similar to spinodal decomposition, but a composition is quenched into the metastable region of the miscibility gap.
C. Crystallization induced decomposition
   The blend is quenched outside the miscibility gap to a temperature below the crystallization/melt coexistence curve. The concentration of the noncrystallizable component increases with crystallization until the miscibility gap is reached inducing demixing.
D. Decomposition-induced crystallization
   The blend is quenched into the miscibility gap to a temperature that lies above the crystallization/melt coexistence curve for the actual composition but lies below the crystallization curve for the binodal composition. When the blend is quenched, demixing occurs resulting in two coexisting phases of which one is able to crystallize. The demixing can result in spinodally as well as in binodally decomposed material.

Only few experimental studies have been performed on polymer blends exhibiting one or more of the phenomena described above (see Table 3.13).

Routes A and C of Fig. 3.41 were discussed by Tanaka and Nishi (1985, 1989) for a system consisting of PCL and PS. In case A coarse spherulite results including PS droplets, while in case C the spherulites are separated and show large droplets on their surface (see Fig. 3.42).

Li et al. (1991, 1993) investigated case B and C for the same system, i.e., PCL/low molecular weight PS, for which the phase diagram is presented in Fig. 3.43.

Table 3.13 Polymer blends showing coupling of demixing and crystallization. The routes describing the type of coupling are explained in the text

Polymer blend	Composition	Type of coupling	References
PCL/PS	40/60	Route B	Li et al. (1991)
	60/40	Route C	
PPE/PEG	12.1/87.9	Route B	Shibanov and Godovsky (1989)
	46/54	Route A	
	93.7/6.3	Route B	
PEG/PPG	88/12	Route B	Shibanov and Godovsky (1991)
	54/46	Route A	
	10.3/89.7	Route B	

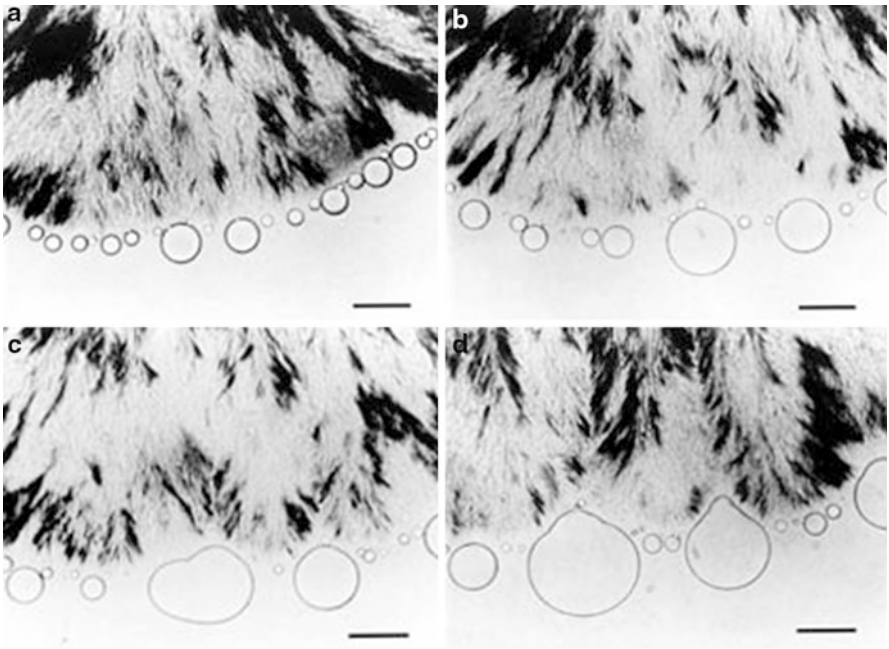

Fig. 3.42 Phase separation behavior at the growth front of the spherulites of PCL during the crystallization process in the PCL/PS 70/30 blend at $T_c = 50$ °C. These morphologies were observed at (**a**) 1,860 min, (**b**) 2,790 min, (**c**) 3,250 min, and (**d**) 4,230 min after quenching (bars: 20 μm) (Tanaka and Nishi 1989)

For route C three different regimes (Fig. 3.44) can still be distinguished depending upon the rate of crystallization, $G = dR/dt$, and the rate of diffusion of the noncrystallizable component, $v_d = (D/t_c)^{1/2}$ (D = diffusion constant and t_c is the correlation time of the macromolecules). Parameters, v_d and G, show a different dependence on temperature (see Fig. 3.45). The growth rate, G, has a maximum

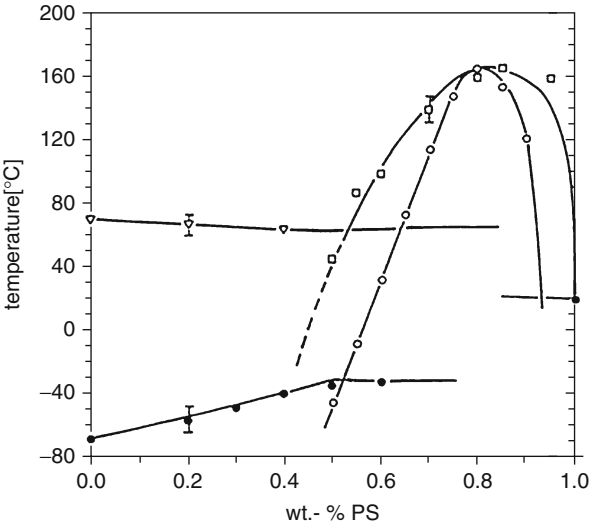

Fig. 3.43 Phase diagram of the PCL/PS blend (*triangles*: homogeneous melt/PCL crystal coexistence curve, *filled circles*: glass-transition curve, *open circles*: spinodal, and *squares*: binodal) (Li et al. 1991)

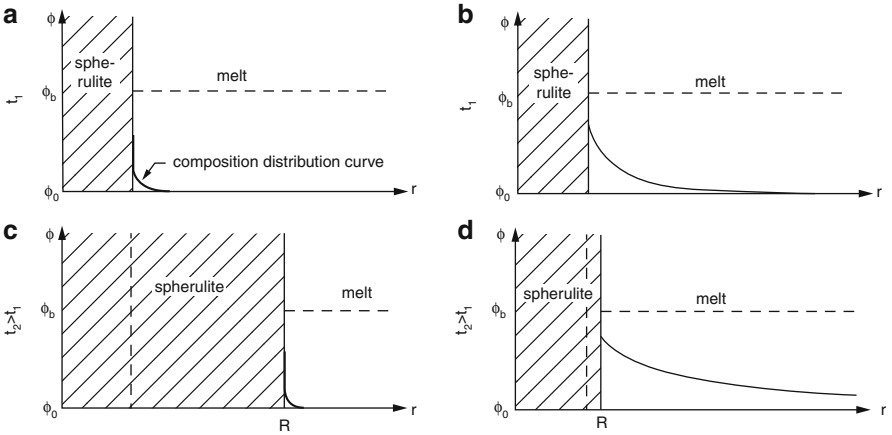

Fig. 3.44 Concentration distribution of PS around a spherulite at different times t and for different ratios G/v_d. ϕ_o, start composition; ϕ_b, binodal composition; and r, local coordinate. (**a**) Regime 1, (**b**) regime 2: the binodal composition is not exceeded, (**c**) as in (**b**) but the binodal composition is exceeded, (**d**) superposition of the concentration distribution curves (*dashed lines*) according to the transition between regime 2 and 3 of two adjacent spherulites (Li et al. 1991)

between the melting temperature and the glass-transition temperature of the blend, whereas the diffusion rate of the amorphous component, v_d, increases with temperature.

1. $v_d << G$: the noncrystallizable component is trapped within the growing crystals. Depending on the composition of the amorphous phase, liquid-liquid

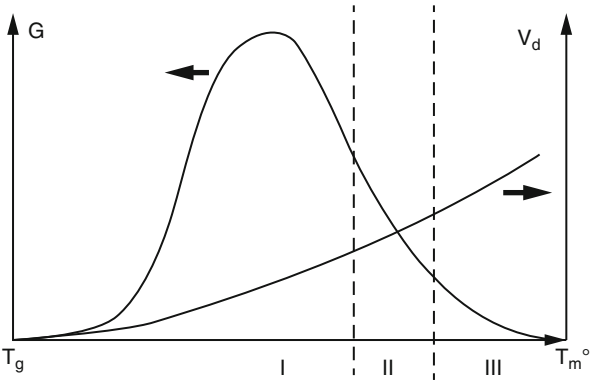

Fig. 3.45 Temperature dependence of the diffusion-driven displacement of the noncrystallizing component, v_d, and the spherulitic growth rate G (Li et al. 1991)

demixing may occur resulting in droplets of noncrystallizing polymer inside the spherulites.

2. $v_d \approx G$: a part of the amorphous component is trapped and another part is segregated from the growing crystals. The concentration of this component increases with crystallization, and finally demixing occurs resulting in the formation of droplets at the spherulite surface.
3. $v_d >> G$: the noncrystalline component is fully segregated into the bulk melt. When the miscibility gap is reached, the melt phase separates homogeneously and binodally.

The crystallization rate is retarded for all regimes, but the extent of hindrance increases from regime 1 to 3. It should be noted that the diffusion of the crystalline polymer occurs on a lamellar scale (about 10 nm), whereas the diffusion of the amorphous component, induced by demixing, takes place on a spherulitic scale (10–20 μm). Under normal processing conditions, crystallization presumably takes place at a higher rate than the demixing.

The morphology resulting from the three regimes are presented in the Fig. 3.46 (regime 1), Fig. 3.47 (regime 2), and Fig. 3.48 (transition from regime 2 to 3) for the PCL/PS system.

A demixing-induced crystallization is shown in Fig. 3.49 (route B in Fig. 3.41) for the binary PCL/PS 40/60 blend.

3.2.7.2 Thermoplastic/Thermosetting Blends

Curing of the thermosetting component and crystallization of the semicrystalline thermoplastic blend partner are two processes that induce phase separation in thermosetting/thermoplastic miscible blend. The new phase morphology that could be generated from the intimately miscible molecules of both components depends on the temperature and kinetics of the curing reaction of the thermosetting resin and of the crystallization of the thermoplastic phase. Semicrystalline thermoplastics like PCL (Guo et al. 2001a, b), PBT (Kulshreshtha et al. 2003a, b), and syndiotactic polystyrene (Schut et al. 2003; Salmon et al. 2005) have been used with curable thermosetting partners with which they form miscible blends before

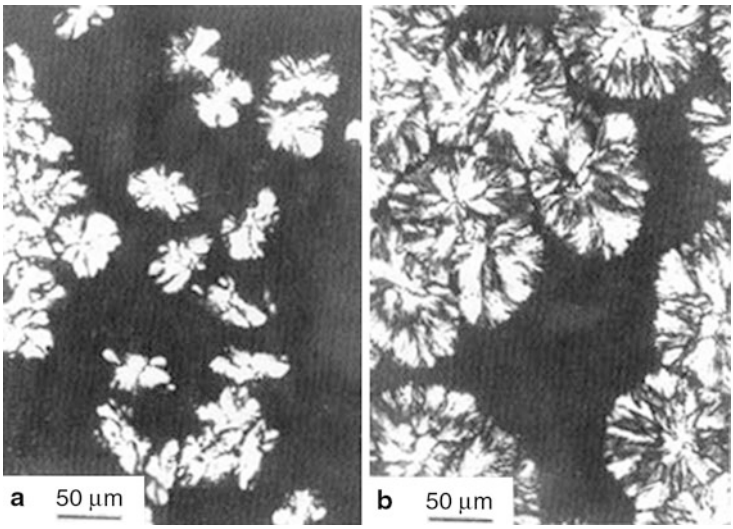

Fig. 3.46 Morphology development in a PS blend with 60 wt% PCL at 44 °C after (**a**) 55 min and (**b**) 126 min (bar: 50 µm) (Li et al. 1991)

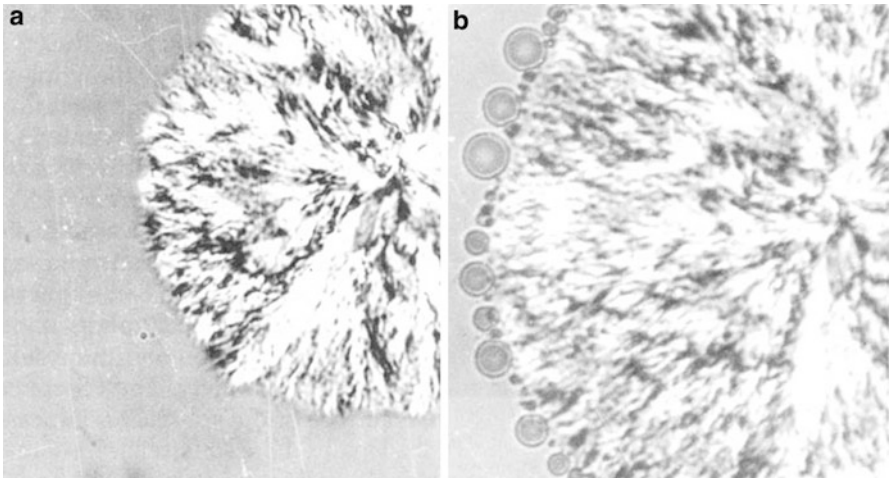

Fig. 3.47 Morphology development in a PS blend with 60 wt% PCL at 49 °C after (**a**) 92 h and (**b**) 142 h (bar: 25 µm) (Li et al. 1991)

any curing or crystallization. Crystallization in thermosetting blends containing a crystallizable thermoplastic component will be affected by the miscibility, the phase behavior and the morphology of the cross-linked blends, and the topological effect of the network (Guo et al. 1991, 2004; Lu et al. 2003; Zheng et al. 2003).

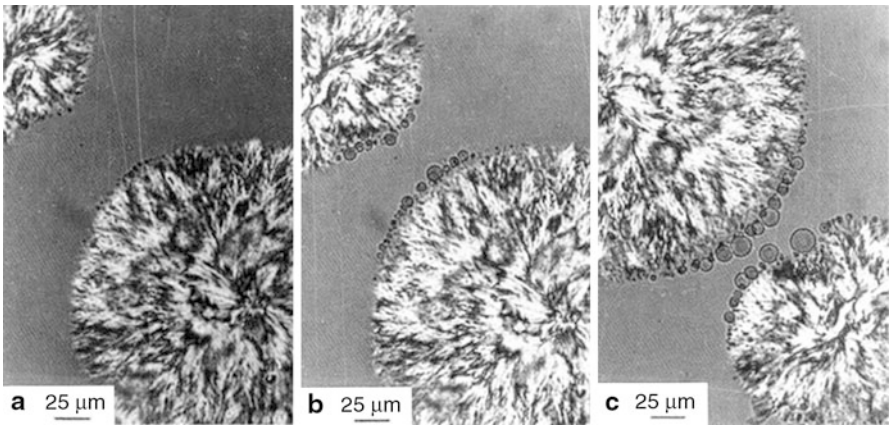

Fig. 3.48 Morphology development in a PS blend with 60 wt% PCL at 51 °C after (**a**) 91.5 h, (**b**) 100 h, and (**c**) 109 h (Li et al. 1991)

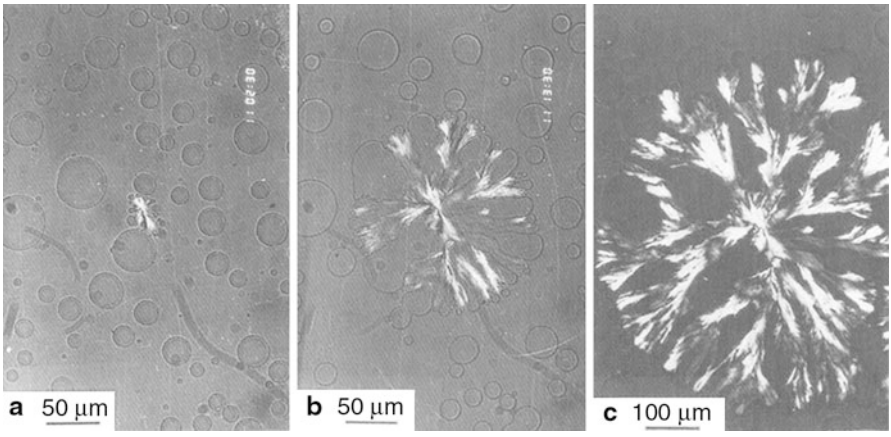

Fig. 3.49 Phase separation followed by crystallization in a PS blend of 40 wt% PCL at 46 °C after (**a**) 2.5 h, (**b**) 13.5 h, and (**c**) 27 h (Li et al. 1991)

By selecting POM/DGEBA/DDS thermosetting/thermoplastic miscible blends, Goossens et al. (2006a, b) could elucidate how the phases are reorganized upon curing of the thermosetting and crystallization of the thermoplastic. Depending on the experimental conditions chosen, crystallization of POM can be investigated before or after the reaction (curing)-induced phase separation (RIPS), i.e., crystallization in homogeneous blend or in a phase-separated one. Three cure temperatures (150, 145, and 140) situated below the melting point of POM were examined. Curing at these temperatures will alter the starting order of the RIPS and crystallization of POM. Both processes will mutually affect each other, leading to complex blend morphologies. Curing at 150 °C is a situation where:

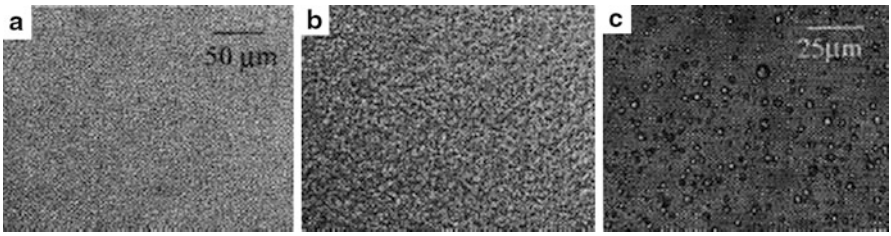

Fig. 3.50 OM pictures of a blend with 10 wt% POM cured at 150 °C for different times: (**a**) 29 min, (**b**) 44 min, and (**c**) 120 min (Goossens et al. 2006a)

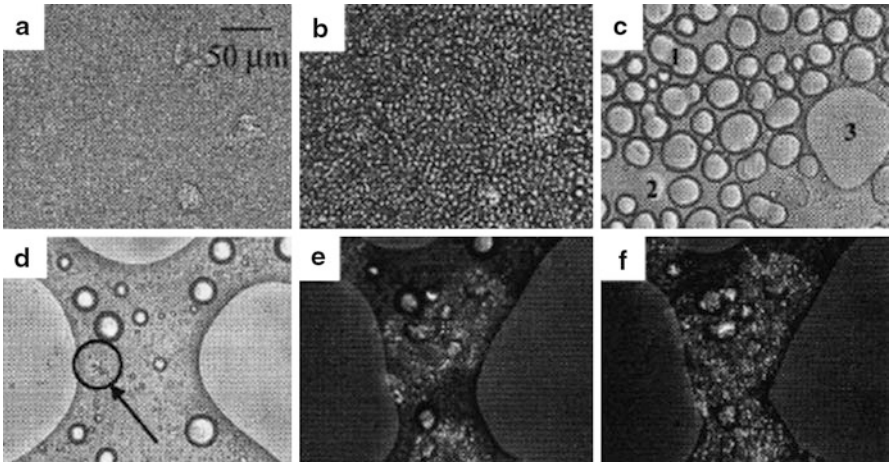

Fig. 3.51 OM pictures of a blend with 20 wt% POM cured at 150 °C for different times: (**a**) 31 min, (**b**) 35 min, (**c**) 41 min, (**d**) 45 min, (**e**) 66 min, and (**f**) 71 min (Goossens et al. 2006a)

(i) *Phase separation precedes the isothermal crystallization* (*curing at* 150 °C). As a consequence of RIPS due to curing, the three initially miscible blends, containing 10, 20, and 30 wt% POM, evolved to a co-continuous and then to a droplet (POM rich)-in-matrix (epoxy rich) phase morphologies (Figs. 3.50, 3.51 and 3.52). For the blends with 10 wt% POM, no isothermal crystallization was depicted because the difference between the cure temperature (150 °C) and the homogeneous crystallization temperature (85 °C) was too large to induce homogeneous crystallization in the dispersed POM-rich droplets. In contrast, at a content of 20 wt%, POM isothermal crystallization was observed after phase separation has set in via successive spinodal demixing, break up into epoxy-rich droplets dispersed in a POM-rich matrix and coalescence which increased particle size. Fifteen minutes after, the liquid-liquid demixing has set in, and growing spherulites were observed in the POM-rich matrix phase in between the epoxy droplets. The growth of spherulites in the POM-rich matrix was also observed during the phase separation process of a 30 wt% POM blend, cured at 150 °C.

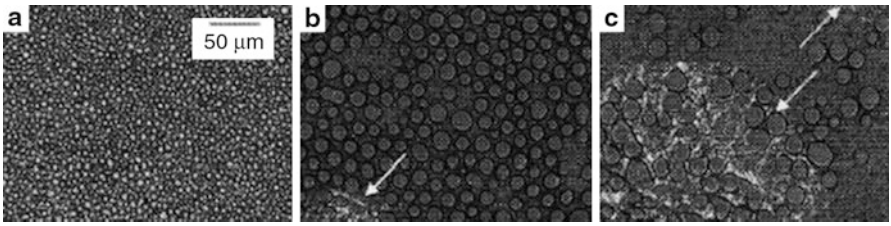

Fig. 3.52 OM pictures of a blend with 30 wt% POM cured at 150 °C for different times: (**a**) 50 min, (**b**) 66 min, and (**c**) 92 min (Goossens et al. 2006a)

(ii) *Isothermal crystallization followed by phase separation* (*curing at* 145 °C). At this curing temperature, isothermal crystallization starts before the liquid-liquid phase separation as caused by the curing of the epoxy resin. Homogeneous blends containing 5 wt% POM developed spherulites after 22 min. Thirty three minutes later, interspherulitic zone starts to phase separate leading to a co-continuous phase structure. While the liquid-liquid phase separation proceeds, the spherulites continue to grow through the POM-rich continuous part of the co-continuous structure. Crystallization stops as the phase structure evolved to a droplet-matrix as POM molecules need to diffuse through the highly viscous cured epoxy. The authors could differentiate between three zones within the POM spherulite: zone 1is the spherulite growth in the homogeneous sample where no RIPS occurs yet, zone 2 is the spherulite growth in the co-continuous structure, zone 3 is limited because of the slow diffusion of very diluted POM molecules in the epoxy-rich matrix, and, finally, zone 4 which represents the volume hat has been phase separated but did not undergo crystallization at 145 °C. Blends containing 10 wt% POM exhibits the same trend. In contrast, increasing the POM content beyond 10 wt% gave a different phase-separated process. For example, the co-continuous structure was found to break up in a phase-inverted structure instead of a particle/matrix structure. Increasing the amount of POM resulted in higher nucleation density and an increased crystallization growth rate.

(iii) *Isothermal crystallization without phase separation* (*curing at* 140 °C). Decreasing the cure temperature to 140 °C will increase the supercooling and consequently the nucleation density. Indeed, when a blend with 20 wt% POM was cured at 140 °C, spherulites appeared as early as 1 min which is a direct result of the higher supercooling. After 20 min the spherulites are almost volume filling due to higher nucleation density and the higher local crystallization rate. This suggests that nearly all the epoxy resin is rejected interlamellar or interfibrillar.

3.2.8 Conclusions

Most of the fundamental and experimental aspects related to the crystallization phenomena occurring in miscible polymer blends are relatively well known. Much research has been done in the 1970s and 1980s, especially the development of the

general theory concerning the crystallization process itself and the concomitant kinetics. These theories could be adapted to simple systems under quiescent conditions. Later, modifications have been made to the original concepts to take into account the effects occurring under processing conditions (for instance, the nonisothermal Avrami theory), unusual phenomena not responding to the simple theory (for instance, the nonlinearity of Hoffman-Weeks plots), coupling of the crystallization with demixing processes, etc.

The addition of a second component to a crystallizable polymer has several profound consequences:

1. Depending on the glass-transition temperature of the added component, the crystallization window is widened or narrowed.
2. The type of added component is also important. Crystallization in the presence of an amorphous component is paralleled to segregation. The segregation can occur into three regions: interspherulitic, interfibrillar, and interlamellar, depending on the ratio of the diffusion rate of the amorphous component and of the crystallization rate of the crystallizable component. In blends of two crystallizable polymers, the phenomena such as separate crystallization, concurrent crystallization, and cocrystallization may take place.
3. The spherulite growth rate changes by blending due to interactions between the components, the necessity of diffusion of both components, the concentration change in the amorphous phase during crystallization, and the possible changes of the glass-transition and melting temperature.
4. The overall kinetics are strongly affected by the type of amorphous component, its influence on the nucleation of the crystallizable component, the degree of miscibility, the presence of secondary nucleation effects, and the molecular weight of both components.
5. The melting behavior is often complex due to phenomena such as reorganization, secondary crystallization, demixing, etc. A depression of the equilibrium melting temperature is often observed.
6. In case of thermosetting/thermoplastic initially miscible blends, the duration and the curing temperature of the thermosetting are crucial conditions which determine the crystallization kinetics, the type of semicrystalline phase morphology generated, as well as the melting behavior of the semicrystalline partner of the blend. Depending on the temperature at which crystallization is carried out, competition between demixing and crystallization can take place.

3.3 Crystallization, Morphological Structure, and Melting Behavior of Immiscible Polymer Blends

3.3.1 Introduction

From a commercial point of view, semicrystalline polymers are of prime importance. Among the four mostly used commodity plastics (PE, PS, PVC, and PP), only PS is completely amorphous. The three semicrystalline polymers account for the

largest volume of the commercial polymer blends. A majority of the polymer blends contains at least one crystalline component. Most polymer blends are immiscible.

The immiscible semicrystalline polymer blends may be classified in terms of crystalline/crystalline systems in which both components are crystallizable and crystalline/amorphous systems in which only one component can crystallize, being either the matrix or the dispersed phase (Utracki 1989). Numerous authors have been investigating the crystallization behavior of immiscible blends. In Tables 3.14 and 3.15, an overview is given of a number of important immiscible crystallizable blend systems.

The properties of the finished articles made from immiscible blends are governed by the morphology created as a result of the interplay of processing conditions and inherent polymer characteristics, including crystallizability. Therefore, a scientific understanding of the crystallization behavior in immiscible polymer blends is necessary for the effective manipulation and control of properties by compounding and processing of these blends.

In the following part, a discussion on the crystallization behavior in immiscible polymer blends is given, including the nucleation behavior, spherulite growth, overall crystallization kinetics, and final semicrystalline morphology. Each topic is illustrated with several examples from the literature to allow the reader to find enough references on the discussed subject for further information.

3.3.2 Factors Affecting the Crystallization Behavior of Immiscible Polymer Blends

The discussion on the crystallization behavior of neat polymers would be expected to be applicable to immiscible polymer blends, where the crystallization takes place within domains of nearly neat component, largely unaffected by the presence of other polymers. However, although both phases are physically separated, they can exert a profound influence on each other. The presence of the second component can disturb the normal crystallization process, thus influencing crystallization kinetics, spherulite growth rate, semicrystalline morphology, etc.

Important factors are:

- Molecular structure and molecular mass of the components
- Blend composition
- Type and degree of dispersion of the phases in the melt state
- Phase interactions (e.g., nature of the interface, migration of nuclei, etc.)
- Melt history (T_{melt}, t_{melt}, etc.)
- Crystallization conditions (e.g., T_c, cooling rate, etc.)
- Physical crystallization conditions (surrounded by melt or solidified material)

These factors influence the crystalline morphology development, resulting in changes of crystallization parameters such as:

- Nucleation density, N
- Spherulite growth rate, G

Table 3.14 Thermal data on immiscible crystalline/amorphous blends (After Nadkarni and Jog 1991)

Comp. A (cryst.)	Comp. B (amorph.)	$T_{g,A}$ (°C)	$T_{g,B}$ (°C)	$T_{c,pure\ A}$ (10°C/min)	$T_{m,\ pure\ A}$	Physical state of the amorph. comp. at T_c	References
LDPE	PS	−123	103	101	115–123	±solidified	Baïltoul et al. (1981)
LDPE	PMMA	−123	100–123	101	115–123	Solidified	
LDPE	PC	−123	147	101	115–123	Solidified	
LLDPE	PS	−123	103	102–110	125	Viscous melt/ ±solid	Müller et al. (1995), Morales et al. (1995)
HDPE	PS	−123	103	118	132–140	Melt	Aref-Azar et al. (1980)
HDPE	PC	−123	147	118	132–140	Solidified	Kunori and Geil (1980)
PP	EPDM[a,b]	−10	100	121	165	Melt	Martuscelli (1984, 1985), Bartczak et al. (1984), Martuscelli et al. (1983), Karger-Kocsis et al. (1979), Greco et al. (1987)
PP	EPR[a,b]	−10	±−45	121	165	Melt	Martuscelli et al. (1982), Coppola et al. (1987), Bartczak et al. (1984), Kalfoglou (1985), Karger-Kocsis et al. (1979), Martuscelli (1985)
PP	PIB[b]	-10	–	121	165	Melt	Martuscelli (1984, 1985), Bartczak et al. (1984), Martuscelli et al. (1982, 1983), Bianchi et al. (1985)
PP	PS	−10	103	121	165	Melt	Bartczak et al. (1987), Wenig et al. (1990), Wei-Berk (1993), Santana and Müller (1994), Han et al. (1977), Hlavatá and Horák (1994)

(*continued*)

Table 3.14 (continued)

Comp. A (cryst.)	Comp. B (amorph.)	$T_{g,A}$ (°C)	$T_{g,B}$ (°C)	$T_{c,pure\ A}$ (10°C/min)	$T_{m,\ pure\ A}$	Physical state of the amorph. comp. at T_c	References
PP	PC	−10	147	121	165	Solidified	
PP	TR (SBS)	−10	–	121	165	Melt	Ghijsels et al. (1982), Karger-Kocsis et al. (1979)
PET	PMMA	70	100–123	150	257	Melt	Nadkarni and Jog (1987)
PET	PS	70	103	150	257	Melt	Quirk et al. (1989)
PET	PPE	70	215	150	257	Solidified	Quirk et al. (1989), Liang and Pan (1994)
PVDF	PVME	−45		140	172		
PEG	PS	−60	103	40	65	Solidified	Lotz and Kovacs (1969)[c], O'Malley et al. (1969)[c]
PEG	PI	−60	10	40	65	Viscous melt	Robitaille and Prud'homme (1983)[d]
POM	PS	−80	103	143	170	Melt	
POM	PC	−80	147	143	170	±solidified	Chang et al. (1991)
PA-6	PC	52	147	199	210	Viscous melt	
PA-6	PS	52	103	199	210	Melt	Ide and Hasegawa (1974), Chen et al. (1988)
PA-6	Elastomer	52	–	199	210		Martuscelli (1984)
sPS	PVME[e]	95	−28	±245	270	Melt	Cimmino et al. (1991, 1993)
PEMA	PMMA	67	105				Kwei et al. (1977)

[a]EPR and EPDM are amorphous only if they are random copolymers
[b]Small and defective PP molecules or amorphous PP chains are partially soluble in the elastomer phase; this can lead to a slightly deviating behavior Martuscelli et al. (1983), Kalfoglou (1985)
[c]Studies have been done on block copolymers of either PEG-PS-PEG or PEG-PS
[d]Studies were done on liquid/liquid phase-separated triblock copolymer PEG-PI-PEG
[e]sPS/PVME is immiscible as long as the PVME content is higher than 10 %

Table 3.15 Thermal data on immiscible crystalline/crystalline blends (After Nadkarni and Jog (1991))

Comp. A (matrix)	Comp. B (minor)	$T_{g,A}$	$T_{g,B}$	$T_{c,A}$	$T_{c,B}$	$T_{m,A}$	$T_{m,B}$	Physical condition for cryst. of A/B		References
LLDPE	PP	−123	−10	102–110	121	125	165	Solid	Melt	Zhou and Hay (1993), Long et al. (1991), Müller et al. (1995), Morales et al. (1995)
LDPE	PP	−123	−10	101	121	115–123	165	Solid	Melt	Teh (1983)
HDPE	EPR[a]	−123	±−40	118		132–140		Viscous melt	Solid	Greco et al. (1987a)
HDPE	PA-6	−123	52	118	199	132–140	225	Solid	Melt	Chen et al. (1988)
HDPE	PP	−123	−10	118	121	132–140	165	Solid	Melt	Bartczak and Galeski (1986), Martuscelli et al. (1980), Rybnikâr (1988)
HDPE	POM	−123	−80	101	143	115–123	170	Solid	Melt	Frensch et al. (1989), Klemmer and Jungnickel (1984)
HDPE	PPS	−123	80	118	256	132–140	280	Solid	Melt	Nadkarni et al. (1987), Nadkarni and Jog (1986), Chen and Su (1993)
PE	PA-11	−123	47	100–120		115–140	180	Solid	Melt	Chen et al. (1988)
PP	LLDPE	−10	−123	121	102–110	165	125	Melt	Solid	Long et al. (1991), Flaris et al. (1993), Zhou and Hay (1993), Plawky and Wenig (1994), Müller et al. (1995)
PP	HDPE	−10	−123	121	118	165	132–140	Supercooled melt	Solid	Bartczak et al. (1986), Noel and Carley (1984), Teh et al. (1994a), Lovinger and Williams (1980),

(*continued*)

Table 3.15 (continued)

Comp. A (matrix)	Comp. B (minor)	$T_{g,A}$	$T_{g,B}$	$T_{c,A}$	$T_{c,B}$	$T_{m,A}$	$T_{m,B}$	Physical condition for cryst. of A/B		References
										Wenig and Meyer (1980), Teh et al. (1994b), Gupta et al. (1982), Martuscelli et al. (1980), Rybnikâr (1988)
PP	LDPE	−10	−123	121	101	165	115–123	Melt	Solid	Bartczak et al. (1984), Martuscelli (1985), Galeski et al. (1984), Teh (1983), Teh et al. (1994a)
PP	EPR[a]	−123	±−30	121		165	±125	Melt	Solid	Greco et al. (1987b), Martuscelli (1984)
PP	PA-6	−10	52	121	199	165	210	Solid	Melt	Liang et al. (1983)[b], Ikkala et al. (1993), Moon et al. (1994), Park et al. (1990), Grof et al. (1989)[b], Ide and Hasegawa (1974)
PP	PA-12	−10		121	154	165	171–179	Solid	Melt	Tang et al. (1994)
PP	PEG	−10	−60	121	38	165	65	Melt	Solid	Bartczak and Galeski (1986), Tang and Huang (1994b)
PP	PVDF	−10	−45	121	140	165	172	Solid		Supercooled melt
Shingankuli et al. (1988)										
PET	HDPE	70	−123	150	118	257	132–140	Melt	Solid	Wilfong et al. (1986)
PET	LLDPE	70	−123	150	102–110	257	125	Melt	Solid	Wilfong et al. (1986)
PET	PP	70	−10	150	121	257	165	Melt	Solid	Wilfong et al. (1986)
PET	PPS	70	80	150	256	257	280	Solid[c]	Melt[c]	Shingankuli et al. (1988))
PPS	HDPE	80	−123	256	118	280	132–140	Superheated melt	Solid	Nadkarni et al. (1987), Nadkarni and Jog (1986), Jog et al. (1993)

PPS	PET	80	70	256	150	280	257	Supercooled melt	Solid	Shingankuli et al. (1988), Jog et al. (1993)
PA-6	PP	52	−10	199	121	225	165	Melt	Solid	Ikkala et al. (1993), Holsti-Mietinen et al. (1992), Park et al. (1990), Ide and Hasegawa (1974), Tang and Huang (1994a)
PA-6	HDPE	52	−123	199	118	225	132–140	Melt	Solid	Chen et al. (1988)
PA-6	LLDPE	52	−123	199	102–110	225	125	Melt	Solid	
PA-6	PVDF	52	−45	199	140	225	172	Melt	Solid	Frensch and Jungnickel (1989, 1991), Frensch et al. (1989)
PA-66	PVDF	60	−45	229	140	264	172	Melt	Solid	Frensch and Jungnickel (1991)
PA-6	POM	52	−80	199	143	225	170	Melt	Solid	
PVDF	PA-6	−45	52	140	199	172	210	Solid[c]	Melt[c]	Frensch and Jungnickel (1989), Frensch et al. (1989)
PVDF	PA-66	−45	60	140	229	172	264	Solid	Melt[c]	Frensch and Jungnickel (1991)
PVDF	PBT	−45	35	140	180	172	225	Solid[c]	Melt[c]	Frensch and Jungnickel (1989), Frensch et al. (1989)
PVDF	PCL	−45	−60	140		172	60	Melt	Solid	

[a]EPDM and EPR copolymers are crystalline if block copolymer and depending on the ethylene/propylene ratio; in blends with PE or PP, they can extract to some extent (depending on the ethylene/propylene ratio) amorphous low molecular weight molecules from the PP or PE phase that slightly influence the crystallization and melting behavior

[b]Study done on fibers

[c]Sometimes coincident crystallization occurs in finely dispersed morphology

– Overall crystallization rate, K
– Total degree of crystallinity, X_c
– Semicrystalline morphology, i.e., shape, size, and texture of the spherulites, interspherulitic boundaries, etc.

To discuss these topics in a systematic way, a distinction will be made between three main blend categories, namely:

1. Blends with a crystallizable matrix and an amorphous dispersed phase
2. Blends with an amorphous matrix and a crystallizable dispersed phase
3. Blends containing two crystallizable components

3.3.3 Blends with a Crystallizable Matrix and an Amorphous Dispersed Phase

In immiscible blends, the phases are separated in the molten state, thus before crystallization of the matrix starts. The dispersed amorphous phase is assumed to be homogeneously distributed in the melt in droplet-like domains.

3.3.3.1 Nucleation Behavior of the Crystallizable Matrix

General Considerations Related to Heterogeneous Nucleation

When a crystallizable component forms the matrix phase in a polymer blend, nucleation can occur via *heterogeneous nucleation* by heterogeneities in a similar way as in the pure component. The heterogeneities, available in the melt, can be residual catalysts, fillers, impurities, crystalline residues (due to incomplete melting), etc. Each type of "heterogeneity" has its own typical activation energy for the formation of an "active nucleus of critical size," corresponding to a certain degree of undercooling ($T_m - T_c$). When $T_{c,1}$ is reached during cooling from the melt, all heterogeneities of type 1 (which have the lowest activation energy) become active and the nucleation of the crystallizable phase is induced. Once the crystallization is initiated by the primary nucleation, it can further spread over the whole available material via secondary nucleation, before any other type of heterogeneity can become active.

Since in immiscible blends the phases are physically separated, the same heterogeneities that nucleate the homopolymer at $T_{c,pure}$ may nucleate the crystallizable matrix. As a result, the crystallization temperature, T_c, of the blend during cooling from the melt will in general not differ that much from the T_c of the pure component.

Some general principles governing the crystallization behavior of homopolymers also remain valid for immiscible polymer blends in which the crystallizable component forms the continuous phase.

The *premelting temperature*, T_{melt}, may have a profound influence on the crystallization temperature of the matrix, T_c, during cooling from the melt (Table 3.16).

The higher the temperature at which the blend is kept in the melt prior to crystallization, the less residual crystalline parts (otherwise leading to self-seeded

Table 3.16 Influence of T_{melt} and $T_{c,iso}$ upon the nucleation behavior in crystalline/amorphous polymer blends

Blend system	Influence of T_{melt}	Influence of $T_{c,iso}$	References
PP/EPDM		x	Martuscelli et al. (1983)
		x	Martuscelli (1985)
PP/EPR		x	Martuscelli et al. (1982)
	x	x	Martuscelli (1985)
PP/PIB		x	Bianchi et al. (1985)
		x	Martuscelli (1985)
PP/PS	x	x	Bartczak et al. (1987)
		x	Wenig et al. (1990)
sPS/PVME[a]		x	Cimmino et al. (1993a)

[a]sPS/PVME is only immiscible in those blends where the amount PVME exceeds 10 %

nucleation) remain in the melt. As a result, fewer nuclei are available to nucleate the melt phase, thus leading to the formation of fewer but larger spherulites.

Another less important factor is the *isothermal crystallization temperature*, $T_{c,iso}$, when the crystallization is carried out at a constant temperature (Table 3.16). When a crystallization experiment is performed at lower temperatures, the activation energy for nucleation of several types of heterogeneities can be overcome. At that $T_{c,iso}$, more nuclei become active, leading to the formation of a larger number of smaller spherulites.

Although most principles for the crystallization of homopolymers remain valid for immiscible blends with a crystallizable matrix, the crystallization behavior can be altered by two phenomena, inherently correlated with immiscible two-phase systems, namely, migration of impurities during melt-mixing and the nucleating activity of the interface between two phases.

Migration of Impurities During the Melt-Mixing Process

During the melt-mixing process, heterogeneous impurities can migrate across the interface between both blend phases (Bartczak et al. 1986). The driving force for this migration is the interfacial free energy of the impurity with respect to its melt phase, $\sigma_{i,1}$. If this interfacial free energy is higher than the interfacial free energy of that impurity within the second melt phase, $\sigma_{i,2}$, it is energetically more favorable for the impurity to move to the second phase. As soon as it has the "possibility," it will migrate across the interface (Galeski et al. 1984).

Several factors determine the "possibility" for the impurities to migrate from one phase to the other phase during the melt-mixing process.

Because the migration of heterogeneities can only occur when they find themselves close enough to the interface, the melt-mixing conditions play an important role (Bartczak et al. 1987; Fig. 3.53). It must be clear that the longer the mixing or the more intense the mixing, the higher the probability that nuclei find themselves somewhere at an interface, where they can easily migrate. Thus, the effect of migration on the crystallization behavior will be more pronounced – migration of

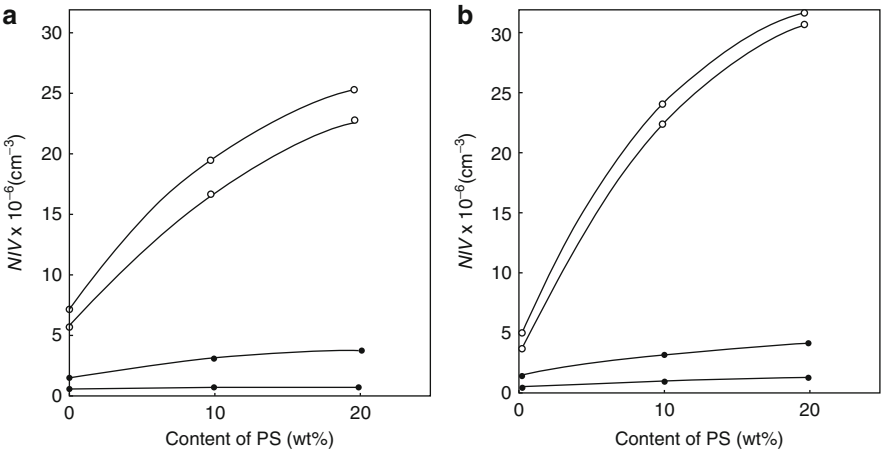

Fig. 3.53 Influence of the amount of dispersed phase, mixing time, and crystallization temperature, T_c, on the amount primary nuclei active for crystallization at T_c in a PP/PS blend. All samples have been molten up at 220 °C; (**a**) 2× mixing, (**b**) 3× mixing; $T_{c,iso}$ was set to 119 °C (▽), 123 °C (Δ), 125 °C (○), and 130 °C (□) (Bartczak et al. 1987)

heterogeneities across the interface will not proceed in the absence of mechanical mixing (Bartczak et al. 1987). Furthermore, the possibility for impurities to be located close enough to an interface stands in direct relation to the phase morphology generated during the melt-mixing (Bartczak et al. 1987).

As the relative amount of the phases changes, the amount of nuclei that can migrate varies, and the effect of these migrating nuclei on the crystallization behavior changes. This can be understood if one assumes an amorphous/crystalline blend system in which heterogeneities migrate from the crystallizable matrix toward the second phase. With increasing amount of the second phase, the total amount of available nuclei is lower, and they will migrate toward a larger volume of the second phase, which may lead to a more than proportional decrease of the nucleation density in the crystallizable phase.

However, the melt morphology also changes with varying content of the phases. By increasing the amount of the second phase, the dispersion becomes coarser due to coalescence of droplets. This implies that larger droplets are formed, and as a consequence, a lower total interfacial contact area is available. Hence, less impurities will find themselves located close enough to the interface to be able to migrate. It should be remarked that a critical volume fraction of the second component could exist, which is able to absorb all active nuclei of the crystallizable matrix. Adding higher amounts of the second component will no longer decrease the number of active nuclei per volume unit of the crystallizable matrix. An example is given for the PP/LLDPE blend, where LLDPE is in the molten state during PP crystallization (and thus can be considered as an amorphous melt) (Fig. 3.54).

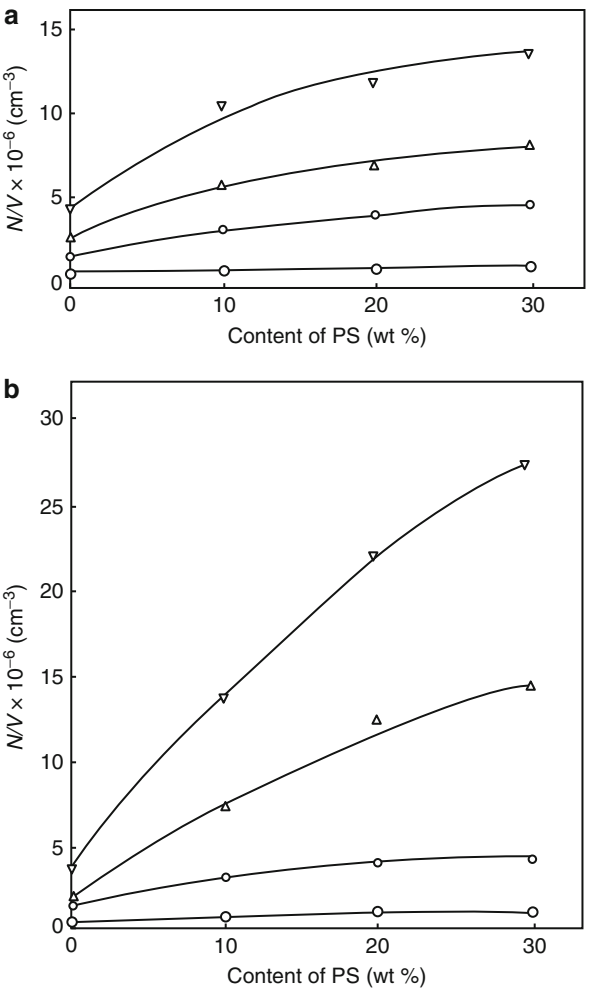

Fig. 3.54 Influence of LLDPE on the nucleation of PP at various temperatures: (**a**) measured as blend volume and (**b**) calculated as PP volume fraction (Long et al. 1991)

Finally, a factor that also may influence the degree of migration is found to be the *interfacial free energy between both phases of the blend in the melt*, $\sigma_{1,2}$. If $\sigma_{1,2}$ is high, due to a high degree of immiscibility between the phases, a sharper interface will be formed. Nuclei close to such a sharp interface are found to migrate fast and efficient (Bartczak et al. 1987), in contrary to partially miscible blends where no evidence could be found for such a fast migration (Galeski et al. 1984; Bartczak et al. 1986).

In general, the migration of heterogeneities from one phase to the other in blends with a crystallizable matrix only slightly affects the crystallization temperature of the matrix during cooling from the melt (Bartczak et al. 1987). More important should be the influence of migration on the final semicrystalline morphology. This aspect will be discussed in Sect. 3.3.3.4.

Nucleating Activity of the Interface

The second phenomenon found to influence the crystallization behavior in immiscible polymer blends is the nucleating activity of the interface (Bartczak et al. 1987; Wenig et al. 1990; Wei-Berk 1993).

In immiscible polymer blends with a high degree of immiscibility such as PP/PS, it has been shown that nucleation at the interface affects the crystallization behavior. Wenig et al. (1990) showed that with increasing the amount of PS in a blend with PP, the nucleation shifted from preferentially thermal (related to the degree of undercooling) to more athermal. This was explained by the effect of heterogeneous surface nucleation at PS interfaces (Fig. 3.53).

However, not all interfaces can produce additional nucleating centers. For immiscible and highly incompatible polymer blends, since their interfacial tension is higher, the interface is very sharp (Helfand and Tagami 1972). Such interfaces can rarely induce new nuclei. Furthermore, on a molecularly smooth surface, a new layer can only be grown after secondary nucleation, and a somewhat lower energy barrier is present, since the surface area which must be created is smaller (Hoffmann et al. 1992). Only an interface which wets well with the crystallizable matrix, so that a crystalline chain can deposit on it, can cause heterogeneous nucleation (Turnbull 1950; Geil 1973). The wetting ability between two melt phases can be calculated from the spreading coefficient F_{12}. An example can be given by the immiscible polymer blend pair PP/PS (Bartczak et al. 1987; Fig. 3.53).

Furthermore, the *physical state* of the second component at the time of matrix nucleation is of importance. It may be presumed that the mode of nucleation of a polymer in the presence of solidified domains of the second polymeric phase is heterogeneous, and therefore the nucleation rate should be higher than in the pure homopolymer. The effect of blending on the nucleation behavior is more subtle and complex in the presence of a molten second component. Factors such as miscibility, relative melt viscosity, and inherent crystallizability all influence the formation of critical size nuclei (Nadkarni and Jog 1991).

Nucleation by the interfaces contributes to the crystallization behavior proportionally to the *total amount of interface* in the blend system. The finer the amorphous droplets are dispersed, the larger the total interfacial contact surface, and thus the higher is the possibility of nucleation at these interfaces.

The main factors determining the melt morphology are the blend composition, the difference in melt viscosity between both phases, and the interfacial tension. Hence, the nucleation effect on the crystallization behavior should be more pronounced in blends containing a higher amount of the dispersed phase, or in blends composed of components with nearly equal melt viscosities. It has to be noticed that due to coalescence, upon increasing the amount of the amorphous component, larger domains are formed. As a result, the total interfacial contact area may not increase proportionally, leading to a less-than-linear increase of T_c with increasing amount of the amorphous component (see Figs. 3.55 and 3.53).

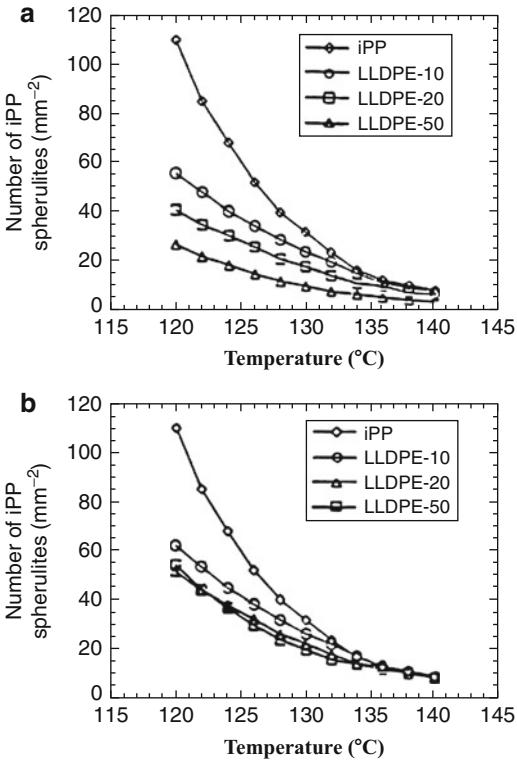

Fig. 3.55 Influence of the amount of dispersed phase, mixing time, T_{melt} and $T_{c,iso}$ on the amount of nuclei per volume unit in the immiscible PP/PS blend (**a**) after 2× mixing, (**b**) after 3× mixing; T_{melt} was set to 190 °C (*open symbols*) or 220 °C (*filled symbols*); $T_{c,iso}$ for experiments was 125 °C (*circles*) or 130 °C (*blocks*) (Bartczak et al. 1987)

An interesting application of the direct relationship between nucleating interfaces and the total amount of the interfacial contact surface can be found in *compatibilized* immiscible blends. In these systems, the dispersed phase size becomes much smaller, strongly increasing the total amount of interface at which nucleation can occur. Some authors reported that this could cause an upward shift in the T_c by up to 10 °C (Wei-Berk 1993). However, other studies in which the crystallization behavior of a compatibilized blend was investigated did not always mention such a clear nucleating activity (Table 3.17).

Finally, the degree of nucleation at the amorphous/semicrystalline interfaces was found to be *temperature dependent*. When the crystallization temperature was raised, the nucleating efficiency of the interface was found to decrease (Bartczak et al. 1987).

In conclusion, the polymer interface can induce some limited number of nucleation events, but does not cause transcrystallinity, as some other crystal surfaces do. Consequently, the amorphous droplet surfaces, either in the solid or molten state, only act as a weak nucleating agent (Bartczak et al. 1987).

Nucleation Behavior of Some Selected Polymer blends

See Table 3.18

Table 3.17 Influence of compatibilizers on the nucleation behavior of the semicrystalline matrix in crystalline/amorphous polymer blends

Blend system	Observations	Explanation	Reference
PA-6/EPR + g-SA	Compatibilization ↓ spherulite size (which was not found in PA-6/EPR blends) + serious ↑ of the interfacial adhesion	Strong nucleation effect of EPR-g-SA on the PP phase	Martuscelli (1984)
PP/PS +PP/PS block	T_c increased (116 → 126 °C) (DSC) along with copolymer content up to 20–25 % of PS phase	Copolymer lowers the interfacial tension → finer dispersion → more surface available for nucleation at interface + more formation of α-phase PP crystals as T_c rises above 125 °C	Wei-Berk (1993)

3.3.3.2 Spherulite Growth of the Crystallizable Matrix

For homopolymers, the temperature dependence of the isothermal spherulite growth rate, G, is described by Eq. 3.43 (Turnbull and Fischer 1949):

$$G_1 = G^{\circ} \exp[-\Delta E/kT_c[\exp] - \Delta F^*/kT_c] \tag{3.43}$$

In the case of immiscible blends with a crystallizable matrix, the spherulite growth can be disturbed to a certain degree by the presence of an amorphous phase component, dispersed in the crystallizable melt.

Phenomena Affecting the Spherulite Growth Rate: Energetic Considerations

Prior to crystallization, the amorphous component exists in the form of droplet-like domains, which at T_c can either be in the molten or glassy state. During the spherulite growth of the crystallizable matrix, small domains may be rejected by the spherulitic growth front either completely to the amorphous interspherulitic zone or only partly over some distance. Furthermore, somewhat larger domains can be occluded by the growing stacks of lamellae after which they eventually can be deformed (Martuscelli 1984; Bartczak et al. 1984). In most cases, a combination of the above-described processes is observed; small droplets are rejected over some distance, coagulate at the growth front, and are engulfed and/or deformed subsequently by the growing lamellar stacks.

The presence of droplet-like domains along the path of the crystallizing growth front can markedly disturb the spherulite growth. The outlined processes require the growth front to perform work against the interfaces, thus dissipating energy. Such energies constitute new energy barriers, controlling the spherulite growth in immiscible blends.

The spherulite growth rate depression is proportional to the type of energy barrier that has to be overcome and can be quantitatively expressed by a modified equation of the spherulite growth rate (Martuscelli 1984):

Table 3.18 Examples of the nucleation behavior of the crystallizable matrix in crystalline/amorphous polymer blends

Blend system (preparation)	Comp.[a]	Observed nucleation behavior (technique used)	Explanation	Reference
LDPE/PS (melt-mix)	90/10	No change		Baïtoul et al. (1981)
	80/20			
	70/30			
	60/40			
HDPE/PS (melt-mix)	90/10	No change		Aref-Azar et al. (1980)
	80/20			
PP/EPR (melt-mix)	95/5	Spherulite size ↓ to less than 1/2 size of PP pure with (EPR)↑ (SALS, O. M.)	EPR is nucleating agent for the production of α-type spherulites (most stable and dense packed)	Karger-Kocsis et al. (1979)
	90/10			
	80/20	Formation of more α-type spherulites with (EPR) ↑ (WAXS, O. M.)		
	60/40	T_c ↑ with (EPR) ↑ (DSC)		
PP/EPR (solvent-mix + melt-mix)	90/10	N/S in PP phase ↑ with (EPR) ↑, mainly at higher (EPR) ⇒ spherulite size ↓ (O. M.)		Martuscelli et al. (1982), Coppola et al. (1987), Kalfoglou (1985)
	80/20			
	(70/30)			
PP/EPR (melt-mix)	95/5	N/S ↑ with (EPR) ↑ (5–7x)	EPR acts as a nucleating agent, probably due to migration of nuclei from EPR to PP phase	Martuscelli (1985)
	90/10	This effect is more pronounced when the % ethylene ↑ or the MW ↓ of the used EPR (O. M.)		
	80/20			
	70/30			
PP/EPDM (solvent cast film)	90/10	N/S in PP phase ↑ with (EPDM) ↑, mainly at higher (EPDM) ⇒ spherulite size ↓ (O. M.)		Martuscelli et al. (1983)
	80/20			
	70/30			

(*continued*)

Table 3.18 (continued)

Blend system (preparation)	Comp.[a]	Observed nucleation behavior (technique used)	Explanation	Reference
PP/PIB (melt-mix)	90/10	N/S is not affected by addition of PIB (O. M., thick sheet cross section)	No additional nucleation effects	Bianchi et al. (1985)), Martuscelli (1985)
	80/20			
	70/30			
PP/PIB (solvent-mix)	90/10	N/S seriously ↑↑ with addition of PIB up to 30 times N/S in PP pure (O. M., thin film)	PIB seems to be an effective nucleating agent	Martuscelli et al. (1983), Martuscelli (1985)
PP/SBS (melt-mix)	75/25	T_c ↑ slightly (±2 °C) with addition of SBS (DSC)	SBS is a weak nucleating agent for PP	Ghijsels et al. (1982)
	50/50			
PP/SBS (melt-mix)	95/5	Spherulite radius ↓ with addition of SBS (O. M., SALS)	SBS is a weak nucleating agent for PP	Karger-Kocsis (1979)
	90/10			
PP/PS (melt-mix)	90/10	N/V ↑ with (PS)↑ (up to 7x N/V found in pure PP)	Mainly migration of nuclei from PS phase to PP phase	Bartczak et al. (1987)
	80/20			
	70/30	This effect is more pronounced with longer mixing times (O. M.)	Some limited nucleating activity of PS droplets at interface because of their high interfacial tension	
PP/PS (solvent-mix)	90/10	N/S ↑ due to addition of PS up to 20 % PS (4×)	Nucleating activity of PS at the interface	Wenig et al. (1990)
	80/20	This increase becomes less pronounced with further (PS) ↑ (O. M.)	When (PS) > 20%, coalescence of droplets occurs ⇒ less ↑ interfacial area	
	70/30			
	60/40	Avrami exponent n ↓ from 3 to 2 (DSC)	Nucleation changes from thermal to athermal due to nucleation at interfaces	
	50/50			

PP/PS (melt-mix)	96/4	T_c ↑ from 121°C (4%PS) to 127°C (40% PS) (DSC)	Nucleating activity of the PS interface on PP	Wei-Berk (1993)
	77/23			
	65/35			
	60/40			
PP/PS (melt-mix)	90/10	No significant change in T_c visible		Santana and Müller (1994)
	80/20			
	70/30			
	50/50			
sPS/PVME[b] (solvent-mix and molten up)	80/20	Formation of larger spherulites with (PVME) ↑ (O. M.)	Migration of impurities during mixing from sPS to PVME phase	Cimmino et al. (1993a)
	70/30	$t_{0.5}$ ↑ during isothermal crystallization (DSC)		
	50/50			

[a]Other compositions than the ones mentioned have been investigated sometimes
[b]PVME and sPS are immiscible as long as the concentration PVME remains larger than 10 % of the blend

Table 3.19 Expressions for the dissipation energy terms and corresponding spherulite growth rates in a crystalline/amorphous polymer blend system (Martuscelli 1984; Bartczak et al. 1984)

Rejection of droplets by growing spherulites	Occlusion of droplets in growing lamellae	Deformation of occluded droplets[a]
$E_1 = 1.5\ (EGR_s\mu_M c/\rho_M r^2)$	$E_3 = 3C\mu_M\Delta F/\rho_M r$	$E_4 = \mathrm{U(K)}\ (3C\mu_M\gamma_{PS}/\rho_M r)$
$G = G_1/(1 + (3\mu_M cEG_1R_s/2\rho_M r^2RT))$	$G = G_1 \exp(-3C\mu_M\Delta F/\rho_M rRT$	$G = G_1 \exp(-\mathrm{U(K)}.(3C\mu_M\gamma_{PS}/\rho_M rRT))$
$E_2 = C\mu_M\rho_P G^2/2\rho_M$		
$G = G_1 \exp(-C\mu_M\rho_P G^2/2\rho_M RT)$		

G_1 is the undisturbed spherulite growth rate
μ_M is the molecular mass of the repetitive unit of the macromolecular chain of the crystallizable matrix
γ_{PS} is the interfacial free energy between the crystallizing solid and the inclusions
ρ_M and ρ_P is the density of the matrix and of the dispersed component
R_s and r is the radius of spherulite and of the dispersed particles, respectively
c is the volume concentration of the noncrystallizable component
R is the gas constant
E is the kinetic energy supply required to move the dispersed droplet along with the motion of the crystallizing front $= 2/3\ G^2\ \Pi r^2\ \rho_P$
[a]The energy of deformation is the sum of two terms: the first is related to change of the surface of particles and the second to deformation of viscoelastic material. U(K) is a complicated function of the coefficient of deformation K of the particles. In the expression of E_4, only the change in surface is taken into consideration with reference to the case where $\Delta F > 0$

$$G = G_1 \exp[-(E_1 + E_2 + E_3 + E_4)/kT_c] \tag{3.44}$$

where G_1 is the spherulite growth rate of the plain crystallizable polymer (theoretically described by the Turnbull-Fisher equation); E_1 is the energy dissipated for rejection (proportional to the melt viscosity); E_2 is the energy needed to overcome the inertia of the drops; E_3 is the energy needed to form a new interface if drops are engulfed; and E_4 is the energy dissipated for deformation of occluded particles.

Theories for the description of these energies for a non-polymeric solidification front were developed by Cissé and Bolling (1971) and by Omenyi et al. (1981). Bartczak et al. (1984) have modified these theories in order to apply them to the case of a crystalline polymeric front that grows according to a spherulite-like morphology, while in the melt, noncrystallizable polymeric domains of spherical shape are present (Table 3.19).

The driving force for rejection, occlusion, or deformation processes is equal to the difference of interfacial free energies (Martuscelli 1984):

$$\Delta F = \gamma_{PS} - \gamma_{PL} \tag{3.45}$$

where γ_{PS} is the interfacial free energy between crystallizing solid and the inclusions, and γ_{PL} is the interfacial free energy between the melt and the inclusions. When ΔF is positive, the particle droplet will be rejected (Wei-Berk 1993).

Table 3.20 Energy dissipated in PP/TR blends for rejection, occlusion, and deformation of the TR droplets by the growing PP lamellae (Martuscelli 1984; Bartczak et al. 1984)

Process	Energy (J/mol PP repeating units)
Rejection	10^{1}–10^{4}
Kinetic energy of rejection	10^{-15}–10^{-14}
Occlusion	10^{-2}–10^{-1}
Deformation: surface change term	10^{-1}–10^{0}
Deformation: viscous term	10^{-7}–10^{-6}

Martuscelli (1984) and Bartczak et al. (1984) have calculated the energies dissipated by growing PP spherulites in a blend with dispersed rubber particles for all the abovementioned phenomena that may disturb the spherulite growth (Table 3.20).

It can be concluded that mainly rejection of small particles and to a lesser extent deformation of large engulfed droplets (requiring the formation of new surface boundaries) cause a depression in the spherulite growth rate.

Factors Influencing the Spherulite Growth Rate, *G*

Several factors determine the amount of energy required by the growth front to be overcome in order to allow the crystallizable matrix to form spherulites.

The first and most important of these is the *crystallization temperature*, T_c. The higher the isothermal crystallization temperature above $T_{c,\max}$, the slower the spherulites will grow. However, higher T_c also implies a lower melt viscosity. In such case, small droplets will be rejected easier, consuming less energy. This is reflected in a spherulite growth rate, nearly independent on the total amount of small amorphous droplets to be rejected, while at lower T_c, it could be clearly seen that the growth rate is much affected by the amount of fine droplets (Fig. 3.56)

The temperature dependence of the spherulitic growth rate has been theoretically treated (Wenig et al. 1990), for several blends composed of a PP matrix in which PS droplets were dispersed. This temperature dependence could be calculated based on the work done by Hoffmann (1983) and by Suzuki and Kovacs (1970) and is defined as follows (Fig. 3.57a):

$$\begin{gathered}\text{for } T < T_g - C_2 : G(T) = 0 \\ \text{for } T_g - C_2 < T < T_m^\circ : G(T) = G^\circ \exp\left[-C_1 C_2/\left(C_2 + T - T_g\right)\right] \exp[(-C_3)/T(T_m^\circ - T)] \\ \text{for } T > T_m^\circ : G(T) = 0\end{gathered} \tag{3.46}$$

where T_g is the glass-transition temperature of the crystallizable component; T_m° is the theoretical melting temperature of the crystalline component; G°, C_1, C_2, and C_3 are parameters describing the growth rate behavior in the blends.

For the crystalline component, the parameters from the WLF equation, C_1 and C_2, can be found from literature (Icenogle 1985). T_g and T_m° can be measured for pure crystallizable component. The parameters G° and C_3 can be calculated from the experiments that give the spherulite growth rate G as

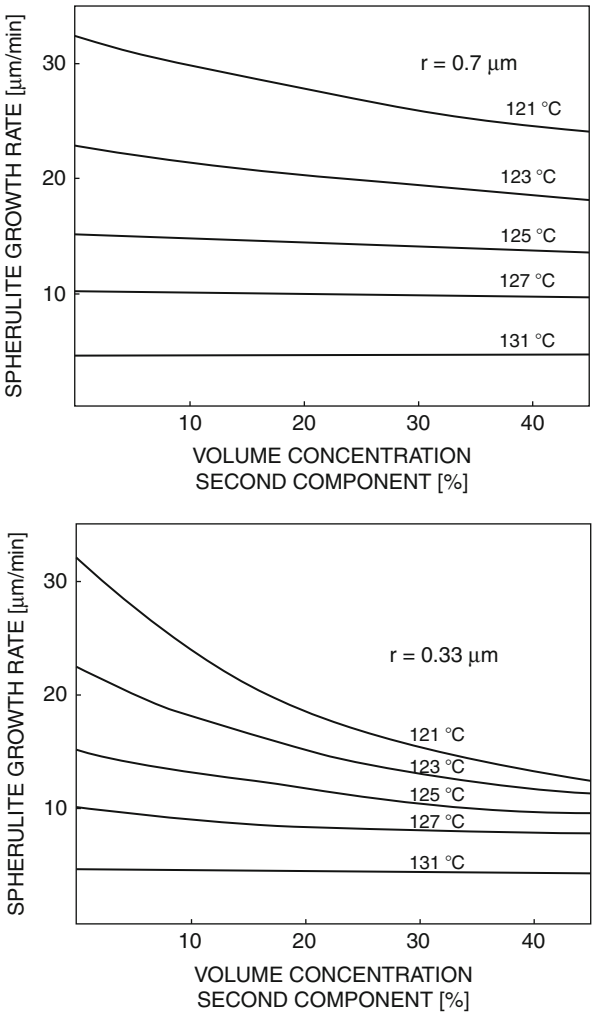

Fig. 3.56 Theoretical estimation for spherulite growth rate depression in immiscible PP-based blends in the case of *rejection* of particles: influence of particle size, $T_{c,iso}$, and volume concentration of the second component (Martuscelli 1984)

a function of temperature T. By plotting the value $\ln G + C_1C_2/(C_2 + T - T_g)$ versus $1/(T(T_m - T))$ for the entire crystallization temperature range, a linear plot is obtained from which the values of G° (intercept) and C_3 (slope) for all the blend compositions can be determined (Fig. 3.57b). Once all these parameters are known, the growth rate can be estimated as a function of temperature for all blend compositions, according to Eq. 3.46.

Secondly, the *blend composition* is of importance as well. The finer the dispersion (i.e., at low content of the amorphous phase, nearby equal melt viscosities of matrix and dispersed phase, etc.), the more droplets need to be rejected. This high energy-consuming process reduces the spherulite growth rate (see Fig. 3.57).

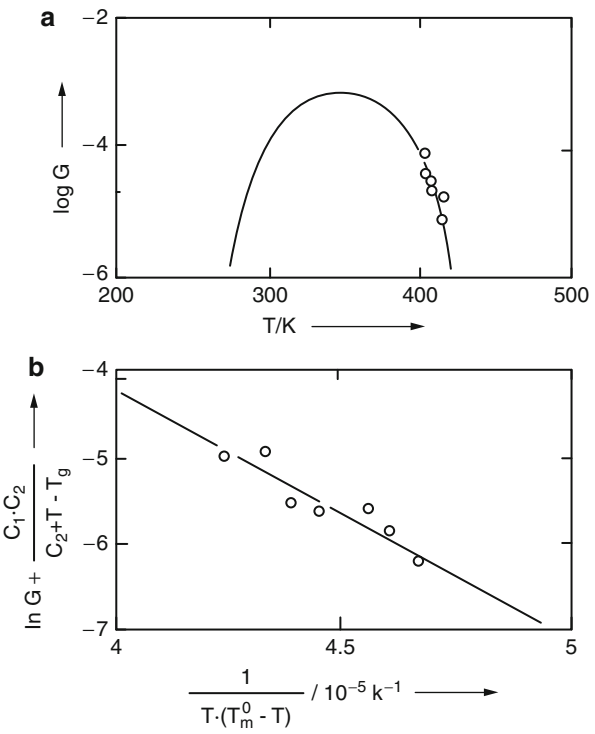

Fig. 3.57 (**a**) Temperature dependence of the spherulite growth rate, G, for PP (experimental values were fitted using the function defined in Eq. 3.46); (**b**) plot to determine the parameters G° and C_3 ($C_1 = 25$, $C_2 = 30$ K, $T_g = 260$ K, $T_m^{\circ} = 460.5$ K) (Wenig et al. 1990)

Spherulite Growth Rate Investigations in Some Typical Polymer Blends
See Table 3.21

3.3.3.3 Overall Crystallization Kinetics

The effect of blending on the overall crystallization rate is the net combined effect of the nucleation and spherulite growth. Martuscelli (1984) observed that in blends of PP with LDPE, crystallized at a T_c high enough to prevent any LDPE crystallization, the overall rate of crystallization of the PP matrix phase (thus in the presence of the LDPE molten droplets) was progressively depressed with increasing content of LDPE (Fig. 3.58).

This can be seen in the plot of $t_{1/2}$ (halftime of crystallization at a fixed $T_{c,iso}$) versus blend composition. The observations agree very well with the findings that the growth rate of the PP spherulites is almost unaffected, while the nuclei density decreases with increasing LDPE content due to impurity migration from PP to LDPE phase.

A different case has also been explored by Martuscelli (1984) for PA-6 blended with an EPR-rubber. As shown in Fig. 3.59, $t_{1/2}$ of the PA-6/EPR blend decreased (faster overall crystallization rate) as the content of the rubbery phase increased, especially at lower concentrations of the EPR phase.

Table 3.21 Examples of the spherulite growth rate, G, of the crystallizable matrix in crystalline/amorphous polymer blends

Blend system	Comp.	G (μm/min)[a] (from O. M.)	$\neq T_c$[b]	Final semicrystalline morphology	Comments	Reference
PP/EPR (thin film)	100/0	32	x	Some droplets are ejected interspherulitically	Small ↓ of G which is composition dependent	Martuscelli et al. (1982)
	90/10	±30				
	80/20	±27		At low (EPR): droplets are ejected for a short distance and then occluded intraspherulitically		Martuscelli (1985)
	70/30	±27 at 121 °C				
PP/EPDM (thin film)	100/0	15	x	Droplets are occluded intraspherulitic	Only small ↓ of G independent of the blend composition	Martuscelli et al. (1983)
	90/10	11				
	80/20	12		Droplets are aligned along radial direction due to coalescence of droplets upon rejection for short distance, followed by deformation		Martuscelli (1985)
	60/40	13 at 125 °C				
PP/PIB (thin film)	100/0	32	x	Most droplets (3–5 μm) are occluded intraspherulitically	Clear depression of G on addition of PIB which is strongly dependent on MW PIB and composition[c]	Martuscelli et al. (1982)
						Martuscelli et al. (1983)
	90/10	23		Sometimes droplets are rejected (for short distance or even interspherul.) if		Martuscelli (1985)
	80/20	20 at 121 °C		MW PIB low		
				(PIB) low (<10 %)		

PP/PS	100/0	2.5	x	PS droplets are occluded intraspherulitically (no rejection or deformation)	G is not changed and is independent on blend composition	Bartczak et al. (1987)
	90/10	2.3				
	80/20	2.5				
	70/30	2.5 at 133 °C				
PP/PS	100/0	3.2	x		G is only slightly ↓ except for 90/10 composition (no explanation)	Wenig et al. (1990)
	90/10	1.6				
	80/20	3.1				
	70/30	2.8			Globally G is independent on composition	
	60/40	2.2 at 133 °C				
sPS/PVME	100/0	2.5	x	Droplets are occluded intraspherulitically	G is ± independent on composition	Cimmino et al. (1991)
	80/20	6.0				
	70/30	7.0			G↑ with (PVME) ↑ due to facilitated transport of chains (PVME and PS chains are partially miscible ⇒ Tg↓)	Cimmino et al. (1993)
	50/50	– at 244 °C				

[a]Some of the listed data were extracted from plots presented in the article
[b]x indicates that the influence of different crystallization temperatures T_c has been investigated
[c]PIB is shown to be partially miscible with the amorphous phase of PP at low concentrations. Hence, the behavior can deviate and exhibit some typical characteristics as in miscible systems

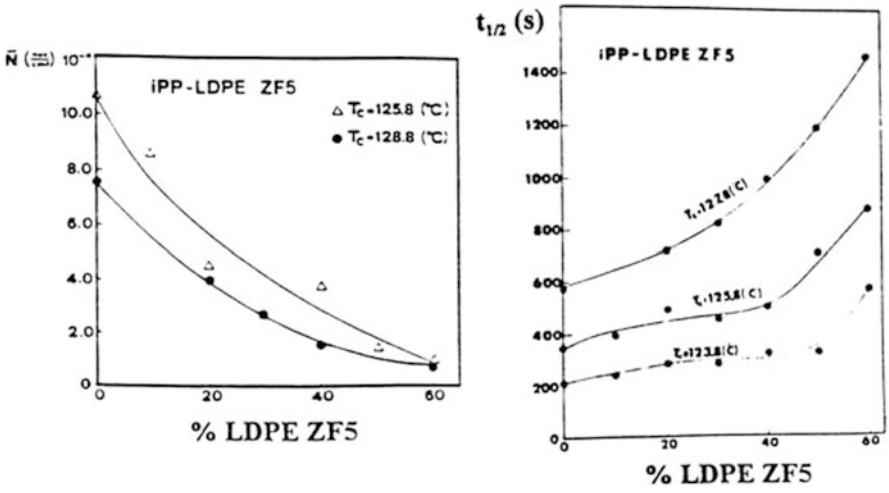

Fig. 3.58 Global crystallization kinetics in immiscible PP/LDPE blends; influence of the amount dispersed phase and the crystallization temperature, T_c, on the halftime for crystallization, $t_{1/2}$ (Martuscelli 1984)

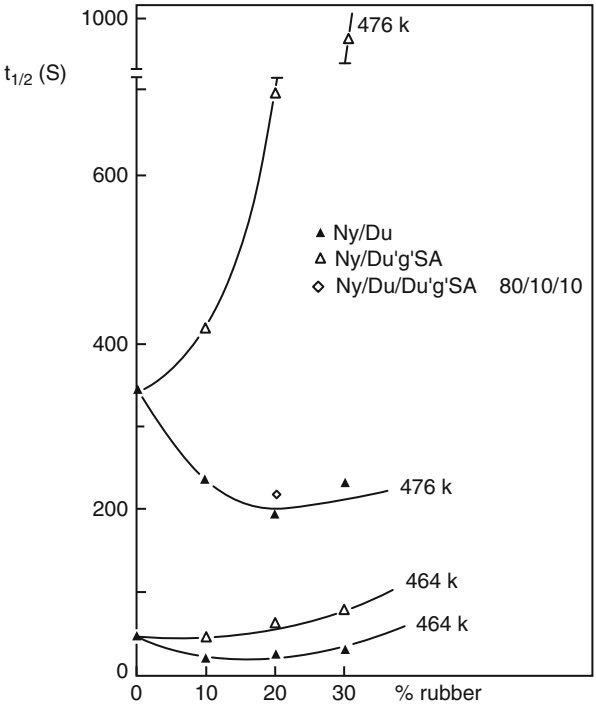

Fig. 3.59 Variation of the halftime of crystallization, $t_{1/2}$, with the percent of added rubber component (EPR) and T_c for PA-6/Dutral and the compatibilized blend PA-6/Dutral-g-SA (Martuscelli 1984)

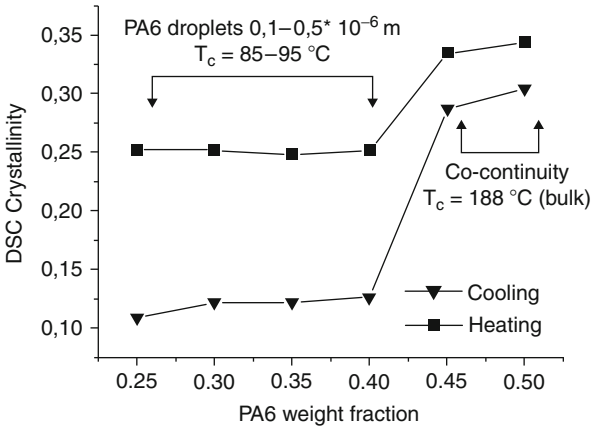

Fig. 3.60 Evolution of DSC crystallinity from cooling (▼) and melting curves (■) versus PA6 droplet size for various (PS/SMA2)/PA6 blend compositions (Tol et al. 2005c)

The reverse could be observed in a compatibilized blend. Because in these blends a serious decrease of the spherulite size was observed, the authors concluded that the compatibilizer acted as a nucleating agent for the PP phase. However, due to the increase of the melt viscosity upon compatibilization, the overall crystallization kinetics was retarded. Additionally, they observed experimentally that ΔF^*(free energy for the formation of a nucleus of critical size) and σ_e (surface free energy of folding) in compatibilized blends were larger than in PA-6 homopolymer. An opposite trend was observed for the physical PA-6/EPR blends. No further investigations have been done to elucidate this phenomenon.

The crystallization kinetics of PA6 in immiscible blends of PS/PA6 and (PS/SMA2)/PA6 have been investigated over very broad temperature range using high cooling rates (Tol et al. 2005c). For immiscible blends with PA6 droplets of micrometer size, exhibiting moderate decrease of crystallization temperature compared to the PA6 bulk crystallization, an athermal nucleation mechanism was suggested based on nucleation process in a very small temperature interval. Blends of PA6/PS compatibilized using SMA2 having submicrometer-sized PA6 droplets, crystallizing at 90 °C (i.e., a supercooling of 100 °C compared to Tc bulk), a random nucleation event was found using isothermal DSC experiments, which is characteristic of a homogeneous nucleation process. This effect was persistent up to 40 wt% PA6 (Fig. 3.60). This concentration is the highest concentrated heterogeneous system reported, exhibiting homogeneous nucleation kinetics. Crystallinities were strongly affected by the confining conditions of the droplets. For 1–30 μm-sized PA6 droplets crystallizing at intermediate temperatures, the crystallinity decreased with decreasing PA6 droplets size from 36 % for bulk PA6 to 22 %. For the submicrometer-sized PA6 droplets, a very strong decrease in crystallinity was found down to 10 %.

3.3.3.4 Final Semicrystalline Morphology

The addition of a second noncrystallizable component to a crystallizable matrix can cause drastic variations of important morphological and structural parameters of the

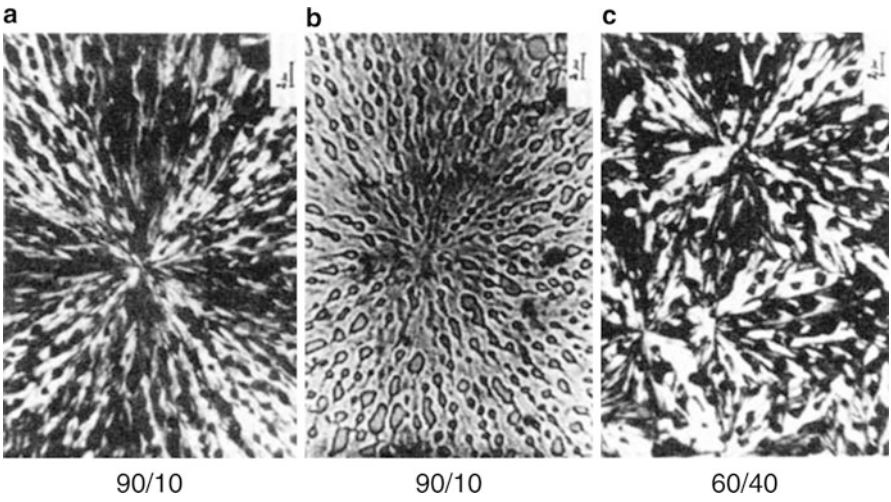

Fig. 3.61 Optical micrographs of melt-crystallized films of PP/EPDM blends at $T_c = 135$ °C; (**a**) 90/10, crossed polarizers; (**b**) 90/10, parallel polarizers; (**c**) 60/40, crossed polarizers (Martuscelli et al. 1983)

semicrystalline phase, such as the shape, size, regularity of spherulites and interspherulitic boundary regions, lateral dimensions of the lamellae, etc. These factors may greatly influence the mechanical behavior and, in particular, the fracture mechanisms and thus are of great importance, especially when the toughening of semicrystalline polymer blends is considered.

The first important parameter determining the final crystalline morphology is the *nucleation density*, *N* (see Sect. 3.3.3.1). An increase in the nucleation density (per volume unit of the crystallizable material) due to migration of nuclei from one phase toward the other, or due to a nucleating activity at the polymer/polymer interface, results in the formation of more numerous but smaller spherulites.

The spherulite *growth rate*, *G*, also plays a role.

- At low *G* values, there is a higher probability that all dispersed particles can diffuse fast enough away from the growth front and be pushed along until complete crystallization. The second phase component will then be found mainly in the interspherulitic regions.
- At high *G* values, even small particles will not be rejected anymore. Hence, the homogeneously distributed droplets will be as such engulfed, rejected into newly formed boundaries behind occluded particles, and eventually deformed. This results in a radial-like distribution of the droplets within the spherulite (Fig. 3.61).
- At intermediate growth rates, the dispersed drops will first be pushed along, but due to an increase of the amount of droplets at the solidification front, they will coagulate and subsequently be engulfed. This results in a spherulite center consisting of pure crystalline material and an outer layer in which dispersed particles are occluded.

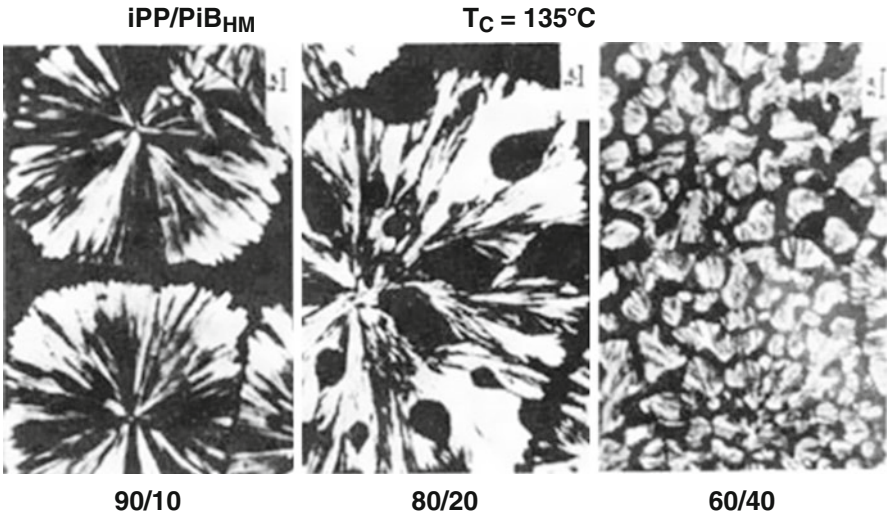

Fig. 3.62 Optical micrographs of isothermally (T_c = 135 °C) crystallized thin films of PP/PIB (HM) blends with different compositions (Martuscelli et al. 1983)

Another parameter strongly influencing the final crystalline morphology is the *blend composition* (Fig. 3.62).

The higher the amount of the amorphous phase, the higher the chance to have a coarse melt morphology containing lots of large, easily coalescing amorphous droplets. In such a case, the crystallizing growth front will mainly engulf and deform these droplets. The resulting crystalline morphology will be heavily disturbed by the second phase component.

Some examples of the final semicrystalline morphology in several immiscible crystalline/amorphous blend systems have already been given in Tables 3.21 and 3.22 for the discussion of the spherulite growth rate (Sect. 3.3.3.2). Some more information about this topic can be found in the articles listed in Table 3.23.

3.3.3.5 Melting Behavior of the Crystalline Matrix in Crystalline/Amorphous Blends

The behavior of binary blends with only one crystallizable component has been studied by several authors, who have investigated different systems. The crystals of the crystallizable matrix have grown in equilibrium with their own melt phase. The presence of separate domains of noncrystallizable component, dispersed in the molten matrix during the crystallization process (owing to the kinetic and morphological effects), may cause a depression of the observed melting temperature, T_m' (Martuscelli 1984). However, the changes in T_m' will be only in the range of a few degrees C.

Some binary systems do not show any depression at all, indicating that T_m' and T_m do not depend on blend composition. This is found when the second dispersed

Table 3.22 Global crystallization kinetics of the crystallizable matrix in some crystalline/amorphous blend systems

Blend system	Comp.	Parameter	$\neq T_c$[a]	Comments	References
HDPE/PS	100/0 90/10 80/20	Avrami exponent (DSC) $t_{0.5}$ (DSC)	x	Unaffected cryst. kinetics (insensitive to blend morphology)	Aref-Azar et al. (1980)
PP/EPR	100/0 90/10	$X_{c,iso}$ *(DSC)*		At (EPR) < 20 %: slight ↓ of X_c due to limited miscibility of aPP and EPR → hindered crystal growth	Kalfoglou (1985)
	80/20 60/40			At (EPR) > 20 % : X_c ↑ with (EPR) ↑ due to nucleating activity of EPR	
PP/PIB	100/0 90/10 80/20 70/30	$X_{c,iso}$ *(WAXS, DSC)*		X_c ↓ with (PIB) ↑	Bianchiet al. (1985) Martuscelli (1985)
PP/PS	100/0 90/10 80/20 70/30 60/40	Avrami exp., n (DSC)		n ↓ from 3 to 2 with (PS) ↑ (due to surface nucleation at PS droplets), and G = cte ⇒ crystallization rate is enhanced and strongly dependent on blend composition	Wenig et al. (1990)
PA-6/EPR	100/0 90/10 80/20 70/30	$t_{0.5}$ (DSC)	x	Serious ↓ in $t_{0.5}$, which is most pronounced at low conc. EPR ⇒ enhanced crystallization kinetics	Martuscelli (1984)
sPS/PVME	100/0 80/20	$t_{0.5}$ (DSC)	x	Seriously retarded kinetics of sPS phase ($t_{0.5}$ ↑) which is composition dependent Effect of N/S ↓ is larger than that of G ↑	Cimmino et al. (1993)

[a]x indicates that the influence of different T_c on the overall crystallization kinetics has been investigated in the article mentioned

phase does not influence the normal crystallization behavior of the matrix polymer: no nucleating activity, no influence on spherulite growth rate, etc.

Some examples of the melting behavior in previously discussed blend systems are given in Table 3.24.

3.3.4 Blends with a Crystallizable Dispersed Phase in an Amorphous Matrix

In immiscible polymer blends, the minor component often forms the dispersed phase, whose shape and size are complex functions of the blend composition, the

Table 3.23 Overview of literature in which the final semicrystalline morphology in immiscible crystalline/amorphous polymer blends has been studied

Blend system	Reference	Composition[a]	Growth rate[b] (rejection ↔ occlusion)	Nucleation density[c] (spherulite size)
PP/EPR	Martuscelli et al. (1982)	x		x
	Coppola et al. (1987)	x		x
	Kalfoglou (1985)	x		x
	Karger-Kocsis et al. (1979)	x		x
	Martuscelli (1985)	x		
PP/EPDM	Martuscelli et al. (1983)	x	x	x
	Martuscelli (1985)	x		
PP/PIB	Martuscelli et al. (1982)	x	x	x
	Martuscelli et al. (1983)	x	x	x
	Bianchi et al. (1985)	x	x	x
	Martuscelli (1985)	x	x	x
PP/PS	Bartczak et al. (1987)	x		x
PEG/PS	Lotz and Kovacs (1969)	x		
sPS/PVME	Cimmino et al. (1991)	x		x
	Cimmino et al. (1993)	x		x

[a]Influence of compositional variations on the semicrystalline morphology has been investigated
[b]Influence of different spherulite growth rates on semicrystalline morphology is discussed
[c]Final spherulite size has been evaluated

melt viscosity of the dispersed phase and the matrix, the viscosity ratio, the interfacial tension, and the processing conditions (Utracki 1989; Folkes and Hope 1993).

The crystallization behavior of a dispersed melt phase, for example, discrete melt droplets, in an amorphous matrix can be dramatically affected compared to that of the bulk polymer. It has been reported by several authors that crystallizable dispersed droplets can exhibit the phenomenon of *fractionated crystallization* originating from the primary nucleation of isolated melt particles by species with different nucleating activities (heterogeneities, local chain ordering)

Table 3.24 Examples of the melting behavior of the crystallizable matrix in some crystalline/amorphous blend systems

Blend system	$T_{m\downarrow}$	$T_m\uparrow$	References
PP/EPR		$T_m\uparrow$ with (EPR) $\uparrow$	Martuscelli et al. (1982)
		Effect is largest at high ethylene content and low MW of EPR	Martuscelli (1984)
		EPR is able to extract selectively defective PP chains $\Rightarrow T_m\uparrow$ and $X_c\uparrow$	Martuscelli (1985)
PP/EPR	$T_m\downarrow$ with (EPR) $\uparrow$ (2 to 3 °C) due to $T_c\downarrow \Rightarrow$ formation of smaller lamellae which melt at slightly lower T_m		Kalfoglou (1985)
PP/EPR	$T_m\downarrow$ with (EPR) $\uparrow$ (3 to 4 °C) due to the formation of smaller spherulites with lower C_p (although $T_c\uparrow$)		Karger-Kocsis et al. (1979)
PP/EPDM	$T_m\downarrow$, min. is observed at 20 % EPDM		Martuscelli et al. (1983)
	EPDM is able to dissolve aPP at low conc. EPDM ($\approx$ diluent-effect)		
PP/PIB	$T_m\downarrow$ with (PIB) $\uparrow$		Martuscelli et al. (1983)
	This effect is largest at high conc. PIBLM or low conc. PIBHM		
	PIB dissolves aPP in low amounts ($\approx$ dilution effect)		
PP/PS	$T_m\downarrow$ with (PS) $\uparrow$ (2 to 3 °C) due to some specific interactions at the interface		Mucha (1986)
			Wei-Berk (1993)
POM/PC	$T_m\downarrow$ with (PC) $\uparrow$ (2 to 3 °C) ΔH_m = cte (per g POM)		Chang et al. (1991)
PEG/PS	$T_m\downarrow$ with (PS) $\uparrow$ (max. 8 °C) due to formation of smaller lamellae if the (PS) in the block copolymer $\uparrow$		O'Malley et al. (1969)
PET/PPE		$T_m\uparrow$ upon addition of PPE to a PET matrix ($\approx$ 2 °C)	Liang and Pan (1994)

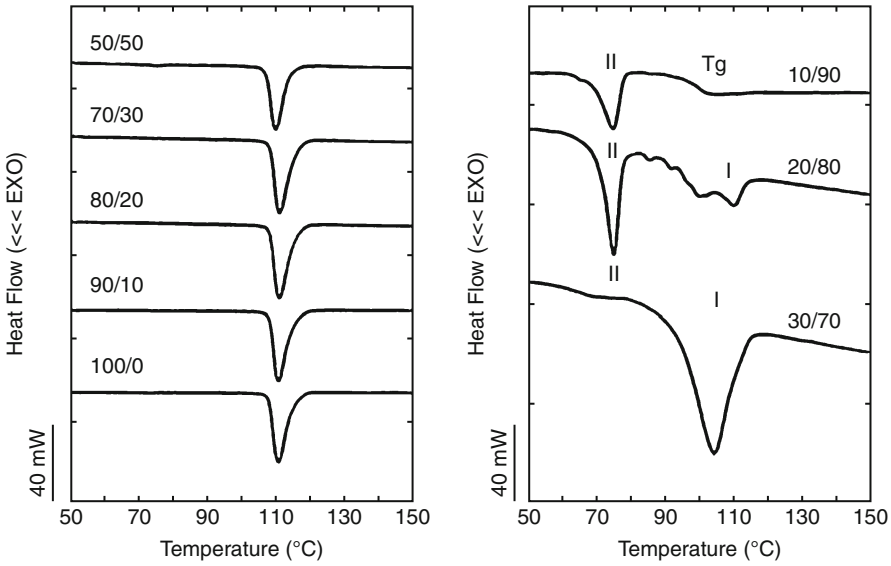

Fig. 3.63 DSC cooling curves (10 °C/min) for PP/PS blends; difference in the crystallization behavior in blends with PP as a matrix phase and as a dispersed phase (Santana and Müller 1994)

(Aref-Azar et al. 1980; Baïltoul et al. 1981; Ghijsels et al. 1982; Robitaille and Prud'homme 1983; Frensch et al. 1989; Santana and Müller 1994; Müller et al. 1995; Morales et al. 1995; Fig. 3.63).

3.3.4.1 The Phenomenon of Fractionated Crystallization of a Dispersed Phase

Crystallization is a phase transition that is controlled by nucleation and growth (Wunderlich 1976). As it has been outlined in Sect. 3.2.2, crystallization during cooling from the melt in homopolymers is initiated by impurities (primary heterogeneous nucleation), after which the crystallizing front spreads over the whole material via the secondary nucleation, before other heterogeneities, requiring a larger degree of undercooling, $\Delta T_{c,i} = T_{mo} - T_{c,i}$, can become active. A single crystallization exotherm is generally observed in DSC thermograms. So, the primary nucleation is the rate-determining step of crystallization. The dynamics of the process depend for a given component only on the temperature.

However, for polymer blends in which the crystallizable phase is dispersed into fine droplets in the matrix, crystallization upon cooling from the melt can sometimes occur in several steps (fractionated crystallization) that are initiated at different undercooling, often ending up with a crystallization at the homogeneous crystallization temperature $T_{c,hom}$ (Aref-Azar et al. 1980; Baïltoul et al. 1981; Ghijsels et al. 1982; Santana and Müller 1994).

The first investigations concerning the crystallization in discrete droplets date from 1880; Van Riemsdyk reported that small gold melt droplets solidify at much

Table 3.25 Crystallization behavior in finely dispersed crystalline droplets

Polymer	Dispersion method	Average droplet size (μm)	ΔT_c, bulk (°C)	ΔT_c, droplets (°C)	Reference
PE	Thermodyn. inert liquid	Some μm	±20	±55[a]	Cormia et al. (1962)
PP	Thermodyn. inert liquid	Some μm	±50	±102[a]	Burns and Turnbull (1966)
PEG	Thermodyn. inert liquid	5	±20	±65[b]	Cormia et al. (1962)
PE	Suspended in silicon oil and sprayed on slides*	1–2	±20	55[a]	Koutsky et al. (1967)
PP	*	1–2	±50	100[a]	Koutsky et al. (1967)
PEG	*	1–2	±20	65[b]	Koutsky et al. (1967)
POM	*	1–2	±30	84[a or b]	Koutsky et al. (1967)
iPS	*	1–2	±	102[b]	Koutsky et al. (1967)
PA-6	*	1–2	±15	100[b]	Koutsky et al. 1967

[a]Crystallization by homogeneous nucleation at $T_{c,hom}$
[b]Nucleating activity of the suspending medium prevents to detect the real undercooling needed to obtain a homogeneous crystallization

larger undercoolings than the bulk material (Van Riemsdyk 1880). Similar observations were made later for other metals (Perepezko and Paik 1982), indicating this to be a basic crystallization phenomenon.

The creation of sufficiently small polymer droplets as a stable suspension was much more difficult. It was therefore only first in 1959 that similar experiments have been reported for polymers (Frensch et al. 1989; Table 3.25).

It was clearly observed that the phenomenon of delayed crystallization was directly related to the size of the dispersed droplets (Koutsky et al. 1967). Only the smallest droplets showed crystallization at much larger undercooling, droplets having a sufficiently large diameter crystallized at temperatures approaching the bulk crystallization temperature, T_c. The explanation for this behavior is obvious: the spectrum of undercoolings at which several crystallization steps occur reflects the difference in nucleating activity of the various heterogeneities available in the melt (Frensch et al. 1989). It can be assumed that if the dispersion of the polymer is so fine that not every droplet contains at least one heterogeneity of type 1, only those droplets containing the latter will crystallize at an undercooling $\Delta T_{c,1}$. Since the droplets are physically not in contact with each other, further growth via secondary nucleation in other crystallizable droplets is impossible. During further cooling, heterogeneities of type 2 requiring the second lowest degree of undercooling, $\Delta T_{c,2}$, can become active in some of the remaining droplets, resulting

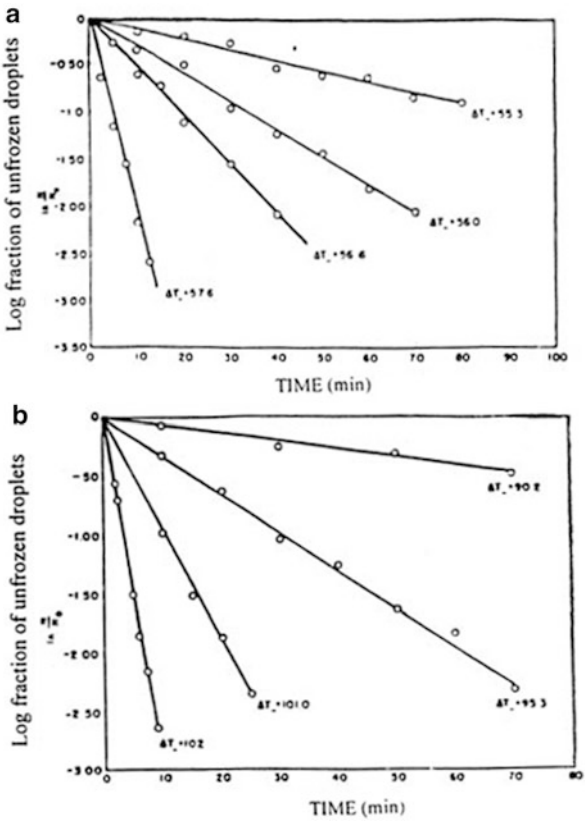

Fig. 3.64 Isothermal homogeneous crystallization of finely dispersed polymer droplets as a function of time (**a**) linear PE, (**b**) PP (Koutsky et al. 1967)

in a second crystallization exotherm. This process goes on until finally some very fine droplets that have not yet been nucleated by the heterogeneous species will crystallize in a homogeneous mode.

In isothermal experiments, the fractionated crystallization of finely dispersed crystallizable droplets is reflected by longer crystallization times before the same degree of crystallinity X_c is obtained. This has been illustrated clearly by Koutsky et al. (1967) in experiments (see Table 3.25) in which finely dispersed droplets of PE and PP in a suspension of silicon oil were crystallized at different undercoolings ΔT_c (Fig. 3.64).

It should be mentioned that the occurrence of a fractionated crystallization is related only to the number densities of dispersed polymer particles and primary heterogeneous nuclei. No direct physical relationship has been found with the number or size of spherulites. These parameters are additionally influenced by the cooling rate and the crystallization temperature (Frensch et al. 1989).

Several factors can influence the fractionated crystallization behavior. An important parameter that has already been discussed is the thermal history of the sample. Crystallizable dispersed droplets that were submitted to premelting at higher temperatures or longer times generally display a shift in the heterogeneous

Table 3.26 Influence of compatibilization on the crystallization behavior of the dispersed phase in amorphous/crystalline polymer blends

Blend system	Compositions	Matrix at T_c	Comments	References
PP/PS +SBS	18/80/2	Melt	SBS did not ↓ particle size (bad compatibilizer because immisc. with PP)	Santana and Müller (1994)
	9/90/1		Nucleation density ↑ because homogeneous nucleation process becomes more heterogeneous (higher T_c)	
			SBS transfers heterogeneities to PP	
LDPE/PS + Kraton G	15/77.8/7.2	Solid	Kraton enhances the formation of a finer dispersed PE phase	Bailtoul et al. (1981)
			Shift of multiple crystallization to lower temp.	
PET/PS +PET-b-PS	23.75/71.25/5	Melt	Addition of block copolymers caused a serious ↓ of droplet size (± 5 μm → 0.2 to 4 μm)	Quirk et al. (1989)
			Compatibilization caused large ↓ of X_c (≈ −10 %)	
PET/PPE +PET-b-PS	23.75/71.25/5	Solid	Addition of block copolymers caused a ↓ of droplet size (± 5 μm → 2 to 4 μm)	Quirk et al. (1989)
			Compatibilization caused X_c ↑ (≈ − 10 to 20 %)	

nucleation spectrum to greater undercooling. The homogeneous crystallization temperature however is not displaced and thus independent of the thermal history (Koutsky et al. 1967). This may become less evident for blends with unstable phase morphology (rapid phase coarsening upon annealing); long residence times in the melt will cause fine droplets to coarsen. Consequently, the newly formed larger droplets have a higher probability to crystallize close to the bulk crystallization temperature of the homopolymer.

The degree of dispersion of the minor phase plays a crucial role. Important factors here are the blend composition, the interfacial tension between both components, the melt viscosity of both components, the processing device and mixing conditions, the blend preparation method, etc.

In this context, it is interesting to evaluate also the influence of compatibilization on the crystallization behavior of the dispersed phase. Since compatibilization reduces the droplet size of the minor phase even more drastically, it can be expected that this can lead to a serious shift of the crystallization temperature toward lower temperatures, resulting in more pronounced fractionated crystallization or even in a homogeneous crystallization. However, this issue is more complex due to numerous other factors involved in the nucleation process. Some examples from the literature are listed in Table 3.26. They illustrate how differently the compatibilization can influence the crystallization behavior of the dispersed phase.

3.3.4.2 Theoretical Considerations of the Fractionated Crystallization

In crystallizable dispersed droplets, several different nucleating heterogeneities (type i) can be present, each having a typical free energy for the formation of a nucleus of critical size, ΔF^*, at an undercooling $\Delta T_{c,i}$:

$$\Delta F^* \approx \Delta y_{pn} / \left(\Delta T_{c,i}\right)^2 \tag{3.47}$$

This free energy is proportional to the specific interfacial free energy difference Δy_{pn} defined as (Wunderlich 1976)

$$\Delta y_{pn} = y_p(m,c) - y_{pn}(m) + y_{pn}(c) \tag{3.48}$$

where the indices refer to polymer (p), melt (m), crystal (c), and nucleus (n); $y_{pn}(m)$ is the interfacial energy between the nucleating species and the polymer melt; $y_{pn}(c)$ is the interfacial energy between the nucleating species and the polymer crystal; and $y_p(m, c)$ is the lateral surface free energy between the crystal and its own melt.

In the case of a homogeneous nucleation, the expression for Δy_{pn} can be simplified to read: $\Delta y_{pn} = 2\ y_p(m, c)$

If one assumes that for the onset of crystallization $\Delta F^*/kT$ must be smaller than a certain critical value (i.e., a nucleus of critical size can be formed at the given temperature), independent of the material, and if one neglects that the crystallization also depends on the temperature-dependent mobility of the crystallizable segments, the following expression for the relation between Δy and the degree of undercooling for two heterogeneities of type 1 and type 2 can be given (Frensch et al. 1989):

$$\Delta y1/\Delta y2 \approx \left(T_{c,1}/T_{c,2}\right).\left(\Delta T_{c,1}/\Delta T_{c,2}\right)^2 \tag{3.49}$$

where $T_{c,1}$ and $T_{c,2}$ represent the temperatures at which nucleation is induced by the heterogeneity of type 1 and 2, respectively (Fig. 3.65).

In the special case of a homogeneous nucleation, Eq. 3.49 can be simplified to read

$$\Delta T_{c,\,hom} = T_c^\circ - T_{c,\,hom} = T_c^\circ/5;\ \text{ i.e.,}\, T_{c,\,hom} = 0.8T_c^\circ \tag{3.50}$$

where T_c° is the crystallization temperature in the bulk polymer (in K).

From the latter (Eq. 3.50), the homogeneous crystallization temperature for each polymer can be estimated in a simple way.

Furthermore, from Eq. 3.49 for heterogeneity of type 1, one may write

$$\Delta y1/y_p(m,c) \approx 62.5\ \left(T_{c,1}/T_c^\circ\right)\left(\Delta T_{c,1}/T_c^\circ\right)^2 \tag{3.51}$$

From this dependence, the relative values of Δy for different heterogeneities can be calculated at the corresponding degrees of undercooling.

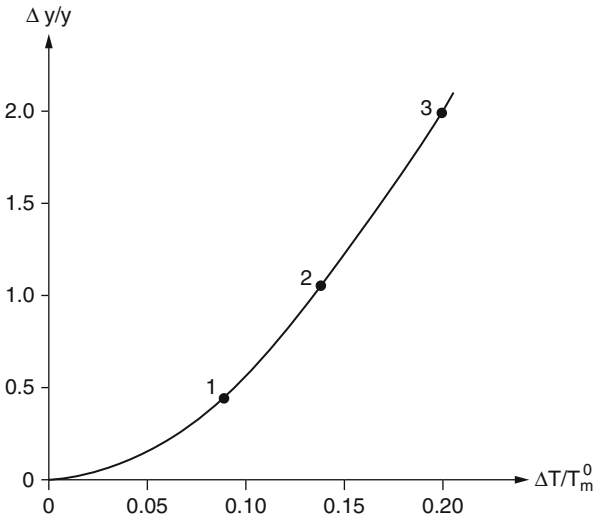

Fig. 3.65 Plots of the relative specific interfacial energy difference $\Delta y/y$ versus the relative undercooling $\Delta T/T^{\circ}_{m}$ at which a heterogeneity nucleates the polymer; (*1*) and (*2*), two different heterogeneous nucleations; (*3*) homogeneous nucleation (Frensch and Jungnickel 1989)

From the fractionated crystallization behavior and the blend morphology, one can determine the number density of the nucleating active species. Among a large number of small polymer droplets, each having a volume V_D, the fraction of droplets that contain exactly z heterogeneities of type 1 (inducing normally crystallization in the bulk polymer at T_c°) follows a Poisson distribution function (Pound and LaMer 1952):

$$f_z^{(1)} = \left[\left(M^{(1)} \cdot V_D\right)^Z / z!\right] \exp\left(-M^{(1)} \cdot V_D\right) \tag{3.52}$$

where $M^{(1)}$ is the concentration of heterogeneities of type 1 and $M^{(1)}.V_D$ is the mean number of heterogeneities of type 1 per droplet with volume V_D.

Hence, the fraction of droplets that contain at least one heterogeneity of type 1 can be given by

$$f_{z>0}^{(1)} = 1 - f_0^{(1)} = 1 - \exp\left(-M^{(1)} \cdot V_D\right) \tag{3.53}$$

Now considering that not all droplets have the same size, $f_{z>0}^{(1)}$ describes that fraction of the droplets (with average volume V_D) that crystallize induced by heterogeneity of type 1. The other droplets will crystallize at a different crystallization step. From the relative intensities of the fractionated crystallization steps, one can estimate the concentration of the different heterogeneities, if the mean size of these droplets is known.

In the special case where the usual crystallization from heterogeneity of type 1 is completely suppressed, Eq. 3.52 can be written as

$$M^{(1)} \cdot V_D << 1 \tag{3.54}$$

Table 3.27 Evaluation of the blend morphology and thermal behavior in immiscible PS/HDPE blends in which HDPE was the minor phase (Aref-Azar et al. 1980)

wt% HDPE	Size-dispersed phase (μm)	Number droplets (cm^{-3})	ΔH_m[a] (J/g)	X_c[b] (%)
1	0.1–0.3	10^{11}–10^{12}	–	–
5	0.3–0.5	10^{10}–10^{11}	163	55
10	2.0–3.0	10^{7}–10^{8}	159	54
20	5–10	10^{6}–10^{7}	184	63

[a]ΔH_m for pure HDPE is 293 J/g
[b]Degree of crystallinity, X_c, for HDPE homopolymer is 80 %

3.3.4.3 Droplet Crystallization in the Presence of a Matrix Melt

In most immiscible crystalline/amorphous polymer blends, the crystallization of the dispersed phase occurs in the presence of a molten matrix phase. In the following description, examples will be categorized according to the major classes, as listed in Table 3.14.

Polyethylene Blends

Blends of PS/HDPE have been investigated by Aref-Azar et al. (1980). Table 3.27 gives an overview of the crystallization behavior in the crystallizable dispersed phase.

It should be noted that the crystallization kinetics is related to the size of the dispersed HDPE droplets and the nucleation density. An increase in the amount amorphous PS caused the HDPE phase to be dispersed into finer droplets that, as a result, exhibited a lower degree of crystallinity, X_c, when isothermally crystallized. Furthermore, a higher degree of undercooling was needed to reach the same X_c in blends where the HDPE phase was dispersed into finer droplets, indicating that crystallization depends on the temperature. The melting behavior of the HDPE phase did not seem to be affected by blending.

Recently, Müller et al. (1995) and Morales et al. (1995) have reported on the crystallization of LLDPE that was finely dispersed in a PS matrix. A good correlation was found between the size of the LLDPE phase and the tendency to crystallize in a fractionated way. The authors showed that the relationship is only sensitive to the volume of the dispersed crystallizable droplets and not to the shape of the droplets.

Polypropylene Blends

Numerous studies have been performed on the crystallization behavior of PP in blends with an amorphous component. However, only few authors paid attention to the crystallization behavior of the PP phase when it formed the minor phase of the blend.

Ghijsels et al. (1982) investigated the multiple crystallization behavior of blends in which the crystallizable PP phase was finely dispersed into a SBS-rubber (TR). In the case where the latter was finely dispersed, the authors found the PP phase to crystallize at much higher undercooling. A serious drop in the degree of crystallinity, X_c, was also reported. The melting behavior of the fractionated crystallized blend did not seem to be markedly affected, e.g., ΔH_m and T_m remained constant, independent of the amount TR added.

Wei-Berk (1993) reported on the crystallization behavior of PP droplets dispersed in a PS matrix. A slight drop in $T_{c,PP}$ (as the PP phase became the minor phase) was observed. However, the author only investigated the behavior in blends containing more than 35 % PP, and did not correlate the crystallization behavior with the blend morphology.

Recently, Santana and Müller (1994) investigated the same polymer blend. These authors reported that droplets having a diameter of less than 6 μm crystallized at higher undercooling ($T_c \approx 78$ °C), while the larger droplets crystallized at $T_c \approx 105$ °C – the latter temperature corresponding to the bulk T_c for the PP used in the studies. The authors referred to the fractionated crystallization behavior caused by a lack of heterogeneities in some of the finely dispersed PP droplets, ending up with the appearance of the homogeneous crystallization peak. Hence, the nucleation mechanism was found to be strongly influenced by the blend morphology.

Polyester Blends

Quirk et al. (1989) investigated the crystallization behavior of PET in a PET/PS 25/75 blend. The PET particle diameter as determined by SEM was found to be in the range of 5 μm, being quite large due to the large difference in interfacial tension between both phases (hindering easy droplet breakup during mixing). Suppression of the cold crystallization in the PET droplets quenched from the melt was observed, along with serious depression of the total degree of crystallinity with increasing content of the amorphous phase.

PBS/PBA crystalline/crystalline miscible blends were recently studied for their crystallization behavior by Yang et al. (2011). Upon blending with PBS, PBA was found to exhibit fractionated crystallization during the nonisothermal crystallization process. The higher isothermal crystallization temperature (TIC) of PBS (e.g., 100 °C) was favorable for the fractionated crystallization of PBA, which was probably attributed to the distribution of PBA in the preexisting PBS matrix. At high TIC of PBS, the phase segregation of PBA was more obvious, that is, PBA can be distributed in the interspherulitic region as well as interfibrillar/interlamellar region of the PBS matrix. However, at low TIC of PBS, the phase segregation was not obvious. The parameters of the crystallization kinetics suggest that PBS suppresses the crystallization of PBA, which was mainly ascribed to the physical confinement effect of PBS on PBA. From the WAXD and FTIR analyses, it was concluded that PBS facilitates the formation of the PBA α-crystal, namely, the PBA polymorphic crystallization can be regulated. From polarized OM observation, the spherulite growth direction and morphology of PBA were found to be controlled by those of PBS. This was mainly ascribed to the induction effect of growth direction of PBS lamellae on PBA ones.

Polyamide Blends

Tol et al. (2005a) intensively described the crystallization phenomenon of polyamide (PA6) semicrystalline component in an immiscible blend with pure PS or (PPE/PS) amorphous miscible mixture. The idea was to have a controlled and a varying glass-transition temperature of the amorphous phase. Two situations

were studied: uncompatibilized blends and reactively compatibilized blends using SMA reactive copolymer. The composition and viscosity ratios of the blend have been selected to generate versatile phase morphologies including the most important ones for the study, i.e., PA6 droplets in (PPE/PS) matrix.

Uncompatibilized PA6/(PPE/PS) Blends

Multiple crystallization peaks were observed in blend systems where PA6 constitutes the dispersed droplets (s 65 and 66). The blends having continuous PA6 phase do not show significant differences in crystallization behavior compared to pure PA6 homopolymer. In contrast, as PA6 content decreases, it forms discrete droplet in the matrix. The multiple crystallization peaks correspond to different degrees of supercooling. As the size of the droplet exceeds a critical size, the PA6 crystallizes around its bulk crystallization temperature (188 °C). When the morphology becomes finer and the concentration of PA6 droplets per unit volume increases, a significant part of the droplets crystallize at higher degree of supercooling as translated by the intensity of the new crystallization peaks. This was ascribed to a heterogeneous nucleation of nuclei having different activities. Three crystallization peaks have been identified in blends with (PPE/PS) matrix. One of these peaks has been formed below ($T_c = 90$ °C), the average vitrification temperature of the matrix ($T_g = 150$ °C). It has been ascribed to a homogeneous nucleation after all the heterogeneities in the droplets have been exhausted. The authors concluded that:

- When the droplet size is small enough and the number of PA6 droplets exceeds the number of nuclei active at T_c bulk, crystallization takes place in different steps, at larger degrees of supercooling, via nucleation by different types of nuclei that need a larger supercooling to become active.
- The crystallization can be affected by the thermal history.
- Self-nucleation experiments generating a larger number of nuclei crystallizing at T_c bulk can lead to a complete suppression of the fractionated crystallization phenomena.
- When the amorphous phase is vitrified prior to crystallization, the nucleation densities increase, leading to less fractionated crystallization in the dispersed droplets.
- The overall crystallization rate, determined after self-nucleation, decreases with decreasing PA6 droplet size (20–1 μm), indicating the disturbing effect of the small dimensions of the micrometer-sized PA6 particles.
- The degree of fractionated crystallization, characterized by the fraction of the droplets that crystallized at temperature below T_c bulk, can be fairly related to the volume average droplet diameter.
- The number of crystallization peaks T_c bulk is very dependent on the droplet size distribution, leading to more peaks for broader distributions (Figs. 3.66 and 3.67).

Reactively Compatibilized PA6/(PPE/PS) Blends

The authors used SMA reactive copolymer that reacts via the anhydride group with the amine groups of the PA6 semicrystalline component of the blend and the

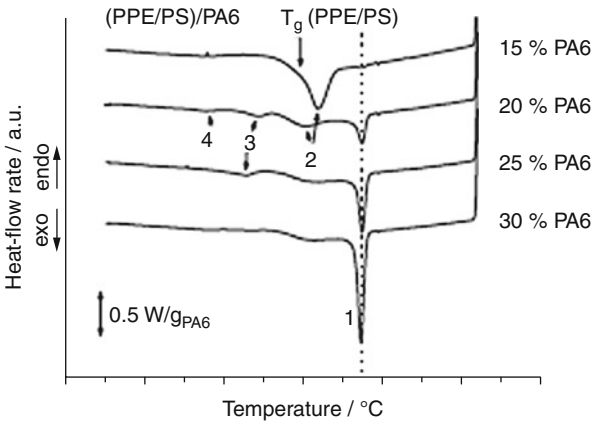

Fig. 3.66 DSC cooling curves for a number of (PPE/PS)/PA6 blend compositions with PA6 droplets (Tol et al. 2005a)

styrene segment ensures miscibility with the PS/PPE mixture. The effects of two copolymers, SMA2 (2 % MA content) and SMA17 (17 % MA), on the crystallization of PA6 in the immiscible (PA6/(PPE/PS)) blends were compared. Figure 3.68 is very illustrative of the effect of the SMA copolymer on the crystallization behavior of the blend. A very strong transition in crystallization behavior is observed when the blend phase morphology evolves from a co-continuous to a PA6-dispersed droplets. Reactive compatibilization with SMA2 strongly decreases the PA6 droplet size in the blend by a factor of 10 (from 1–2 to 0.1–0.2 μm on average). In addition, due to compatibilization, the droplet distribution is less polydisperse compared to uncompatibilized blends. An enormous retardation of the crystallization is induced by the reactive compatibilization. The bulk crystallization around 188 °C (peak1) is completely suppressed, and a crystallization peak emerges around 85 °C (peak 3 in Fig. 3.68a, peak4 in Fig. 3.68b), about 100 °C lower than the bulk crystallization temperature. The authors performed additional experiments combining the phase morphology (droplet size and distribution measurement) and crystallization phenomena and draw the following conclusions on the effect of the reactive compatibilization on crystallization of PA6 in compatibilized immiscible PA6/(PPE/PS) blends:

– Fractionated crystallization is strongly enhanced in the submicron-sized PA6 droplets per unit volume leading to a marked delay of crystallization to very high supercooling and ultimately to crystallization at temperatures as low as 85 °C.
– A clear relation between the number of dispersed PA6 droplets per unit volume and the intensity of the homogeneous nucleation peak at this very low crystallization temperature has been found.
– Abundant reaction of the reactive copolymer with the PA6 seems to reduce the mobility of PA6 chain segments, leading to an increased fractionated crystallization in the PA6 droplets.

Ethylene-1-octene copolymer was also used as an amorphous blend partner of PA6 in PA6/ethylene-1-octene blend reactively compatibilized using PE-g-MA reactive copolymer (Sanchez et al. 2006). Because of the dispersed phase

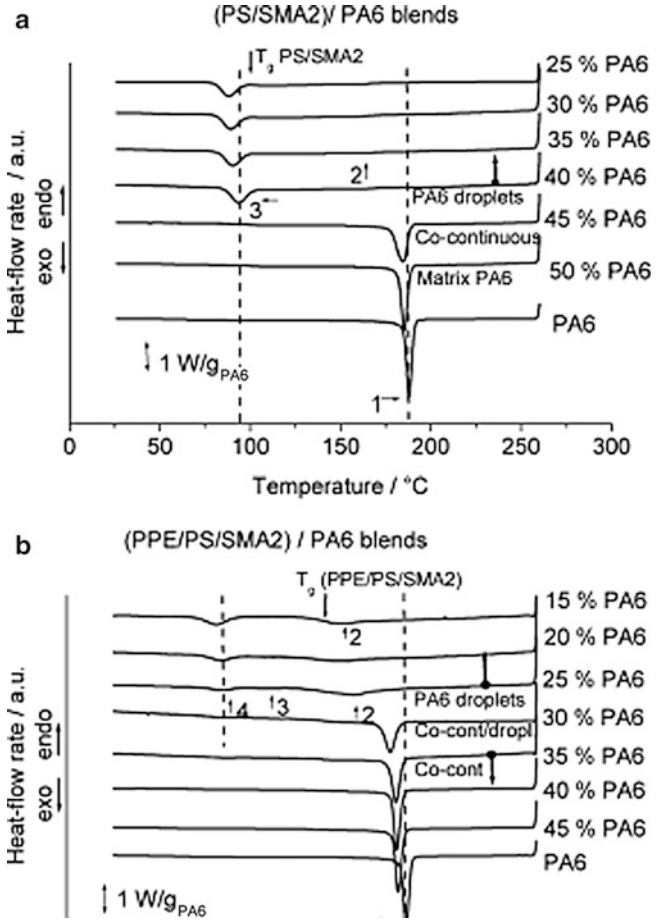

Fig. 3.67 DSC cooling curves at 10 K/min for (**a**) PS/PA6 and (**b**) (PPE/PS)/PA6 blend compositions (Tol et al. 2005a)

morphology, fractionated crystallization was observed, leading to an extra supercooling of PA6 (50 °C compared to bulk crystallization temperature). Self-nucleation experiments the authors used were able to demonstrate, as expected, that a lack of heterogeneities is at the origin of the fractionated crystallization.

Yordanov et al. (2005) have considered fractionated crystallization in blends of LDPE/PA6 reactively compatibilized using each of the three different types of reactive copolymers: EAA, EGMA, and SEBS-g-MA. As expected the SEBS-MA, owing to the efficient reaction of the maleic anhydride groups with the amine groups of PA6, resulted in the most significant particle size reduction of the dispersed phase. As a direct consequence, the most visible fractionated crystallization was obtained with this copolymer. Compatibilization with EGMA could not lead to PA6/LDPE blends that exhibit fractionated crystallization because of a lack of interfacial

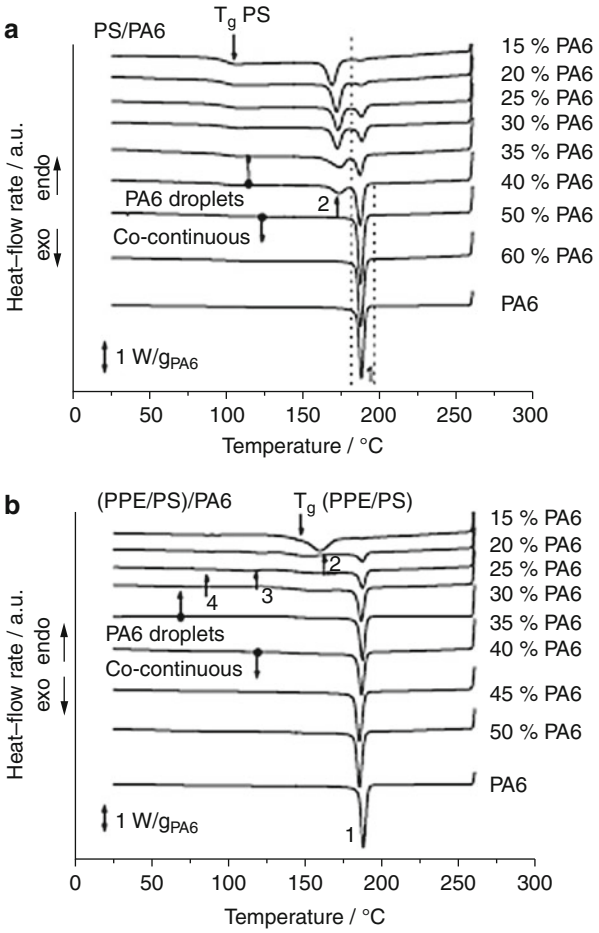

Fig. 3.68 DSC crystallization curves for different compositions of (**a**) (PS/SMA2)/PA6 blends and (**b**) (PPE/PS/SMA2)/PA6 blends. (PS/SMA2 ratio 92/8 w/w, (PPE/PS/SMA2)/PA6 80/20, and 85/15: 95/5 w/w (PPE/PS)/SMA2 (Tol et al. 2005b)

reaction and thus inefficiency in reducing particle size. The authors performed self-nucleation experiments and concluded that the lack of nuclei is responsible for the fractionated crystallization at high supercooling and not the absolute particle size reduction.

Other Blends

Robitaille and Prud'homme (1983) studied the crystallization in the liquid/liquid phase-separated melt of the triblock copolymer PEG-PI-PEG having a minor amount of PEG. The authors reported a lower degree of crystallinity of the PEG domains along with a slight melting-point depression. Due to the fine dispersion of PEG, the droplets only crystallized at much higher undercoolings (up to 60 °C lower than the bulk T_c), and less perfect crystalline lamellae were formed. These lamellae consequently melted at lower temperatures than the usual T_m. The bulk T_c has disappeared completely. The authors related this behavior to the

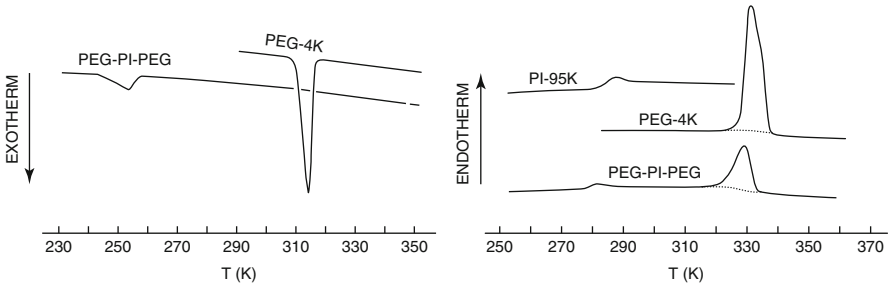

Fig. 3.69 DSC cooling and heating curves for the PEG-PI-PEG block copolymer, a pure PEG sample, and PI; the homogeneous crystallization of the PEG segment at much higher degrees of undercooling does not really influence its melting behavior (Robitaille and Prud'homme 1983)

lack of heterogeneities available in the PEG microdomains, which are hence nucleated at much lower temperatures by a homogeneous nucleation mechanism (Fig. 3.69).

Tang and Huang (1994a) investigated that the crystallization behavior of PA-6 is an EPDM matrix. The fractionated crystallization of the PA-6 occurs when the PA-6 content decreased below 15 wt%. Two crystallization peaks were observed, one around the bulk $T_{c,PA\text{-}6}$ and another at about 25 °C lower, caused by the smaller PA-6 droplets having a lack in heterogeneous nuclei. The ratio of the α/γ crystalline form was not altered by the fractionated crystallization, indicating that the lower crystallizing droplets do not crystallize in another crystalline form as in the bulk.

Fractionated crystallization of the POM crystalline phase in (PS/PPE) miscible amorphous phase has been investigated by DSC, and the results were correlated to the blend phase morphology (Everaert et al. 2000). This model blend was selected to investigate both the influence of the blend phase morphology and of the physical state of the amorphous PS/PPE matrix on the crystallization behavior of the minor POM phase. To have a varying Tg of the amorphous matrix, the PS/PPE composition has been varied as 85/15, 60/40, 50/50, and 40/60 wt:wt% to have tg's of 114 °C, 134 °C, 144 °C, and 156 °C, respectively. Interesting relationships were established between the crystallization features and the parameters of the phase morphologies developed in the blend. Figure 3.70 shows the absolute degree of crystallinity of the POM crystalline phase as a function of the average particle diameter of the POM dispersed as minor phase in PS/PPE amorphous matrix (the composition of Ha4 and Ha7 are 85/15 and 50/50 PS/PPE, respectively). The authors could not correlate the degree of crystallinity to the POM particle diameter. In contrast, as the fraction of POM droplets should reflect all homogeneously crystallized material, a correlation between both parameters could be found (Fig. 3.71). To elucidate a possible effect of the phase morphology of the blend on the crystallization of the crystalline polymer, the authors have asked and discussed the following key questions: (i) What determines the onset of fractionated crystallization and/or the offset of heterogeneous nucleation at T_c, bulk?

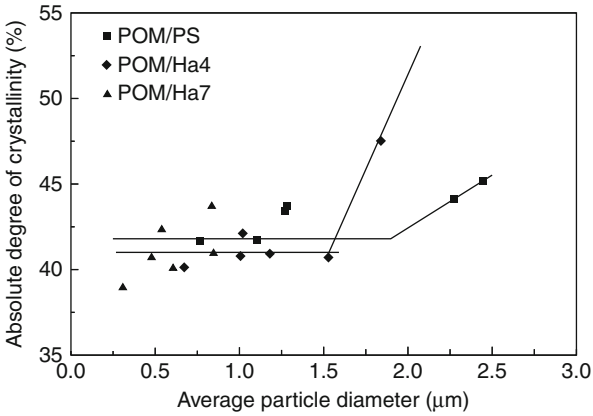

Fig. 3.70 Relationship between the absolute degree of crystallinity, X_c, of the POM phase and the average particle diameter of the POM droplets (Everaert et al. 2000)

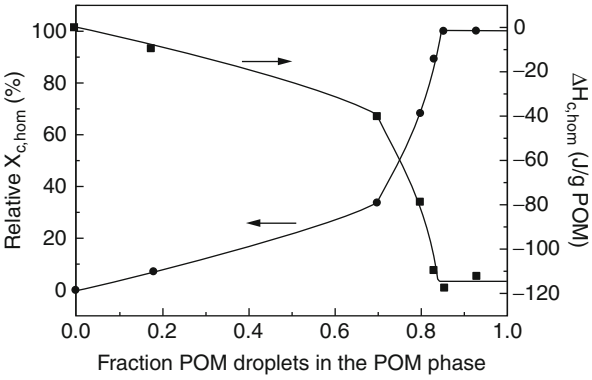

Fig. 3.71 Correlation between the fraction of POM droplets in POM/Ha7 blends with a composite-like phase morphology and the intensity of the homogeneous crystallization peak (Everaert et al. 2000)

(ii) Is fractionated crystallization solely related to the blend phase morphology? (iii) Under what conditions are multiple crystallization peaks possible, and what determines their number and extent? (iv) What causes the decrease of the crystallinity in fractionated crystallizing samples? The onset of fractionated crystallization was found to coincide with the center of the phase inversion region. In contrast, the morphological parameters and blend composition that could influence the offset of fractionated crystallization were less evidenced. The data presented in Table 3.28 reveal the effect of the POM content in POM/(PS/PPE) blend systems on the final degree of crystallinity, X_c, as calculated directly from fractionated crystallization.

The semicrystalline phase morphology and crystallinity of POM in POM/(PS/PPE) blends were studied with respect to fractionated crystallization (Everaert et al. 2003). The degree of crystallinity decreases with decreasing POM content with a visible shift from bulk to homogeneous crystallization. Analysis of WAXD reflections indicate that the decrease in X_c is not solely due to the formation of thinner lamellae at higher degrees of undercooling.

Table 3.28 Influence of the POM content in POM/(PS/PPE) blend systems on the final degree of crystallinity, X_c, as calculated directly from fractionated crystallization curves. X_c for POM is 54 %

Wt % POM	POM/PS	POM/Ha4	POM/Ha6	POM/Ha7	POM/Ha8
5	42[a]	41[a]	40[a]	39[a]	47[a]
10	42	41[a]	41[a]	41[a]	36[a]
15	43[a]	43[a]	39[a]	43	46
20	43	41	39	41	46
30	44	41	42	41	47
40	45	48	45	44	51
60	53[b]	46	51	53	52[b]

[a]Only one crystallization exotherm around 95 °C (homogeneous nucleation)
[b]Only one crystallization exotherm around 145 °C (bulk nucleation)

3.3.4.4 Droplet Crystallization in the Presence of a Glassy Amorphous Matrix

The crystallization of dispersed domains in the presence of a solidified matrix has not yet been a field of active research. Some examples are given below.

Polyethylene Blends

The thermal behavior of PS/LDPE blends has been investigated by Baitoul et al. (1981). A clear indication of the fractionated crystallization was deduced from the appearance of two additional crystallization peaks around 71 °C and 64 °C in all blends in which LDPE was the dispersed phase. Furthermore, the crystallization kinetics was found to slow down severely when the content of PS was raised.

Kunori and Geil (1980) investigated the melting behavior of the binary PC/HDPE blends, in which the weight percentage PE varied between 2 % and 10 %. The melting temperature of the HDPE droplets did not seem to be affected.

Polypropylene Blends

The majority of published papers on the crystallization of PP in blends concerns those blends in which the T_g of the amorphous component falls below the crystallization temperature of PP. The crystallization of PP in the presence of a glassy amorphous matrix has seldom been reported.

The well-known blend PC/PP has been intensively investigated by Favis and his co-workers (1987, 1988, 1990, 1992). Morphology development, rheology, compatibilization, etc., were studied, but no results on the thermal behavior of these blends were reported.

Polyester Blends

Quirk et al. (1989) have reported the crystallization behavior in blends of PPE with PET. Since the blend components showed only a small difference in the interfacial tension, quite small dispersions could be obtained ($d \approx 4$ μm). The authors reported that the glassy PPE matrix enhanced the cold crystallization of PET after being quenched. Decreasing the PPE content from 75 to 50 wt% resulted in the nearly

disappearance of the cold crystallization exotherm. This behavior was found to be opposite to that in a PS/PET blend (where PET crystallizes surrounded by a PS melt). No clear explanation has been given here.

A similar result for PPE/PET blends has been reported by Liang and Pan (1994). The authors found the cold crystallization temperature, $T_{c,\,cold}$, in the dispersed PET phase to be markedly lower than that of the virgin PET, indicating that PPE may partly act as nucleating agent to promote the nucleation of the PET component.

Other Blends

O'Malley et al. (1969) described the thermal behavior of PEG/PS blends in which PEG was dispersed into fine droplets. A clear indication of fractionated crystallization combined with a simultaneous decrease in the total degree of crystallinity with increasing weight fraction of PS has been observed. Again, a slight decrease of the melting temperature, T_m, with about 2 °C was detected, although ΔH_m remained unaffected. This was attributed by the authors to the formation of less perfect crystalline lamellae during the crystallization at higher undercooling.

Chang et al. (1991) reported on the melting behavior in PC/POM blends. The blends were found to behave in a similar way as the above-described PEG/PS blend.

3.3.5 Conclusions

It can be stated that the crystallization behavior of a semicrystalline polymer phase, dispersed into an amorphous matrix, is characterized by:

(i) Fractionated crystallization or homogeneous nucleation if the minor phase is finely dispersed. Annealing or large droplets resulted in the appearance of a crystallization peak close to the bulk T_c° of the homopolymer.

(ii) A decrease in the overall degree of crystallinity, X_c, after cooling from the melt, most pronounced in finely dispersed blend morphologies.

(iii) A slight decrease of the melting temperature due to the formation of less perfect crystalline lamellae at higher undercoolings. A decrease of the overall melting enthalpy, ΔH_m, could be observed clearly, only in blends where the crystallizable dispersed phase did not undergo recrystallization upon heating.

3.3.6 Binary Polymer Blends Containing Two Crystallizable Phases

A large number of polymer blends consists of two crystallizable phases (Table 3.15); hence, more studies have been carried out on the thermal behavior of crystalline/crystalline polymer blends.

The morphology of a polyblend consisting of two crystallizable polymers can vary depending on the processing conditions and the relative rates and temperature of crystallization of the constituent polymers. These can either crystallize at the same time (coincident crystallization, see further) or separately in a sequential

manner, leading to different morphologies and hence different properties. As such, in blends of two semicrystalline polymers, the physical properties may be altered not only by the blend composition and the phase morphology but also by changing their relative crystallization behavior. Therefore, it is important to study the effect of blending on the crystallization behavior of each component in the blend, to understand the structure development as influenced by melt-processing.

Because the phases are physically separated in the melt, the theory concerning the crystallization behavior as discussed above can be combined to understand the crystallization and melting behavior of most crystalline/crystalline polymer blends. In general, both crystallizable phases crystallize separately around their characteristic bulk T_c-value (as long as the minor phase is not dispersed into very fine droplets). The T_c-values can be somewhat shifted due to the migration of heterogeneities from one phase toward the other phase or due to the nucleating activity of one – crystalline or crystallizing – phase at the interface with the second phase. However, changes in the nucleation density of both phases will be more clearly reflected in the spherulite size of each blend component with respect to the homopolymer. This can have important consequences for the final mechanical properties of the blend (Friedrich 1978, 1979).

In the following overview, a survey of the most important topics concerning crystallization behavior in immiscible crystalline/crystalline polymer blends is given. Because the physical state of the second phase affects the crystallization mode of the phase under consideration, a distinction has been made for blends crystallizing in a melt environment and those crystallizing when the second phase has solidified.

3.3.6.1 Crystallization of the Matrix in the Presence of a Molten Dispersed Phase

For most commonly studied polymer blends, crystallization of the matrix occurs in the presence of a molten dispersed phase. The crystallization behavior of the continuous phase can be compared to that found for crystalline/amorphous blend systems in which the dispersed amorphous phase was in the molten state.

Polyethylene Blends

Because of the low crystallization temperature of the polyethylenes (HDPE, LDPE, LLDPE, etc.) (see Table 3.15), in most commonly used blends, the dispersed phase has already solidified before the PE matrix starts crystallizing. However, Greco et al. (1987a) studied the crystallization of HDPE ($T_c \approx 118$ °C) in an 80/20 binary blend with EPR elastomers containing a different ethylene/propylene ratio. The HDPE phase was reported to exhibit higher T_c-values during cooling from the melt, indicating enhanced nucleation, due to the nucleating effect of the EPR copolymers on the HDPE matrix. Furthermore, the melting point, T_m, shifted to slightly higher temperatures relative to the homopolymer due to better crystal perfection as a result of the dissolution of some low molecular weight ("defective") HDPE molecules into the EPR copolymer phase during the melt-mixing process. The latter phenomenon was directly related to the ethylene content in the copolymer.

Polypropylene Blends

Blends of isotactic polypropylene, PP, with a polyethylene are immiscible and, owing to their commercial importance, have been the subject of intensive studies. In these blends, PP crystallization mostly takes place in the presence of molten PE droplets.

Long et al. (1991) investigated the crystallization behavior in blends of PP with LLDPE. They found the crystallization temperature of the PP matrix, T_c, to decrease slightly upon the addition of LLDPE. However, the degree of crystallinity, X_c, and the spherulite growth rate, G, were not affected. The authors concluded that the overall crystallization rate of PP in the matrix decreased due to a decreasing primary nuclei density. The latter was confirmed in O. M. experiments by the increased size of the PP spherulites upon the addition of LLDPE. However, Zhou and Hay (1993) reported that with the addition of LLDPE to PP, the crystallization rate remained similar as for the PP homopolymer.

Flaris et al. (1993) investigated also the same blend system and reported that blending had a pronounced effect on the lamellar morphology. Furthermore, the isothermal crystallization experiments indicated that the spherulite growth rate, G, and the nucleation density of the PP phase were enhanced. The authors suggested that these observations could be related to the formation of additional nucleation sites, which arise from the polymer-polymer interfaces created by the blending.

Because three different observations were reported on the crystallization of the PP matrix in which LLDPE droplets are dispersed, no unambiguous conclusions on this matter can be given. A serious investigation of all factors playing a role here is necessary in the future.

Blends composed of a PP matrix with LDPE as the minor dispersed phase have been intensively investigated by Teh (1983), Bartczak et al. (1984), Galeski et al. (1984), and recently Teh et al. (1994a). All authors found LDPE to act primarily as an efficient nucleating agent for the PP matrix, reducing the average PP spherulite size, and to induce the formation of some large β-form PP crystals at the interface with the LDPE phase that melt at a lower temperature, $T_m = 155\ ^\circ\mathrm{C}$ as compared to normal α-form PP crystals with $T_m = 165\ ^\circ\mathrm{C}$. Galeski et al. (1984) and Bartczak et al. (1984) revealed that the nucleating activity of the LDPE phase was mainly attributed to the migration of heterogeneous impurities from LDPE to PP during the melt-mixing process. Furthermore, Galeski et al. (1984) showed the spherulite growth rate of the PP matrix to be unaffected by the dispersed molten LDPE droplets and showed that these droplets were not rejected by the growing PP spherulites.

In the case of PP/HDPE blends, the influence of the HDPE component was more complex and dependent on the physical state of the dispersed HDPE droplets. At a T_c high enough to prevent any HDPE crystallization, the overall rate of crystallization of the PP matrix in isothermal crystallization was found to be strongly reduced by the addition of HDPE (Bartczak et al. 1986). Since the spherulite growth rate of PP was found to be constant and independent of the blend composition (Teh et al. 1994a), this decrease has been attributed to a decrease in the nucleation density of the PP phase. Bartczak et al. (1986) related this to the migration of heterogeneous nuclei from the PP phase toward the HDPE melt during

melt-blending. As a result, the PP spherulite size was found to increase (Bartczak et al. 1986; Teh et al. 1994b). The same observations were reported for PP/HDPE blends cooled slowly from the melt (Plesek and Malac 1986).

However, in the case of either an isothermal crystallization at temperatures below the crystallization temperature of HDPE or crystallization at a higher cooling rate, there may have been migration of nuclei from the PP toward the HDPE phase, but the overall number of heterogeneous nuclei was increased due to the presence of HDPE crystallites that may have acted as additional nucleating centers for PP (Lovinger and Williams 1980; Gupta et al. 1982; Bartczak et al. 1986; Plesek and Malac 1986; Teh et al. 1994a, b). This results in a drastic reduction of the PP spherulite size (Noel and Carley 1984; Lovinger and Williams 1980; Plesek and Malac 1986). Moreover, Bartczak and Galeski (1986) reported that spherulitic crystallization of a polymer near the interface can cause its deformation, increasing the interfacial area, and can lead to an improvement of toughness and impact properties.

Greco et al. (1987b) studied the crystallization in immiscible PP/EPR blends. The average spherulite size in the PP phase was smaller than in the homopolymer. The higher the PP contents (*C*-3) in EPR, the stronger the nucleating effect for the matrix. The authors experimentally showed that migration of impurities could not cause this effect and that the copolymer composition was the most important factor. An increase in the PP content of the EPR caused a higher miscibility (defective PP molecules could be partially dissolved in the EPR phase), leading to more perfect PP crystallites melting at a higher T_m, and also caused a stronger nucleating effect.

Pukansky et al. (1989) investigated both the crystallization and melting behavior and the global blend morphology in PP/EPDM blends over the whole composition range. Blends quickly cooled from the melt did not show significant changes in the crystallization behavior of the PP matrix. However, blends crystallized at a fixed rate of 10 °C/min behaved differently. Thermograms of the blends containing between 5 and 50 vol% EPDM showed a second melting peak at lower temperature, corresponding to the melting of the β-form of PP. Furthermore, the authors reported that small amounts of EPDM slightly increased the $T_{c,PP}$, but did not affect the degree of crystallinity. Dispersed EPDM droplets thus seem to promote the formation of the hexagonal β-form of PP.

An overview of the effects affecting the primary nucleation in immiscible PP-based blends is provided in Table 3.29.

Polyethylene Terephthalate Blends

Wilfong et al. (1986) reported on the effects of blending low concentrations (1–10 wt%) **polyolefin** with PET on the crystallization and toughening behavior of the latter. The authors studied blends of PET with LLDPE, HDPE, PP, and poly (4-methylpentene-1), all of them having a lower melting point than PET (Table 3.15). Polyolefin melts did not enhance the nucleation of PET, although the spherulite size of the PET matrix was found to be 2.5–3 times larger than for the homopolymer, with a broader spherulite size distribution. Both the crystallization

Table 3.29 Overview of the phenomena influencing heterogeneous primary nucleation in polypropylene-based immiscible blends (After Bartczak et al. 1995)

Blend system[a]	Migration of impurities[b]	Crystallization of the second component[b]	Influence of the interface[b]	References
PP/LLDPE	—[c]	—	-	Zhou and Hay (1993)
	↓↓	—		Long et al. (1991)
		—	↑↑	Flaris et al. (1993)
PP/LDPE	↑↑	↑[c]	↑	Bartczak et al. (1984), Teh (1983), Galeski et al. (1984), Teh et al. (1994a)
PP/HDPE	↓↓↓			Bartczak et al. (1986), Teh et al. 1994a, b
	↓↓↓[d]	↑↑↑[d]		Lovinger and Williams (1980), Gupta et al. (1982), (Bartczak et al. (1986), Teh et al. (1994)
PP/EPR	——	—		Greco et al. (1987b)

[a]Data concerning the crystallization of the matrix polymer (mentioned first in the blend code)
[b]↑ indicates an increase of the nucleation density in the blend, ↓ indicates a decrease of the nucleation density (the number of arrows is related to the intensity of the effect)
[c]— indicates that the authors did not find evidence explicitly for the mentioned topic to influence the nucleation of PP in the blend system described
[d]Found for samples crystallized nonisothermally

rate and the degree of crystallinity were found to be reduced by blending. This was attributed to the expense of energy that was required by the crystallizing growth front to reject and deform the polyolefin dispersed molten droplets. Martuscelli (1984) and Bartczak et al. (1984) have calculated that the rejection and/or deformation of dispersed droplets by the crystallizing growth front can cause a marked depression of the spherulite growth rate, G.

Poly(phenylene sulfide) Blends

Poly(phenylene sulfide), PPS, is an expensive, high-performance but brittle specialty resin. Blending can offer a good alternative both in toughness improvement and cost reduction (Nadkarni and Jog 1991).

Shingankuli et al. (1988) and Jog et al. (1993) investigated the influence of blending PPS with PET on its thermal and crystallization behavior. Blending was found to enhance the PPS nucleation. Isothermal crystallization experiments revealed that the crystallization time of PPS decreases along with the crystallization induction time. Both parameters were found to depend on composition. Optical microscopy confirmed this and revealed that the size of PPS spherulites in PPS/PET blends was drastically reduced as compared to the homopolymer. Furthermore, the degree of crystallinity of the PPS phase decreased with increasing PET concentration. However, dynamic crystallization experiments showed a constant value of $T_{c,PPS}$. The authors have related the accelerated crystallization of PPS in a blend with PET to the nucleation at the interface of the PET droplets. Owing to its supercooled state, the PPS matrix consists of highly ordered chains.

Nadkarni and Jog (1986), Nadkarni et al. (1987), and Jog et al. (1993) investigated the crystallization in blends of PPS with three types of HDPE, having a different melt flow index. In contrast to the PPS/PET blends, PPS crystallizes now in a superheated HDPE melt environment. From the dynamic cooling experiments, it was found that the presence of the HDPE melt suppresses the crystallization of PPS. The crystal growth rate, G, of PPS was found to remain unchanged, but its nucleation density was reduced as the concentration of HDPE in the blend increased or when the melt viscosity of the HDPE phase decreased. As a consequence, the overall crystallization rate of PPS was found to be retarded.

Other Blends

Chen et al. (1988) reported about blends of polyamides with a polyolefin. PA-11/LDPE blends and PA/HDPE blends both showed an increase of the melting temperature of the PA-11 matrix due to the addition of the polyolefin. No further attention was paid to this phenomenon.

Holsti-Miettinen et al. (1992) and Ikkala et al. (1993) recently studied the crystallization behavior of PA-6 blended with PP. No shift of the crystallization temperature of the PA-6 matrix was observed in the blends; the dispersed PP droplets did not influence the crystallization behavior of the matrix.

Frensch and Jungnickel (1989) investigated the influence of blend composition on the crystallization and melting behavior of PA-6/PVDF blends and PBT/PVDF blends. The crystallization of the PA-6 matrix and PBT matrix was promoted by the dispersed molten PVDF phase, as indicated by the rise in their T_c in the blends, while their relative crystallinity remained unaffected. The authors assigned this increase in T_c to migration of nucleating heterogeneities from the dispersed PVDF phase toward the matrix phase during melt-mixing of the blends.

3.3.6.2 Crystallization of the Matrix in the Presence of a Solidified Dispersed Phase

The crystallization of a polymer in the presence of solidified domains of the second phase takes place through a heterogeneous nucleation process. Since the rate of heterogeneous nucleation is higher than that of homogeneous nucleation, and since primary nucleation is the rate-controlling step for polymer crystallization, the crystallization rate is expected to be higher in such blends when compared to homopolymers (Nadkarni and Jog 1991).

Polyethylene Blends

On account of their commercial interest, the crystallization of HDPE, LDPE, and LLDPE in blends with PP has been extensively investigated. In these systems, the PP phase solidified already before the PE matrix starts crystallizing.

In the case of LDPE/PP blends, not much attention has been focused on the case where the LDPE phase forms the matrix. Teh (1983) reported no shift in the melting temperature of the LDPE matrix in the presence of solidified PP domains. Bartczak and Galeski (1986) observed that the LDPE crystallinity remained unaffected by blending.

Zhou and Hay (1993) investigated the crystallization behavior in LLDPE/PP blends. The crystallization rate of the LLDPE matrix, measured from isothermal DSC experiments, was not really affected by the dispersed PP domains. However, its degree of crystallinity slightly decreased with increasing PP content in the blend. According to the authors, this could be ascribed to the lower degree of perfection of the LLDPE crystals.

More extensive investigations have been performed on HDPE/PP blends by Martuscelli et al. (1980) and Bartczak and Galeski (1986). From the isothermal crystallization experiments, it was found that the rate of crystallization of the HDPE matrix was markedly reduced upon addition of small amounts of PP (10 wt%). The authors attributed this phenomenon to the increased melt viscosity of the sample caused by the presence of solidified PP domains. Moreover, Plesek and Malac (1986) have calculated from the surface tensions of the homopolymers at T_c that PP crystallization will not cause the nucleation of the HDPE phase, while in the reverse case HDPE crystals will induce the nucleation of PP.

Similar results were reported by Nadkarni and Jog (1986) and Nadkarni et al. (1987) for HDPE/PPS blends. The degree of crystallinity of HDPE in blends with a HDPE matrix was not affected by blending. The degree of supercooling required for initiating nonisothermal crystallization of HDPE was surprisingly not affected by the presence of solid PPS domains. However, isothermal crystallization halftimes for HDPE in the blends containing more than 10 wt% PPS were longer than for the HDPE homopolymer. Again, this has been attributed by the authors to the increased melt viscosity due to the presence of solidified PPS domains.

Frensch et al. (1989) reported on the crystallization of HDPE in a blend with POM. The HDPE matrix crystallized in all samples at almost the same temperature and to the same extent, independent of the extrusion time.

Polypropylene Blends

The majority of papers related to the crystallization of isotactic polypropylene(PP)-based blends concern those where the PP matrix crystallizes in the presence of a molten dispersed phase of polyethylenes and olefinic elastomers. As a result, crystallization of a PP matrix in the presence of a solidified dispersed polymer has seldom been reported (Nadkarni and Jog 1991).

Shingankuli (1990) studied the crystallization behavior of PP in the presence of solidified PVDF domains. A higher crystallization temperature of the PP matrix phase was observed, indicating an enhanced nucleation in the blends. The degree of crystallinity of PP was found to increase by about 30 % to 40 % with increasing PVDF content. Isothermal crystallization studies also confirmed the acceleration of the overall crystallization rate in terms of shorter crystallization halftimes for PP.

More efforts have recently been dedicated in understanding the crystallization behavior in PP/PA-6 blends. Holsti-Miettinen et al. (1992), Moon et al. (1994), and Ikkala et al. (1993) found that the crystallization temperature of the PP matrix by cooling from the melt rises by about 10 °C by adding PA-6. Ikkala et al. (1993) observed that the largest temperature increase was caused at a PA-6 concentration of about 20 wt%; in this case, the PA-6 dispersion size was quite small (2.5 μm).

Moon et al. (1994) have related this temperature shift to the migration of heterogeneous nuclei toward the PP matrix during the melt-mixing process, together with the nucleating agent-like behavior of the solidified PA-6 domains. No change of the melting peak has been noticed (Park et al., 1990). Grof et al. (1989) performed some isothermal crystallization experiments on fibers of the PP/PA-6 blend. In accordance with the cited findings, the latter authors reported a decrease both in the crystallization halftime and the induction time for crystallization of PP in PP/PA-6 blends, while no change in the degree of crystallinity was observed.

Tang and co-workers (1994) investigated briefly the crystallization behavior of PP in blends with PA-12. The melting point remained unaffected by blending. However, a slight shift of the crystallization peak (about 2.5 °C), upon cooling from the melt, was reported for blends comprising 33 wt% PA, along with an increase of the height of the T_c peak. The PP matrix has been nucleated by the dispersed PA-12 domains. The authors related this to the fine morphology; at the interface of the phases, epitaxial crystallization had also been observed. This was also the reason why the PA-12 phase in the blends only existed in the γ-form. However, it should be mentioned that these PP/PA-12 blends were prepared from solution.

Polyethylene Terephthalate Blends

Only few papers related to the crystallization of a PET matrix in immiscible crystalline/crystalline blends have been published.

Shingankuli et al. (1988) investigated the thermal behavior of PET blends with the glass fiber-reinforced polymer PPS. Dynamic crystallization experiments revealed that the PET crystallization behavior was significantly altered by blending. Upon the addition of PPS, both the onset temperature for crystallization and the peak value, T_c, showed a dramatic shift to higher temperatures (up to 20 °C). Also, the degree of crystallinity significantly increased in the blends. The author attributed the phenomenon to the heterogeneous nucleation induced by the glass fibers in the PPS phase and the nucleating activity of the already solidified PPS domains. As a result, the PET matrix in the blends became richer in heterogeneous nucleating sites as compared to virgin PET. Isothermal experiments confirmed these conclusions and showed that the crystallization halftime of PET decreased drastically in the blends (attributed to the enhanced nucleation). Furthermore, an increase of the onset of melting of the PET matrix (15 °C) with increasing content of PPS in the blends has been observed. The melting behavior PET in the blends has been explained by the formation of larger and more perfect crystallites (due to the nucleation at higher temperatures) with a narrower size distribution and by an increased degree of crystallinity.

Other Blends

Frensch and Jungnickel (1989, 1991) and Frensch et al. (1989) have investigated the thermal behavior of polyvinylidene fluoride, PVDF, in blends with polyamides, in relation to the blend morphology. PA-6 droplets could be finely dispersed into the PVDF matrix. The crystallization temperature of the PVDF matrix did not seem to be affected in the blends. A similar behavior was observed in PVDF/PA-66 blends.

Investigations on the crystallization behavior of PVDF in a blend with polybutyleneterephthalate, PBT, have been reported by Frensch and Jungnickel (1989) and Frensch et al. (1989). PBT dispersed droplet size was found to be an order of magnitude larger than the dispersed PA droplets in PVDF blends. However, in this case, the $T_{c,PVDF}$ displayed a shift to higher temperatures (2–8 °C) upon blending with PBT, which was attributed to the nucleating efficiency of amorphous or crystallizing PBT domains (which subsequently crystallized coincidentally with the PVDF matrix).

3.3.6.3 Crystallization of the Dispersed Phase in the Presence of a Matrix Melt

Immiscible blends most often show a two-phase morphology consisting of a continuous matrix and a droplet-like dispersed phase beyond the phase inversion region. From Sect. 3.2.3, it is clear that the crystallization behavior of droplets can be dramatically affected as compared to the homopolymer.

In summary, (i) dispersed drops can have an altered nucleation density, caused by the migration of heterogeneous nuclei during the melt-mixing process, they can be nucleated by a crystallizing or solidified matrix, the interface can induce some additional nucleating centers, etc. (ii) The smallest dispersed droplets can suffer from the lack of heterogeneous impurities in each droplet, what may result in a fractionated crystallization. In some cases, this can give rise to the coincident crystallization of the dispersed phase with the (lower crystallizing) matrix (see Sect. 3.2.4.6).

Polyethylene as Dispersed Phase

Because of the low crystallization temperature of all polyethylenes as compared to most other commonly used thermoplastics, crystallization will proceed most often in an already solidified matrix. No literature could be found on the crystallization behavior of PE in a molten matrix environment.

Polypropylene as Dispersed Phase

Typical polymer blends with isotactic polypropylene, PP, are the PP/PE blends, in which PP is the first crystallizing component.

Zhou and Hay (1993) investigated the crystallization in LLDPE/PP blends. They reported that the extent of crystallization in PP droplets is seriously hindered by the low nucleation density of PP, resulting in a serious drop of the degree of crystallinity during the isothermal measurements. From these experiments, it could be predicted that cooling from the melt would result in a fractionated crystallization (30 wt% PP) or even homogeneous crystallization (10 wt% PP). Similar results had already been reported by Long et al. (1991), Pukanszky et al. (1989), and recently Müller et al. (1995) and Morales et al. (1995). The latter authors even mentioned that the retarded crystallization of PP droplets in some cases finally resulted in the coincident crystallization of PP with the LLDPE matrix. Furthermore, a partial change in the crystallographic form from α to the lower melting β-form was observed. Lovinger et al. (1977) reported that the β-form is nucleated at a lower rate than the α-form and hence promoted on homogeneous nucleation.

Teh (1983) reported only the melting behavior of LDPE/PP blends – no shift in $T_{m,PP}$ was seen. An enhancement in the formation of the β-form PP spherulites in the LDPE melt was observed.

Blends of HDPE with PP have been studied by several authors. However, not much attention has been focused on the crystallization behavior of the dispersed phase yet.

Polyamide as Dispersed Phase

Several blends with polyamides, crystallizing at high temperatures, have been studied. Chen et al. (1988) investigated the phase morphology and melting behavior of HDPE/PA-11 and LDPE/PA-11 75/25 blends. The melting point of the dispersed PA-11 phase was found to be unaffected by blending.

Several studies have been performed on the thermal behavior of PP/PA-6 blends. Park et al. (1990) reported a melting-point depression for the dispersed PA-6 phase (about 4 °C), having an average particle size of 2–5 μm at 25 wt% PA-6 in the blend. However, the relations between the crystallization phenomena and the blend morphology were not explored. Ikkala et al. (1993) have investigated the correlation between the blend morphology, crystallization, and melting behavior of the minor component in PP/PA-6 blends. The PA-6 phase was reported to crystallize at its bulk temperature. However, compatibilization (resulting in the formation of a finer dispersion) did not show any crystallization exotherm around the bulk $T_{c,PA\text{-}6}$. This could be explained by the retarded crystallization caused by a lack of heterogeneous nuclei in the PA-6 droplets. Finally, the nucleating activity of both blend components on each other caused the coincidental crystallization of the PA-6 with the PP matrix.

Moon et al. (1994) also investigated the thermal behavior of PP/PA-6 70/30 blends. The authors reported the T_c of the PA-6 droplets to rise remarkably (by about 14 °C) as compared to the T_c of the virgin PA-6. This rise in $T_{c,PA\text{-}6}$ was explained by analogy to findings of Khanna et al. (1988a, b) on pure virgin PA-6 homopolymer, suggesting that melt extrusion of PA-6 would lead to a more ordered molecular arrangement that persisted in the molten state due to hydrogen bonding, and as such caused a faster crystallization. This has been confirmed by crystallization experiments on melt-extruded PA-6 homopolymer. The results of the blends as compared to melt-mixed pure PA-6 agree with those reported by Ikkala et al. (1993) – no shift in the $T_{c,PA\text{-}6}$ was caused by blending. Furthermore, they also reported that compatibilization of the blends caused a decrease of the dispersed phase size, leading to fractionated and subsequently coincident crystallization.

Frensch and Jungnickel (1989) and Frensch et al. (1989) tried to elucidate the crystallization behavior of the minor phase in the binary PVDF/PA-6 blends, in relation to the final blend morphology. They reported that the crystallization of the PA-6 droplets was fractionated and/or retarded, depending on the number of mixing cycles and dispersion size. The smaller the PA-6 droplets, the more pronounced the retardation of the crystallization peak ($\Delta T \approx 40$ °C). Nevertheless, the melting endotherm remained unaffected. They concluded that part or all of the PA-6 phase finally coincidentally crystallized with the PVDF matrix due to the specific mutual nucleating efficiency of both components.

A similar behavior has been reported by Frensch and Jungnickel (1991) for PVDF/PA-66 blends. In this case, the undercooling associated with the retarded crystallization was about 90 °C higher than the one for the bulk crystallization! The size of the dispersed PA-66 droplets has been found to be only about 0.3 μm. The authors concluded that the appearance of fractionated and coincident crystallization is correlated with the low interfacial energies between the amorphous melt phases, providing a high level of dispersion, and between the crystalline phases, providing a nucleating efficiency.

Other Blends

Shingankuli et al. (1988) reported on the crystallization of dispersed PPS domains in a PET matrix. The onset of crystallization of the dispersed PPS domains decreased (by about 7 °C) with decreasing PPS content, together with the crystallization peak and the degree of crystallinity. The authors concluded that the PPS crystallization was retarded mainly when the PPS content in the blends was below 20 wt%. Furthermore, the onset of melting of the PPS fraction remained nearly unaffected, except for those blends containing less than 20 wt% PPS. In the latter case, the onset of melting seriously decreased (by about 30 °C), whereas the melting peak temperature and heat of fusion remained constant. This can be attributed to the lower crystallization temperature of the PPS droplets leading to the formation of less perfect, lower melting crystallites.

Klemmer and Jungnickel (1984) have reported on the fractionated crystallization of POM in an HDPE matrix. They found an additional crystallization peak of POM to occur 14 °C lower than the bulk crystallization peak. This was attributed to the fractionated crystallization of POM, caused by an interface-induced additional inhomogeneous nucleation and crystallization. It was shown that this phenomenon only occurs in those blends where the number of the dispersed particles was higher than the number of available heterogeneous particles. Moreover, the preparation method clearly influenced the fractionation due to the change of the particle sizes – fractionated crystallization has been observed only in melt-mixed blends.

Frensch and Jungnickel (1989) and French et al. (1989) have investigated PVDF/PBT blends and related their thermal behavior with the blend morphology. Similar to PVDF/PA-6 blends, the PBT droplet crystallization was completely suppressed in an 85/15 blend and finally crystallized coincidentally with the PVDF matrix. Again this phenomenon could be related to the fine dispersion of PBT droplets, in number exceeding the available nuclei. Shorter melt-mixing cycles caused a coarser dispersion leading only to a fractionated crystallization of PBT at $T_{c,bulk}$ and at $T_{c,PVDF}$.

3.3.6.4 Crystallization of the Dispersed Phase in the Presence of an Already Solidified Matrix

Polyethylene as Dispersed Phase

PP/PE blends have been studied extensively by several authors. Zhou and Hay (1993) reported that the dispersed LLDPE droplets in PP/LLDPE blends showed problems in nucleating at the normally expected bulk crystallization temperature, T_c. Also, a serious decrease of the degree of crystallinity from isothermal measurements, as the LLDPE content decreased, could be observed. Contrary to these

observations, Müller et al. (1995) recently stated that the LLDPE droplets do not exhibit fractionated crystallization when they are dispersed in a PP matrix (although they do in a PS matrix), because of the nucleating effect of the solidified PP matrix on the LLDPE droplets.

Galeski et al. (1984) and Teh et al. (1983) have investigated PP/LDPE blends. No shift of the melting peak for LDPE has been observed. Both authors showed migration of the impurities during the melt-mixing process from the PP toward the LDPE phase. No further details on the crystallization behavior of the LDPE droplets themselves were reported.

Nadkarni and Jog (1986) have reported on PPS/HDPE blends. The degree of crystallinity of HDPE was reduced when HDPE was the minor phase. Furthermore, the $T_{c,HDPE}$ shifted to somewhat lower temperatures (by about 5 °C) but only in those blends with a low HDPE content. Isothermal crystallization halftimes for HDPE in its blends with PPS decreased as the HDPE content decreased, indicating an enhanced nucleation from the solidified PPS interfaces.

Chen et al. (1988) have investigated the melting behavior of 75/25 PA-6/HDPE and PA/LDPE **blends**. No shift has been observed in the melting point. No attention has been focused to the crystallization of the PE droplets.

Polypropylene Blends

Blends of PA-6 with PP dispersed as fine droplets have been examined recently by several authors.

Ikkala et al. (1993) investigated the thermal behavior and morphology of blends of PA-6 in which PP had been dispersed. In binary blends, PP droplets crystallized even at somewhat higher temperature (by about 5 °C) than the PP homopolymer, attributed to the nucleating activity of the solidified PA-6 matrix toward the dispersed PP phase. Morphological investigations revealed that the PP dispersion in the blends was quite coarse; so nearly every droplet contained the heterogeneities that usually nucleate PP. However, upon compatibilization, this behavior changed. Compatibilizers that formed an immiscible interlayer between PA-6 and PP and caused a reduction of the dispersed particle size gave rise to a retarded crystallization of the PP phase in a PA-6/PP 80/20 blend, decreasing the $T_{c,PP}$ by 50° C! This behavior was directly caused by the small size of the dispersed phase and the prevented nucleation from the solidified matrix. Blends containing 40 wt% PP did not crystallize in a retarded way due to their coarser droplet size, but clearly were not nucleated by the PA-6 phase as seen from $T_{c,PA\text{-}6} = T^{\circ}_{c,PA\text{-}6}$. Similar results have been presented by Holsti-Miettinen et al. (1992).

Other Blends

Tang and Huang (1994b) investigated the relation between blend morphology and crystallization behavior in PP/PEG blends, prepared by solution blending. They reported that the PEG phase crystallized fractionated at different degrees of undercooling, but was always nucleated heterogeneously. The authors related the different crystallized fractions to PEG droplets of different sizes; the largest droplets crystallized at the bulk crystallization temperature.

Shingankuli et al. (1988) studied the crystallization behavior of dispersed PET droplets in a PPS matrix. A serious increase of the crystallization temperature of the dispersed PET phase (by about 20° C) during cooling experiments from the melt was explained as a result of the nucleating activity of the glass fibers in the PPS matrix, but also from the solidified PPS itself. As a result, the crystallization became more heterogeneous and the crystallization peak width decreased drastically. A corresponding increase in the onset of melting for PET (about 15 °C) was attributed to the formation of thicker and more perfect PET crystallites in the blends.

Frensch and Jungnickel (1989) and Frensch et al. (1989) have studied PA-6/PVDF blends. The authors reported that the finely dispersed PVDF droplets crystallized fractionated at different undercoolings. Again this could be directly related to the lack of heterogeneous nuclei in some of the smallest droplets. Increasing the blend composition or decreasing the mixing cycles caused the crystallization of the PVDF droplets to shift to higher temperatures, due to the formation of a coarser morphology. A similar behavior has been reported for PA-66/PVDF blends (Frensch and Jungnickel 1991).

A reverse case however has been reported by the same authors for the crystallization of dispersed PVDF droplets in a solidified PBT matrix. In the latter case, $T_{c,PVDF}$ even shifted to higher temperatures (by about 5 °C) than for homopolymer crystallization. The shift seemed to become less pronounced as the number of mixing cycles increased. No explanation for this behavior was reported. The melting endotherm of the PBT droplets was not affected by the blending.

3.3.6.5 Coincident Crystallization in Crystalline/Crystalline Polymer Blends

A few authors have observed coincident crystallization of both phases in crystalline/crystalline immiscible blends. This phenomenon was reported for blends in which the minor phase exhibits a higher degree of undercooling for crystallization due to its fine dispersion (see Sect. 3.2.3) and the matrix phase crystallizes at its bulk T_c that is lower than that of the minor phase. An additional factor that should be taken into account is that a heterogeneous nucleation is promoted on surfaces with a high interfacial tension (Helfand and Sapse 1975) (i.e., a crystallizing phase boundary). This can lead to the "coincident crystallization" of both phases, as it has been reported by Frensch and Jungnickel (1989, 1991) and by Frensch et al. (1989).

Principle of Coincident Crystallization

It has been observed that this phenomenon is connected with the phase dispersion of the minor component and is enhanced when the dispersion becomes finer. Upon cooling from the melt, a finely dispersed phase can exhibit fractionated crystallization, what implies that none, or only part of the dispersed droplets crystallize at their bulk T_c. This type of crystallization is related to the lack of heterogeneities in the droplets, required for nucleation at the bulk T_c.

When the blend is now further cooled, two possible ways of primary nucleation are possible. In the first case, the matrix phase is nucleated by heterogeneous species present in this phase, and, instantly, newly created crystals appear. Hence,

the crystallization temperature of the matrix will be situated at its bulk T_c. The second possibility for coincident crystallization occurs in the case one finds again a single crystallization peak for the matrix phase, which however takes place above its bulk T_c. Some novel mutual nucleating mechanism was suggested in such blends; a molten component (minor phase) acts as nucleating substrate for the matrix, which instantaneously crystallizes (Frensch and Jungnickel 1989).

For both cases, when the Δy-value (see Sect. 3.2.3.2) between these newly formed crystals and the melt of the minor phase is smaller than that of all other heterogeneities present in the minor phase (except probably the nuclei of "type 1" normally nucleating around the bulk $T_{c,minor}$), its associated specific undercooling must be so small that the crystals can induce the crystallization of that minor phase from the instant of their own creation (Frensch et al. 1989). Consequently, a single *coincident* crystallization peak will be registered in DSC thermograms.

It is clear that this phenomenon is phase morphology-dependent. Only in those blends where the minor phase is dispersed into sufficiently fine droplets, this phase has the opportunity to exhibit fractionated crystallization. Hence, only at low blend compositions and/or good matching viscosities of both phases (where the capillary number C_a predicts droplet breakup being dominant above coalescence) the occurrence of coincident crystallization is possible.

Examples of Coincident Crystallization

Frensch and Jungnickel (1989, 1991) and Frensch et al. (1989) have investigated the crystallization behavior of PVDF/PA-6, PVDF/PA-66, and PVDF/PBT blends. The PVDF/PA-6 blends showed a composite droplet-type morphology (finely dispersed matrix droplets encapsulated in the minor phase droplets) that disappeared after sufficiently long mixing cycles. Along with these observations, coincident crystallization was found in PVDF/PA-6 blends for an 85/15 and 75/25 composition only. The influence of morphological changes could be significant; after four mixing cycles, the dispersed PA-6 droplets became finer and did not contain small PVDF inclusions anymore. Along with this observation, only one single coincident crystallization peak could be found from DSC. The small exotherm at 184 °C caused by some larger PA-6 domains containing the PVDF inclusions with a small exotherm at 113 °C had disappeared completely by the mixing (Fig. 3.72). PVDF crystallization was found to be initiated by nucleation from heterogeneities of "type 1" at the bulk $T_{c,PVDF}$. A similar behavior has been reported for PVDF/PA-66 blends by Frensch and Jungnickel (1991).

A second system investigated by the authors was the PVDF/PBT blend. Similar effects could be observed. However, coincident crystallization in the PVDF/PBT 85/15 blend occurred at a somewhat higher temperature than the bulk $T_{c,PVDF}$. It could be concluded that in this case, the PBT melt induced the crystallization of the PVDF matrix phase.

Besides the cases of coincident crystallization reported previously, recent investigations on PP/PA-6 blends in which a compatibilizing agent had been used to obtain finer and more homogeneous dispersed phase morphology also mentioned coincident crystallization of the PA-6 droplets with the PP matrix (Ikkala et al. 1993; Moon et al. 1994). However, this has not been observed in the binary blend.

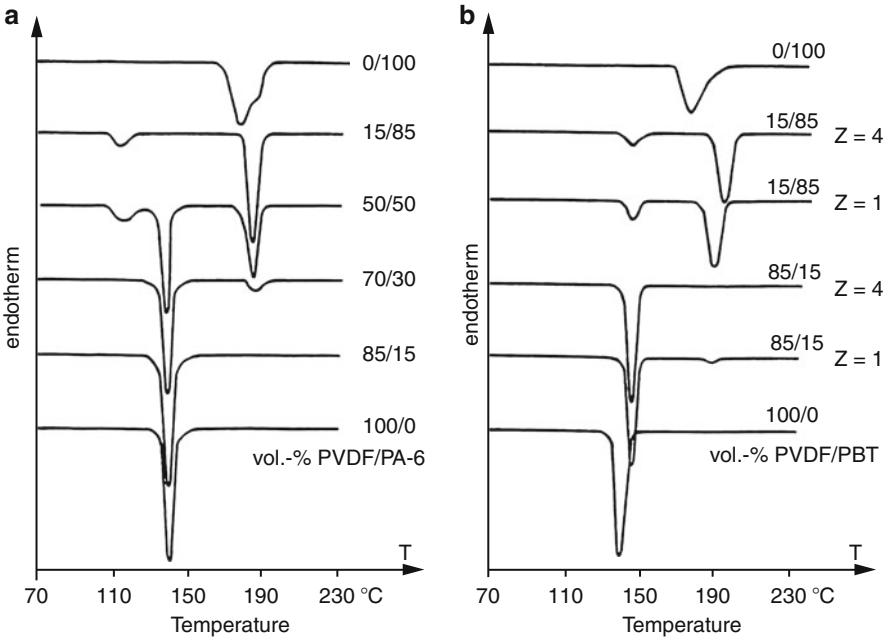

Fig. 3.72 Retarded and/or fractionated crystallization causing coincident crystallization in PVDF/PA-6 and PVDF/PBT blends. Influence of the blend composition (**a**) and the number of extrusion cycles *Z* (**b**) (Frensch and Jungnickel 1989)

3.3.6.6 Effect of Compatibilization on the Crystallization Behavior in Crystalline/Crystalline Polymer Blends

Blending offers an interesting means of tailoring product properties to specific applications. However, in the case of immiscible polymer pairs, the desired properties are not achieved readily without a compatibilizer, which enhances the phase dispersion and stability, as well as a good adhesion between the phases. This can be effectuated by physical or reactive methods (Folkes and Hope 1993). Compatibilization strongly affects the blend phase morphology, and as such, it also may influence the crystallization behavior of the blend (Flaris et al. 1993). Because both factors are related to the final properties of the blend, it is worth paying attention to these phenomena.

Several authors have investigated the influence of compatibilization on the global blend morphology. However, only a few authors really tried to understand the effect of compatibilization in crystalline/crystalline polymer blends on the crystallization kinetics, melting behavior, and semicrystalline morphology of the components. In Table 3.30, some recent results on this topic are summarized.

From the data presented in this table, it appears that in contrast to binary blends without a compatibilizer, the crystallization of the minor component in compatibilized blends cannot be solely explained by the size of the dispersion (Ikkala et al. 1993; Flaris et al. 1993; Tang and Huang 1994a; Holsti-Miettinen et al. 1995). Other factors

Table 3.30 Influence of a compatibilizing agent on the crystallization behavior of binary crystalline/crystalline polymer blends

Blend system[a] +compatibilizer	Studies on the influence of	Crystallization	Explanation	Reference
PP/PA-6 + MAH-g-PP 70/30	Concentration compatibilizer (in phr)	PP matrix: $T_{c,PP}$ matrix ≈ cte PA-6 droplets: $T_{c,PA\text{-}6}$ ↓ from 195 °C (0phr) to 188 °C (1.5 phr) $X_{c,PA\text{-}6}$ also ↓ From > 2 phr MA = > coincident crystallization of PA-6 with PP matrix ($\Delta T = 60$ °C)	Increase of phr MA-g-PP => Interfacial tension ↓ => Dispersion size PA-6 ↓↓ => Lack of heterogeneities in each droplet => Retarded crystallization Constraint effect of grafted PA-6 chains is negligible	Moon et al. (1994)
PP-g-MA/PA-6 77/23 50/50	Composition	*PP matrix: $T_c \approx T_{c,bulk}$ *PA-6 dispersed: fractionated crystallization = > Coincident cryst. with PP	Compatibilization => Interfacial tension ↓ => Droplet size ↓ => Lack of heterogeneity of type 1 — > crystallization by nuclei of type 2 which in his turn induces PP-MA crystallization	Tang and Huang (1994a)
PA-6/PP +MAH-g-PP +MAH-g-SEBS +FA-g-EBA +GMA-g-E EA 80/20 60/40	Composition Type of compatibilizer	*PA-6 matrix: $T_c \approx T_{c,bulk}$ *PP dispersed 20 % – > Depending on type of compatibilizer: • Cryst. around $T_{c,bulk}$ • Retarded cryst. ($\Delta T \approx 50$ °C) *PP dispersed 40 %: no large shift down of T_c	* If PA-6/PP phases in direct contact (no comp or analog. comp. as MA-g-PP) => PA-6 nucleates PP droplets => No lack of nuclei in droplets => $T_c \approx T_{c,bulk}$ *If SEBS, EBA, or E EA => immiscible interlayer between phases => Small droplets with lack of nuclei => T_c ↓↓ *PP droplets are large (coalescence) and contain enough heterogeneities to cryst. at $T_{c,PP}$	Holsti-Miettinen et al. (1992) Ikkala et al. (1993)
PP/PA-6 +MAH-g-PP +MAH-g-SEBS +FA-g-EBA +GMA-g-E EA 80/20 60/40	Composition Type of compatibilizer	*PP matrix: $T_c \approx T_{c,bulk}$ but slight ↑ in T_c (10 °C) in case of binary blend and MAH-g-PP *PA-6 dispersed: coincident crystallization with PP	*PA-6 has nucleating effect on PP cryst. at interface if in direct contact SEBS, EBA, and E EA form immiscible interlayer between PA-6 and PP => no nucleation => $T_{c,PP} \approx T_{c,bulk}$ *Compatibilization => serious reduction of PA-6 droplet size => lack of nucleating species => retarded cryst.	Holsti-Miettinen et al. (1992) Ikkala et al. (1993)

(*continued*)

Table 3.30 (continued)

Blend system[a] +compatibilizer	Studies on the influence of	Crystallization	Explanation	Reference
PP/PEG[a] + (PP-MA)-g-PEG 75/25 50/50	Composition	*Isothermal cryst. rate of both PP and PEG ↑ with compatibilizer Growth rate remains cte. Avrami exp. PP = cte. Avrami exp. PEG: 1 - > 2. *Fractionated cryst. of PEG is reduced by adding the compatibilizer	Mutual nucleation between PP and PEG	Tang and Huang (1994b)
PP/LLDPE + EP blockpol. + SEBS triblock + SEBS-g-MA 72/18/10	Type of compatibilizer	• Nucleation density at $T_c = 135$ °C: – ↑↑ with EP – ↓ with SEBS • Spherulite growth rate ↑ upon compatibilization • Interfacial free energy of PP crystal surfaces ↓ with compatibilization	• Compatibilization changes the interface morphology = > Additional nucleation sites from interfaces • Finer dispersion of LLDPE can cause more unidimensional growth of crystals	Flaris et al. (1993)
PP/LLDPE + EP blockpol. + Butyl rubber + EPR + SEBS triblock 72/18/10	Type of compatibilizer	• $T_{c,PP}$ ↑ (3–4 °C) when compat. is added: – Peak temp. independent on type of compat. – Onset temp. is dependent on type compat. • Half-width of exotherm ↓ strongly by addition of compat., independent of type used	• Rate of nucleation ↑ • Crystal size distribution becomes more uniform due to higher nucleation rate	Plawky and Wenig (1994)
PA-6/ionomer 90/10 80/20 70/30 60/40	Concentration of ionomer	• Dramatic ↑ in crystallization halftimes • $T_{c,PA\text{-}6}$ ↓ with [ionomer] ↑ (by ±4 °C) • Relative X_c ↓ with [ionomer] ↑ • Much wider distribution of PA-6 crystallite sizes	Strong interactions between PA-6 and ionomer impeded the crystallization of PA-6	Willis et al. (1993)

[a]All blend systems listed have been prepared by melt-mixing, except when indicated with

affecting the crystallization are the type of compatibilizer and its degree of miscibility with one or both of the blend components, the amount of compatibilizer added, the amount of interface created, and other effects.

The general influence of a compatibilizer on the crystallization behavior of an immiscible polymer blend system is still far from being well understood. However, abstract can be made between two main classes. A first class consists of compatibilizers that form a kind of "immiscible" interlayer between the two phases. Examples are given by Holsti-Miettinen et al. (1992) and Ikkala et al. (1993) for PP/PA-6 blends to which MAH-g-SEBS, FA-g-EBA, and GMA-g-E EA have been added. The compatibilizer prevents direct nucleating effects from one phase on the other. As such, only the size of the dispersion relative to the nucleation density of the dispersed phase and the nucleating effect of the compatibilizing agent itself play a role in the crystallization behavior (Fig. 3.73). Remark however that the size of the dispersion is often directly related to the concentration of the compatibilizer added (Moon et al. 1994).

A second class consists of compatibilizers that have an analogous chemical structure compared to one or two of the blend components. Here, the influence of a compatibilizer on the crystallization behavior of both phases is complex. Several factors have to be taken into account: nucleating effect of the matrix on the dispersed phase or from the dispersed phase on the matrix, the size of the dispersed phase relative to the nucleation density of that phase (and thus to the composition, content of the compatibilizer, etc.), nucleating effect of the compatibilizer itself, interactions of the compatibilizing agent and one or both phases which can impede the crystallization, cocrystallization of the compatibilizer with one of the phases, etc. An illustration is given in Figs. 3.72 and 3.73. Again, the concentration of compatibilizer plays a crucial role (Fig. 3.74).

Compatibilization seems to be of industrial interest in several ways: besides the improvement of the phase dispersion and adhesion, leading to superior mechanical properties, it also often can prevent the minor crystallizable dispersed phase from fractionated or retarded crystallization, which make faster production times and higher thermal stability of the products possible.

3.3.6.7 Conclusions on the Crystallization Behavior of Immiscible Crystalline/Crystalline Polymer Blends

The scientific literature on crystallization in polymer blends clearly indicates that the crystallization behavior and the semicrystalline morphology of a polymer are significantly modified by the presence of the second component even when both phases are physically separated due to their immiscibility. The presence of the second component, either in the molten or solid state, can affect both nucleation and crystal growth of the crystallizing polymer. The effect of blending on the overall crystallization rate is the net combined effect on nucleation and growth.

From the above literature survey, it is clear that the physical state of the second phase at the moment of crystallization is of utmost importance.

The crystallization of a *continuous matrix in which the dispersed phase is in the molten state* can be influenced by several phenomena. One of the most important

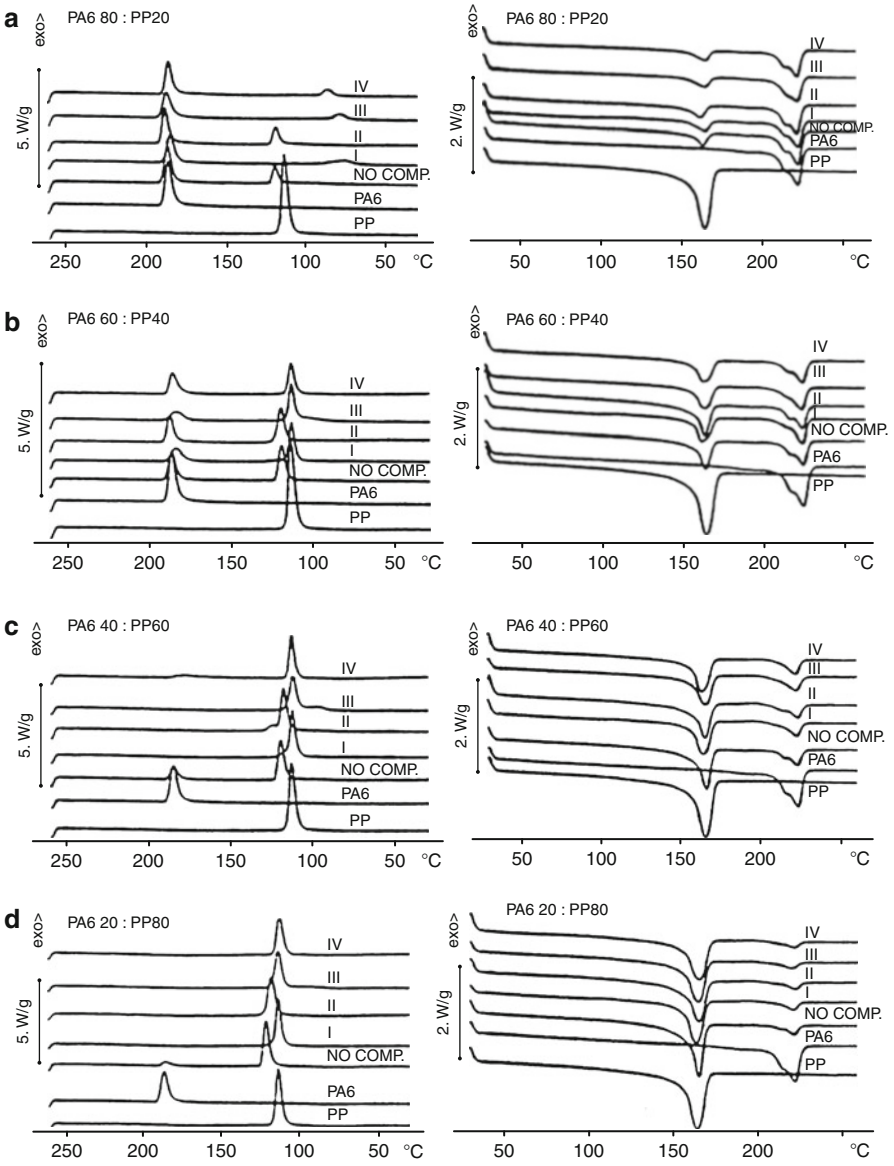

Fig. 3.73 Influence of compatibilization (10 wt%) on the crystallization and melting behavior of PA-6/PP blends with various blend compositions. Compatibilizer types used were EBA-g-FA (I), PP-g-MAH (II), SEBS-g-MAH (III), and E EA-GMA (IV) (Ikkala et al. 1993)

factors that play a role here is the possibility that impurities and nuclei migrate during the melt-mixing process, hence altering the nucleation density of the components. Furthermore, the interface may enhance the nucleation, mostly due to highly ordered structures in supercooled melt droplets.

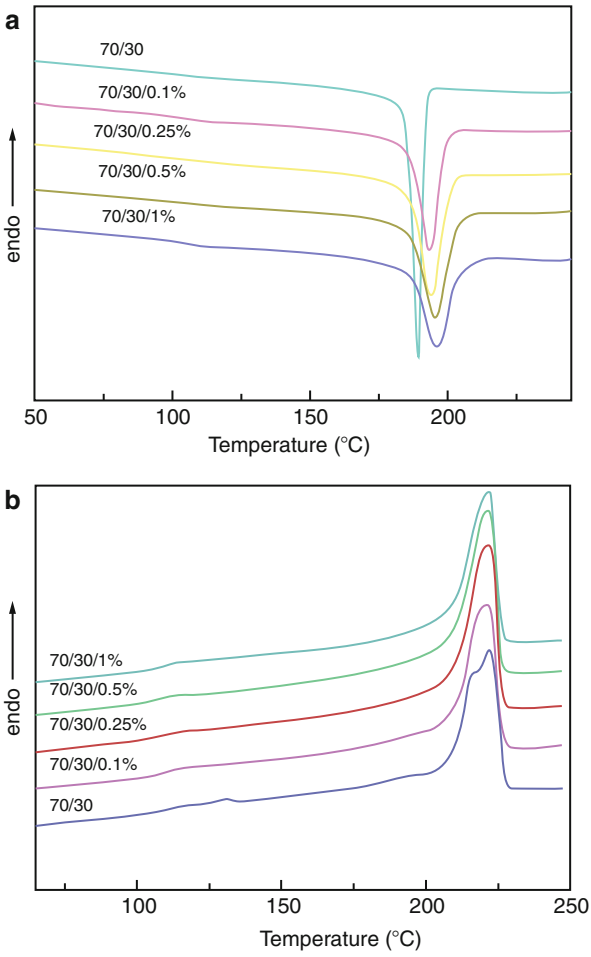

Fig. 3.74 DSC (**a**) cooling and (**b**) heating curves of PA6/ABS (70/30 wt) blends with various contents of MWNTs (Liu et al. 2012)

It should however be mentioned that the crystal growth rate, G, is generally not affected. Only in some exceptional cases where the growing crystallizing front rejects and/or deforms finely dispersed melt droplets, a decrease of G has been reported. It can thus be concluded that the matrix always crystallizes around its bulk temperature. Migration of nuclei, nucleation effects, etc., result in a shift of the $T_{c,matrix}$ by 5–10 °C, on average. The melting behavior of the matrix remains in general unaffected.

In the case of the *crystallization of the matrix in the presence of already solidified or crystallizing particles*, migration of nuclei still can play an important role. However, several other phenomena have to be taken into account. First of all, the solidified domains can act as efficient nucleators. Furthermore, retarded crystallization of finely dispersed droplets can nucleate the matrix and leads to coincident crystallization of both phases. Finally, it has been reported that epitaxial crystallization at the interfaces sporadically occurs. All these phenomena lead to an increased heterogeneous nucleation of the matrix phase.

Although most often also here the crystal growth rate is not affected, some authors have reported that finely dispersed solidified domains can increase the melt viscosity of the matrix in such a way that the crystallization rate becomes depressed. Again, the matrix component will crystallize around its bulk temperature. The abovementioned phenomena can eventually alter the spherulite size and shift the T_c of the matrix on average by 5–10 °C. The melting behavior remains normally unaffected.

The crystallization and melting behavior of a dispersed phase is highly different from the behavior of the continuous phase and much more sensitive for changes.

Droplets crystallizing in a melt matrix can just crystallize at their bulk temperature or show shifts of their T_c as a result of migration of nuclei, as has been outlined for matrix crystallization in the melt.

However, an important additional factor that plays a role here is the size of the dispersed phase. When the number of finely dispersed droplets exceeds the available heterogeneities of "type 1," fractionated or even homogeneous crystallization will occur, leading to shifts in the crystallization temperature by sometimes up to 100 °C (as compared to the homopolymer). This can result in a change of the crystal polymorphic form, coincident crystallization with a lower crystallizing matrix component, etc. However, the melting peak in the latter case will only be slightly depressed (by 2–4 °C) due to the formation of less perfect crystallites at lower temperatures. Additionally, it has been demonstrated that compatibilization can induce drastic changes in the blend phase morphology and thus in the crystallization and melting behavior.

In the case where *dispersed droplets crystallize in an already solidified matrix*, the same phenomena as in the previously described case can influence the thermal behavior of the dispersed phase. Additionally, nucleation from the already solidified matrix will play a distinguished role. An induction of heterogeneous nuclei often can reduce the fractionated crystallization or even bring the T_c back at its bulk temperature.

3.3.7 Crystallization in Immiscible Polymer Blends Containing Nanoparticles

Solid particles can be used as fillers dispersed in a matrix composed of one polymer or copolymer but can also be added in a miscible and immiscible binary, ternary, or multicomponent blend. The objective of the addition of fillers is diverse. They can be used as fillers to reduce the price of the composite and to improve the properties of the material (mechanical, aspect, chemical, etc.). Nanoparticles are among the category of fillers, the particle size of which is in the nanometer scale. They are considered as a new generation of particles which is progressively occupying a strategic position in the area of material development. Carbon nanotubes (CNTs) are nanoparticles that have been widely used in various fields owing to their remarkable mechanical, thermal, and electrical properties. One of the most intriguing applications of CNTs is the polymer/CNTs composites. Because of the combination of low density,

nanometer scale diameter, high aspect ratio, and, more importantly, unique physical properties such as extremely high mechanical strength and modulus, CNTs have emerged as potential reinforcing filler in polymer composites with excellent performance and multifunction. Nanoparticles can also be added to polymer matrices for specific effect of modifying a single but discrete property such as crystallization of homopolymers. In this application, they are nucleating agents as they enhance the crystallization of the polymer matrix where they are dispersed via a heterogeneous nucleation process. The use of nanoparticles as nucleating agents and more generally as crystallization modifiers in polymer blends is poorly reported in literature. Only few reports deal with this particular application of nanoparticles. Bose et al. (2007) performed an interesting investigation on fractionated crystallization in reactively compatibilized PA6/(amorphous)ABS blends. They added multiwall carbon nanotubes (MWNT) as heterogeneous nucleating agents. SMA- or SMA-modified MWNT were able to reduce significantly the particle size of PA6 up to a concentration of 1 wt% SMA. Fractionated crystallization was observed in both reactively compatibilized and non-compatibilized 20 PA6/80ABS blends. Delayed crystallization was reported for both types of blends due to lack of heterogeneities because of indirect but crucial effect of particle size reduction.

Pillin and Feller (2006) investigated the crystallization of the PBT minor phase in an EEA continuous matrix by DSC and SEM. When PBT is the minor phase, PBT crystallizes at a lower temperature of 105°C. Introducing different CB nanoparticles into the EEA continuous phase at contents increasing from 0.02 to 5 wt% resulted in important modifications of the PBT crystallization. A new PBT exotherm appeared at $T_c = 144$ °C on the addition of CB, becoming really visible at $T_c = 158$ °C and finally moving to $T_c = 185$ °C at high content. The areas corresponding to the new peaks were found to increase to the detriment of that of the fractionated crystallization at $T_c = 105$ °C. Morphological studies and interfacial tension measurements were made to understand the surprising activity of the CB. Moreover, the substitution of the EEA phase with a less polar component as, e.g., LLDPE, confirmed the importance of the strong interactions developed by EEA with CB aggregates.

Liu et al. (2012) have recently investigated the morphology, melting, crystallization, and mechanical properties for similar blend combination of PA6/ABS with MWNT nanotubes. PA6/ABS blends (70/30 and 50/50 wt) with 0, 0.1, 0.25, 0.5, and 1 wt% MWNTs were studied. Figures 3.75 and 3.76 show the crystallization and melting behaviors of PA6/ABS (70/30 wt) and (50/50 wt) blends with different contents of MWNTs. By incorporating MWNTs, the crystallization peak of PA6 shifted to higher temperature regions, the same effect has been reported in various polymer/CNTs composites (Li et al. 2006; Assouline et al. 2003; Valentini et al. 2003). The crystallization onset temperature (Tco) and the crystallization peak temperature (Tcp) increase with increasing the content of MWNTs. In PA6/ABS (70/30 wt) blends, PA6 crystallized at 191.4 °C, and with the incorporation of 1 wt% MWNTs, PA6 started to crystallize at 203.6, i.e., 12.2 °C higher than that of PA6 in simple (nonmodified blends). In PA6/ABS (50/50 wt) blend, the increment in Tco is also 12.2 °C. The long fibrillar MWNTs provided ideal

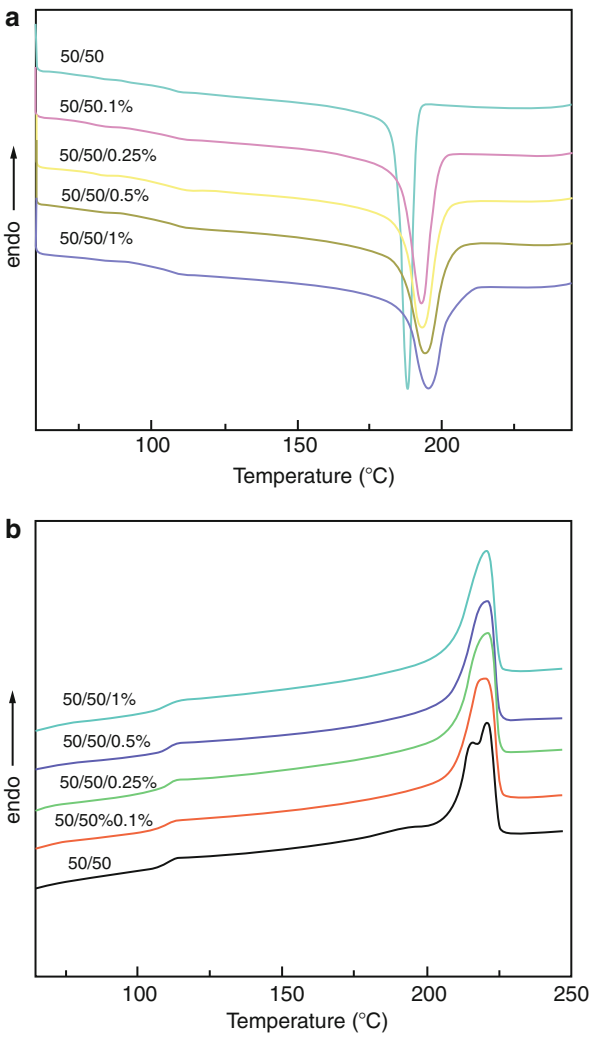

Fig. 3.75 DSC (**a**) cooling and (**b**) heating curves of PA6/ABS (50/50 wt) blends with various contents of MWNTs (Liu et al. 2012)

nucleation sites for PA6 chains (Gong et al. 2000). Indeed, the nucleation ability of MWNTs was quite high and effective. When the content of MWNTs in PA6 increases, more heterogeneous nucleation sites are available, leading to higher Tco and Tcp. Additionally, a weak exotherm at about 110 °C is found in Fig. 3.75a, c, which is often referred to as fractionated crystallization. This phenomenon often appears when the crystallizable polymer exists as the minor phase in a dispersed droplets form. In the composition the authors selected, PA6 acts mainly as the matrix. Indeed, fractionated crystallization is less visible, because numerous new interfaces are introduced during melt-mixing which can cause heterogeneous nucleation (Turbull et al. 1950; Helfand et al. 1977). In the melting endotherms,

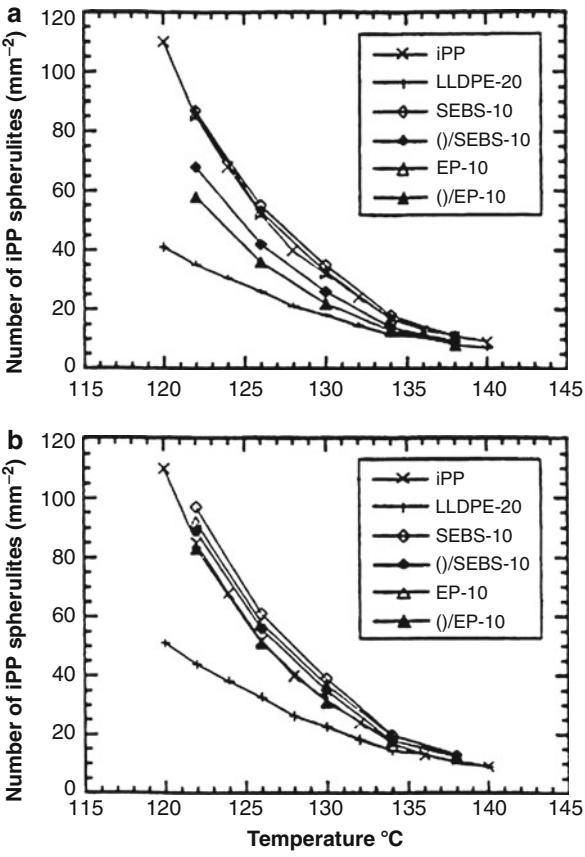

Fig. 3.76 The effect of compatibilizers (SEBS) and (EP) on the nucleation of isotactic PP at various temperatures: (**a**) measured as blend volume and (**b**) calculated as PP volume fraction (Long et al. 1995)

PA6 forms two melting peaks in both PA6/ABS (70/30 wt) and PA6/ABS (50/50 wt) simple blends. The double melting peaks were not due to the existence of two crystal forms but originated from the different distribution of the lamellar thickness (Helfand et al. 1977). According to the authors, the introduction of MWNTs in the blends provides a large amount of nucleation sites for end tethering of PA6 chains to form the α-phase crystals with similar lamellar thickness and restrain reorganization or recrystallization during the heating process in DSC scanning (Phang et al. 2006), which results in only one melting peak of PA6. The favorable formation of α-phase crystals in the presence of MWNTs also facilitates the enhancement of mechanical properties of the blends (Zhang et al. 2004).

The fractionated crystallization behavior of polypropylene (PP) droplets in its 20PP/80PS blends in the presence of hydrophilic or hydrophobic fumed silica nanoparticles was studied by using differential scanning calorimetry, scanning electron microscopy, and transmission electron microscopy by Huang et al. (2013). The fractionated crystallization of PP droplets in the PS matrix was promoted by adding a low content of hydrophobic or hydrophilic nanoparticles due

to their morphological refinement effect. However, discrepancies in the fractionated crystallization behavior of PP droplets occurred as the nanoparticle content increased. The crystallization became dominated by the heterogeneous nucleation effect of high content of hydrophilic nanoparticles. The authors ascribed this decrease to possible migration of the nanoparticles preferentially into PP droplets during mixing, significantly suppressing their fractionated crystallization (cause heterogeneous nucleation).

3.4 General Conclusion

Crystallization and melting phenomena in multicomponent polymer-based materials has been and is still a subject of scientific activity for a large number of academic and industrial research centers. That is because a wide spectrum of properties of many polymer materials depends on the crystallization process and on their extent of crystallinity as a result of the processing operations. The huge volume of literature of various types dealing with the crystallization and melting features is a strong witness of the above statements. The present chapter can be considered as a smart guide rather than an exclusive review work for people involved with the study of crystallization both for academic and applied research programs. The chapter has been split, although not really simple to achieve, into miscible, immiscible, and nanoparticles containing polymer blends. The miscible blends section has been divided into subsections of thermoplastic/thermoplastic and thermoplastic/thermosets. In the former system, the segregation of the molecules of the amorphous component from the crystallizing front is affected by the T_g, the kinetics of diffusion of the amorphous component, the crystallization kinetics, and the supercooling. In the latter blend system, the temperature and time of curing of the thermosetting affect strongly the crystallization features of the crystallizable thermoplastic component.

In miscible blends, segregation of the amorphous component competes with crystallization of the crystallizable one. Interspherulitic, interfibrillar, and interlamellar are the regions where segregation can take place during the crystallization of the crystallizable componenet. The balance between the diffusion rate of the amorphous component and the crystallization rate of the crystallizable component determines one or the other of the segregation type. In miscible blends of two crystallizable components, separate crystallization, concurrent crystallization, or cocrystallization may take place upon cooling from above the two individual melting temperatures of both blend components. Examples of blend systems leading to similar behavior were selected from literature and summarized herein. These phenomena were already reported in the first edition of the handbook and are maintained unmodified in the present chapter as no important new concepts were reported since then.

In immiscible blend systems, the accent was put on the fractionated crystallization features. A new and interesting work has been done since the first edition. This is extensively highlighted in the present chapter. The phenomenon is significant when the crystallizable phase is dispersed in the amorphous phase of the second blend component. Reactively compatibilized blends were compared to uncompatibilized

ones. The effect of compatibilization was shown to indirectly affect the crystallization behavior of the blends as it effects only and mainly causes particle size reduction. That results in more fractionated crystallization as the number of heterogeneities becomes insufficient to locate in all the crystallizable dispersed particles.

Dedication and Acknowledgments Professor Emeritus Dr. Gabriël Groeninckx would like to dedicate this chapter to all his former master and Ph.D. students, postdocs, and colleagues of the Laboratory for Macromolecular Structure Chemistry of the Catholic University of Leuven (KU Leuven, Heverlee, Belgium) for their valuable contribution in the field of polymer blends and related domains. He also would like to fully express his acknowledgments to the KU Leuven where he spent his scientific career from 1965 to 2010. And last but not least, he also has the great pleasure of dedicating this chapter 5 to his wife Anne-Marie and his children Christine, Filip, and Mark but also to his grandchildren Maartje, Nikolaas, Lineke, Noortje, and Luca. Each of them made him very happy in their own way.

3.5 Cross-References

▶ Interphase and Compatibilization by Addition of a Compatibilizer
▶ Miscible Polymer Blends
▶ Morphology of Polymer Blends
▶ Polymer Blends Containing "Nanoparticles"
▶ Reactive Compatibilization

Notations and Abbreviations

AN Acrylonitrile
aPMMA Atactic poly(methyl methacrylate)
aPS Atactic polystyrene
BR Butyl rubber
CPE Chlorinated polyethylene
DDS 4,4′-diaminodiphenylsulfone
DGEBA Diglycidyl ether of bisphenol A
DHDPE Deuterated high-density polyethylene
EBA Ethylene butylacrylate
EEA Elastomeric copolymer from ethylene and ethyl acrylate
EGMA Ethylene glycidyl methacrylate
EPDM Elastomeric terpolymer from ethylene, propylene, and a non-conjugated diene
EPR Elastomeric ethylene-propylene copolymer
EPR-g-SA Elastomeric ethylene-propylene copolymer grafted with styrene acrylonitrile
ER Epoxy resin
EVAc Poly(ethylene-*co*-vinyl acetate) (random)
FVA Poly(vinyl acetate-*co*-di-*n*-tetradecyl fumarate) (alternating)

GMA Glycidyl methacrylate copolymer
HDPE High-density polyethylene
iP(*p*-Me-S) Isotactic copolymer of styrene and *p*-methyl styrene
iPEMA Isotactic poly(ethyl methacrylate)
iPMMA Isotactic poly(methyl methacrylate)
iPS Isotactic polystyrene
LDPE Low-density polyethylene
LLDPE Linear low-density polyethylene
MA or MAH Maleic anhydride
MCDEA 4,4′-methylenebis(3-chloro-2,6-diethylaniline
P(4-Me-pentene) Poly(4-methyl pentene)
$P(E)_{0.43}(K)_{0.57}$ Random copolymer of phenyl ether and phenyl ketone
P(iPr-vinyl ether) Poly(isopropyl-vinyl ether)
P(sec-But-vinyl ether) Poly(sec-butyl vinyl ether)
PA-11 Polyamide 11
PA-12 Polyamide 12
PA-6 Polyamide 6
PA-66 Polyamide 66
PAr Polyarylate
PBA Poly(1,4.butylene adipate)
PBT Polybutyleneterephthalate
PC Bisphenol-A polycarbonate
PCDS Poly(1,4-cyclohexane-dimethylene succinate)
PCL Poly-e-caprolactone
PDPA Poly(2,2-dimethyl-1,3-propylene adipate)
PDPS Poly(2,2-dimethyl-1,3-propylene succinate)
PE Polyethylene
PEA Poly(ethylene adipate)
PECH Poly(epichlorohydrin)
PED *n*-Dodecyl ester terminated poly(ethylene glycol)
PEE Poly(ester-ether) segmented block copolymers
PEEEK Poly(ether ether ether ketone)
PEEK Poly(ether ether ketone)
PEEKK Poly(ether ether ketone ketone)
PEG Polyethylene glycol (also PEO)
PEI Poly(ether imide)
PEK Poly(ether ketone)
PEKK Poly(ether ketone ketone)
PEMA Polyethylmethacrylate
Penton Poly[3,3-bis(chloromethyl)oxetane]
PET Polyethyleneterephthalate
PET-b-PS Block copolymer of PET and PS segments
Phenoxy Poly(hydroxy ether of bisphenol A)
PI Di-*n*-octadecyl ester of itaconic acid

PI Polyisoprene
PIB Polyisobutene
PMMA Polymethylmethacrylate
POM Polyoxymethylene
PP Isotactic polypropylene
PPE, PPO Poly(2,6-dimethyl 1,4-phenylene ether), GE Co. trade name
PPG Poly(propylene glycol)
PPS Poly(phenylene sulfide)
PS Atactic polystyrene
PSMA Poly(styrene-*co*-maleic anhydride)
PVAc Poly(vinyl acetate)
PVC Polyvinyl chloride
PVDF Poly(vinylidene fluoride) (sometimes expressed as PVF_2)
PVF Poly(vinyl fluoride)
PVME Polyvinylmethylether
RIPS Reaction-induced phase separation
SAN Poly(styrene-*co*-acrylonitrile)
SARAN P(VCl_2-VC), P(VCl_2-VA), or P(VCl_2-AN) random copolymers of vinylidene chloride (VCl_2) with vinyl chloride (VC), vinyl acetate (VA), and acrylonitrile (AN), respectively
SBS Elastomeric styrene-butadiene-styrene triblock polymer (also TR)
SD Spinodal decomposition
SEBS Styrene-ethylene/butylene-styrene triblock polymer
SMA Poly(styrene-*co*-maleic anhydride)
sPMMA Syndiotactic poly(methyl methacrylate)
sPS Syndiotactic polystyrene
TR Thermoplastic rubber (also SBS)
UHMWPE Ultra-high-molecular-weight polyethylene
VDF-HFA Copolymer of vinylidene fluoride and hexafluoro acetone
VDF-TFE Copolymer of vinylidene fluoride and tetrafluoro ethylene
VLDPE Very low-density polyethylene
compat. Compatibilization, compatibilized, etc.
conc. Concentration
cryst. Crystallization, crystalline, crystallize
cte Constant
DSC Differential scanning calorimetry
etc. Et cetera
exp. Exponent
HM High molecular weight
LCST Lower critical solution temperature
O. M. Optical microscopy (also OM)
phr. Parts per hundred
[(*polymer*)] Amount/concentration of the cited polymer
SALS Small-angle light scattering (also SALLS)

SAXS Small-angle X-ray scattering
SEM Scanning electron microscopy
temp. Temperature
UCST Upper critical solution temperature
WAXS Wide-angle X-ray scattering
WLF Williams, Landel, and Ferry
C_1, C_2, C_3 WLF constants
***C*-2** Carbon chain with 2 C-atoms; i.e., ethylene
***C*-3** Carbon chain with 3 C-atoms; i.e., propylene
C_p Heat capacity under constant pressure
E_1 Energy dissipated for rejection of droplets during spherulite growth
E_2 Energy to overcome the inertia of droplets during spherulite growth
E_3 Energy required to form new interfaces when droplets are engulfed
E_4 Energy dissipated for deformation of occluded particles during spherulite growth
F_{12} Spreading coefficient
$f_z^{(1)}$ Fraction of dispersed droplets of volume V_D that contain z heterogeneities of type 1
G Isothermal spherulite growth rate
G^o Theoretical spherulite growth rate
G_1 Undisturbed spherulite growth rate of the homopolymer described by the Turnbull-Fisher equation
$M^{(1)}$ Concentration of heterogeneities of type 1
MW Molecular weight
n Avrami exponent
N Nucleation density
N/S Nucleation density normalized per unit area
K Overall crystallization rate
$t_{0.5}$ Halftime of crystallization at a fixed $T_{c,iso}$
T_c Bulk crystallization temperature upon cooling from the melt
T_c^o Crystallization temperature of the bulk homopolymer
$T_{c,cold}$ Cold crystallization temperature
$T_{c,hom}$ Homogeneous crystallization temperature
$T_{c,i}$ Crystallization temperature at which heterogeneities of type i become active
$T_{c,iso}$ Isothermal crystallization temperature
$T_{c,\max}$ Optimal isothermal crystallization temperature which yields the highest overall crystallization
T_g Glass-transition temperature
T_m Measured melting temperature of the crystalline phase
T_m^o Theoretical melting temperature for crystalline lamellae of infinite thickness
T_m' Observed melting temperature of the crystalline phase in blends
T_{melt} Premelting temperature
t_{melt} Time the polymer is kept in the melt
V_D Average volume of dispersed polymer droplets

Vol% Volume percentage
wt% Weight percentage
X_c Total degree of crystallinity
y_p **(*m*, *c*)** Lateral surface free energy between the crystal and its own melt
y_{pn} **(*m*)** Interfacial energy between the nucleating species and the polymer melt
y_{pn} **(*c*)** Interfacial energy between the nucleating species and the polymer crystal
z Number of heterogeneities of type 1, inducing crystallization in the bulk polymer at T_c°

Symbols: Greek Letters

ΔE Activation free energy for the transport of chains through the liquid–solid interface
ΔF Difference of interfacial energies; driving force for rejection, engulfing, and/or deformation of dispersed droplets during spherulite growth
ΔF^* Free energy for the formation of a nucleus of critical size
ΔH_m Total melting enthalpy of the crystalline polymer fraction
$\Delta T_{c,hom}$ Degree of undercooling required for homogeneous crystallization
$\Delta T_{c,i}$ Degree of undercooling required before a heterogeneity of type i can become active
Δy_i Specific interfacial energy difference between a nucleating species of type i and the polymer
Δy_{pn} Specific interfacial energy difference between a nucleating species and the polymer
γ_{PS} Interfacial free energy between the crystallizing solid and the inclusions
γ_{PL} Interfacial free energy between the liquid polymer melt and the inclusions
σ_o Surface free energy of folding
$\sigma_{1,2}$ Interfacial free energy between two phases of a blend in the melt
$\sigma_{i,1}$ Interfacial free energy of an impurity with respect to melt phase 1
$\sigma_{i,2}$ Interfacial free energy of an impurity with respect to melt phase 2

References

H. Abe, Y. Doi, M. Satkowski, I. Noda, Macromolecules **27**, 50 (1994)
J. Albuerne, L. Marquez, A.J. Muller, J.M. Raquez, P. Degee, P. Dubois, Macromolecules **36**, 1633 (2003)
G.C. Alfonso, T.P. Russell, Macromolecules **19**, 1143 (1986)
A. Aref-Azar, J. Hay, B. Marsden, N. Walker, J. Polym. Sci., Polym. Phys. Ed. **B18**, 637 (1980)
E. Assouline, A. Lustiger, A.H. Barber, C.A. Cooper, E. Klein, E. Wachtel, J. Polym. Sci. Part B: Polym. Phys. **41**(520) (2003)
M. Aubin, Y. Bédard, M.-F. Morrissette, R.E. Prudhomme, J. Polym. Sci., Polym. Phys. Ed. **B21**, 233 (1983)
M.J. Avrami, Chem. Phys. **7**, 1103 (1939)
M. Baïtoul, H. Saint-Guirons, P. Xans, P. Monge, Eur. Polym. J. **17**, 1281 (1981)

V. Balsamo, F. von Gyldenfeldt, R. Stadler, Macromol. Chem. Phys. **33**, 197 (1996)
V. Balsamo, D. Newman, L. Gouveia, L. Herrera, M. Grimau, E. Laredo, Polymer **47**, 5810 (2006)
C.A. Barron, S.K. Kumar, J.P. Runt, ACS Polym. Prepr. **2**, 610 (1992)
Z. Bartczak, A. Galeski, Polymer **27**, 544 (1986)
Z. Bartczak, A. Galeski, E. Martuscelli, Polym. Eng. Sci. **24**, 1155 (1984)
Z. Bartczak, A. Galeski, M. Pracella, Polymer **27**, 537 (1986)
Z. Bartczak, A. Galeski, N.P. Krasnikova, Polymer **28**, 1627 (1987)
Z. Bartczak, E. Martuscelli, A. Galeski, in *Polypropylene: Structure*, *Blends and Composites*, vol. 2, ed. by J. Karger-Kocsis (Chapman & Hall, London, 1995)
D.C. Bassett, R.H. Olley, I.A.M. Al Raheil, Polymer **29**, 1745 (1992)
L. Bianchi, S. Cimmino, A. Forte, R. Greco, F. Riva, C. Silvestre, J. Mater. Sci. **20**, 895 (1985)
J. Boon, J.M. Azcue, J. Polym. Sci., Part A-2 **6**, 885 (1968)
J. Boon, G. Challa, D.W. Van Krevelen, J. Polym. Sci., Part A-2 **6**, 1791 (1968)
J.R. Burns, D. Turnbull, J. Appl. Phys. **37**, 4021 (1966)
E. Calahorra, M. Cortazar, G.M. Guzman, Polymer **23**, 1322 (1982)
M. Canetti, P. Sadocco, A. Siciliano, A. Seves, Polymer **35**, 2884 (1994)
F.-C. Chang, M.-Y. Yang, J.-S. Wu, Polymer **32**, 1394 (1991)
H.-L. Chen, R.S. Porter, J. Polym. Sci., Polym. Phys. Ed. **B31**, 1845 (1993)
T.H. Chen, A.C. Su, Polymer **34**, 4826 (1993)
C.C. Chen, E. Fontan, K. Min, J.L. White, Polym. Eng. Sci. **28**, 69 (1988)
F. Chen, R.A. Shanks, G. Amarasinghe, Polymer **42**, 4579 (2001)
H. Chen, M. Pyda, P. Cebe, Thermochim. Acta. **492**, 61 (2009)
S.Z.D. Cheng, M.-Y. Cao, B. Wunderlich, Macromolecules **19**, 1868 (1986)
J.W. Cho, S. Tasaka, S. Miyata, Polym. J. **25**, 1267 (1993)
S. Cimmino, E. Martuscelli, C. Silvestre, Macromol. Chem. **16**, 147 (1988)
S. Cimmino, E. Martuscelli, C. Silvestre, M. Canetti, C. De Lalla, A. Seves, J. Polym. Sci., Polym. Phys. Ed. **B27**, 1781 (1989)
S. Cimmino, E. Di Pace, E. Martuscelli, C. Silvestre, Polym. Comm. **32**, 251 (1991)
S. Cimmino, E. Di Pace, E. Martuscelli, C. Silvestre, Polymer **34**, 2799 (1993a)
S. Cimmino, E. Martuscelli, C. Silvestre, A. Cecere, M. Fontelos, Polymer **34**, 1207 (1993b)
J. Cissé, G. Bolling, J. Cryst. Growth **10**, 56 (1971)
N.E. Clough, R.W. Richards, T. Ibrahim, Polymer **35**, 1044 (1994)
F. Coppola, R. Greco, E. Martuscelli, H.W. Kammer, C. Kummerlowe, Polymer **28**, 47 (1987)
R. Cormia, F. Price, D. Turnbull, J. Chem. Phys. **37**, 1333 (1962)
G. Crevecoeur, G. Groeninckx, Macromolecules **24**, 1190 (1991)
G. Crevecoeur, Ph.D. dissertation, KU Leuven, 1991
C.A. Cruz, J.W. Barlow, D.R. Paul, Macromolecules **12**, 726 (1979)
G. Defieuw, Ph.D. dissertation, KU Leuven, 1989
G. Defieuw, G. Groeninckx, H. Reynaers, Polymer **30**, 2158 (1989a)
G. Defieuw, G. Groeninckx, H. Reynaers, Polymer **30**, 595 (1989b)
G. Defieuw, G. Groeninckx, H. Reynaers, *Contemporary Topics in Polymer Science: Multiphase Macromolecular Systems*, vol. 6 (Plenum, New York, 1989c), p. 423
G. Defieuw, G. Groeninckx, H. Reynaers, Polymer **30**, 2164 (1989d)
F. Defoor, G. Groeninckx, H. Reynaers, P. Schouterden, B. Van Der Heyden, J. Appl. Polym. Sci. **47**, 1839 (1993)
G. Dreezen, M.H.J. Koch, H. Reynaers, G. Groeninckx, Polymer **40**, 6451 (1999a)
G. Dreezen, Z. Fang, G. Groeninckx, Polymer **40**, 5907 (1999b)
G.C. Eastmond, Adv. Polym Sci. **59**, 40 (2000)
G.H. Edward, Br. Polym. J. **18**, 88 (1986)
A. Escala, R. S. Stein, in *Multiphase Polymers*, ed. by S. L. Cooper, G. M. Ester. Advance in Chemistry Series, vol. 176 (American Chemical Society, Washington, DC, 1979), p. 455
A. Eshuis, E. Roerdink, G. Challa, Polymer **23**, 735 (1982)
V. Everaert, G. Groeninckx, L. Aerts, Polymer **41**, 1409 (2000)

V. Everaert, G. Groeninckx, M.H.J. Koch, H. Reynaers, Polymer **44**, 3491 (2003)
B.D. Favis, J. Appl. Polym. Sci. **39**, 285 (1990)
B.D. Favis, Makromol. Chem., Macromol. Symp. **56**, 143 (1992)
B.D. Favis, J.P. Chalifoux, Polym. Eng. Sci. **27**, 1591 (1987)
B.D. Favis, J.P. Chalifoux, Polymer **29**, 1761 (1988)
B.D. Favis, C. Lavallee, A. Derdouri, J. Mater. Sci. **27**, 4211 (1992)
A.C. Fernandez, J.W. Barlow, D.R. Paul, Polymer **27**, 1799 (1986)
V. Flaris, A. Wasiak, W. Wenig, J. Mater. Sci. **28**, 1685 (1993)
M.J. Folkes, P.S. Hope (eds.), *Polymer Blends and Alloys* (Blackie Academic and Professional, London, 1993)
H. Frensch, B.-J. Jungnickel, Colloid Polym. Sci. **267**, 16 (1989)
H. Frensch, B.-J. Jungnickel, Plast. Rubber Compos. Process. Appl. **16**, 5 (1991)
H. Frensch, P. Harnischfeger, B.-J. Jungnickel, in *Multiphase Polymers: Blends and Ionomers*, eds. by L. Utracki, R. A. Weiss. ACS Symposium Series, vol. 395 (American Chemical Society, Washington, DC, 1989), p. 101
C. Friedrich, Progr. Colloid Polym. Sci. **66**, 299 (1979)
A. Galeski, Z. Bartczak, M. Pracella, Polymer **25**, 1323 (1984)
K.P. Gallagher, X. Zhang, J.P. Runt, G. Huynh-ba, J.S. Lin, Macromolecules **26**, 588 (1993)
P.H. Geil, *Polymer Single Crystals* (Wiley, New York, 1963), p. 229
P.H. Geil, *Polymer Single Crystals* (R. E. Krieger, New York, 1973)
A. Ghijsels, N. Groesbeek, C.W. Yip, Polymer **23**, 1913 (1982)
X.Y. Gong, J. Liu, S. Baskaran, R.D. Voise, J.S. Young, Chem. Mater. **12:1**, 1049 (2000)
S. Goossens, G. Groeninckx, Macromolecules **39**, 8049 (2006)
S. Goossens, G. Groeninckx, J. Polym. Sci.: Part B: Polym. Phys. **45**, 2456 (2007)
S. Goossens, B. Goderis, G. Groeninckx, Macromolecules **39**, 2953 (2006)
R. Greco, M. Mancarella, E. Martuscelli, G. Ragosta, Y. Jinghua, Polymer **28**, 1922 (1987a)
R. Greco, M. Mancarella, E. Martuscelli, G. Ragosta, Y. Jinghua, Polymer **28**, 1929 (1987b)
D. Grenier, R.E. Prud'homme, J. Polym. Sci., Polym. Phys. Ed. **B18**, 1655 (1980)
I. Grof, O. Durcova, A. Marcincin, Acta Polym. **40**, 344 (1989)
Q. Guo, Makromol. Chem. **191**, 2639 (1990)
Q. Guo, G. Groeninckx, Polymer **42**, 8647 (2001)
Q. Guo, X. Peng, Z. Wang, Polymer **32**, 53 (1991)
Q. Guo, C. Harrats, G. Groeninckx, M.H.J. Koch, Polymer **42**, 4127 (2001a)
Q. Guo, C. Harrats, G. Groeninckx, H. Reynaers, M.H.J. Koch, Polymer **42**, 6031 (2001b)
Q. Guo, S. Slavov, P.J. Halley, J. Polym. Sci.: Part B: Polym. Phys. **42**, 2833 (2004)
A.K. Gupta, V.B. Gupta, R.H. Peters, W.G. Harland, J.P. Berry, J. Appl. Polym. Sci. **27**, 4669 (1982)
A.K. Gupta, S.K. Rana, B.L. Deopura, J. Appl. Polym. Sci. **44**, 719 (1992)
A.K. Gupta, S.K. Rana, B.L. Deopura, J. Appl. Polym. Sci. **51**, 231 (1994)
B.R. Hahn, O. Herrmann-Schönherr, J.H. Wendorff, Polymer **28**, 201 (1987)
C.D. Han, C.A. Villamizar, Y.W. Kim, S.J. Chen, J. Appl. Polym. Sci. **21**, 353 (1977)
J.E. Harris, L.M. Robeson, J. Polym. Sci., Polym. Phys. Ed **B25**, 311 (1987)
J.E. Harris, L.M. Robeson, J. Appl. Polym. Sci. **35**, 1877 (1988)
J.E. Harris, S.H. Goh, D.R. Paul, J.W. Barlow, J. Appl. Polym. Sci. **27**, 839 (1982)
J.N. Hay, J. Polym. Sci., Polym. Chem. Ed. **A14**, 2845 (1976)
E. Helfand, A. Sapse, J. Chem. Phys. **62**, 1327 (1975)
E. Helfand, Y. Tagami, J. Chem. Phys. **56**, 3592 (1972)
E. Helfand, Z.R. Wasserman, J. Appl. Phys. **56**, 251 (1977)
D. Hlavatá, Z. Horák, Eur. Polym. J. **30**, 597 (1994)
J.D. Hoffman, Polymer **24**, 3 (1983)
J.D. Hoffman, J.J. Weeks, J. Chem. Phys. **37**, 1723–1741 (1962a)
J.D. Hoffman, J.J. Weeks, J. Res. Natl. Bur. Stand., Sect. A **66**, 13–28 (1962b)
J. D. Hoffman, G. T. Davis, J. I. Lauritzen, in *Treatise on Solid State Chemistry*, vol. 3, chapter 7, ed. by N. B. Hannay (Plenum, New York, 1976)

J.D. Hoffmann, R.L. Miller, H. Marand, D.B. Roitman, J. Nat. Bur. Stand. **79A**, 671 (1992)
R. Holsti-Miettinen, J. Seppälä, O.T. Ikkala, Polym. Eng. Sci. **32**, 868 (1992)
R. Holsti-Miettinen, M. Heino, J. Seppälä, J. Appl. Polym. Sci. **57**, 573 (1995)
B.S. Hsiao, B.B. Sauer, J. Polym. Sci., Polym. Phys. Ed. **B31**, 901 (1993)
S.-R. Hu, T. Kyu, R.S. Stein, J. Polym. Sci., Polym. Phys. Ed. **B25**, 71 (1987)
B. Huang, J. Wang, D. Pang, in *Third European Symposium on Polymer Blends* (PRI), Cambridge, UK, 1990, p. B3
S.D. Hudson, D.D. Davis, A.J. Lovinger, Macromolecules **25**, 3446 (1991)
R.D. Icenogle, J. Polym. Sci., Polym. Phys. Ed. **B23**, 1369 (1985)
F. Ide, A. Hasegawa, J. Appl. Polym. Sci. **18**, 963 (1974)
O.T. Ikkala, R.M. Holsti-Miettinen, J. Seppälä, J. Appl. Polym. Sci. **49**, 1165 (1993)
R.L. Imken, D.R. Paul, J.W. Barlow, Polym. Eng. Sci. **16**, 593 (1976)
J.J. Iruin, J.I. Eguiazabal, G.M. Guzman, Eur. Polym. J. **25**, 1169 (1989)
W.H. Jo, S.J. Park, I.H. Kwon, Polym. Int. **29**, 173 (1992)
J.P. Jog, V.L. Shingankuli, V.M. Nadkarni, Polymer **34**, 1966 (1993)
A.M. Jonas, T.P. Russell, Y.D. Yoon, Macromolecules **28**, 8491 (1995)
J.M. Jonza, R.S. Porter, Macromolecules **19**, 1946 (1986)
N.K. Kalfoglou, Angew. Makromol. Chem. **129**, 103 (1985)
N.F. Kalfoglou, D.D. Sotiropoulou, A.G. Margaritis, Eur. Polym. J. **24**, 389 (1988)
M.R. Kamal, E. Chu, Polym. Eng. Sci. **3**, 27 (1983)
J. Karger-Kocsis, A. Kallo, A. Szafner, G. Bodor, U.S. Senyei, Polymer **20**, 37 (1979)
H.D. Keith, F.J. Padden Jr., J. Appl. Phys. **34**, 2409 (1963)
H.D. Keith, F.J. Padden Jr., J. Appl. Phys. **35**, 1286 (1964)
F.H. Khambatta, F.P. Warner, T.P. Russell, R.S. Stein, J. Polym. Sci-A2 **14**, 1391 (1976a)
F.B. Khambatta, F. Warner, T. Russell, R.S. Stein, J. Polym. Sci., Polym. Phys. Ed. **B14**, 1391 (1976b)
Y.P. Khanna, R. Kumar, A.C. Reimschuessel, Polym. Eng. Sci. **28**, 1607 (1988a)
Y.P. Khanna, A.C. Reimschuessel, A. Banerjie, C. Altman, Polym. Eng. Sci. **28**, 1600 (1988b)
N. Klemmer, B.-J. Jungnickel, Colloid Polym. Sci. **262**, 381 (1984)
J.A. Koutsky, A.G. Walton, E. Baer, J. Appl. Phys. **38**, 1832 (1967)
J. Kressler, H.W. Kammer, Polym. Bull. **19**, 283 (1988)
J. Kressler, P. Svoboda, T. Inoue, in *ACS Polymer Preprints*, vol. 33, p. 612. Papers presented at the Washington, DC. Meeting, August 1992
J. Kressler, P. Svoboda, T. Inoue, Polymer **34**, 3225 (1993)
B. Kulshreshtha, A. Ghost, A.K. Misra, Polymer **44**, 4723 (2003a)
B. Kulshreshtha, A.K. Ghost, A. Misra, J. Macromol. Sci. Phys. **B42**, 307 (2003b)
S.K. Kumar, D.Y. Yoon, Macromolecules **24**, 5414 (1991)
T. Kunori, P.H. Geil, J. Makromol. Sci., Phys. Ed. **B18**, 135 (1980)
T.K. Kwei, H.L. Frisch, Macromolecules **11**, 1267 (1978)
T.K. Kwei, G.D. Patterson, T.T. Wang, Macromolecules **9**, 780 (1976)
T.K. Kwei, H.L. Frisch, W. Radigan, S. Vogel, Macromolecules **10**, 157 (1977)
T. Kyu, P. Vadhar, J. Appl. Polym. Sci. **32**, 5575 (1986)
T. Kyu, S.-R. Hu, R.S. Stein, J. Polym. Sci., Polym. Phys. Ed. **B25**, 89 (1987)
M.P. Lattimer, J.K. Hobbs, M.J. Hill, P.J. Barham, Polymer **33**, 3971 (1992)
J.I. Lauritzen, J.D. Hoffman, J. Appl. Phys. **44**, 4340 (1973)
Y. Lee, R.S. Porter, Macromolecules **20**, 1336 (1987)
Y. Lee, R.S. Porter, J.S. Lin, Macromolecules **22**, 1756 (1989)
Y. Li, B.-J. Jungnickel, Polymer **34**, 9 (1993)
Y. Li, M. Stein, B.-J. Jungnickel, Colloid Polym. Sci. **269**, 772 (1991); and '*Mitteilungen aus dem Deutschen Kunststoff-Institut*', Nr° 53, April, Darmstadt, 1991
W. Li, R. Yan, B. Jian, Polymer **33**, 889 (1992)
P. Li, Y. Huang, M. Kong, Y. Lv, Y. Luo, Q. Yang, G. Li, Colloid Polym. Sci. **291**, 1693 (2013)
B. Liang, L. Pan, J. Appl. Polym. Sci. **54**, 1945 (1994)

B.R. Liang, J.L. White, J.E. Spruiel, B.C. Goswami, J. Appl. Polym. Sci. **28**, 2011 (1983)
A.M. Liquori, G. Anzuino, V.M. Coiro, M. D'Alagni, P. de Santis, M. Savino, Nature **206**, 358 (1965)
X.Q. Liu, W. Yang, B.H. Xie, M.B. Yang, Mater. Design. **34**, 355 (2012)
Y. Long, Z. Stachurski, R.A. Shanks, Polym. Int. **26**, 143 (1991)
B. Lotz, A.J. Kovacs, ACS Div. Polym. Chem., Polym. Prepr. **10**, 820 (1969)
A.J. Lovinger, M.L. Williams, J. Appl. Polym. Sci. **25**, 1703 (1980)
A.J. Lovinger, J.O. Chua, C.C. Gryte, J. Polym. Sci., Polym. Phys. Ed. **B15**, 641 (1977)
H. Lu, S.X. Zheng, Polym. **44**, 4689 (2003)
J.H. Magill, J. Appl. Phys. **35**, 3249 (1964)
K. Mai, M. Zhang, H. Zeng, S. Qi, J. Appl. Polym. Sci. **51**, 57 (1994)
L. Mandelkern, *Crystallization of Polymers* (McGraw-Hill, New York, 1964)
L. Mandelkern, F.A. Quinn, P.J. Flory, J. Appl. Phys. **25**, 830 (1954)
C. Marco, M.A. Gomez, J.G. Fatou, A. Etxeberria, M.M. Elorza, J.J. Iruin, Eur. Polym. J. **29**, 1477 (1993)
E. Martuscelli, Polym. Eng. Sci. **24**, 563 (1984)
E. Martuscelli, in *Polymer Blends and Mixtures*, ed. by D. J. Walsch (Dordrecht, Springer, 1985), pp. 217–243
E. Martuscelli, G.B. Demma, in *Polymer Blends: Processing*, *Morphology and Properties*, ed. by E. Martuscelli, M. Kryszewski, R. Palumbo (Plenum, New York, 1980a)
E. Martuscelli, M. Pracella, M. Avella, R. Greco, G. Ragosta, Makromol. Chem. **181**, 957 (1980b)
E. Martuscelli, C. Silvestre, G. Abate, Polymer **23**, 229 (1982)
E. Martuscelli, C. Silvestre, L. Bianchi, Polymer **24**, 1458 (1983)
E. Martuscelli, M. Pracella, P.Y. Wang, Polymer **25**, 1097 (1984)
H.-S. Moon, B.-K. Ryoo, J.-K. Park, J. Polym. Sci., Polym. Phys. Ed. **B32**, 1427 (1994)
R.A. Morales, M.L. Arnal, A.J. Müller, Polym. Bull. **35**, 379 (1995)
L.B. Morgan, Phila. Trans. Roy. Soc. Lond. **247**, 13 (1954)
D. Morin, Y. Zhao, R.E. Prud'homme, J. Appl. Polym. Sci. **81**, 1683 (2001)
B.S. Morra, R.S. Stein, J. Polym. Sci., Polym. Phys. Ed. **B20**, 2261 (1982)
B.S. Morra, R.S. Stein, Polym. Eng. Sci. **24**, 311–318 (1984)
B.S. Morra, Ph.D. dissertation, University of Amherst, MA, 1980
M. Mucha, Colloid Polym. Sci. **264**, 859 (1986)
A. J. Müller, M. L. Arnal, R. A. Morales, in *Europhysics Conference Abstracts*, 19D, P2, Prague, 17–20 July 1995
V.M. Nadkarni, J.P. Jog, J. Appl. Polym. Sci. **32**, 5817 (1986)
V.M. Nadkarni, J.P. Jog, Polym. Eng. Sci. **27**, 451 (1987)
V.M. Nadkarni, V.L. Shingankuli, J.P. Jog, Int. Polym. Proc. **2**, 53 (1987)
V.M. Nadkarni, J. P. Jog, in *Two-phase Polymer Systems*, ed. by L. A. Utracki (Hanser Publishing, Munich/New York, 1991)
G. Natta, P. Corradini, D. Sianesi, D. Morero, J. Polym. Sci. **51**, 527 (1961)
G. Natta, I.W. Bassi, D. Sianesi, G. Caporiccio, E. Torti, J. Polym. Sci., Polym. Chem. Ed. **A3**, 4263 (1965)
M.K. Neo, S.H. Goh, Eur. Polym. J. **27**, 927 (1991)
T. Nishi, T.T. Wang, Macromolecules **8**, 909 (1975)
O.F. Noel, J.P. Carley, Polym. Eng. Sci. **24**, 488 (1984)
S. Nojima, H. Tsutsui, M. Urushihara, W. Kosaka, N. Kato, T. Ashida, Polym. J. **18**, 451 (1986)
S. Nojima, D.J. Wang, T. Ashida, Polym. J. **23**, 1473 (1991)
O. Olabishi, L.M. Robeson, M.Y. Shaw, *Polymer-Polymer Miscibility* (Academic, New York, 1979)
J.J. O'Malley, R.G. Crystal, P.F. Erhardt, ACS Div. Polym. Chem., Polym. Prepr. **10**, 796 (1969)
S. Omenyi, A. Neumann, W. Martin, G. Lespinard, R. Smith, J. Appl. Phys. **52**, 789 (1981)
C.J. Ong, F.P. Price, J. Polym. Sci. Polym. Symp. **63**, 45 (1978a)
C.J. Ong, F.P. Price, J. Polym. Sci. Polym. Symp. **63**, 59 (1978b)
T. Ozawa, Polymer **12**, 150 (1971)

S.J. Park, B.K. Kim, H.M. Jeong, Eur. Polym. J. **26**, 131 (1990)
J.H. Perepezko, J.S. Paik, Undercooling Behaviour of Liquid Metals, in *Rapidly solidified Amorphous and Crystalline Alloys*, ed. by B.H. Kear, B.C. Giessen, M. Cohen (North Holland, New York, 1982)
F.C. Pérez-Cardenas, D.E.L. Felipe, L. Castillo, R. Vera-graziano, J. Appl. Polym. Sci. **43**, 779 (1991)
I.Y. Phang, J.H. Ma, L. Shen, T.X. Liu, W.D. Zhang, Polym. Int. **55**, 71 (2006)
I. Pillin, J.-F. Feller, Macomol. Mater. Eng. **291**, 1375 (2006)
J. Plans, W.J. MacKnight, F.E. Karasz, Macromolecules **17**, 810 (1984)
U. Plawky, W. Wenig, J. Mater. Sci. Lett. **13**, 863 (1994)
M. Plesek, Z. Malac, in *Morphology of Polymers*, ed. by B. Sedlacek, Proceedings of the 17th Europhysics Conference on Macromolecular Physics, Prague, 15–18 July 1985 (1986)
G.M. Pound, V.K. LaMer, J. Am. Chem. Soc. **74**, 2323 (1952)
A. Prasad, H. Marand, Bull. Am. Phys. Soc. **36**, 632 (1991)
B. Pukanszky, F. Tudos, A. Kallo, G. Bodor, Polymer **30**, 1399 (1989)
R.P. Quirk, J.-J. Ma, C.C. Chen, K. Min, J.L. White, in *Contemporary Topics in Polymer Science*, *Vol. 6*, *Multiphase macromolecular Systems*, ed. by B. M. Culbertson (Plenum, New York/London, 1989)
J.M. Rego Lopez, U.W. Gedde, Polymer **29**, 1037 (1988)
M.C. Righetti, M.L. Di Lorenzo, M. Angiuli, E. Tombari, P. La Pietra, Eur. Polym. J. **43**, 4726 (2007)
P.B. Rim, J.P. Runt, Macromolecules **16**, 762–768 (1983)
P.B. Rim, J.P. Runt, Macromolecules **17**, 1520–1526 (1984)
C. Robitaille, J. Prud'homme, Macromolecules **16**, 665 (1983)
S. Rostami, Polymer **31**, 899–904 (1990)
M. Run, Y. Hao, C. Yao, Thermochim. Acta. **51**, 495 (2009)
J.P. Runt, Macromolecules **14**, 420 (1981)
J. Runt, P.B. Rim, S.E. Howe, Polym. Bull. **11**, 517 (1984)
J.P. Runt, L.M. Martynowicz, in *Multicomponent Polymer Materials*, ed. by D. R. Paul, L.H. Sperling, Advance in Chemistry Series, vol. 211 (American Chemical Society, Washington, DC, 1986)
J.P. Runt, C.A. Barron, X.-F. Zhang, S.K. Kumar, Macromolecules **24**, 3466 (1991)
T.P. Russell, R.S. Stein, J. Macromol. Sci., Phys. Ed. **B17**, 617 (1980)
T.P. Russell, R.S. Stein, J. Polym. Sci. Polym. Phys. Ed. **B21**, 999 (1983)
F. Rybnikâr, J. Macromol. Sci. Phys. Ed. **B27**, 125 (1988)
H. Saito, B. Stühn, Macromolecules **27**, 216 (1994)
H. Saito, T. Okada, T. Hamane, T. Inoue, Macromolecules **24**, 4446 (1991)
N. Salmon, V. Carlier, J. Schut, P.M. Remiro, I. Mondragon, Polym. Int. **54**, 667 (2005)
I. Sanchez, E.A. Di Marzio, Macromolecules **4**, 677 (1971)
O.O. Santana, A.J. Müller, Polym. Bull. **32**, 471 (1994)
P. Schouterden, G. Groeninckx, H. Reynaers, C. Riekel, M.H.J. Koch, Polym. Bull. **13**, 533 (1985)
K. Schulze, J. Kressler, H.W. Kammer, Polymer **34**, 3704 (1993)
J. Schut, M. Stamm, M. Dumon, J. Galy, J.F. Gerard, Macroml. Symp. **202**, 25 (2003)
C.K. Sham, G. Guerra, F.E. Karasz, W.J. MacKnight, Polymer **29**, 1016 (1988)
Y.D. Shibanov, Y.K. Godovsky, Progr. Colloid Polym. Sci. **80**, 110 (1989)
Y.D. Shibanov, Y.K. Godovsky, Makromol. Chem., Macromol. Symp. **44**, 61 (1991)
V.L. Shingankuli, J.P. Jog, V.M. Nadkarni, J. Appl. Polym. Sci. **36**, 335 (1988)
V. L. Shingankuli, Ph.D. thesis, Bombay University, India, 1990
C. Silvestre, S. Cimmino, E. Martuscelli, F.E. Karasz, W.J. MacKnight, Polymer **28**, 1190 (1987a)
C. Silvestre, F.E. Karasz, W.J. MacKnight, E. Martuscelli, Eur. Polym. J. **23**, 745 (1987b)
H.H. Song, D.-Q. Wu, M. Ree, R.S. Stein, J.C. Phillips, L. LeGrand, B. Chu, Macromolecules **21**, 1180 (1988)
H.W. Starkweather Jr., J. Appl. Polym. Sci. **25**, 139 (1980)
R.S. Stein, in *Newer Methods of Polymer Characterization*, chapter 4 (Wiley, New York, 1964)

R.S. Stein, F.B. Khambatta, F.P. Warner, T. Russell, A. Escala, E. Balizer, J. Polym. Sci., Polym. Symp. **63**, 313 (1978)
R.S. Stein, T.P. Russell, B.S. Morra, M. Wai, J. Gilmer, in *Structural Order in Polymers*, ed. by F. Ciardelli, P. Giusti (Pergamon, New York, 1981), p. 195
T. Suzuki, A. Kovacs, Polym. J. **1**, 82 (1970)
P. Svoboda, D. Svobodova, T. Chiba, T. Inoue, Eur. Polym. J. **44**, 329 (2008)
H. Tanaka, T. Nishi, Phys. Rev. Lett. **55**, 1102 (1985)
H. Tanaka, T. Nishi, Phys. Rev. A **39**, 783 (1989)
T. Tang, B. Huang, J. Appl. Polym. Sci. **53**, 355 (1994a)
T. Tang, B. Huang, J. Polym. Sci., Polym. Phys. Ed. **B32**, 1991 (1994b)
T. Tang, H. Li, B. Huang, Macromol. Chem. Phys. **195**, 2931 (1994)
K. Tashiro, M.M. Satkowski, R.S. Stein, Y. Li, B. Chu, S.L. Hsu, Macromolecules **25**, 1809 (1992a)
K. Tashiro, R.S. Stein, S.L. Hsu, Macromolecules **25**, 1801 (1992b)
K. Tashiro, M. Izuchi, F. Kaneuchi, C. Jin, M. Kobayashi, R.S. Stein, Macromolecules **27**, 1140 (1994a)
K. Tashiro, M. Izuchi, M. Kobayashi, R.S. Stein, Macromolecules **27**, 1121 (1994b)
K. Tashiro, M. Izuchi, M. Kobayashi, R.S. Stein, Macromolecules **27**, 1128 (1994c)
K. Tashiro, M. Izuchi, M. Kobayashi, R.S. Stein, Macromolecules **27**, 1134 (1994d)
J.W. Teh, J. Appl. Polym. Sci. **28**, 605 (1983)
J.W. Teh, H.P. Blom, A. Rudin, Polymer **35**, 1680 (1994a)
J.W. Teh, A. Rudin, J.C. Keung, Adv. Polym. Technol. **13**, 1 (1994b)
D.G. Thomas, L.A.K. Staveley, J. Chem. Soc. 4569 (1952)
R.T. Tol, V.B.F. Mathot, G. Groeninckx, Polymer **46**, 369 (2005a)
R.T. Tol, V.B.F. Mathot, G. Groeninckx, Polymer **46**, 383 (2005b)
R.T. Tol, V.B.F. Mathot, G. Groeninckx, Polymer **46**, 2955 (2005c)
D. Turbull, J. Chem. Phys. **18**, 198 (1950)
D. Turnbull, J. Chem. Phys. **18**, 198 (1950)
D. Turnbull, R.E. Cech, J. Appl. Phys. **21**, 804 (1950)
D. Turnbull, J.C. Fisher, J. Chem. Phys. **17**, 71 (1949)
W. Ullmann, J.H. Wendorff, Compos. Sci. Technol. **23**, 97 (1985)
L.A. Utracki, *Polymer Alloys and Blends* (Hanser Publishers, Munich, 1989)
P. Vadhar, T. Kyu, Polym. Eng. Sci. **27**, 202 (1987)
L. Valentini, J. Biagiotti, J.M. Kenny, S. Santucci, Compos. Sci. Technol. **63**, 1149 (2003)
F. Van Antwerpen, D.W. Van Krevelen, J. Polym. Sci., Polym. Phys. Ed. **B10**, 2423 (1972)
D.W. Van Krevelen, *Properties of Polymer* (Elsevier, New York, 1976)
A.D. Van Riemsdyk, Ann. Chim. Phys. **20**, 66 (1880)
M. Vandermarliere, Ph.D. dissertation, KU Leuven, 1986
M. Vanneste, G. Groeninckx, Polymer **35**, 1051 (1994)
M. Vanneste, G. Groeninckx, Polymer **36**, 4253 (1995)
M. Vanneste, Ph.D. dissertation, KU Leuven, 1993
G. Vidotto, D.L. Levy, A.J. Kovacs, Kolloid Z. Z. Polym. **230**, 289 (1969)
D.J. Walsh, S. Rostami, V.B. Singh, Macromol. Chem. **186**, 145 (1985)
Z. Wang, B. Jiang, Macromolecules **30**, 6223 (1997)
T.T. Wang, T. Nishi, Macromolecules **10**, 421 (1977)
Z. Wang, X. Wang, D. Yu, B. Jiang, Polymer **38**, 5897 (1997)
Z. Wang, A.N. Lijia, B. Jiang, X. Wang, H. Zhao, Polym. J. **30**, 206 (1998)
F.P. Warner, W.J. MacKnight, R.S. Stein, J. Polym. Sci., Polym. Phys. Ed. **B15**, 2113 (1977)
C. Wei-Berk, ACS **68**, 299 (1993)
W. Wenig, K. Meyer, Colloid Polym. Sci. **258**, 1009 (1980)
W. Wenig, F.E. Karasz, W.J. MacKnight, J. Appl. Phys. **46**, 4194 (1975)
W. Wenig, H.-W. Fiedel, A. Scholl, Colloid Polym. Sci. **268**, 528 (1990)
D.L. Wilfong, A. Hiltner, E. Baer, J. Mater. Sci. **21**, 2014 (1986)
M.L. Williams, R.F. Landel, J.D. Ferry, J. Am. Chem. Soc. **77**, 3701 (1955)

J.M. Willis, B.D. Favis, C. Lavallé, J. Mater. Sci. **28**, 1749 (1993)
E.M. Woo, J.W. Barlow, D.R. Paul, J. Appl. Polym. Sci. **28**, 1347 (1983)
B. Wunderlich, *Macromolecular Physics* (Academic, New York, 1973)
B. Wunderlich, in *Macromolecular Physics*, *Vol.2*, *Crystal Nucleation-Growth-Annealing* (Academic, New York/San Francisco/London, 1976)
J. Yang, P. Pan, L. Hua, Y. Xie, T. Dong, B. Zhu, Y. Inoue, X. Feng, Polymer **52**, 3460 (2011)
C. Yordanov, L. Minkova, Eur. Polym. J. **41**, 527 (2005)
H. Zhang, R.E. Prud'homme, J. Polym. Sci., Polym. Phys. Ed. **B24**, 723 (1987)
W.D. Zhang, L. Shen, I.Y. Phang, T.X. Liu, Macromolecules **37**, 256 (2004)
S.X. Zheng, Q. Guo, Y.L. Mi, Polymer **44**, 867 (2003)
X.-Q. Zhou, J.N. Hay, Polymer **34**, 4710 (1993)
A. Ziabicki, Appl. Polym. Symp. **6**, 1 (1967)
A. Ziabicki, *Fundamentals of Fibre Formation: The Science of Fibre Spinning and Drawing* (Wiley, New York, 1976), p. 111